The Oceanography, the Biogeochemistry and the Fluxes of Carbon Dioxide in the Benguela Upwelling System

Pedro Manuel Scheel Monteiro

Thesis Presented for the Degree of

DOCTOR OF PHILOSOPHY

UNIVERSITY OF CAPE TOWN

Rondebosch 7700

SOUTH AFRICA

September 1996

Declaration

I Pedro Manuel Scheel Monteiro declare that this thesis is my own unaided work, both in concept and execution and that apart from the normal guidance of my supervisors, I have received no assistance except as is provided in the acknowlegements.

Acknowledgements

A number of people from the oceanographic community, friends and family were instrumental in making this enterprise conceptually, logistically and emotionally possible:

My colleague Grev Nelson whose door was always open. He generously shared in the excitement of new ideas and made many hours available to talk and philosophise about the ocean and its complexity which made this work that much more enjoyable and creative. The wind-driven Ekman transport calculations were all carried out using software designed and made to work by Grev Nelson. My friend and colleague Trevor Probyn for the many discussions and guidance on ideas in development. Every idea in this thesis had to survive the rigours of a late afternoon discussion at the Club. Dick Loewenthal whose prodigious and exact understanding of chemical equilibrium theory as well as his excitement with the whole project gave me the understanding and the confidence to step into it more seriously. The Chapter on the modified Deffeys vector plots has been submitted for publication as a joint paper with Dick Loewenthal. Geoff Brundrit for being my oceanographic mentor starting many years ago with the indelible notions of scales of spatial and temporal variability. John Field for the support, even when things were not looking good, and all his advice in the write up phase. I was financially partly supported by the Sea Fisheries Research Institute and I would like to particularly thank Vere Shannon and Andy Payne for allowing me to integrate this study into my work at the Institute.

I would also like to thank Claudia Melo for assisting with many of the analyses particularly those on the Hondeklip Bay transect and the sediment ammonium measurements from the Henties Bay transect. Mike Lucas for collecting the samples and doing the pH measurements from the Olifants River transect and for always being a strong supporter of this project. Caroline Zauner for writing the code for the programmes which were used to calculate the carbonate species equilibria. Geoff Bailey for inviting me to join the Hondeklip Bay transect and Mike Bremner for similarly inviting me to be part of the Henties Bay transect off Namibia.

My daughters Sofia and Catarina who despite their young age asked the most penetrating question: why do you do this ? and demanded an answer understandable to 4 and 6 year-olds. They like all my family put up with sometimes erratic behaviour and long hours of non-availability at home. Amanda Youngleson for having been there and supportive in the early stages of the project and Joeke Singles for helping me through to the end. Joeke put her architectural hand to paper in the beautifully coloured maps. Finally, but not least to my parents for providing me with the support and having the foresight years ago to make it possible to get to where I am.

Pedro M. Ş. Monteiro

Marine Biology Research Institute
University of Cape Town
Rondebosch 7700
South Africa

The Oceanography, the Biogeochemistry and the Fluxes of Carbon Dioxide in the Benguela Upwelling System

September 1996

ABSTRACT

The aim of this study was to quantitatively investigate the mechanisms which drive carbon fluxes in an eastern boundary coastal upwelling system of which the Benguela is one of four comparable examples in the world. Three hypotheses describe the way the key aspects of the problem:

- The Benguela upwelling system is, by virtue of its high primary production and sediment organic carbon accumulation rates, an important CO_2 sink.
- The carbon export flux and the magnitude of the CO_2 sink in the Benguela System can be predicted from the C:N stoichiometry provided by the Redfield Ratio.
- The inorganic carbon pump through coccolithophore production plays a minimal role in driving changes to the magnitude of both the carbon export flux and the air - sea CO_2 flux in the Benguela System

Carbon and nitrogen bulk water concentrations together with relevant physical parameters were measured along three transects which spanned the Benguela System defining the physical and biogeochemical characteristics of waters at the key stages of the upwelling cycle. The carbonate chemical system is characterized using Total Alkalinity and pH as master variables measured using the potentiometric Gran titration technique and pH on the NBS scale. This methodology provides an estimated uncertainty in the

calculated PCO_2 values of 10μatm which is thought to be adequate for the process orientated nature of this study where fluxes are driven by PCO_2 gradients of between 100 and 1500μatm. A modified Deffeys type vector plot is formulated to assist in interpreting the relative importance of the organic (C_{Org}) and inorganic (C_{Ing}) carbon pumps. The oceanographic sections provide two important insights into the advective characteristics of the Benguela System. Firstly, that the water which outcrops at each of the six upwelling centres has a more recent history along the inner shelf (< 100m depth) rather than being advected straight up from depths of 200-350m as was thought to be the case. Secondly, the water on the shelf does not share a common source. The results suggest that the Benguela System is supplied with South Atlantic Central Water (SACW) at predominantly three sites suitable for the advection of slope water onto the shelf. This is the basis for the "gate" hypothesis which defines a novel advective regime for the system. It also formed the physical basis for the box model used to quantify the carbon fluxes. The benthic remineralization flux is shown to be a key process in modifying shelf based SACW and providing the variable biogeochemical characteristics to waters which outcrop at the surface. The key mechanism is the stoichiometric disequilibrium in the remineralization fluxes of carbon and nitrogen. Measured C:N disequilibria of > 50, especially in the northern part of the system, limit and in some cases reverses the CO_2 drawdown potential associated with the nitrate flux. An NH_4^+ adsorption mechanism was proposed to account for these observations. Similar C:N disequilibria (10 < C:N < 20) were measured in the surface uptake of CO_2 and NO_3^- by post upwelling phytoplankton blooms. The significance and the mechanistic basis for the uptake disequilibria is also discussed with special focus on their association with Dissolved Organic Carbon (DOC) production. The carbon fluxes in the Benguela System are modelled using a spreadsheet based box model. The inputs are annual Ekman fluxes (1.1 - 1.4 Sv) calculated from two (1992: ENSO and 1994 non-ENSO conditions) one year hourly wind records from each upwelling centre and respective carbon and nitrogen concentrations in newly upwelled and aged upwelled waters. The model

confirm the first hypothesis that the Benguela System is indeed a small CO_2 sink (0.34 - 1.5 million tons C y^{-1}), but this result is dependent on the magnitude of the labile DOC pool. The labile DOC pool is assumed to be 30% of the total DOC production. The dynamics of DOC are identified as the biggest gap of knowledge in closing the carbon budget of the Benguela System. The C:N stoichiometric measurements show that using the Redfield ratio to calculate carbon production and export fluxes will underestimate their magnitude. Finally, using the modified Deffeys vector plots, it is shown that in the experimental time scale, the inorganic carbon deposition and remineralization pathway is insignificant in the Benguela System.

TABLE OF CONTENTS

1. INTRODUCTION: CARBON FLUXES IN THE GLOBAL OCEAN AND THE BENGUELA UPWELLING SYSTEM : AN OVERVIEW 4

1.1 Statement of the Problem and Background 4

1.2 CO_2 Variability and Fluxes in the Global Ocean System 8

1.3 Carbon Fluxes and Open Ocean Upwelling Systems 18

1.4 Coastal upwelling: the Benguela Upwelling System 21
1.4.1 Physical Characteristics 22
1.4.2 Biogeochemical Characteristics: 27

1.5 Aims and Hypotheses 37

1.6 Approach 38

2. THE CHARACTERIZATION OF THE CARBONATE SYSTEM IN SEA WATER 42

2.1 Introduction 42

2.2 Concepts, and Definitions 45
2.2.1 Weak Acid-Base Equilibria 45
2.2.2 Activity Scales: 48
2.2.3 The Sea Water Weak Acid-Base System 50

2.3 Sampling and Analytical Methods 65
2.3.1 Carbonate System 65

2.4 Other Sampling and Analytical Methods 77
2.4.1 Nutrients 77
2.4.2 Sediments 77

3. A CARBONATE STOICHIOMETRY VECTOR PLOT 79

3.1 Background 79

3.2 Effects of the addition / removal of carbonate species on TAlk, TAcy and TCO_2. 82

3.3 The Deffeys Model Approach 83

3.4 Modified Deffeys Approach: 86
3.4.1 Intensive Parameters in Modified Deffeys Plots: PCO_2 89
3.4.2 Application of the Vector Model to Simulated Upwelling Systems 93
3.4.3 The PCO_2 - C_{Org}:C_{Ing} stoichiometry dynamics of pre-upwelled waters 93
3.4.4 Combined Effects of Stoichiometry and Temperature on PCO_2 Dynamics in Post - Upwelled Waters. 95

3.5 Nitrate Correction to Total Alkalinity 99

4. SHELF SCALE PHYSICAL OCEANOGRAPHIC PROCESSES AND THEIR IMPACT ON THE DISTRIBUTION OF CO_2 PARAMETERS IN THE BENGUELA SYSTEM 101

4.1 Background 101

4.2 Physical Processes Critical to Carbon Fluxes in the Benguela System 104
4.2.1 Advection: Longshore and Cross Shelf 104
4.2.2 Benthic Boundary Layer (BBL) Turbulence: 107
4.2.3 Surface Layer (SL) Turbulence and Stratification: 108
4.2.4 Role of turbulence and stratification on CO_2 dynamics in the surface layer: 109
4.2.5 The role of physical forcing on CO_2 fluxes across the boundaries of the surface layer. 111
4.2.6 Physical Modelling of the CO2 Flux across the Thermocline Boundary 114

4.3 Methods: Cruises and sampling 115
4.3.1 Henties Bay Transect: Northern Benguela Sub-System 115
4.3.2 Hondeklip Bay Transect: Central Benguela Sub-System 117
4.3.3 Olifants River Transect: Southern Benguela Sub-System 119

4.4 Results and Discussion 120
4.4.1 Henties Bay Transect: Northern Benguela System 120
4.4.2 Hondeklip Bay Transect: Central Benguela Sub-System 131
4.4.3 Olifants River Transect: Southern Benguela System 142

4.5 Further Discussion: New Insights 154
4.5.1 The "Gate" hypothesis 154
4.5.2 Benthic Boundary Layer (BBL) Turbulence 161
4.5.3 BBL turbulence conceptual model: 162

5. SHELF SCALE BIOGEOCHEMICAL PROCESSES I: BENTHIC REMINERALIZATION 168

5.1 Background 168

5.2 Methods 173

5.3 Results and Discussion 174
5.3.1 Northern Sector: Henties Bay Transect 174
5.3.2 Central Sector (CS): Hondeklip Bay Transect 184
5.3.3 Southern Sector (SS): Olifants River Transect 192

5.4 Further Discussion 199
5.4.1 Remineralization of Organic Carbon 200
5.4.2 Remineralization of Calcium Carbonate: 204
5.4.3 C:N Remineralization Stoichiometry and Pathways 205
5.4.4 NH_4^+ Adsorption Model 208

6. SHELF SCALE BIOGEOCHEMICAL PROCESSES II: SURFACE LAYER UPTAKE AND EXPORT 212

6.1 Background 212
6.1.1 C:N Stoichiometric Disequilibrium in the Surface Layer 213
6.1.2 Carbon Stoichiometry (C_{Org}:C_{Ing}) 216

6.2 Methods 216

6.3 Results and Discussion 220
6.3.1 Walvis Bay Upwelling Cell (Northern Benguela) 220
6.3.2 Cape Frio Upwell Cell (Northern Sector) 226
6.3.3 Namaqua Upwelling Cell (Central Sector) 227
6.3.4 Luderitz Upwell Cell (Central Sector) 232
6.3.5 Cape Columbine Upwelling Cell (Southern Sector) 233
6.3.6 Cape Peninsula Upwelling Cell (Southern Sector) 237

6.4 Further Discussion: 238
6.4.1 C: N uptake stoichiometry in the surface layer: contradictions with existing paradigms. 242
6.4.2 The decoupling of C and N uptake: a simple model 246
6.4.3 Partitioning of carbon export flux into POC and DOC fluxes. 254
6.4.4 The C_{Org}: C_{Ing} stoichiometry of carbon fluxes: 258

7. CARBON FLUXES IN THE BENGUELA SYSTEM: A BOX MODEL APPROACH 262

7.1 Background 262

7.2 Model Assumptions 268
7.2.1 Physical assumptions: Advective Flux Pathways 268
7.2.2 Biogeochemical assumptions: Parameter concentrations and stoichiometry 269

7.3 Model Inputs and Outputs 271
7.3.1 Physical Inputs: Equatorward Wind Driven Ekman Transport 272
7.3.2 Biogeochemical Inputs: parameter concentrations and stoichiometry 280
7.3.3 Model Outputs: Carbon Fluxes 287

7.4 Model Results I: Standard Runs: 1992 and 1994 winds 288
7.4.1 Net air - sea CO_2 fluxes in the Benguela System 289
7.4.2 Organic Carbon Fluxes Predicted by the Model for the Benguela System 299

7.5 Model Results Part II: Perturbation Runs 314
7.5.1 C:N Stoichiometry of Remineralization and Uptake 314
7.5.2 Carbon pump stoichiometry: Org:Ing 317
7.5.3 Temperature: the solubility pump 319

7.6 Appendix 1: 320

8. CLOSURE 323

8.1 Conclusions 323

8.2 Other Highlights 328
8.2.1 The "Gate" Hypothesis 328
8.2.2 The Total Acidity - Total Alkalinity Vector Plots 330

9. LITERATURE CITED 332

Chapter 1

1. Introduction: Carbon Fluxes in the Global Ocean and the Benguela Upwelling System : an Overview

1.1 Statement of the Problem and Background

Global concerns about observed and predicted anthropogenically driven increases in atmospheric CO_2 are largely motivated by its uncertain feedback on climate through the Greenhouse effect (Mitchell, 1989; IPCC, 1990; Keeling and Whorf, 1994; IPCC, 1996). The potential socio-economic risks associated with climate change have recently been perceived to be serious enough to enter the global political agenda (IPCC, 1990; IPCC, 1996). These include *inter alia*: changes in rainfall patterns and their impact on agriculture, increases in sea level and their impact on coastal infrastructure, changes in the characteristics of winds and heating and their impact on global circulation, regional circulation and coastal fisheries (IPCC, 1990; Hsieh and Boer, 1992; Rhamstorf, 1994; Denman *et al.*, 1996; IPCC, 1996; Melillo *et al.*, 1996). The atmospheric CO_2 inventory has increased by 28% from its pre-industrial (mid-19th century) levels of pCO2 ~ 280 μatm to present levels of 358 - 360μatm (Keeling and Whorf, 1994). While natural CO_2 variability is a well known phenomenon, at no other time in the quaternary has the rate of increase (~0.3 μatm y-1) and projected end values (1500 μatm by 2100) been so high (Neftel *et al.*, 1985; Barnola *et al.*, 1987; Barnola *et al.*, 1995). The scale of the anthropogenic perturbation is put into perspective by comparison to simulated extremes of natural perturbations. Models predict that if the ocean operated a 100% efficient biological pump, atmospheric pCO2 would drop to 160 μatm while at the other extreme, in an abiotic "Strangelove" ocean pCO2 is expected to increase to only 450μatm (Siegenthaler and Sarmiento, 1993).

Two aspects of anthropogenically driven climate change were instrumental in catalysing a new approach to its understanding and predictive modelling:

- Firstly, it was no longer a local or regional problem as had been the case with most pollution issues. It had become a global one, both in respect of the forcing factors (fossil fuel emissions and land use changes), as well as in the response (biosphere research and improvements in the efficiency of energy usage).
- Secondly, due to the complexity of not only the physical and biogeochemical mechanisms but also their temporal and spatial scales of interaction, the solution required a radical shift in approach. It had to rely less on the deterministic - empirical and uni-disciplinary approaches which had characterized many oceanographic and pollution studies up to the mid 70's and more on integrated approaches from the planning to the modelling and interpretation phases. However, the key aspect to this integrated strategy is the development of quantitative models which could be used to not only organize relevant issues, but also serve as a platform from which to plan sampling strategies and provide some predictive capability.

The initial contribution of the international marine science community was the Joint Global Ocean Flux Study (JGOFS) programme and the physically orientated World Ocean Circulation Experiment (WOCE) (JGOFS, 1990; JGOFS' 1992). These aimed to formulate and execute co-ordinated global scale sampling programmes which could address the need for constraining of physical and biogeochemical dynamic models outputs and predictions.

Concerns about anthropogenically driven global warming are not new. The issue entered the domain of environmental science the 1930's as a result of the above average warming experienced between 1925 - 1935 (Callendar, 1938; Hansen and Lebedeff, 1988). Subsequent cooling from the 1940's to

early 1960's diminished scientific interest on the problem until the late 1950's - early 1960's when the first results from the atmospheric CO_2 monitoring at Mauna Loa began to indicate the increasing CO_2 trend (Callendar, 1958; Keeling, 1960). By then pioneering carbon budget geochemical box models (Revelle and Suess, 1957) started to show that the oceans could have an important role in governing the dynamics of CO_2 in the atmosphere. These modelling attempts were limited by the lack of oceanographic data required to constrain their outputs. This served as a prime motivation for the GEOSECS sampling programme which aimed at not only providing the required data coverage but also to improve the accuracy and precision of sampling and analytical methods (Broecker and Peng, 1982).

The problem of global warming and its association to anthropogenic emissions of CO_2 re-surfaced when once again global mean temperatures were on a rapid increase rate reaching new high end records through the whole decade of the 1980's (Hansen and Lebedeff, 1988; IPCC, 1990). By the time the issue of anthropogenically driven climate change was once again highlighted in the developed world's scientific and political arena in the mid-1980's, the following factors in the marine science community had converged:

- sampling techniques in sea water had expanded the spatial (remote sensing) and temporal (monitoring moorings) resolution of the data sets and analytical techniques improved in accuracy, precision and detection limits to allow measurement of very small changes in biogeochemical parameters. This applied particularly to CO_2 parameters for which changes of 1μM for TCO_2 and 1μatm for PCO_2 could be achieved, allowing interannual changes to be resolved with greater certainty (Johnson *et al.,* 1987; Dickson, 1994).
- remote sensing had become a scientific tool which allowed the very serious obstacle of instantaneous regional and basin scale CO_2 variability to be addressed both in the physical (temperature and winds) (Gower, 1981; Etcheto *et al.,* 1991) and biogeochemical (ocean colour) domains

(Platt and Sathyendranath, 1988; Aiken *et al.*, 1992; Balch and Byrne, 1994).

- understanding CO_2 variability in terms of underlying physical and biogeochemical mechanisms and their forcing - response scales had expanded dramatically which formed the basis for the development of the modelling capacity (box to dynamic models) and, coupled to it,
- the increase in relatively cheap processing power had rendered model simulation a much more accessible day to day tool for individuals and groups. This afforded a more coherent design of sampling strategies (spatial and temporal scales) as well as a more rigorous hypothesis testing mechanism. It also made data communication on a global scale instantaneous and the mass storage and access to collective data sets possible.

The JGOFS programme which evolved out of the need to understand the natural mechanisms which govern the rates of atmospheric CO_2 increase, took an open ocean focus on the basis that the largest CO_2 reservoirs and fluxes were on that ocean scale (JGOFS, 1990; Ducklow, 1995). The view held that small changes in the large open ocean fluxes of CO_2 could impact on the net air - sea fluxes. This strategic approach has biased much of the sampling and modelling effort towards the assumption that the variability of CO_2 fluxes is driven by the "solubility pump". Recently, there has been an increasing awareness that the ocean margins with their greater rates of new production might play a significant role in both short term and long term CO_2 dynamics (Brink *et al.*, 1995; Hutchings *et al.*, 1995; Summerhayes *et al.*, 1995). The long term role was emphasised by the view that the intensification of the biological pump in glacial periods occurred mainly at the ocean margins (Berger *et al.*, 1989). This applies particularly to coastal upwelling systems such as the Benguela System which is the focus of this study.

1.2 CO_2 Variability and Fluxes in the Global Ocean System

The natural variability in the magnitude of the atmospheric CO_2 reservoir is a well measured phenomenon whether as a result of tectonic activity at the Permo-Triassic boundary 250 My (Thackeray *et al.*, 1990), planetary orbital forcing time scales of 10,000 - 100,000 y (; Barnola *et al.*, 1995) or El Nino events of < 10 years (Siegenthaler, 1990). Recent (< 200,000y BP) variability of CO_2 measured from the Vostok ice core appears to constrain the range of natural pCO2 variability to 175 - 300 μatm (Barnola *et al.*, 1987). This has been subsequently confirmed by other high resolution ice core measurements (Neftel *et al.*, 1985; Etheridge *et al.*, 1993; Barnola *et al.*, 1995). Fossil fuel emissions since the industrial revolution have been increasing the CO_2 inventory of the atmosphere at a rate > 0.25 μatm y-1 (Barnola *et al.*, 1995). A comparable "rapid" natural rate of increase is 2 orders of magnitude lower (Barnola *et al.*, 1995). This contrast is emphasised by the composite plot of the data sets from the Vostok ice core (160,000 - 4000 BP) (Barnola *et al.*, 1994), Sipple ice core (1734 - 1953) (Neftel *et al.*, 1994) and the contemporary Mauna Loa record (1958 - Present) (Keeling and Whorf, 1994) (Fig. 1.1). The anthropogenic input dominated mainly by fossil fuel combustion (IPCC, 1996) has increased the magnitude of the atmospheric CO_2 reservoir by ~25% from 600 - 750 Gt C (Giga Tons = 10^9 tons) which corresponds to a pCO2 increase from 278 - 360 μatm in the same period. This measured increase in atmospheric CO_2 accounts for approximately 50% of all anthropogenic CO_2 emissions with the balance being taken up by the terrestrial biosphere and the oceans (Siegenthaler and Sarmiento, 1993). An annual CO_2 budget based on the CO_2 emissions in the decade 1980-89 is shown on Table 1.1 (Siegenthaler and Sarmiento, 1993). It highlights the following three issues:

- the degree of uncertainty (0.6 - 2.5 Gt C y^{-1}) in CO_2 emissions from land use changes.
- the magnitude of the oceanic sink ~ 2 Gt C y^{-1}.

- the magnitude and the uncertainty of the carbon removal which cannot be presently accounted for in the oceanic sink, the so called "missing carbon".

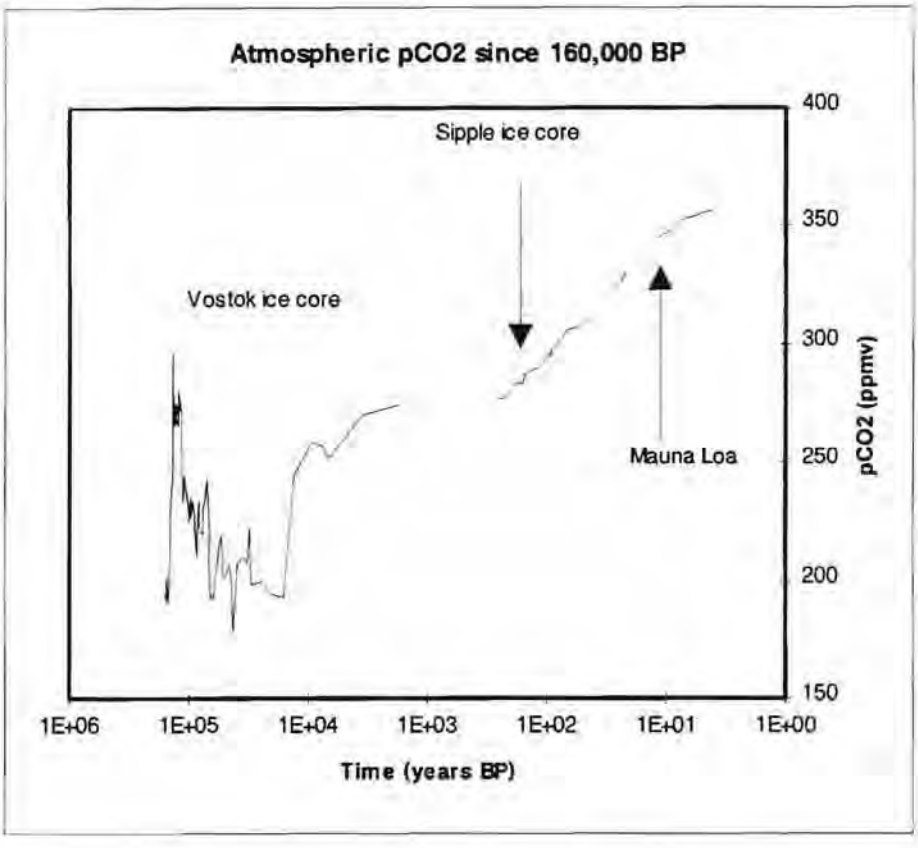

Fig. 1.1: A log scale composite time series of atmospheric pCO_2 since 160,000 BP. It includes data from the Vostok and Sipple ice cores (Barnola *et al.*, 1994), (Neftel *et al.*, 1994) and from the contemporary record of Mauna Loa Station (Keeling and Whorf, 1994). It emphasises the magnitude of the impact of the anthropogenic CO_2 input which started with the industrial revolution which also coincides approximately with the beginning of the Sipple record (1734 - 1953).

Table 1.1: Global CO_2 budget: [Gt C y^{-1}] from: (Siegenthaler and Sarmiento, 1993)

Emissions from Fossil Fuels:	5.4 ±0.5
Emissions from Deforestation	0.6 - 2.5
Atmospheric Build up	3.2 ±0.2
Oceanic Uptake	2.0 ±0.6
"Missing Carbon"	1.8 ±1.3

One of the main obstacles to constraining the role of the oceans in the global CO_2 budget with confidence is that the anthropogenic fluxes are relatively small compared to the magnitude of natural annual exchange between the ocean and the atmosphere (90 Gt C y^{-1}) and between the surface and deep ocean (100 Gt C y^{-1}) (Fig.1.2). With these relative magnitudes, small shifts in the natural annual exchange fluxes could have a major impact in the net CO_2 sink - source nature of the oceanic system. These sorts of shifts are likely part of the explanation for the observed natural variability of atmospheric CO_2 reservoir in the paleo-record.

The uncertainty in the estimates of the net uptake of CO_2 by the oceans also reflects to some degree the effects of the different assumptions which underlie global carbon flux models as well as the spatial - temporal resolution of the data sets used to constrain them. The recent estimates of the oceanic sink fall into 2 groups: the higher estimates (-2 Gt C y^{-1}), which form the basis for the budget on Table 1.1 and include the 1 dimensional box models (2.32 Gt C y^{-1}) (Siegenthaler and Oeschger, 1987), HILDA (2.15 Gt C y^{-1}) (Siegenthaler and Joos, 1992), Princeton GCM (1.9 Gt C y^{-1}; (Sarmiento *et al.*, 1992) and the lower estimates which range from 0.8 Gt C y-1 (Tans *et al.*, 1990) to 1.6 Gt C y^{-1} (Enting *et al.*, 1995; Taylor, 1995). The latter group of modelling techniques simulate more complex interactions and require that all mechanisms be explicitly included. This suggests that any unknown mechanisms not explicitly included will contribute to a lower estimate of the global oceanic sink. The Tans et al., 1990 model is such an example: if factors such as the effects of skin temperature (0.4 Gt C y^{-1}), natural CO_2 fluxes (0.55Gt C y^{-1}) and carbon monoxide (0.25Gt C y^{-1}) are included, the final estimate is adjusted to -2 Gt C y^{-1} which brings it into line with the higher estimates (Siegenthaler and Sarmiento, 1993). It is significant that independent CO_2 flux calculations using a combination of ^{13}C and ^{14}C observations also predict an oceanic sink of 2.1Gt C y^{-1} (Quay *et al.*, 1992).

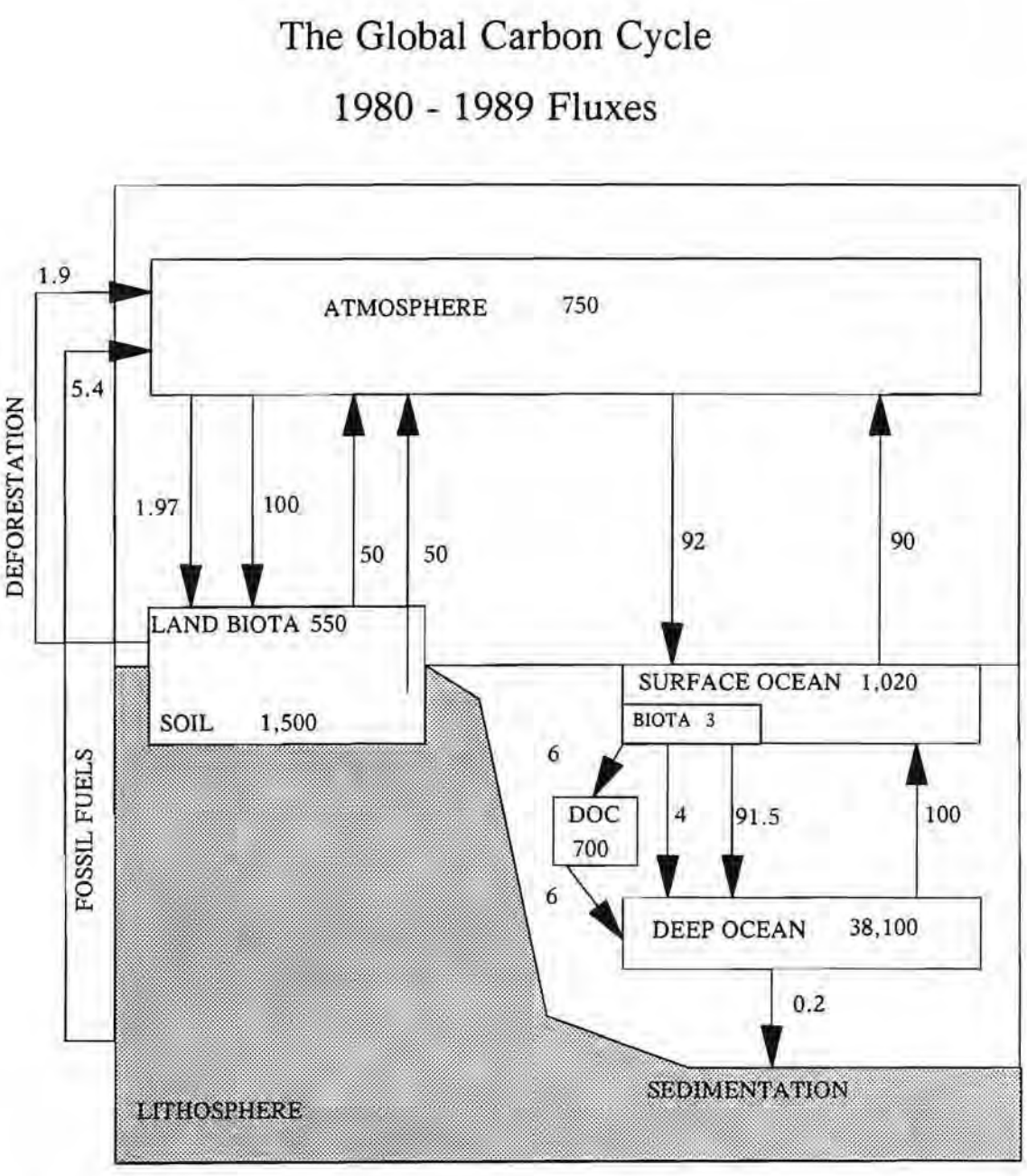

Fig. 1.2: A conceptual model of the global carbon cycle with fluxes (Gt C y^{-1}) and reservoir sizes (Gt C) based on contemporary (1980 - 1989) CO_2 content of the atmosphere. It shows that the net CO_2 uptake fluxes by the oceans (2 Gt C y^{-1}) and the terrestrial biosphere (1.97 Gt C y^{-1}) is offset by the fossil fuel (5.4 Gt Cy^{-1}) and deforestation (1.9 Gt C y^{-1}) fluxes. The annual net input of CO_2 to the atmosphere (3.33 Gt C y^{-1}) amounts to approximately 0.5% of the atmospheric reservoir. These net fluxes are two orders of magnitude smaller than the natural annual exchange fluxes which suggest that small changes in the latter can match the magnitudes of the anthropogenic components. It also shows that the magnitude of the carbon fluxes linked to the biological pumps (10 Gt C y^{-1}) are 10% of the total transported from the surface to the deep ocean. The balance (91.5 Gt C y^{-1}) is transported through the activity of the solubility pump. Adapted from Siegenthaler and Sarmiento, 1993.

The magnitude and direction of the air - sea CO_2 flux is governed by the biogeochemically driven pCO2 - PCO_2 gradient and the physical wind driven transfer velocity (Liss and Merlivat, 1986; Wanninkhof, 1992; Farmer *et al.*, 1993). The biogeochemically driven PCO_2 gradient is in turn, driven by the transport of carbon out of the surface layer into intermediate and deep waters. The conventional view is that this transport is mediated by 2 "pumps":

- the physically driven **solubility pump** which is driven by the combination of increased CO_2 solubility in cool sub-polar and polar waters coupled with the subduction of these waters into the intermediate (Antarctic Intermediate Waters (AAIW), Central Waters (SACW) and deep (NADW) oceanic depths (Volk and Hoeffert, 1985; Reid, 1989). This mechanism for the drawdown of atmospheric CO_2 drives the largest CO_2 sink pathway (~90 Gt C y^{-1}) (Siegenthaler and Sarmiento, 1993).
- The **biological pump** transports CO_2 and CO_3^{2-} against the ocean water column gradient, maintaining the observed relative TCO_2 depletion at the surface and enrichment in the deep (Broecker and Peng, 1982; Volk and Hoeffert, 1985; Longhurst and Harrison, 1989). The biological pump is generally divided into two further pumps (Volk and Hoeffert, 1985; Longhurst and Harrison, 1989): the **organic carbon pump,** also referred to as the carbon export flux, mediates the vertical transport of carbon (POC). Its magnitude is considered to approximate closely with temporally integrated new production (Eppley and Peterson, 1979; Platt *et al.*, 1989). The **inorganic carbon pump** mediates the transport of carbon (PIC) generated by coccolithophore activity across the permanent pycnocline (Honjo, 1976; Volk and Hoeffert, 1985; Fernandez *et al.*, 1993; Westbroek *et al.*, 1993). In the intermediate, deep or benthic domains these particulate fluxes are remineralized or accumulated and buried (Berner, 1982; Broecker and Peng, 1982). The biological pump has been suggested to contribute a flux of 10 Gt C y^{-1} or approximately 10% of the

total carbon transport (sum of solubility and biological pumps) from the surface to the deep ocean (Siegenthaler and Sarmiento, 1993).

One of the anomalies which characterizes existing "carbon pump" formalism is that it does not easily accommodate the important DOC export flux (Farrington. 1992 ; Hedges, 1992; Ducklow, 1995; Guo *et al.*, 1995; Sondergaard and Middelboe, 1995). Although DOC is strictly speaking a product of the biological pump, its transport from the surface to the deep water domains is physically mediated by turbulent diffusion or subduction (King and Devol, 1979; Gargett, 1984). A simpler formalism may assist in conceptually defining each of the fluxes more precisely.

It is suggested that "pump" categories be defined firstly, in terms of common transport mechanisms (sedimentation of particulates or turbulent diffusion and advection of dissolved fractions) and secondly, in terms of organic or inorganic synthesis pathways. The particulate pump (PP) would comprise both the particulate organic carbon (POC) and the particulate inorganic carbon (PIC) export fluxes. The dissolved pump (DP) would comprise both the dissolved inorganic carbon (TCO_2) and the dissolved organic carbon (DOC) export fluxes. In this instance, the dissolved inorganic carbon flux corresponds to the "solubility pump".

In most global carbon flux modelling the biological pump is maintained as a constant unchanging turnover or completely ignored (Siegenthaler and Sarmiento, 1993; Taylor, 1995). Such an approach does not reflect an important characteristic of solubility and biological pumps in the ocean: their heterogeneity. Because of differences in their key forcing mechanisms the solubility and biological pumps are concentrated in a spatially heterogeneous way. The solubility pump activity is primarily focused in areas where subduction of cold polar or sub-polar waters occurs (Keeling, 1968; Takahashi, 1989; Tans *et al.*, 1990; Taylor, 1995). The biological pump intensifies in the vicinity of coastal upwelling areas where critical forcing

factors of nutrient supply, light and phytoplankton seeding converge. These conditions sustain production in open ocean upwelling systems or generate synoptic scale blooms in coastal upwelling systems. The spatial separation is clearly seen in the contrast between Fig. 1.3a (Takahashi, 1989) which reflects the impact of the solubility pump on surface PCO_2 and Fig.1.3b which reflects the distribution of the activity of phytoplankton production. The first, shows the CO_2 deficit or ingassing areas, where the flux < 0, as being primarily around the sub - polar seas where cooling and subduction occurs (Southern Ocean and North Atlantic). Conversely, the biological pump is concentrated in areas where upwelling is the dominant advective process (Fig. 1.3 b) along the coastal margins and the equatorial and polar upwelling systems. The long term effects of the intensification of the biological pump in upwelling systems is supported by the distribution of organic rich sediments where burial of new production is concentrated (Fig. 1.4).

In respect of CO_2 drawdown fluxes the aspect of total production which is of primary concern, particularly in upwellling areas, is NO_3^- driven new production (Dugdale and Goering, 1967; Eppley and Peterson, 1979; Platt *et al.*, 1989; Ducklow, 1995) which drives the carbon export flux from the surface domain. This link between intensity of the biological pump and upwelling is important in the context of global change because it makes the biological pump and its predicted impact on carbon fluxes particularly susceptible to expected changes in wind intensity and wind regimes.

The global distribution of new production in respect of different oceanic (upwelling and non-upwelling) regimes is shown on Table 1.2 which was adapted from Chavez and Toggweiler, 1995. It shows that upwelling systems (coastal and open ocean), which account for 40% of the ocean area, contribute 67% of the total new production. This increases to 80% if the estuarine contribution to ocean new production is excluded. Although there has been an increase in the research effort in upwelling systems, particularly open ocean systems, the biological pump is widely seen and modelled to be a

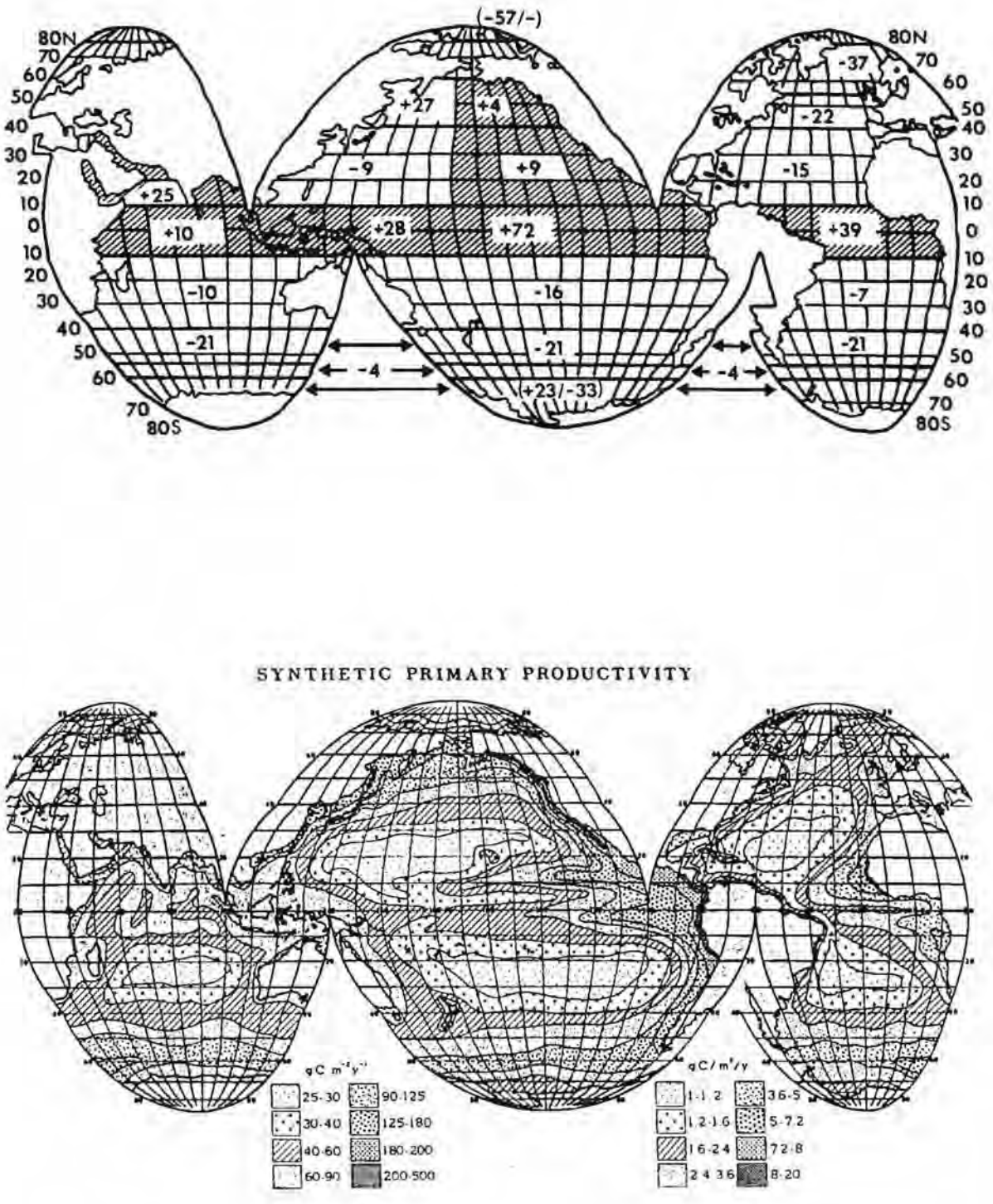

Fig. 1.3a, b: These global maps depict the distribution of PCO_2 difference between the ocean and the atmosphere (Fig. 1.3a) and surface productivity (Fig. 1.3b). This comparison emphasises the spatial mismatch between the distribution of ΔPCO2 which is largely governed by the solubility pump and vertical water fluxes and biological activity which is mostly concentrated at ocean margins. It suggests that to fully model the impact of the biological pumps on global carbon fluxes that models should include physical and biogeochemical processes which intensify at the regional scale of coastal margins. (adapted from Takahashi, 1989 and JGOFS, 1992)

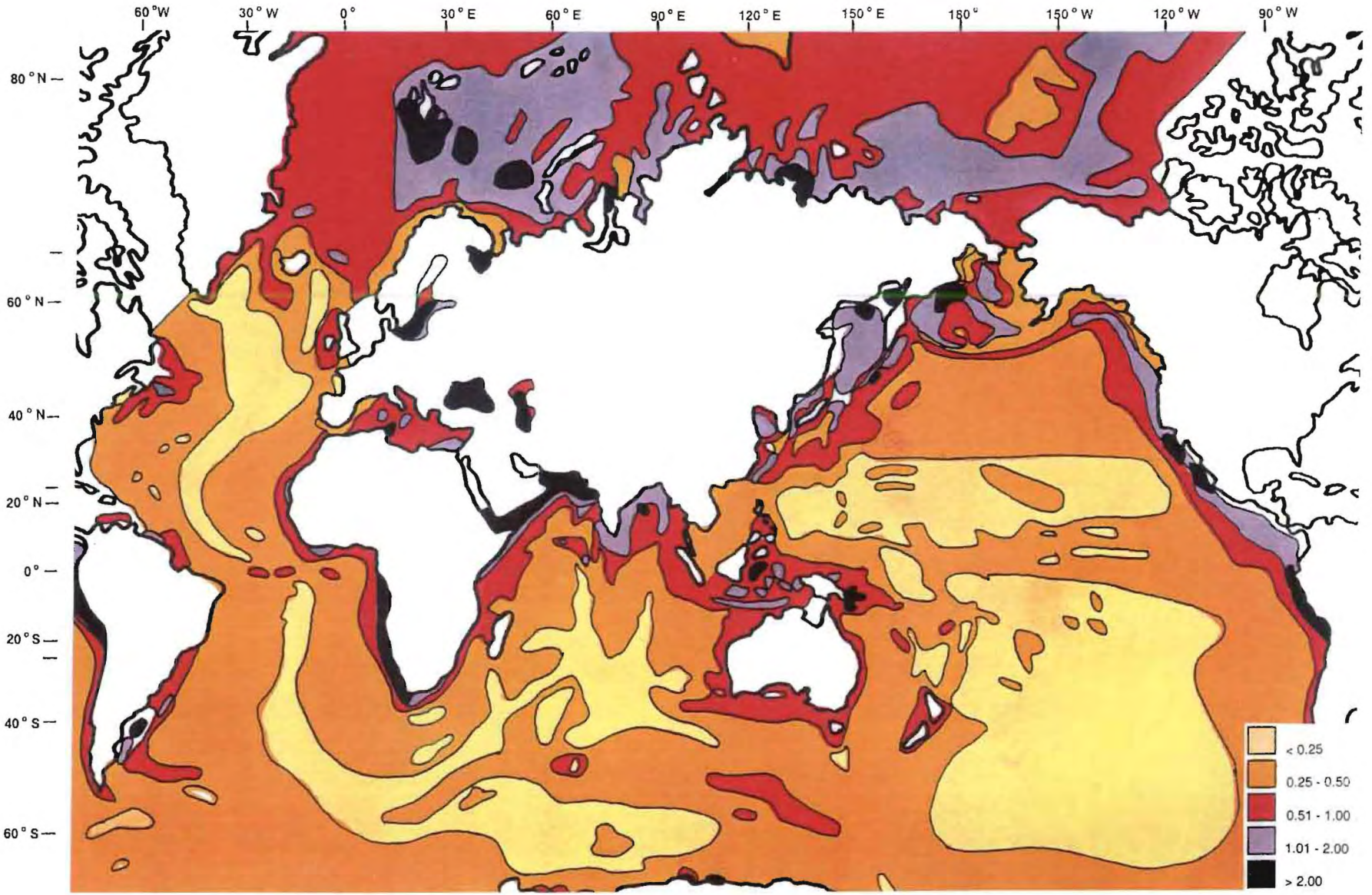

Fig. 1.4: Shows the global distribution of organic carbon in the ocean sediments. It not only provides support for the long term impact of enhanced activity at the ocean margins but also focusses attention to the eastern boundary upwelling systems where, with the exception of the NW African system, the highest concentrations of organic carbon are consistently located. This indicates that these systems may provide an important contribution to global new production. (Adapted from Romankevich, 1984, Geochemistry of Organic matter in the ocean, Springer, in JGOFS, 1990)

"constant background" and contribute little to PCO_2 variability (Siegenthaler and Sarmiento, 1993; Taylor, 1995). This view has not stimulated the acquisition of spatially and temporally distributed high resolution data similar to PCO_2 measurements used to constrain physical models.

Table 1.2: Estimates of annual upwelling rates, new production and surface area (from: Chavez and Toggweiler, 1995)

Region	System	Upwelling Rates (Sv)	New Production (Gt C y^{-1})	Area (m^2*10^{-12})	
Trop. Open Ocean:	upwelling	60	1.5 (21%)	30	(8%)
	turb. diff.		0.7 (9.5%)	60	(17%)
Southern Ocean:	upwelling	30	1.1 (15.5%)	77	(22%)
S.Tr. Gyre	turb. diff.		0.5 (7%)	114	(32%)
S.Ar. Gyre	upwelling	7	0.3 (4%)	22	(6%)
Monsoon	upwelling	15	0.4 (5.5%)	5	(1.5%)
Coastal	upwelling	15	0.8 (11%)	4	(1%)
	west. bound.	20	0.7 (9.5%)	45	(12.5%)
	estuarine		1.2 (17%)		
Total		147	7.2	357	(100%)

Although the focus of this study is on the Benguela System, an eastern boundary coastal upwelling system, it is useful to briefly overview the main characteristics of open ocean upwelling systems. This will provide a conceptual and quantitative basis for a comparative discussion of the results and model outputs.

1.3 Carbon Fluxes and Open Ocean Upwelling Systems

As was shown in Table 1.2 upwelling systems fall into two broad categories:

- open ocean systems, which include equatorial (mainly Pacific and Atlantic 5°N - 5°S), Southern Ocean and Pacific sub arctic gyre and
- secondly, the coastal upwelling which include the 4 major eastern boundary systems, the western boundary currents and monsoon systems. It should be noted that upwelling associated with western boundary currents is not primarily wind driven by caused by dynamic upwelling (Angel *et al.*, 1995; Summerhayes *et al.*, 1995) favourable winds may assist to get the relatively shallow thermocline into the euphotic zone.

Open ocean upwelling of 97 Sv (Table 1.2) accounts for the bulk (76%) of all wind driven upwelling (excludes western boundary upwelling 20 Sv) and its importance in global exchange between the intermediate - deep and surface ocean is underpinned by its close agreement with the magnitude of 100 Sv attributed to total upwelling in global flux models (Watson, 1995). The discrepancy between the sum of all upwelling fluxes (147 Sv: Table 1.2) and the global vertical exchange flux of 100 Sv used in models (Watson, 1995) emphasises the extent to which global scale modelling studies exclude the important coastal upwelling component which amounts to 24% of the total. This suggests that ignoring the role of coastal upwelling may lead to larger than expected uncertainties in the global carbon budget. Upwelling in open ocean systems is driven by a divergent wind stress curl across the equator and in the southern ocean (Reverdin, 1995). The importance of these water fluxes is that they not only advect CO_2 enriched water into the surface layer but also introduce new nutrients into the euphotic zone which drives new production (Dugdale and Goering, 1967; Chavez and Toggeweiler, 1995; Ducklow, 1995). This limits or even reverses CO_2 outgassing. Estimates of global new production vary quite substantially between the lowest value of 3.4 - 4.7 Gt C y^{-1} (Eppley and Peterson, 1979) and 22 Gt C y^{-1} (Packard *et al.*,

1988). It appears that the tendency is for values to be revised upwards but the higher estimates include an unquantified DOC production and export flux (Ducklow, 1995). Central to the variability in new production is the issue of non-Redfield C:N stoichiometry which is thought to be an important co-factor in DOC production (Sambrotto *et al.*, 1993; Toggweiler, 1993; Ducklow, 1995). Such behaviour has to be explicitly included into sampling programmes and its effects tested through modelling. The global new production rate used in this study, 7.2 Gt C y^{-1} (Table 1.2) is based on the estimate by Chavez and Toggweiler, 1995. The contribution of total upwelling new production (4.8 Gt C y^{-1}) to global new production is 67% (Chavez and Toggeweiler, 1995), while the open ocean upwelling contribution to total global new production is 40% (Table 1.2). Despite these magnitudes of new production, open ocean upwelling systems are net CO_2 sources which in the case of the equatorial systems contribute approximately 2 Gt C y^{-1} (Pacific ~ 0.6 Gt C y^{-1}) of CO_2 into the atmosphere (Murray *et al.*, 1994; Chavez and Smith, 1995; Watson, 1995). Short term changes to the net rates of CO_2 exchange between the ocean and the atmosphere have been observed in association with ENSO events when the equatorial Pacific CO_2 degassing flux (0.6 Gt C y^{-1}) is cut-off or reduced (Siegenthaler, 1990). Transient phenomena are very useful perturbations to help constrain the predicted magnitudes of the outgassing fluxes (Keeling and Whorf, 1993).

Degassing of CO_2 occurs in conjunction with persistently observed high surface nutrients and low chlorophyll (in the equatorial Pacific Chla ~ 0.21 mgm-3 and NO_3^- ~ 5 mmolm-3) (Chavez and Smith, 1995). This suggests that phytoplankton growth rates in these systems are ecologically constrained to a slow or delayed utilization of upwelled NO_3^- which limits annual new production. (Cullen, 1991; Chavez and Smith, 1995). While a range of potential mechanisms have been suggested (Cullen, 1991), primary production in these systems is largely dominated by regenerated production which has no impact on upwelled CO_2 because it generates no new biomass (Dugdale and Goering, 1967). It requires the destruction of biomass to

recycle both carbon and nitrogen and sustain production. The net effects are the observed low chlorophyll concentrations, a persistence of non-zero surface NO_3^- concentrations and elevated CO_2 degassing rates due to both high TCO_2 and warming and of aged upwelled waters (Watson, 1995). However, the modest rates of new production characteristic of these systems is compensated by their total surface area which, as was stated above, accounts for 70 % of ocean surface (Table 1.2).

In the equatorial Pacific upwelling system, total annual primary production rates are estimated to average 328 g C m^{-2} y^{-1} cf. Coastal systems: California and Peru: 716 g C m^{-2} y^{-1} (Chavez and Smith, 1995), Benguela: 584 g C m^{-2} y^{-1} (Brown *et al.*, 1991). These rates are estimated to turnover 3.65 Gt C y^{-1} in the equatorial Pacific, and 0.153 Gt C y^{-1} in the Benguela system. From the measured NO_3^- flux, the maximum rate of new production, assuming that the Redfield ratio holds, is 1.3 Gt C y^{-1} yielding an upper limit to the f-Ratio of 0.36 (Chavez and Smith, 1995). The observed average f-Ratio is ~ 0.18 which results in a calculated new production rate and carbon export flux of 50 - 70 g C m^{-2} y^{-1} or 0.65 Gt C y^{-1} (Chavez and Smith, 1995). The export flux from open ocean new production results in an estimated burial flux of 0.009 Gt C y^{-1} which is ~ 30% of the total burial of organic carbon of marine origin only (excludes terrestrially derived organic matter deposited in deltaic fans) (Berner, 1982).

Open ocean upwelling systems such as the Equatorial Pacific and Atlantic as well as the Southern Ocean have, because of the strong open ocean focus of the JGOFS and WOCE programmes benefited from an intense carbon flux orientated sampling programmes (Ducklow, 1995). This has gone a substantial way to constraining their contribution to the global carbon budget. The same cannot be said for coastal systems where a potentially important contribution to the biological pump is supported by the following:

- Productivity rates in coastal upwelling systems are not only higher than in open ocean systems but also driven by a much higher proportion of new

production (f-Ratio > 0.2) . This is supported by the observation that they occupy 1% of the ocean area but contribute 11% of new production (Chavez and Toggeweiler, 1995).

- In periods of globally enhanced production such as during the glacial periods this production concentrates particularly along the margins (Berger *et al.*, 1989)
- Eastern boundary coastal upwellling systems account for 3.4% of the annual burial of marine carbon (Berner, 1982)

1.4 Coastal upwelling: the Benguela Upwelling System

The Benguela System is one of 4 major wind driven eastern boundary upwelling systems including the Humbolt (Peru-Chile) system, the Californian (California - Oregon) system, and the NW African - Iberian system (Barber and Smith, 1981). The Arabian sea or Somali system is also an important coastal upwelling system but it is driven by offshore seasonal SW monsoon winds rather than the long shore component of equatorward winds (Barber and Smith, 1981). Coastal upwelling systems have been the subject of intensive physical, biogeochemical and ecological research over the past two decades (Barber and Smith, 1981; Richards, 1981; Payne *et al.*, 1987; Payne *et al.*, 1992; Hutchings *et al.*, 1995; Summerhayes *et al.*, 1995). The primary goal of this effort was to understand the foodweb dynamics which give rise to their lucrative but highly variable fisheries (Crawford, 1987 ; Hutchings, 1992). The ecological basis for the fact that 50% of the world fish catches come from coastal upwelling systems which occupy 1% of the ocean surface area (see Table 1.2) was first articulated by (Ryther, 1969) as a hypothesis: *the very productive fisheries in coastal upwelling systems were supported by a short and efficient food chain (1.5 trophic levels) linking elevated production and biomass of large diatoms directly to mostly phytophagous pelagic fish.* This hypothesis stimulated a change in the approach to research in upwelling systems from a largely descriptive one to a more mechanistic emphasis

(Barber and Smith, 1981). Recent research in the Benguela System has both followed this general shift and pioneered new perspectives on the dynamics of upwelling systems (Payne *et al.*, 1987; Payne *et al.*, 1992; Shannon and Nelson, 1996). This work was co-ordinated by the Benguela Ecology Programme (BEP) (Siegfried and Field, 1981) and its precursors the Kelp Bed Programme (Field *et al.*, 1981) and the Cape Upwelling Experiment (Shannon, 1985). These recent developments are now overviewed with the objective of setting the scientific background into which this study fits.

1.4.1 Physical Characteristics

The physical characteristics of the Benguela System are central to understanding and modelling of carbon fluxes for two main reasons:

- NO_3^- which supports phytoplankton production is supplied by wind driven advection of South Atlantic Central Water (SACW) which outcrops at various upwelling centres (Andrews and Hutchings, 1980; Brown and Hutchings. 1987a) and,
- phytoplankton dynamics (seeding, succession and growth are governed by the characteristics (frequency, strength and persistence) of wind induced turbulence (Hutchings *et al.*, 1995).

The aim of this study is not to describe the oceanography of the Benguela System but rather to focus on those features which are relevant to carbon flux modelling. However, a brief historical overview of the development of oceanographic insight is appropriate.

Although the earliest dedicated oceanographic work in the Benguela System was done by (Defant, 1936), the modern oceanographic era started with the pioneering work of Hart and Currie in the 1950's which is reported in (Currie, 1953; Hart and Currie, 1960). This work set out an advective framework for

the Benguela System which, only recently, with the advent of high resolution monitoring of spatial and temporal variability has been slightly adjusted. These earlier studies established that the Benguela System was driven by pulsed equatorward winds. This forcing upwelled SACW from 200-300m through Ekman transport while at the same time generating an equatorward barotropic shelf current and a poleward slope resident compensation current (Currie, 1953; Hart and Currie, 1960). The next major advance was the understanding of the dynamics of mesoscale features which characterized frontal zones (Bang, 1973; Bang and Andrews, 1974). Such was the contribution of these earlier studies that recent, and widely quoted (Barange, Pillar, and Hutchings. 1992 ; Summerhayes *et al.,* 1995; Shannon and Nelson, 1996) conceptual re-interpretation of frontal characteristics in the Benguela System from (Barange and Pillar, 1992) have not added any new insights. The period between 1975 and the end of the 1980's decade was characterized by technologically driven advances in the dynamics of the Benguela System. The use of remote sensing (Shannon *et al.*, 1985) and autonomous current meter - temperature moorings (Nelson, 1989) allowed the scales of spatial and temporal variability to be defined. The most important outcome of these advances was a better understanding of the coupling dynamics between physical forcing and biological response specifically by phytoplankton. Primary production is the key component in carbon flux measurement and modelling. This most recent work is overviewed in (Nelson and Hutchings, 1983; ; Shannon and Nelson, 1996) where, from the advection perspective, the most important advance was the magnitude of the sub-surface poleward flow across the shelf (Nelson, 1989; Shannon and Nelson, 1996). Much of the recent work, especially that which focused on frontal dynamics provided the basis to define the system's spatial boundaries which were adopted as a starting point for this study (Shannon and Nelson, 1996).

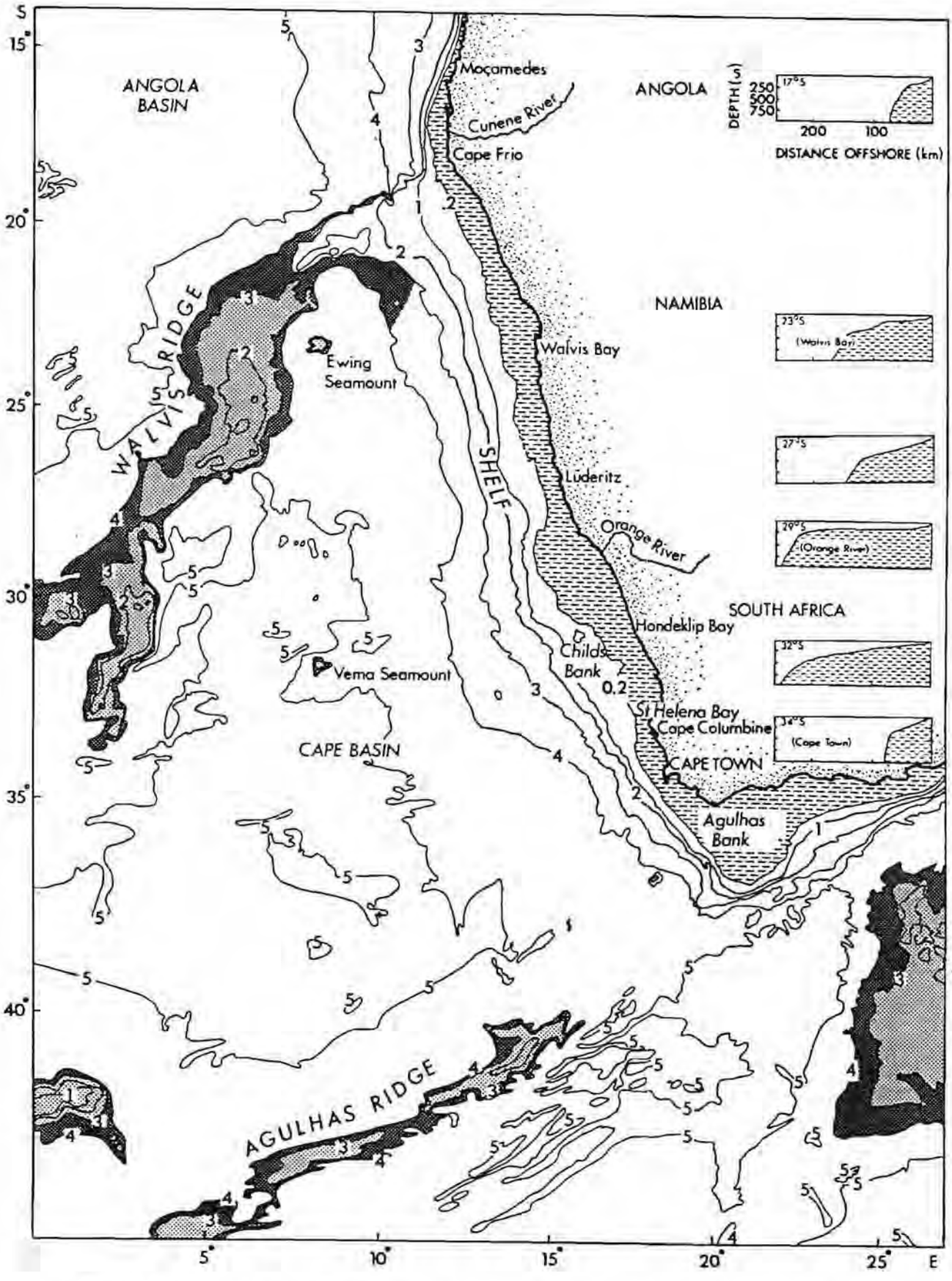

Fig. 1.5: A map of the South East Atlantic ocean depicting the spatial dimensions of the Benguela System. It shows the upper and lower boundaries of the system (Cape Frio and the Cape Peninsula in the imediate vicinity of Cape Town) as well as the 200m bathymetric contour which closely approximates the shelf break western boundary of the upwelling system. The six main upwelling centres of Cape Frio, Walvis Bay, Luderitz, Namaqua (Hondeklip Bay), Cape Columbine and Cape Peninsula (Cape Town) are also shown.

Benguela System Boundaries

The conventionally accepted view on the boundaries of the Benguela System were examined by (Shannon and Nelson, 1996) and spatially positioned in Fig. 1.5. The shelf system is divided into two regions: the northern and the southern Benguela System separated by the Luderitz upwelling centre which acts as an environmental barrier (Agenbag and Shannon, 1988; Shannon and Nelson, 1996). The area defined by each region is 104,000 km^2 and 179,000km^2 for the southern and northern sectors respectively (Brown *et al.*, 1991). The northern boundary of the northern Benguela System is the Angola front with a seasonally driven meridional displacement between 14 - 17 °S (Shannon and Nelson, 1996). Its maximal southward excursion occurs in the late summer (March) and, typically, extends to a depth of 50m (Shannon and Nelson, 1996). The southern boundary of the Benguela System is taken to be either the Agulhas current retroflection area (Shannon and Nelson, 1996) located at approximately 37 °S or the Cape Peninsula 34°S (Andrews and Hutchings, 1980). The latter was adopted in this study (Fig. 1.5).

The seaward boundaries of the Benguela System are characterised by complex meso-scale and synoptic scale dynamics which were recently overviewed by Shannon and Nelson, 1996. These dynamics make it difficult to define unambiguously spatially and temporally continuous frontal zones as system boundaries. For the purposes of this study a simplified approach was taken akin to the original notions of Hart and Currie, 1960 and recently revisited by Barange and Pillar, 1992. Two important frontal features define seaward boundaries of the Benguela System:

- the **oceanic front** which demarcates the boundary between aged upwelled water and south - east Atlantic surface water and can therefore be considered to be the outer boundary of the upwelling system. This front, first characterised by Hart and Currie, 1960, is closely associated

with the semi- continuous shelf edge equatorward jet located along the 300-400m bathymetric range which is also sometimes known as the shelf break front (Shannon and Nelson, 1996). The zonal dynamics of these fronts have been well described using remote sensing imagery (Lutjeharms and Stockton, 1987) and in many instances they cannot be separated (Shannon and Nelson, 1996). For the purposes of this study and in line with previous usage (Brown *et al.*, 1991) the outer or westward boundary of the Benguela System is taken to be the 200m depth contour which is both convenient and also lies approximately along the mid point of the zonal excursions of the oceanic front. This provides for a system divided into two sub-systems, northern and southern, separated by the Luderitz upwelling cell and with areas of 179,000 and 104,000 km^2 respectively (Brown *et al.*, 1991).

- the **upwelling fronts** which demarcate the boundary between newly upwelled (cold: 9 - 12°C) and aged upwelled water (warmed: > 12°C) in the surface domain are associated closely with the individual upwelling centres (Lutjeharms and Meeuvis. 1987). The 6 main upwelling centres identified in Shannon and Nelson, 1996, Cape Frio (18 °S), Walvis Bay (23°S), Luderitz (27°S), Namaqua (30°S), Cape Columbine (33°S) and Cape Peninsula (34°S) (Fig. 1.5) were all used in the development of the box model for the Benguela System (Chapters 4 and 7).

Most of the biogeochemical activity from phytoplankton blooming to CO_2 uptake and air - sea fluxes occur closely linked to the turbulence and advective characteristics of the surface domain between the two frontal zones. Those are addressed in detail in the context of the Chapter 4 which deals with physical processes.

1.4.2 Biogeochemical Characteristics: Phytoplankton Production

On the basis of the Ryther hypothesis (Ryther, 1969), much of the early foodweb research in the Benguela System focussed on quantifying primary production, particularly during various stages of the upwelling cycle (Andrews and Hutchings, 1980b; Brown and Hutchings, 1987b). Research also provided insight into how primary production processes are linked to physical forcing mechanisms and their scales of variability (Andrews and Hutchings, 1980; Field *et al.*, 1981; Hutchings, 1981). Of particular note, were the early studies which showed the clear links between synoptic scale wind events, upwelling and bloom development and decay (Brown and Hutchings, 1987 b). This helped to establish a key feature of coastal upwelling - that the magnitude of post upwelling phytoplankton blooms are limited by the NO_3^- flux advected by each upwelling event (Andrews and Hutchings, 1980; Brown and Hutchings, 1987 a). This feature of the Benguela System and other coastal upwelling systems is in sharp contrast to open ocean upwelling systems discussed above where incomplete utilization of upwelled NO_3^- was a consistent feature (Chavez and Smith, 1995).

The work of Brown *et al.*, 1991 showed the Benguela system to be one of the most productive of the 4 main eastern boundary coastal upwelling systems. Annual rates of total phytoplankton production have been constrained to range from an upper value of $274*10^6$ tons C y^{-1} (Cushing, 1969) to a more recent $154*10^6$ tons C y^{-1} (Brown *et al.*, 1991) . By comparison, estimates for the Chile-Peru and California systems are $156*10^6$ and $30*10^6$ tons C y^{-1} respectively (Cushing, 1969). Notwithstanding the serious problems linked to the spatial or temporal scaling up of field data (Platt *et al.*, 1989), the lower figure for the Benguela System was produced with a higher degree of confidence given the much larger number of measurements which underpin it (N=187 between the Northern and Southern sectors) (Brown *et al.*, 1991). This estimate of total net production in the Benguela System is approximately

0.16 - 0.3% of the estimated total oceanic annual production (50 - 100*10^9 tons C y^{-1}). The spatial breakdown of annual net primary production and biomass shows that while the productivity rates in the southern Benguela sub-system compare well with those in the northern sub-system (77.4*10^6 tons C y^{-1} and 76.4*10^6 tons C y^{-1} respectively) the biomass in the latter is close to 4 fold higher than in the former (2.6*10^6 and 0.67*10^6 tons C respectively) (Brown *et al.*, 1991). In terms of the Ryther hypothesis that the short food chain in upwelling systems should operate at 20% efficiency, these total production values should yield an annual fish production of 111 million tons. This compares unfavourably with the estimate of 2.5 million tons by Hutchings, 1992.

As biological production data sets began to reflect more reliable system averages (Brown *et al.*, 1991) it soon became apparent that the relationship between fish (9 tons fish km^{-2} y^{-1} ~ 2.5 tons C m^{-2} y^{-1}) and phytoplankton (544 tons C km^{-2} y^{-1}) production in the Benguela System was well below the 20% efficiency predicted by the Ryther hypothesis. The transfer efficiency of free energy up the food chain was being limited by factors not addressed by the Ryther hypothesis and which could also have significant implications for carbon fluxes.

Recent research into the feeding ecology of anchovy further challenged the Ryther notions by showing that these fish which comprise the bulk of the fishery feed primarily on zooplankton (James, 1987). These results which were further supported by stable isotope measurements (Monteiro *et al.*, 1990; Sholto-Douglas *et al.*, 1990) showed that trophic dynamics in the Benguela System were more complex than predicted by Ryther. Not only were fish occupying higher trophic positions but the carbon flux pathways had to be modelled as complex webs in which microbial processes were an important part (Moloney, 1992). It was clear that the size-based trophic interactions which determined the production and utilization of carbon in the Benguela System manifested initially at the primary production level

(Moloney, 1992). Phytoplankton production showed a clear breakdown into a dominance by large or chain forming cells under upwelling conditions and conversely, small cells during quiescent periods (Pitcher *et al.*, 1991; Pitcher *et al.*,. 1992) . This was consistent with earlier observations in the Peruvian system (Huntsman *et al.*, 1981) and predictions by Margalef, 1978. This size based division was closely linked to the concepts of new and regenerated production (Dugdale and Goering, 1967) and hence the apparently low trophic efficiency of the system. Measuring and understanding the dynamics of new production was not only important to modelling trophic efficiency but also to predicting carbon export flux.

The study of phytoplankton new production dynamics in the Benguela System developed along two interrelated approaches: the biophysical interactions approach focussed on the links between physical forcing and their impact on adaptive strategies such as seeding and succession (Margalef, 1978; Garrison, 1981; Huntsman *et al.*, 1981; Pitcher *et al.*, 1989; Pitcher *et al.*, 1991; Denman and Gargett, 1995). The biogeochemical approach focussed on the relationship between the relative supply and uptake of nitrogen (NO_3^- and NH_4^+), the limiting nutrient, and its control on the magnitudes of new and regenerated production (Dugdale and Goering, 1967; Harrison, 1978; Probyn, 1985; Probyn. 1992). Each approach provided an important independent contribution. The biophysical approach provided the ecological basis for new production whereas the biogeochemical approach provided a means to quantify it. The insights derived from these two approaches in respect of CO_2 dynamics in the Benguela System are now addressed in further detail starting with the biogeochemical approach.

The Biogeochemical Approach: Relative NO_3^- uptake rates

The breakthrough in separately quantifying new and regenerated phytoplankton production was the development of ^{15}N uptake methods (Dugdale and Goering, 1967; Harrison, 1978; Glibert *et al.*, 1982; Probyn,

1985). After the notion of NO_3^- limitation, quantifying new and regenerated production from nitrogen uptake rates marked the next biggest step in estimating carbon production and export fluxes in coastal upwelling systems. The measurement and ecological implications of new and regenerated production in the Benguela system was based on the pioneering work of Probyn (1985) and subsequent field measurements in the southern (Probyn, 1987; Probyn, 1990) and northern (Probyn, 1988) Benguela system. The ecological significance of the results, in particular the size based trophic relationships in the plankton foodweb, was synthesised by Probyn, 1992. The relationship between physical forcing and new - regenerated production was synthesised by Hutchings et al., 1995 and Brink et al., 1995. The most significant outcome of the new production work was the finding that in the Benguela System the average f-ratio was unexpectedly low compared to other coastal upwelling systems (Probyn, 1992). The averages for the northern (0.3) and southern (0.2 in summer and 0.3 in autumn) halves of the system compare unfavorably with values of 0.5 - 1 for the Californian (Eppley *et al.*, 1979) and Peruvian (MacIsaac *et al.*, 1985) systems.

Because of its definition, the f-ratio can be used to calculate carbon new production from the above total net production values. These calculated values of new production of $23.3*10^6$ tons C y^{-1} for the northern sector and a range of 15.3 - 23.0 * 10^6 tons C y^{-1} for the southern sector and a total of 38.5 - $46.2*10^6$ tons C y^{-1} for the whole system. This total is in agreement with the value of $47*10^6$ tons C y^{-1} calculated from the relationship between integrated NO_3^- (0-30m) concentrations and temperature with satelite based SST images (Waldron and Probyn, 1992). This value represents approximately 0.6% of the estimated total global ocean new production of $7200*10^6$ tons C y^{-1} or 6% of total coastal new production (Table 1.2). This compares well with the fact that its area ($0.28*10^{12}$ m^2) is approximately 7% of the total area occupied by coastal upwelling systems (Table 1.2). More recently, a similar calculation was repeated for the southern Benguela System only, using a time series of satelite thermal images (Waldron, 1996). This more accurate estimate of

carbon export flux of $5.6*10^6$ tons C y^{-1}, calculated assuming Redfield stoichiometry, is sharply lower than the equivalent value calculated above of 15 - $23*10^6$ tons C y^{-1} from an f-ratio of 0.2 - 0.3. The lower new production flux value predicts an f-ratio of < 0.1 for the southern Benguela System which is inconsistent with average field measurements (Probyn. 1992). The discrepancy between the two estimates highlights the problems of scale in comparing *in situ* and bulk based measurements (Platt *et al.*, 1989). This is an issue into which the modelling approach in this study will be able to provide some quantitative contribution.

Overall, these total and new production values from the Benguela System combined with the complete utilization of upwelled NO_3^-, support the notion that it is a very productive system which is potentially capable of generating a CO_2 drawdown from the atmosphere. This form the basis of the **first hypothesis**: *that the Benguela upwelling system is an important CO_2 sink by virtue of its high primary production and sediment organic carbon accumulation rates,.*

Estimates of new production from NO_3^- supply rates, such as those above, are predicated on the widely held assumption that the carbon export flux can be calculated from the NO_3^- flux and the Redfield ratio of 6.6 (Waldron and Probyn. 1992 ; Waldron, 1996). On the basis of recent doubts about the robustness of this paradigm (Sambrotto *et al.*, 1993) it became necessary to test its validity in the Benguela System. This forms the basis for the **second hypothesis**: *that the carbon export flux and the magnitude of the CO_2 sink in the Benguela System can be predicted from the C:N stoichiometry provided by the Redfield Ratio.*

One of the most important ecophysiological changes measured by ^{15}N uptake in the growth of a post upwelling phytoplankton bloom is the "shift up" in the uptake rate of NO_3^- in the early stages of bloom development which characterises new production (Probyn. 1992). This is, a sharp increase in

the uptake rate of NO_3^- until this nutrient supply is exausted. This "shift up" is closely linked to the degree of wind induced physical turbulence where high turbulence favours rapid uptake of NO_3^- and new production and quiescent conditions favour NH_4^+ uptake and regenerated production. This relationship between physical forcing and new - regenerated production was effectively synthesised in a diagramatic form by Probyn in Brink *et al.*, 1995. The ecological context for these observations is provided by the findings of the biophysical coupling studies which are briefly overviewed below.

Biophysical Approach: Adaptation Strategies to a Physically Dynamic System

Recent advances have been made in understanding the links between physical forcing mechanisms and their impact on seeding and succession of phytoplankton in the Benguela System (Pitcher *et al.*, 1992 ; Hutchings *et al.*, 1995). These phytoplankton bloom characteristics are thought to govern the magnitude and direction of air - sea CO_2 fluxes over a temporal range of hours to seasons.

The main physical forcing mechanisms operating at the upper boundary of the ocean in upwelling systems are the wind and solar heating which together govern advection and turbulent mixing - stratification characteristics in the surface layer (see Chapter 4). It is particularly the temporal characteristics (frequency and strength) of pulsed wind events which have a direct bearing on phytoplankton dynamics in the vicinity of upwelling centres (Garrison, 1981; Huntsman *et al.*, 1981; Pitcher *et al.*, 1992 ; Pitcher *et al.*, 1996). Over and above providing the required nutrient flux, wind induced advection and turbulent mixing impact on phytoplankton bloom dynamics in two ways: they govern the phytoplankton seeding mechanism (refuge vs. fugitive) and species succession (Hutchings *et al.*, 1995). In so doing they provide the ecological link between physical forcing and the dominance of new and regenerated production.

Seeding

Seeding of upwelled water with phytoplankton can occur through two mechanisms: with the **refuge** strategy, resting spores deposited mainly by diatoms onto the sediments are advected to the surface layer where they form the pioneer populations of newly upwelled water. Alternatively, with the **fugitive** strategy, seeding of newly upwelled water is provided through surface mixing with aged upwelled water which is already seeded with a residual population from the previous upwelling event(s) (Huntsman *et al.*, 1981; Pitcher *et al.*, 1989; Pitcher, 1990; Hutchings *et al.*, 1995). The two mechanisms are adaptive strategies for competition in an environment whose physical dynamics are pulsed between turbulent and stratified conditions on synoptic to seasonal time scales. Diatoms are best adapted to take advantage of both strategies which gives them the species dominance in the context of active upwelling in the Benguela System (Hutchings *et al.*, 1995). Their ability to form rapidly sinking spores which are also resistant to the benthic remineralization mechanisms ensures that they maintain a pioneer status in active upwelling. Small cells (dinoflagellates, small diatoms, coccolithophores) which typically have slow or negligible sinking rates are best adapted for quiescent surface layer environments which characterize the relaxation phase of an upwelling cycle (Hutchings *et al.*, 1995).. In conditions of weak upwelling or a relaxation after an upwelling event, aged surface waters tend to be advected polewards (see Chapter 4) and mix with newly upwelled waters close to the coast. These are the conditions which enhance *fugitive* seeding of upwelled waters and are typically found in the mid-late summer in both the southern and northern Benguela System (Pitcher *et al.*, 1992) at which time the prevalence of red tides also increases (Pitcher *et al.*, 1996). Whether newly upwelled water gets seeded with diatoms net - nanno plankton: large, aggregate or small chain forming cells which have relatively fast sinking rates or dinoflagellates which have negligible sinking rates, there are clear implications for the CO_2 drawdown flux.

Succession

In an upwelling cycle the physical environment of the surface layer changes from that of wind induced turbulence to quiescent and stratified conditions which follow the relaxation of equatorward wind stress (Huntsman *et al.*, 1981; Pitcher *et al.*, 1992 ; Hutchings *et al.*, 1995). These changing conditions open a number of environmental windows to which a range of phytoplankton may be best adapted. In the Benguela System the succession sequence is typically "small diatoms - large diatoms - dinoflagellates - micro-flagellate community" which are progressively adapted to reducing levels of turbulence (Hutchings *et al.*, 1995). The extent of the succession depends largely on the temporal dynamics of the upwelling inducing equatorward winds. Where upwelling is ongoing or pulsed but with short relaxation times the succession sequences will be short and dominated by diatoms. Alternatively, where the relaxation periods are long dinoflagellate or even coccolithophore blooms can develop and dominate the community (Mitchell-Innes and Winter, 1987; Pitcher *et al.*, 1996)

The seeding mechanisms and the succession sequences are probably interrelated in that similar physical forcing conditions lead to *refuge* seeding and short diatom dominated sequences and alternatively *fugitive* seeding and longer dinoflagellate succession sequences. This is borne out by data from both the northern and southern Benguela sub-systems. In the northern sub-system diatoms dominate dinoflagellates by 1 -2 orders of magnitude throughout the year except in the late summer when the upwelling rate is at a minimum (Shannon, 1985; Shannon and Pillar, 1986). This situation reverses in the January - March period of reduced equatorward wind stress. Similarly, in the southern sector, dinoflagellates become dominant when upwelling intensity decreases in the late summer and dinoflagellate dominated red tides become more common (Pitcher *et al.*, 1996).

This type of relationship suggests that those parts of the system where, because of physical constraints, short succession sequences dominate, will be characterised by a higher export flux than where the converse holds. This overview described the ecological basis for the relationship provided by Probyn in (Brink *et al.*, 1995) between the degree of turbulence and new or regenerated production.

Coccolithophore Activity

The largest gap in the overall understanding of phytoplankton dynamics in the Benguela System centres on the ecological dynamics of coccolithophorids (Giraudeau and Bailey, 1995). Coccolithophorids contribute to the plankton community in the nannoplankton size range of 4 -24 μ (Giraudeau and Bailey, 1995) which, in terms of the size - production relationships presented above, suggest that they contribute largely to regenerated production. They are therefore considered to make an insignificant input into foodweb energy flows particularly to fish and resulting in their ecological role being largely overlooked. This applies both to the mechanisms which govern or trigger coccolithophore blooms as well as their contribution to the transport of carbon from the surface layer to the sediments. Most field observations of coccolithophore blooms are incidental reports linked to other ongoing planktonic studies (Shannon and Pillar, 1986). Such reports appear to indicate that their occurrence is highest along the Namibian coast where the largest blooms of 3 - 6.8 * 10^6 cells l^{-1} were recorded (Shannon and Pillar, 1986; Giraudeau *et al.*, 1993). This prevalence of coccolithophre blooms in the northern Benguela sub-system was suported by images of a large coastal bloom off Walvis Bay taken from the space shuttle (Holligan, pers.com). There is only one major bloom record for the southern Benguela sub-system when standing stocks of 2.3 * 10^6 cells l^{-1} were recorded along a transect northwest of Cape Town (Mitchell-Innes and Winter, 1987). In most instances the dominant species were identified as *Emiliania huxleyi* and *Gephyrocapsa oceanica* (Mitchell-Innes and Winter, 1987; Giraudeau and Bailey, 1995).

Recent increased interest in the physical and biogeochemical mechanisms behind coccolithophore blooms has been driven by their importance as proxies for paleo-oceanographic reconstructions in the Benguela System (Giraudeau, 1992). Three recent sampling cruises when a deliberate effort was made to investigate the oceanographic context of coccolithophore blooms (Mitchell-Innes and Winter, 1987; Giraudeau, 1992; Giraudeau and Bailey, 1995) have shown one common and perhaps surprising feature: the highest numbers were always measured within the upwelling front. However in all instances the occurrences coincided with stratified or at least quiescent conditions which lends support to the view that seeding of blooms from *fugitive* populations is an important aspect. Further support for this view comes from the observation that the largest recorded blooms in both the northern and southern Benguela sub-system occured under El Nino conditions when upwelling rates weaken (Mitchell-Innes and Winter, 1987). Under these conditions the upwelling front would move closer to the coast and favour the *fugitive* re-seeding from aged waters and with a lower input of newly upwelled waters, longer successional sequences would also be expected to develop.

The apparent minor role of coccolithophores in the Benguela System is not consistent with geochemical observations that $CaCO_3$ appears to be the single most important biogenic contstituent in the sediments on the shelf (Rogers and Bremner, 1991). While other calcareous organisms such as benthic and pelagic foraminefera are important, a survey of coccolithophore species in the sediments of the Benguela System has shown that they are a major contributor of $CaCO_3$ to the sediments (Giraudeau, 1992). Unfortunately, due to their very different sizes coccoliths and foraminifera tests are not normally quantified simultaneously. While it is possible to explain why $CaCO_3$ should be preserved in Benguela System sediments, the question which remains unanswered is whether coccolithophores contribute to this flux through continuous low level "blooms" of $< 10^6$ cells l^{-1} as were

observed in Namibia and off the Namaqua upwelling cell (Giraudeau, 1992; Giraudeau and Bailey, 1995) or through a few very large events of $5\text{-}10*10^6$ cells l^{-1}. The low incidence of observed surface coccolithophore blooms and their simultaneous important role as a sediment constituent indicate that their short term role in carbon fluxes and CO_2 variability is small but, in the long term coccoliths could be an important carbon export route. This forms the basis for the **third hypothesis**: *that the stoichiometry of the organic and inorganic pumps (C_{Org} : C_{Ing}) plays an insignificant role in the magnitude of both the carbon export flux and the air - sea CO_2 flux in the Benguela System*

1.5 Aims and Hypotheses

The aims of this study are two fold:

- to conceptually and quantitatively describe the physical and biogeochemical processes which drive the carbon fluxes in the Benguela System and use them to,
- formulate a box model whose output is to be used to test the aforementioned three hypotheses:

- The Benguela upwelling system is an important CO_2 sink by virtue of its high primary production and sediment organic carbon accumulation rates,.
- The carbon export flux and the magnitude of the CO_2 sink in the Benguela System can be predicted from the C:N stoichiometry provided by the Redfield Ratio.
- The inorganic carbon pump, through coccolithophore production, plays a minimal role in driving changes to the magnitude of both the carbon export flux and the air - sea CO_2 flux in the Benguela System

1.6 Approach

There are *inter alia* two approaches to address these issues:

- firstly, the empirical - deterministic approach which, has been widely used in the global CO_2 sampling programmes, entails an intensive surface sampling programme of CO_2 parameter transects to map the spatial variability of surface PCO_2. This approach which has been widely used in the global CO_2 sampling programmes is suited to inverse modelling studies. Such studies would provide an answer to the first hypothesis. However, its non-mechanistic basis would not allow it to address the underlying biogeochemical dynamics which are the focus of the remaining two hypotheses.
- secondly, a mechanistic approach where sampling strategies are directed towards identifying key driving physical and biogeochemical forcing which can then be incorporated into the box model. This provides a quantitative method to test the degree to which the complexity of the problem is understood and forms the basis of the approach adopted in this study. With this approach, even if the fluxes characteristic of the Benguela System were too small to impact on the global CO_2 budget, new insights would still provided into mechanisms which drive the biological pumps in their role in CO_2 variability in the ocean in general.

This study is divided into three main parts:

Part 1 which comprises Chapters 2 and 3 addresses the methods which were used or developed to characterise the carbonate chemistry and quantify changes in its chemical state. Chapter 2 provides both the theoretical and practical details of the methods used to sample and quantify the two carbonate system master variables (Total Alkalinity and pH). Chapter 3 describes a vector ploting method which assists in independently and directly

quantifying the contributions by the organic and inorganic pumps to changes in the state of the carbonate system in sea water and its links to PCO_2.

Part 2 which comprises Chapters 4 to 6 is the body of the study in which the results obtained are presented and discussed to prepare the physical and biogeochemical inputs and assumptions which underpin the box model. Each of these chapters addresses **3 questions**:

1: to what extent do the results support recent understanding of the key physical and biogeochemical forcing in the system ?

2: what new perspectives can be obtained from the way in which aspects of the results do not support existing ideas ?

3: what qualitative assumptions and quantitative inputs do the results and discussion provide for the box model ?

These questions form the basis for the short summaries which end Chapters 4 - 6. The approach to Part 2 is best described with the assistance of a simplified conceptual depiction of 3 biogeochemical stages of the upwelling cycle (Fig. 1.6). The diagram depicts the main physical and biogenic flux pathways as well as the end-members that they link (Fig. 1.6). The first sub-surface stage (1) is the wind driven upwelling of shelf based and poleward flowing SACW. This water, which is biogeochemically modified by the impact of benthic remineralization flux (BREF) outcrops as newly upwelled water (UPW) where it undergoes physical and biogeochemical ageing (2) to form aged upwelled water (AUW). The main biogeochemical activity which follows upwelling is new production which generates the vertical flux of organic carbon (3) which in turn, and depending on the characteristics of UPW, will result in a net ingassing or outgassing of CO_2.

The physical processes which drive both advection and turbulence in each of the stages are addressed in Chapter 4. The oceanographic data (physical and biogeochemical) are discussed with a view to testing the extent to which they are consistent with the most recent ideas on the advective and turbulence characteristics of the Benguela System. Some new insights are

The 3 biogeochemical stages of the upwelling cycle

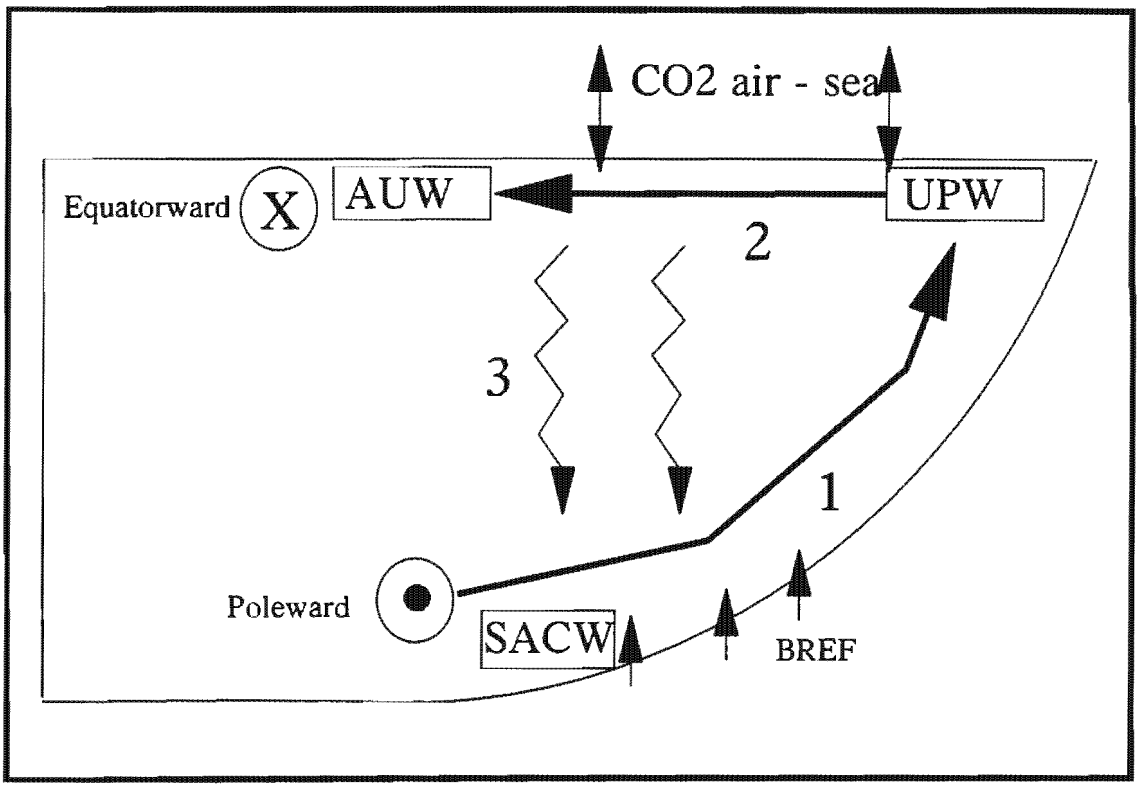

1: Upwelling of South Atlantic Central Water (SACW) which has been modified by the benthic remineralization flux (BREF)

2: Ageing of newly upwelled waters (UPW) to aged upwelled waters (AUW).

3: the sedimentation flux from new production during the ageing of UPW

Fig. 1.6: The 3 main stages of the upwelling cycle which formed the original basis for the approach to this study are depicted as a conceptualised cross-shelf section.

also developed. The mechanisms which govern changes to the biogeochemical characteristics of poleward flowing sub-surface SACW on the shelf (stage 1) are discussed in Chapter 5. The mechanisms which govern changes in the biogeochemical characteristics during the surface based ageing phase (2) are discussed in Chapter 6. Of particular importance in both cases are the roles of changing C:N and C_{Org} : C_{Ing} stoichiometry on PCO_2 and the biogeochemical characteristics of the end members.

Part 3 comprises Chapters 7 and 8. In Chapter 7 the input data and assumptions derived from Part 2 coupled to wind based Ekman transport are modelled to quantify the annual air - sea CO_2 fluxes and organic carbon fluxes (stage 3) in the Benguela System with a view to addressing the 3 hypotheses. Chapter 8 is a summary which assesses the extent to which the study was able to address the hypotheses as well as to suggest some new directions and identify aspects of the Benguela System which may require further attention.

Chapter 2

2. The Characterization of the Carbonate System in Sea Water

2.1 Introduction

The study of oceanic carbonate biogeochemistry poses a dual challenge. Firstly, it requires quantitative measurement and modelling of chemical equilibria in high ionic strength solutions where departures from ideality pose specific theoretical and experimental difficulties in accurately predicting speciation and phase behaviour. Secondly, it provides the basis for an improved mechanistic insight into some of the complex interactions which drive global climate change through perturbations to the oceanic carbonate equilibria. This chapter focuses on the first aspect with an objective of setting the theoretical and analytical base from which to analyse carbon biogeochemistry in the Benguela System.

The reliability of CO_2 measurements in the ocean has been one of the key concerns of the JGOFS programme (Dickson, 1990; JGOFS, 1992). It stimulated intensive evaluation and standardization of general core methodology (UNESCO, 1994) and particularly sampling and analysis of carbonate parameters (Dickson, 1993; Dickson, 1994; Dickson, 1995). With an annual increase in atmospheric CO_2 of 2 Gt C y^{-1} (IPCC, 1996) the PCO_2 in the surface layer should increase by approximately 7μatm (Wallace, 1995). Thus, for the purposes of monitoring anthropogenically linked interannual changes in surface ocean PCO_2 the required accuracy of both calculated and directly determined PCO_2 must be better than 7μatm. The best existing methodology which includes coulometry, TCO_2 measurement, direct PCO_2 measurement and total alkalinity (TAlk) measurement can be used to give an accuracy of ~ 1μatm in the calculated PCO_2 values (Johnson *et al* 1987; Dickson, 1994; UNESCO, 1994).

With knowledge of the respective equilibrium / dissociation constants, the carbonate equilibrium system in sea water can be fully described with known values for a minimum of 2 carbonate master variables (intensive or conservative), total borate (B_T) and if appropriate, a variable for each of the lower order weak acid systems (Skirrow, 1975; Jagner, 1981; Dickson, 1994). In line with the quest for the requirements for the JGOFS programme, the carbonate master variables are usually selected from a suite of parameters (TCO_2 , TAlk and PCO_2) whose concentrations can be most accurately determined. This study was constrained by existing material resources and had to rely instead on the use of pH and TAlk as the only master variables with which to determine the carbonate system in the Benguela. This imposed some limitations on the precision of the calculated fluxes based on calculated PCO_2 gradients which preclude the results from being used as part of a global data set to monitor interannual changes in PCO_2 arising from changes to the atmospheric CO_2 inventory. However, in this study the main objective was to identify and quantify biogeochemical mechanisms which drive CO_2 variability within the various stages of the upwelling cycle (see Chapter 1: Approach). The magnitude of these gradients was in most instances at least 5 times larger than the estimated upper boundary of uncertainty in the calculated PCO_2 (~20μatm). It is envisaged that once the first order biogeochemical processes in the Benguela System have been mechanistically and numerically constrained it will be necessary to implement a monitoring programme where the highest accuracy and precision would be with improved precision. This is probably best implemented through international co-operation.

Thus while the use of pH as a master variable is not suited for CO_2 monitoring programmes looking at small anthropogenically driven interannual changes its degree of precision and low cost are well within the boundaries of accuracy required for process orientated biogeochemical studies. This will be even more so in the future when widespread use is made of carefully calibrated

profiling pH probes whose accurate use will provide the only means to high resolution 3 dimensional view of CO_2 variability induced by the biological pumps and their underlying mechanisms.

Central to the modelling of perturbations of the marine carbonate system, especially when pH is a master variable, is the weak acid - base theory which underlies its speciation in a non ideal environment: sea water. The theory is relevant to both the experimental determination of specific aqueous equilibrium master variables as well as the interrelationships which allow for the remaining variables to be quantified. The approach in this Chapter is:

- to address the theoretical considerations which underlie the carbonate system equilibrium and its characterization with particular reference to a critical evaluation of the pH (NBS) scale and Total Alkalinity (TAlk), the master variables used in this study.

- to present the sampling and analytical procedures used to characterize the carbonate system in this study with particular reference to procedures adopted to reduce the risk of experimental error and

- to present a sensitivity analysis of the sources of error and their impact on calculated PCO_2 values.

- to present a brief outline of additional sampling and analytical methods used to characterize nitrate and ammonium in both the water column and sediments.

2.2 Concepts, and Definitions

2.2.1 Weak Acid-Base Equilibria

Dissolved salts provide sea water with two important properties in respect of its aqueous chemistry: a high but nearly constant ionic strength (0.7M) provided by the principal ionic matrix and a weak acid - base pH buffer control provided by the minor ionic species. The concentrations of the main contributors to the principal and minor ion reservoirs are summarized on Table 2.1 (Whitfield and Turner, 1981).

Table 2.1: Concentrations (mmol/l) of the main major ions and minor ions which make up the background electrolyte and the weak acid - base system in sea water respectively (from: Whitfield and Turner, 1981).

Major ions:		**Weak acid - base ions**	
Cl^-	558.65		
Na^+	479.12	HCO_3^-	2.20
Mg^{2+}	54.49	$B(OH)_4^-$	0.43
Ca^{2+}	10.51	F^-	0.06
K^+	10.45	HPO_4^{2-}, $Si(OH)_4^-$	< 0.02
SO_4^{2-}	28.90		

The principal ionic matrix and the weak acid-base systems present govern the equilibrium, phase behaviour and characterization of the carbonate systems set out below.

A thermodynamic definition of acid - base equilibria is provided by the law of mass action which relates the activities of the components to their equilibrium constant (K) (Stumm and Morgan, 1970; Pytkowicz, 1983). For a generic weak acid HX which dissociates into H^+ and X^-

$$HX \text{ <----------> } X^- + H^+ \qquad \text{eq. 2.1}$$

$$K = \{X^-\}\{H^+\}/\{HX\} \quad \text{or} \qquad \text{eq. 2.2}$$

$$\ln K = \ln\{H^+\} + \ln\{X^-\} - \ln\{HX\} \qquad \text{eq. 2.3}$$

Where {X} is the activity of species X. The activities of the acid - base equilibrium pair can be separated into mass and activity coefficient components as shown on eqs. (2.4).

$$K = [X^-]\gamma_{X^-}\,[H^+]\gamma_{H+}/[HX]\,\gamma_{HX} \qquad \text{eq. 2.4}$$

Where [X] = concentrations and γ = activity coefficient. The difficulty which arises from trying to implement this thermodynamic definition of equilibrium in the context of non ideal solutions or "real" solutions, is that it is not possible to experimentally quantify or theoretically model single ion activity coefficients without non-thermodynamic assumptions (Loewenthal and Marais, 1984). The important characteristics of low and higher ionic strength solutions (such as sea water) in respect of departures from thermodynamic ideality are summarized as follows (Loewenthal and Marais, 1984):

Low Ionic Strength (Low Salinity):

1: The activity coefficients are almost completely determined by long range electrostatic effects which can be suitably modelled using the Debye-Hückel model or a modification of it such as the Davies model.

2: The hydrogen ion activity $\{H^+\}$, can be estimated potentiometrically with minimal error on a conventional scale because the residual liquid junction potential effects (between buffers and test solution) are negligible.

3: There are negligible ion pairing effects.

High Ionic Strength (High Salinity) $\mu > 0.1$:

1: Activity coefficients cannot be modelled easily due to numerous effects , *inter alia* hydration effects, which become significant and require further non-thermodynamic assumptions. The theory is both conceptually and numerically complex.

2: Residual liquid junction potentials are significant. This makes the interpretation of the pH not only more problematic in respect of thermodynamic rigour, but also prone to irreproducible residual effects. These can contribute to the uncertainty in the final CO_2 flux calculations.

3: The effects of ion pairing become significant. This has an interactive effect on pH and the distribution of free and ion paired species.

Because of these departures from ideality, it is not possible to use strictly defined thermodynamic relationships to measure or model ionic equlibria in sea water (Jagner, 1981; Loewenthal and Marais, 1984). Alternatives, based on a range of conventional scales are the only choice. The particular option adopted in this study, the NBS (operational) scale, to characterize sea water carbonate equilibria is now critically discussed with special emphasis on how the underlying assumptions compare with the Sea Water Scale (SWS) (Hansson, 1973) which has become the more favoured choice for oceanographic work (Dickson, 1984, Dickson, 1994).

There are two possible approaches to address the problem of non ideal behaviour of ions in multi-component high ionic strength solutions. Firstly, semi-empirical models for single ion activity coefficients can be developed based on a number of non-thermodynamic assumptions to model the effects of ion pairing, hydration and long range electrostatic interactions (Loewenthal and Marais, 1984). These models offer the advantage of flexibility in that they can be used over a wide range of ionic strength and electrolyte composition.

Although the most recent versions of these models have provided outputs which closely model observations, they are numerically complex requiring extensive computing power. However, the flexibility makes them useful in the context of industrial effluents where compositional changes are part of the process. Fortuitously, sea water is closely a constant ionic environment which allows some operational simplifications to be made which are the basis for the second approach.

The second approach, generally used for sea water based equilibrium studies, is to use experimentally determined equilibrium constants (Millero, 1979; Culberson, 1981; Dickson and Millero, 1987). This is possible only where there is a coherence between the scale on which the "activity" of the H+ ion and the equilibrium constants are measured. Use of these conventional scales give (with varying degrees of thermodynamic rigour) relationships between the equilibrium constant and the stoichiometric concentrations of weak acids and bases. As was shown above (eq. 2.5), the activity can be expressed as a product of the stoichiometric concentration and the activity coefficient terms. The next step in the simplification process is to assess whether the chemical composition of sea water allows that the activity coefficients γ_+ and γ_- to be ignored (i.e.: as being equal to unity. The simplest approach is to define conditions whereby it is possible to define activity coefficients γ_+ and γ_- as being equal to unity. Two conventional activity scales satisfy this approximation.

2.2.2 Activity Scales:

The Infinite Dilution Scale:

In this scale the activity coefficient γ_i approaches unity as the concentration of all solutes, c_i , approach zero. In terms of the law of mass action from eq. (2.4):

$$\lim_{c_j \to 0} K = [X][H]/[HX] \qquad \text{eq. 2.6}$$

When this condition holds, the activity coefficients become unity and the equilibrium constant is then a simple function of the stoichiometric concentrations and becomes a concentration scale. An alternative and more widely used form, mixed constants, makes use of the operationally defined activity of the hydrogen ion on the NBS scale where $pH_o = -\log\{H^+\}$. On this operational scale, on which K is also determined, the above expression becomes:

$$\lim_{c_i \to 0} K = 10^{-pH_o} \frac{[X]}{[HX]} \qquad \text{eq. 2.7}$$

In practical terms, for this condition to hold, the concentration of the dissolved solutes should not exceed 10^{-4}M. Though this is a widely used approach in low salinity waters, it does not apply to sea water where the ionic strength reaches 0.7M. A special form of the same expression is used to apply the NBS scale to sea water. In this approach the solution is considered to be a constant ionic medium (Loewenthal and Marais, 1984).

The Constant Ionic Medium Scale (CIMS):

The principle of activity coefficients approaching unity in solutions of high ionic strength is similar to that described above except that it in this case the activity coefficient tends to unity as the concentration of the solution tends to that of the ionic medium when the equilibrating weak acid concentrations approach zero (Stumm and Morgan, 1970; Loewenthal and Marais, 1984).

$$\lim_{[X],[HX] \to 0} K' = 10^{-pH_0} \frac{[X]}{[HX]} \qquad \text{eq. 2.8}$$

The relation in eq.(2.8) holds for a solution of constant ionic medium when the background electrolyte has a total concentration greater than 10 times that of the equilibrating weak acid species (Culberson, 1981). In this case the equilibrium constant is referred to as the apparent equilibrium constant because it incorporates all the non measurable deviations from ideality in sea water. For sea water the ratio of weak acid-base concentrations to background electrolyte is more than 100 (Table 2.1), and, with the added fact that the ratio of principal components remains closely constant (Whitfield and Turner, 1981), it satisfies the criteria for the use of a CIMS. This allows the development of equilibrium expressions based on a measurable scale to characterize carbonate species in the complex aqueous matrix of sea water.

2.2.3 The Sea Water Weak Acid-Base System

Activity Scale:

Sea water can be classified as a high ionic strength solution of mixed electrolytes but with a constant composition in all but the most extreme environments such as some pore waters and hydrothermal environments where special biogeochemical circumstances predominate. Table (2.1) lists a breakdown of the main components which make up the background electrolyte and the main weak acid - base systems in sea water. In the oceans, though the salinity (total ionic strength) may vary by about 10% (32-36 practical salinity units psu) the relative composition remains largely constant. These characteristics of sea water make it appropriate that the constant ionic medium activity scale be adopted to model concentrations and equilibria in ocean systems. The issue then arises as to how pH and the corresponding equilibrium scale K should be operationally defined. In

practice the two most commonly used methods are via the National Bureau of Standards Scale (NBS) (Bates, 1973) and the Sea Water Scale (SWS) (Hansson, 1973) concentration scales (Culberson, 1981; Loewenthal and Marais, 1984).

pH Scales:

As was shown above pH, or the "activity " of the hydrogen ion, is fundamental to the utilization of weak acid - base equilibria in solution. The activity of the hydrogen ion is an indicator of the state of proton transfer equilibria in solution. The added attraction for using pH as a master variable in sea water carbonate equilibria is its apparent albeit sometimes deceptive simplicity of use and its low cost. The incompatibility between the thermodynamic definition of $\{H^+\}$ (Culberson, 1981; Dickson, 1984) and its practical potentiometric determination as pH relative to an electrode potential, is at the core of much of the difficulty associated with the use of this parameter as a master variable in sea water equilibria. These are discussed in more detail below.

Three different conventional pH scales have been developed to make pH measurements in sea water both simple and reproducible while retaining varying degrees of thermodynamic rigour. Only two of these NBS and SWS have been widely implemented and will now be critically compared

The basic definition of pH is $pH = -\log_{10}\{H^+\}$, the activity of the hydrogen ion on a log scale. pH is usually determined using potentiometric methods and is best expressed as an electrode potential. The electrochemical relationship between of the activity of H^+ and the half cell potential is given by the Nernst equation for the hydrogen half cell (Stumm and Morgan, 1970; Culberson, 1981; Loewenthal and Marais, 1984):

$$E_H = E_{H0} + RT/nF * \ln \{H^+\} \qquad \text{eq. 2.9}$$

Where E_H is the potential for the hydrogen electrode, E_{H0} is the standard electrode potential for the hydrogen electrode (Stumm and Morgan, 1970; Loewenthal and Marais, 1984). It is however not possible to either measure the activity of a single ion nor to practically operate a half cell without a reference half cell (Loewenthal and Marais, 1984). The most widely used reference half cell for pH determinations is the Ag/AgCl with a liquid junction of KCl (Culberson, 1981). This basic potentiometric architecture applies to almost all pH measurements regardless of convention.

The corresponding reference half cell potential is:

$$E_{ref} = E_{0ref} - RT/nF * \ln \{Cl^-\} - E_{ljp} \qquad \text{eq. 2.10}$$

which depends on two additional factors: the activity of the Cl^- ion and the liquid junction potential (E_{ljp}). To overcome these problems, the reference electrode is operated within a saturated KCl solution where the activity of the Cl^- ion remains constant and the electrodes are calibrated against standard buffers which minimizes the liquid junction potential problem. These will be shown to be important steps in simplifying the relationship between pH and the electrode potential. The various pH scales in sea water differ mostly depending on how they treat the liquid junction potential problem in a practical way.

NBS Scale:

The NBS scale is a scale derived as an extension of the operationally defined pH and apparent equilibrium constants on the infinite dilution scale (eqs. 2.7 and 2.8). The principle which underlies this scale is that all deviations from ideality (hydration, ion pairing and long range electrostatic interactions) are

incorporated into the definition of the apparent equilibrium constant (pK_i') on the same scale. Because absolute activities cannot be measured directly, potentiometric pH determinations make use of reference buffer solutions whose hydrogen ion activities or concentrations are defined. In the case of the NBS scale the buffers are low salinity solutions whose hydrogen ion activities can be satisfactorily predicted using the Davies equation (Loewenthal and Marais, 1984).

Expressions can be formulated giving the electrochemical potential of the cell in both buffer and test solutions.

The hydrogen cell potential in a buffer:

$$E_b = E^* + RT/F * 2.303\log \{H^+\}_b + E_{ljp} + \{Cl^-\} \qquad \text{eq. 2.11}$$

The hydrogen cell potential in sea water:

$$E_{sw} = E^* + RT/F * 2.303\log \{H^+\}_{sw} + E_{ljp(sw)} + \{Cl^-\} \qquad \text{eq. 2.12}$$

defining $pH = -\log \{H^+\}$ and re-arranging eq. 2.12,

$$pH_{sw} = pH_b + (E_b - E_{sw})/ Z - (E_{ljpb} - E_{ljpsw})/Z \qquad \text{eq. 2.13}$$

where $Z = 2.303RT/F$. It shows that the effect of measuring pH relative to a buffer scale is that because the activity of the Cl^- remains constant, the $\{Cl^-\}$ term become zero. This leaves an expression which shows the dependence of sea water pH on the potential difference between the sample and buffer, due to their different $\{H^+\}$ and a residual liquid junction potential term $\Delta E_{ljp}/Z$. This residual liquid junction potential term is negligible in the case of infinite dilution because the ionic strength of the buffer is almost the same as the sample solution. In sea water, on the other hand, the potential which is generated at the liquid junction is not the same between the low ionic strength

NBS buffer and the high ionic strength sea water solution. It is the apparent difficulty of reproducing this term accurately in measurements between samples which undermines the thermodynamic rigour of the NBS scale in sea water applications (Dickson, 1984). It has been estimated that this irreproducibility of the residual liquid junction potential introduces an uncertainty of about 0.005 pH units (Culberson, 1981).

The assumption with this method is that the residual liquid junction potential (ΔE_{ljp}) is constant and can be included into the apparent equilibrium constant, which is generally correct provided that all sample measurements are done using the same electrode set. This assumption is criticized by Dickson,1984 and Dickson, 1994 who favoured the SWS scale, unfortunately he does not give actual figures for the estimate of errors between the different scales.

Total Hydrogen Ion Concentration Scale:
(Hansson Scale or Sea Water Scale (SWS)):

This scale, also commonly referred to as the Sea Water Scale (SWS) was developed by Hansson, 1973 with a view to addressing two important shortcomings of the NBS scale:

1: The SWS scale provides a pH scale which though strictly also conventional is thermodynamically more rigorous than the NBS scale. The hydrogen ion "activity" is defined in terms of a concentration scale.

2: Because this method makes use of buffers made up in a constant ionic medium of artificial sea water, (Dickson, 1994) it supposedly overcomes the problem of irreproducibility of residual liquid junction potentials which is a source of uncertainty in the NBS scale.

pH (SWS) is defined as:

$$pH(SWS) = - \log (c_{H+} + c_{HSO4^-}) = -\log (c_{H+T}) \qquad \text{eq. 2.14}$$

which is the mass balance of the free protons (c_{H^+}) and those taken up by the formation of the bisulphate (C_{HSO4^-}) the sum of which give the total hydrogen ion concentration (Culberson, 1981). Difficulties which arise with this scale are twofold: firstly, (c_{HSO4^-}) varies with salinity, and secondly, because of the dependence of β_{HSO4^-} on temperature, salinity and pressure, the ratio c_{H+}/C_{H+T} also changes. Like the problem of the residual liquid junction potential for the NBS scale, this effect is incorporated into the carbonate equilibrium constants determined for the SWS scale. However, it diminishes the apparent simplicity of the theoretical basis of this scale which means that like the NBS scale the SWS scale is also an operational scale.

Each pH scale offers advantages and conceptual problems but the preferred scale for oceanographic work has become the SWS in which ionic strength is adjusted to suit the sea water salinity range (Dickson, 1984; Dickson, 1994). Much work has been done to refine the required buffers equilibrium constants for carbonate, borate and other minor weak acid sub-systems in the SWS (Dickson, 1994). This should be the pH scale of choice for future work in the Benguela System. However, as this study was initiated on the NBS scale it was considered prudent to retain this scale for the sake of continuity.

Equilibrium Constants and Species Equilibria of Carbonate and Secondary Weak Acid Systems in Sea Water

Carbonate equilibrium constants were experimentally determined in sea water for the NBS scale by Merbach et al., (1973) whose determinations superseded the earlier pioneering work of Lyman and Buch (Pytkowicz, 1983). The results were more recently fitted into polynomial functions to obtain a statistically valid dependency on temperature (0 - 50°C), salinity (0 - 40psu) and pressure (Millero, 1979). Statistical comparisons of the errors

arising in the use of equilibrium constants from either the NBS or the SWS show that neither offers an intrinsic advantage (Millero, 1979; Dickson and Millero, 1987). The critical issue is that if pH is used as a master variable to characterize the carbonate system, the pH and equilibrium constants must be on the same scales. This is important because the apparent equilibrium constants (K') incorporate different simplifying assumptions which in the case of NBS scale include ion pairing effects, hydration effects, liquid junction potential effects (Loewenthal and Marais, 1984). The functional dependence of NBS scale apparent equilibrium constants for the sea water weak acid sub-systems with physical forcing variables (t,S,P) were obtained from Millero, 1979. The equilibrium functions are now defined on the NBS scale for the main weak acid sub-systems in sea water.

Carbonate Subsystem:

Carbonate species are involved in physico-chemical equilibria across all three phases; gas, aqueous and solid (Stumm and Morgan, 1970; Pytkowicz, 1983). In this study, only those equilibria occurring in the aqueous phase are explicitly discussed as these are the ones which determine the magnitude of the PCO_2 which then defines the magnitude of the air - sea CO_2 flux. The precipitation - dissolution pathways between the aqueous and solid phases are largely kinetically controlled and their importance in the CO_2 fluxes lies in their net impact on the concentration and speciation of the aqueous phase (Broecker and Peng, 1982; Pytkowicz, 1983).

From the point of view of CO_2 exchange between the oceans and the atmosphere, the solubility of CO_2 is the most important equilibrium reaction as it establishes the partial pressure of CO_2 in the water. The CO_2 gas flux across the air - sea boundary is a function of the physical coefficient of turbulent exchange velocity (K_w) and the biogeochemically driven partial pressure gradient across the air -sea boundary (Liss and Merlivat, 1986). The solubility equilibrium (eq. 2.15) defines the gradient by providing the

magnitude of the PCO_2 value in the aqueous system. Carbon dioxide dissolves in sea water to form a composite species [H_2CO_3*] made up of molecularly dissolved CO_2 and a very minor (~ 0.26%) contribution of the carbonic acid H_2CO_3 species (Pytkowicz, 1983).

$$CO_2 + H_2O \text{ <----------> } H_2CO_3^* \qquad \text{eq. 2.15}$$

The equilibrium constant for this equation, also referred to as Henry's Constant K_H, is given by:

$$K_H = [H_2CO_3^*]/[CO_2] \qquad \text{eq. 2.16}$$

or in a more useful way, where CO_2 is expressed as a partial pressure PCO_2, the solubility coefficient (α)(Skirrow, 1975 from Weiss, 1974). The dependence of solubility coefficient (α) on temperature, salinity and pressure is given in Skirrow, 1975 from Weiss, 1974. The most important aspect of this relationship is that temperature is a first order effect inversely correlated to solubility.

Dissolved CO_2 equilibrates with the remaining protolytic species of the carbonate system with the following equilibria:

$$H_2CO_3^* \text{ <----------> } HCO_3^- + H^+ \quad K_1' \qquad \text{eq. 2.17}$$

$$HCO_3^- \text{ <----------> } CO_3^{2-} + H^+ \quad K_2' \qquad \text{eq. 2.18}$$

in each case the equilibrium constant is apparent and operationally based on the NBS scale.

$$K1' = [HCO_3^-][H^+]/[H_2CO_3^*] \qquad \text{eq. 2.19}$$

$$K2' = [CO_3^{2-}][H^+]/[HCO_3^-] \qquad \text{eq. 2.20}$$

where $[H+] = 10^{-pHNBS}$ eq. 2.21

The relationships between speciation (log [species concentration]) and pH are graphically summarized in Fig. (2.1) which emphasises the important role of pH and indicator of the state of the weak acid equilibria.

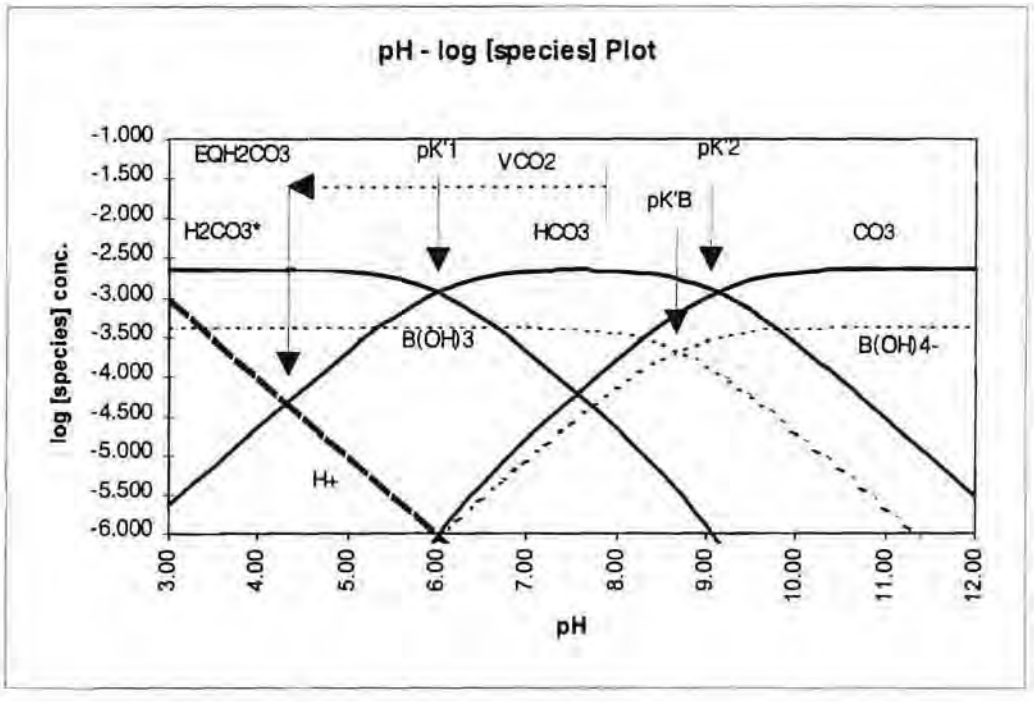

Fig. 2.1: Log [species] plot showing the relationship between carbonate and borate species concentrations against pH. It shows the pH of the $H_2CO_3^*$ equivalence point (EQH2CO3) which is used to calculate Total Alkalinity as well as VCO_2 which is the volume of strong acid required to titrate the sample from a pH 8 to the $H_2CO_3^*$ equivalence point. It also shows the pK values for the carbonate (pK_1 and pK_2) and borate (pK_B) weak acid sub-systems. The plot was set up assuming a TCO_2 of 2.3mM.

It shows that for a carbonate system where total dissolved inorganic carbon (TCO_2) equals 2.3 mmol/l at the pH of sea water (pH ~ 8) that the carbonate species concentrations are dominated by $[HCO_3^-] > [CO_3^{2-}] >> [H_2CO_3^*]$. It shows how biogeochemical processes which decrease the pH (respiration; $CaCO_3$ precipitation) shift the equilibrium so that $[H_2CO_3^*]$ increases which also increases PCO_2. Conversely, when the pH increases (photosynthesis, $CaCO_3$ dissolution) $[H_2CO_3^*]$ and PCO_2 decrease. The plot also includes

borate sub-system species equilibria ([$B(OH)_4$-]; [$B(OH)_3$]) as well as the pK values for K'_1 (~6.0), K'_2 (~9.2) and K'_B (~8.8) (Fig. 2.1).

Borate Sub-system

The borate sub-system, in terms of concentration, is the second most important weak acid system in sea water (Stumm and Morgan, 1970; Pytkowicz, 1983). No significant components of the borate sub-system are active in the marine biogeochemical cycles which could modify total boron B_T concentrations. B_T can therefore be modelled as a conservative parameter and parametrized by salinity, S, with the following function (Culkin, 1965 from Millero, 1979):

$$B_T = 0.01212 * S \text{ (mmol/l)} \qquad \text{eq. 2.22}$$

The borate weak acid equilibrium comprises two species; the borate anion [$B(OH)_4$-] and the protonated boric acid [$B(OH)_3$]:

$$B(OH)_3 + H_2O \text{ <----------> } B(OH)_4^- + H^+ \qquad \text{eq. 2.23}$$

where the equilibrium constant KB is:

$$K_B = [B(OH)_4^-]\,[H^+] / [B(OH)_3] \qquad \text{eq. 2.24}$$

The borate equilibrium constant is also defined on the NBS scale and its functional dependence on t,S,P was determined by Millero, 1979. The borate equilibrium constant and its t,S,P dependence on the SWS is summarized in Dickson and Goyet, 1994.

Minor sub-systems

The role of minor weak acid sub-systems such as SO_4^- - HSO_4^-, F^- - HF, PO_4^{3-} - H_3PO_4 are insignificant at their normal concentrations and natural pH range in sea water. They have to be considered only in special circumstances where concentrations are elevated such as in pore waters or hydrothermal vents or when the pH drops sufficiently low, such as during a Gran titration (Jagner, 1981). In the latter conditions which apply to the determination of total alkalinity TAlk, the protonated species concentrations are no longer insignificant. This last special case which is pertinent to this study will be addressed more fully in the context of the determination of TAlk by Gran titration.

Whereas in theory it would be possible to determine carbonate species equilibria in sea water using intensive variables from the equilibrium equations, in practice it is not possible to measure single ion activity coefficients except for H^+ which is constrained by a conventional scale (Culberson, 1981; Loewenthal and Marais, 1984). PCO_2 can be accurately measured (Dickson, 1984) but its determination is, because of its relationship to K_H (Henry's constant), also dependent on the careful and accurate control of environmental variables such as t,S,P. Three other mass balance (TCO_2) and capacity parameters (Total Alkalinity and Total Acidity) can be use to define the carbonate system with the added advantage that they are independent of physical environmental variables (t,S,P) (Stumm and Morgan, 1970; Pytkowicz, 1983; Loewenthal and Marais, 1984). Of these, TCO_2 and TAlk can be measure with high precision.

Capacity and Mass Parameters: Conservative Variables

Capacity and mass parameters are useful for measurement, characterization of weak acid sub-systems and prediction of changes in state arising from chemical perturbations (Stumm and Morgan, 1970). This arises for two

reasons. Firstly, they are conservative with respect to physical forcing factors such as temperature (t), salinity (S) and pressure (P) (Pytkowicz, 1983). Secondly, they change in a simple stoichiometric way with the addition and removal of carbonate species (Loewenthal and Marais, 1984). In contrast, the individual weak acid species concentrations, *inter alia* $[H_2CO_3]$, $[HCO_3^-]$, $[CO_3^{2-}]$, are governed by (t,S,P) dependent equilibrium expressions (Pytkowicz, 1983). Consequently, the individual species concentrations not only change with physical forcing factors, but also in a complex way with the addition and removal of weak and strong acid-base species. The ensuing discussion deals with the definitions of alkalinity and acidity in a general way prior to returning to the specifics of the parameters in the marine environment.

Capacity Parameters: Alkalinity and Acidity

Capacity parameters, alkalinity (alk) and acidity (acy), are defined respectively as measures of the proton accepting and donating capacity respectively of an aqueous solution of one or more weak acids (Stumm and Morgan, 1970). Proton accepting or donating capacity is measured relative to a reference or equivalent solution (Stumm and Morgan, 1970; Loewenthal and Marais, 1984). This comprises a set of reference species, one for each weak acid system present. Weak acid systems in sea water are dominated by the carbonate subsystem with a second order contribution from the borate subsystem and lower order contributions *inter alia* from sulphate, phosphate, fluoride, silicate subsystems (Pytkowicz, 1983). Contributions from the lower order subsystems are significant only under special circumstances such as in the course of certain Gran titrations (Jagner, 1981), and perhaps in the context of the chemistry of some pore water samples. For the sake of completeness these lower order weak acid subsystems are also considered initially. However, in the pH range of natural sea water their role is negligible (Stumm and Morgan, 1970).

The sea water carbonate subsystem comprises three species ($H_2CO_3^*$, HCO_3^- ,CO_3^{2-}) and the borate subsystem two (H_3BO_3, $B(OH)_4^-$) any of which can be used as reference species. For the lower order subsystems it will be shown that the least protonated species are the most convenient to use as reference species (ie: SO_4^{2-} and F^-). In general practice, reference species are selected from a standpoint of convenience relating both to ease of measurement and change in state arising from a biogeochemically driven perturbation.

From the standpoint of measurement, the solution alkalinity with $H_2CO_3^*$, H_3BO_3, SO_4^{2-} and F^- as reference species, termed Total Alkalinity (TAlk) is most amenable to accurate determination (Stumm and Morgan, 1970). The normal method for determination of TAlk, by Gran titration, provides a very accurate measure of the protons to be added (via strong acid addition) to convert the sample solution to an equivalent solution which has zero proton accepting capacity (Stumm and Morgan, 1970). Solution acidity with CO_3^{2-}, $B(OH)_4^-$, SO_4^{2-} and F^- as reference species is termed Total Acidity (TACy). This parameter is not amenable to accurate determination for numerous reasons (Loewenthal and Marais, 1984). It can however be determined through the interrelationship between capacity and mass parameters discussed below.

Equations for TAlk and TAcy are formulated from proton balance considerations (Loewenthal and Marais, 1984). The expression for TAlk comprises the sum of all the subsystem alkalinities each with their respective reference species (eq. 2.1):

$$\overline{TAlk = H_2CO_3^*Alk + H_3BO_3Alk + H_2OAlk + SO_4^{2}Alk + F\,Alk +} \qquad \text{(eq. 2.25)}$$

Where XAlk = proton accepting capacity of a particular weak acid subsystem with reference species X.

The same expression in terms of species concentrations becomes (eq. 2.26):

$TAlk = \{2*[CO_3^{2-}] + [HCO_3^-]\} + \{B(OH)_4^-\} + \{[OH^-] - [H^+]\} + \{ - [HSO_4^-]\} + \{ - [HF]\} + ...$ eq. 2.26

The expression for TAcy comprises the sum of all subsystem acidities each with their respective reference species (eq. 2.27):

$TAcy = CO_3^{2-}Acy + B(OH)_4^-Acy + H_2OAcy + SO_4^{2-}Acy + F^-Acy +$ eq. 2.27

Where Y-Acy = proton donating capacity of a particular weak acid subsystem with reference species Y.

The same expression in terms of species concentrations becomes:

$TAcy = \{2*[H_2CO_3^*] + [HCO_3^-]\} + \{[H_3BO_3]\} + \{(H^+) - [OH^-]\} + \{[HSO_4^-]\} + \{[HF]\}$ ... eq. 2.28

Note that for the lower order subsystems (SO_4^{2-}, F^-) the same reference species apply to both TAlk and TAcy. The reason being that in the overall relationship linking TAlk, TAcy to the mass parameters the lower order terms then cancel out (see below). In any case, in the pH range of sea water the concentrations of the lower order terms (H_2OAlk / H_2OAcy and lower terms) are negligible compared with the carbonate and borate subsystems and can be ignored (Stumm and Morgan, 1970). The total capacity parameter expressions (eqs. 2.29, 2.30) now simplify to the sum of the carbonate and borate subsystem species:

$TAlk = H_2CO_3\ Alk + B(OH)_4^-Alk$ eq. 2.29

$TAcy = CO_3^{2-}Acy + B(OH)_3\ Acy$ eq. 2.30

Because it is not possible to experimentally determine TAcy it has to be quantified indirectly. This is done through the accurate determination of other system parameters and the use of an interrelationship linking TAcy to these parameters. Perhaps the most appropriate choice to measure are TAlk and the two total mass parameters (TCO_2 and B_T) all of which can be determined with high precision (Dickson, 1994).

Mass Parameters

For each subsystem, these parameters provide a mass balance of the sum of concentrations of the individual weak acid species. For the carbonate and borate subsystems, the respective mass balances are:

$$TCO_2 = [H_2CO_3^*] + [HCO_3^-] + [CO_3^{2-}] \qquad \text{eq. 2.31}$$

$$B_T = [\ B(OH)_3\ ] + [\ B(OH)_4^-\ ] \qquad \text{eq. 2.32}$$

Where [X] is the concentration of species X (mM).

The desired relationship linking TAcy to TAlk and the mass parameters TCO_2 and B_T is obtained by adding the expressions for the two capacity parameters (eqs. 2.26, 2.28),

$$TAlk + TAcy = 2 * TCO_2 + B_T \qquad \text{eq. 2.33}$$

An equation in which the lower order weak acid terms fall away. This interrelationship shows that TAcy can be accurately determined provided that TCO_2, B_T and TAlk are accurately measured.

2.3 Sampling and Analytical Methods

2.3.1 Carbonate System

Sampling: pH

Although pH is not part of the core JGOFS methods (UNESCO, 1994) a number of detailed protocols exist which address the procedural requirements and problems in some detail (Jagner, 1981; Grasshoff, 1983; Dickson, 1994). The sampling protocol used in this study was adapted from the most recent protocol which was designed to be used for pH measurement in the SWS scale (Dickson, 1994). The procedural steps took cognisance of the potential sources of error in the method and tried as far as possible to control them so as to minimize the uncertainty. A detailed discussion of the error estimates and their impact on calculated PCO_2 values is set out below.

Water samples were in all cases obtained from 5 litre General Oceanics Niskin bottles triggered on a Neil - Brown CTD-Rosette system. pH samples were collected into 120ml BOD bottles after flushing with 3 bottle volumes through a siphon system identical to that used for Winkler oxygen determinations. After spiking with 50µl of a 50% saturated solution of $HgCl_2$ the BOD bottles were tightly stoppered and equilibrated to a constant temperature in a water bath (20.0°C or 25.0°C) for 2 hours prior to pH measurement.

Sampling: Total Alkalinity

Total Alkalinity samples were taken from the same BOD bottles used for pH analysis after the pH determinations had been completed. These provided 2 50ml replicates. In most instances they were done in the course of the cruise but if that was not possible they were done ashore within 2 weeks.

Analysis: pH

pH determinations were carried out in all cases with a Radiometer pHM 84 meter with a 3 decimal point display and a Radiometer (GK2401C) combined reference - glass electrode. A new electrode was purchased for each field trip and used for the entire period which was usually approximately 2 weeks. The calibration of the pH electrode was done using NBS buffers (Radiometer pH 4 (S1316) and pH 7 (S1326) equilibrated to the same temperature as the samples in a water bath at either 20.0°C or 25.0°C. The electrode assembly included a rubber fitting which when the electrode was placed inside a BOD bottle would create a seal between the electrode and the bottle neck. When not in use the electrode was stored in pH 4 NBS buffer to minimise bacterial growth on the glass membrane and the ceramic liquid junction frit.

In the calibration procedure the electrode itself was allowed to equilibrate to the working temperature in the pH 7 buffer prior to the measurement. The calibration itself was an iteration procedure between pH 7 and pH 4 buffers until stable values (±0.002) were obtained from both buffers at the appropriate temperature. Usually, stable and reproducible values were obtained by the 2nd iteration. Prior to measuring the sample pH values the electrode was immersed into filtered sea water, also at the working temperature, for 15-20 mins to condition the electrode. The change in the ionic strength between the NBS buffers (low ionic strength) and sea water (high ionic strength) induces changes to the liquid junction potential discussed in detail earlier. It usually took no more than 5-10 minutes for stability to be reached. This process also insured that the whole electrode assembly, including the KCl bridge and reference electrode were stabilized at the working temperature.

Samples were measured in sequence starting from the deepest one where potential problems associated with DOM or bacterial films were least likely. In each case the electrode was immersed into the BOD bottle until the seal was

in place after which it normally did not take more than 1 minute for a stable reading to be achieved (in practice a 3 minute period was adopted). All the readings were taken with no stirring of the sample to minimize the problem of irreproducibility arising from a difference in stirring potentials between the buffers and the sea water samples. If not addressed, this factor can contribute an uncertainty of more than 0.01 pH units to the readings (Culberson, 1981). At the end of the sample batch, the electrode was washed with MilliQ water and stored in pH 4 buffer until the following calibration. The electrode was calibrated before every new batch of samples.

The effectiveness of the method in yielding reproducible results is best assessed in the context of field samples where a number of samples are taken at different depths within a well mixed layer. This was done in the Hondeklip Bay transect (see Chapter 4) where on the outer part of the transect there was a well mixed surface layer of 20-30m. The number of readings, means and standard deviations are summarized on Table 2.2:

Table 2.2: Assessment of the uncertainty associated with pH measurements in the sea. Samples taken from a well mixed surface layer from the Hondeklip Bay transect

Station	Samples	pH (mean)	pH (SD)
117	4	8.169	0.004
119	5	8.224	0.005
121	4	8.222	0.003

Considering that even in a well mixed layer there could be some slight variations in biological activity these standard deviations reflect a conservative assessment of the potential measurement error. The impact of this experimental error on the CO_2 fluxes is addressed below in the context of all sources of error.

Analysis: Total Alkalinity

Total alkalinity is defined as the proton accepting capacity of a solution of weak acids with reference to the most protonated form of the carbonate and borate species. The practical expression of this definition in respect of carbonate solutions is: the mass concentration of protons required to shift the equilibrium of a carbonate solution to the $H_2CO_3^*$ equivalence point (Fig. 2.1). The volume of strong acid (V_{CO2}) required to shift the equilibrium from its natural pH (pH_N) to the $H_2CO_3^*$ equivalence point (EQ_{H2CO3^*}) is the equivalence volume. Its determination provides a measure the Total Alkalinity (TAlk) and in this study (V_{CO2}) was obtained using a potentiometric Gran titration (Hansson and Jagner, 1973; Jagner, 1981; Almgren *et al* 1983; Loewenthal and Marais, 1984). A major practical advantage of this measurement is that in line with the definition of total alkalinity (eq. 2.26) it is independent of any CO_2 losses which occur during the acidification.

The Gran Titration

The Gran linearization technique (Gran, 1952) whose use in the characterisation of sea water was proposed by (Dyrssen and Sillen, 1967), is based on the assumption that in each part of the titration curve on either side of the equivalence point there exist a dominant reaction (Jagner, 1981; Loewenthal and Marais, 1984). In this study the $H_2CO_3^*$ equivalence point (Fig. 2.1) the chosen part of the titration curve was beyond the equivalence point where $pH < pH_{CO2} \sim 4$. In this pH region the increase in $[H^+]$ is proportional to the amount of strong acid added (Jagner, 1981). It does not therefore require that it be conducted in a sealed reaction vessel. In this method the following definitions hold:

V_0 :- Sample volume (50.00ml)

V_x :- Acid (HCl ~ 0.1M) volume added.

V_{CO2} :- Volume of acid required to reach the equivalence point

M_{HCl} : - Acid strength (Molarity)

$$TAlk = \frac{(V_{co2} - V_x) \cdot M_{HCl}}{(V_0 + V_x)} \qquad \text{eq. 2.34}$$

In the pH region of the $H_2CO_3^*$ equivalence point $TAlk \equiv -[H^+]$ because all other terms of the TAlk mass balance (eq. 2.26) become insignificant. Thus eq.(2.34) can be re-arranged as:

$$[H^+] (V_0 + V_x) = (Vx - V_{CO2}) M_{HCl} \qquad \text{eq. 2.35}$$

This yields the first Gran function (F1):

$$F_1 = (V_0+V_x) [H^+] = (V_x - V_{CO2}) M_{HCl} \qquad \text{eq. 2.36}$$

The Gran plot is generated by plotting F_1 vs V_x. From the right-hand side of eq. 2.36 the plot will be linear and the extrapolation will intercept the X axis at V_{CO2}.

The example described above is not applicable to real sea water because it does not make provision for the effect of other protonated weak acid species in the pH range 3 - 4. The equilibrium reactions which can generate significant side reactions are:

Equilibria	Total Conc. (mmol/l)
$SO_4^{2-} + H^+ <----------> HSO_4^-$	28
$F^- + H^+ <----------> HF$	0.073
$HCO_3^- + H^+ <----------> H_2CO_3$	2

Table 2. Spreadsheet display used to calculate the H2CO3 equivalence volume VCO2 from the results of a Gran titration (Vx and pH). The output is the Gran Function F1 which is corrected for the minor side reactions. The statistics of the regression are also shown as are the equilibrium constants calculated for the experimental temperature and salinity.

Vco2 (ml)	0.969

ample Vo	Acid Vol.									
V0	VX	PH	H+	HSO4-	HF	HCO3	SUM	F1	TEMP	SALT
50	0.00	8.000	1.00E-08	2.55E-09	2.46E-10	1.86E-03	1.86E-03	9.28E-02	15	34.7
	1.118	3.669	2.14E-04	5.45E-05	4.91E-06	7.99E-06	2.82E-04	1.44E-02		
	1.131	3.639	2.30E-04	5.84E-05	5.24E-06	7.46E-06	3.01E-04	1.54E-02		
	1.150	3.590	2.57E-04	6.54E-05	5.82E-06	6.66E-06	3.35E-04	1.71E-02		
	1.200	3.483	3.29E-04	8.36E-05	7.28E-06	5.21E-06	4.25E-04	2.18E-02		
	1.250	3.390	4.07E-04	1.03E-04	8.80E-06	4.21E-06	5.24E-04	2.68E-02		
	1.300	3.320	4.79E-04	1.22E-04	1.01E-05	3.58E-06	6.14E-04	3.15E-02		
	1.350	3.258	5.52E-04	1.40E-04	1.14E-05	3.11E-06	7.07E-04	3.63E-02		
	1.400	3.204	6.25E-04	1.58E-04	1.27E-05	2.75E-06	7.99E-04	4.11E-02		
	1.450	3.156	6.98E-04	1.77E-04	1.39E-05	2.46E-06	8.91E-04	4.59E-02		
	1.500	3.114	7.69E-04	1.95E-04	1.50E-05	2.23E-06	9.81E-04	5.05E-02		
	1.550	3.076	8.39E-04	2.12E-04	1.61E-05	2.05E-06	1.07E-03	5.52E-02		
	1.600	3.040	9.12E-04	2.31E-04	1.71E-05	1.88E-06	1.16E-03	5.99E-02		

Total Concentrations		mol/l
SO4	F	HCO3
0.028008	7.24E-05	0.001983

POLYNOMIAL CONSTANTS					
Carbonate (MERBACH, 1973)				SO4	F
K1s	K1	K2s	K2	KSO4	KF
0.0221	290.9097	0.9805	207.6548	647.58	1590.2
34.02	-14554.2	-92.65	-11843.8	6.3451	12.641
	-45.0575		-33.6485	0.019085	1.525
		-0.03294		0.5208	0.7223
				0.7223	

Regression Output:		
Constant		-0.09203
Std Err of Y Est		0.000125
R Squared		0.999944
No. of Observations		12
Degrees of Freedom		10
X Coefficient(s)	0.095019	
Std Err of Coef.	0.000225	

EQUILIBRIUM CONSTANTS					
lnK1	ln(K1)s	ln(K1*)	K1*	KSO4	KF
-14.7846	0.826019	-13.9586	8.67E-07	9.103537	340.0077
ln(K2)	ln(K2)s	ln(K2*)	K2*		
-24.0196	2.737748	-21.2618	5.72E-10		

The inclusion of these side reactions is shown in equation 2.37. In this modified form the Gran function is now written as $F_{1'x}$.

$$F_{1'x} = (V_0+V_x)\ ([H^+]_x + [HSO_4^-]_x + [HCO_3^-]_x + [HF]_x) \qquad \text{eq. 2.37}$$

where x refers to the value after V_x ml of strong acid have been added. The concentrations of each of the protonated species are calculated using the respective equilibrium or dissociation constants and their respective temperature and salinity dependence functions (Jagner, 1981).

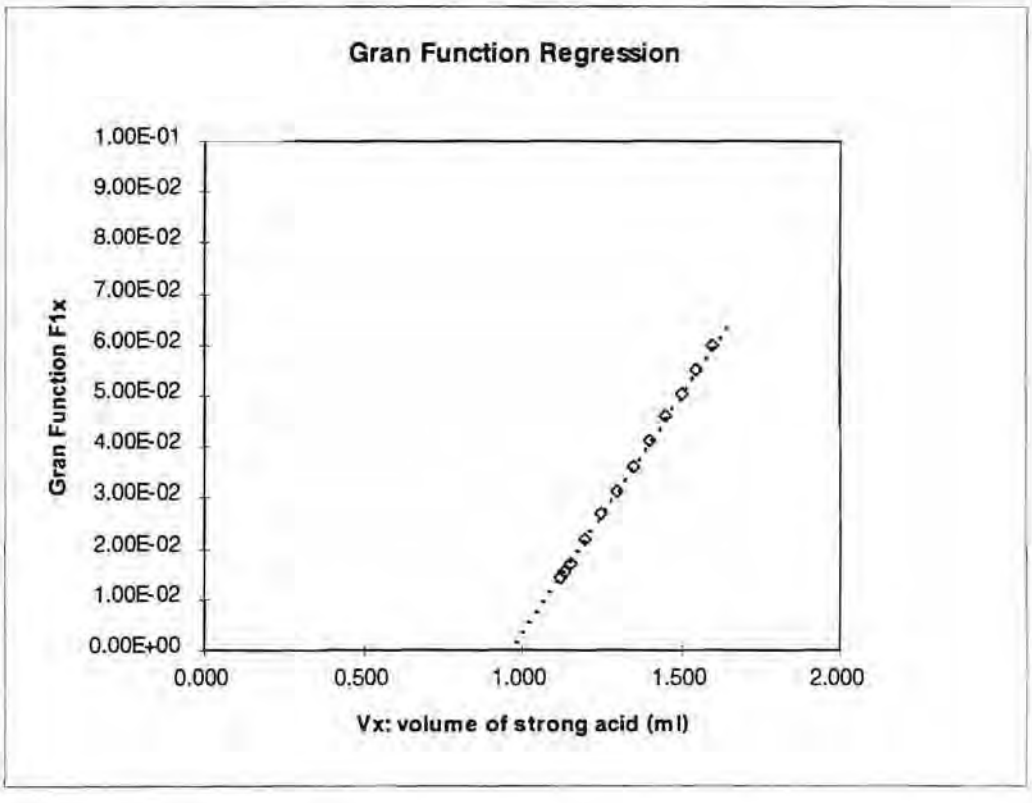

Fig 2.2: Plot of a Gran function (F'_1) regression showing the linearity of the relationship beyond the $H_2CO_3^*$ equivalence point. The equivalence volume V_{CO2} is calculated by extrapolating the regression to the point $F'_1 = 0$.

An example of the numerical procedure used to calculate the equivalence volumes for the sea water samples is shown on Table 2.3. The titration data is in the first 3 columns (V_0: sample volume; V_x: acid added; pH: pH

corresponding to the acid volume added). In all cases an initial amount of HCl was added to bring the pH to below 4 (typically 1.1ml). The Gran titration was carried out in the pH range 3-4. For each point in the titration a value for the Gran function F_{1x} was calculated (corrected for all side reactions using equilibrium constants whose values in respect of t and S were calculated from polynomial functions whose constants are also given). A linear regression was executed between F_1 and V_x whose intercept at $F_1 = 0$ gives the equivalence volume (V_{CO2}). A typical regression is depicted in Fig. 2.2 where the linearity of the relationship is emphasised by an $r^2 > 0.9999$.

The use of several (N > 10) points in the titration to calculate the equivalence volume not only provides confidence in its value but is a key aspect of the accuracy of the Gran method.

The methodological steps adopted were as follows:

Preparation of reagents and standards

Internal Standard: the anhydrous Na_2CO_3 (AnalaR) internal standard was dried at 280°C for 6 hours (Dickson, 1994) and cooled in a silica gel desiccator under vacuum. An amount of the dried Na_2CO_3 was precisely weighed to make up a standard with a nominal concentration of 1.25mM which corresponds to an Alkalinity of 2.5 mM. The standard was made up in a 0.7M NaCl (AnalaR) solution (Dickson, 1994) to simulate the ionic strength of sea water. The standard was used to calibrate the strong acid.
Strong Acid: the strong acid used for the Gran titrations was ~ 0.1M HCl made up in 0.6M NaCl solution. The acid was calibrated prior to every batch of samples being processed.
External Standard: An external TAlk standard (Batch 21) was obtained towards the end of the field programme from Dr A.G. Dickson's laboratory with the following characteristics: Salinity: 34.53psu; TAlk: 2258 ± 1.2 µmol/kg (measured by Prof. Frank Millero) (AG Dickson, pers.com.).

Determination of the NaCl background electrolyte blank

The first step of the calibration procedure was to constrain the blank introduced by the use of 0.7M NaCl as a background electrolyte to distilled water. This was done by running a Gran titration (3 replicates) of a 0.7M NaCl blank solution and calculating its own equivalence volume. Typically this value was a significant 3 - 4% of the equivalence volume for the Na_2CO_3 standard which made it an essential correction.

Standardization of the acid (~ 0.1M HCl)

The acid was standardized against the internal Na_2CO_3 standard (3 replicates) using a Gran titration procedure which had to agree to within 0.002 ml. The acid strength used for the subsequent calculation of the sea water sample alkalinities was corrected for the 0.6M NaCl used as a background electrolyte. The calculation is done according to eq.(2.38) where the acid strength M_{HCl} is a function of the molarity of the Na_2CO_3 standard (M_{Na2CO3}), the volume of standard (VNa2CO3), the equivalence acid volume (VeHCl) corrected for the NaCl blank (V_{eNaCl}).

$$M_{HCl} = (M_{Na2CO3} * V_{Na2CO3})/ (V_{eHCl} - V_{eNaCl})*2 \qquad \text{eq. 2.38}$$

The standardized acid is immediately used to run the Gran titration on the sea water samples.

Determination of TAlk in sea water samples

Sea water sample TAlk were determined through the Gran titration procedure with HCl whose molarity had been standardized with the internal Na_2CO_3 standard.

The value of TAlk is calculated with expression eq. 2.39 where M_{HCl} is the standardized strength of the strong acid, V_{eHCl} is the equivalence volume calculated from the Gran titration regression and V0 is the sample volume which was in the course of this work 50.00ml.

$$TAlk = M_{HCl} * V_{eHCl} / V_0 \qquad \text{eq. 2.39}$$

The high degree of confidence in the results generated by this method are supported by TAlk values produced when the procedure was applied to the external standard. The standard was sent with a certified TAlk of 2258 μmol/Kg Total Alkalinity (AG Dickson, Pers.Comm). This corresponded to an equivalent concentration of 2311 μmol/l (ϱ = 1.0236) on the molarity scale. The average of 10 TAlk standard runs from the Gran titration for the same external standard was 2310μmol/l where the 1μmol/l difference (< 0.1%) is insignificant.

Calculations: Species and Capacity Parameters

The calculation of the carbonate system intensive and conservative variables was carried out with the following steps executed through an algorithm coded in Turbo Pascal:

Using pH (NBS) values measured at laboratory temperature conditions (pHLAB) and TAlk obtained from the Gran titration and NBS scale equilibrium constants (at lab temperatures), the corresponding TCO_2 values were calculated.
The *in situ* pH (pHSEA) was then calculated by solving the cubic expression in terms of $[H^+]$ using TA, TCO_2, B_T and equilibrium constant values calculated for in situ (t,S,P) (Millero, 1979).

The cubic expression was solved for $[H^+]$ using a Newton's method approach which was initiated by an approximate guess and stopped by a convergence where the difference was less than $1*10^{-12}$.

Using the *in situ* pH and TAlk values the intensive variables (H2CO3*, HCO_3^-, CO_3^{2-} and PCO_2) were calculated for the actual physical conditions pertaining to the sample site and depth.

The programme **inputs** were sample number, depth (D)(m), *in situ* temperature (TSEA)(°C), salinity (SAL) (psu), total alkalinity (TAlk) (mmol/l), laboratory pH (pHLAB) and laboratory temperature (TLAB). The programme **outputs** were (Table 2.4) sample number, D, TSEA, SAL, TAlk(mmol/l), total acidity (TACY) (mmol/l), carbonate alkalinity (CAlk)(mmol/l), TCO_2 (mmol/l), *in situ* pH (pHSEA), H2CO3* (mmol/l), $[HCO_3^-]$ (mmol/l), $[CO_3^{2-}]$ (mmol/l) and PCO_2 (µatm). The example given on Table 2.4 below refers to inputs obtained from Millero, 1979 as a benchmark to test that the routines would produce the expected outputs. The observed insignificant difference in the calculated PCO_2 value (472 µatm vs. 471 µatm) is ascribed to differences in the Newton's Method sub-routine.

Sensitivity analysis of the impact of experimental error on PCO_2

A sensitivity analysis of the impact which measurement uncertainty in the input variables (t,S,TAlk,pH) has on the PCO_2 and other carbonate intensive variables is summarized in Table (2.4).

The first set of 3 values tests the effect of an uncertainty of 0.01 pH units in the pH determinations where the reference pH was 8.000 and other input variables are fixed. It shows that the impact on PCO_2 is to induce an uncertainty of 19µatm which even though it is a worst case scenario (realistically ~ 10µatm) emphasises the limitations of pH as a master variable when changes in PCO_2 are small. In the Benguela System where variability

in PCO_2 values is high (160 - > 1000 μatm) the constraint of a 10μatm uncertainty will not impact significantly on CO_2 flux predictions.

Table 2.4a, b: Results from a sensitivity analysis of the main potential sources of error: pH (8.000±0.01), Talk (2.451±0.005 mM) and temperature (25.00±0.05°C) and salinity (35.00±0.01) (Table 2.4a). The impact of these ranges of uncertainty are summarized in Table 2.4b where pH can be seen to be the only significant factor in respect of PCO_2.

Variable	D	TSEA	SAL	TA	TACY	CA	TCO2	PHSEA	H2CO3	HCO3	CO3	PCO2
Benchmark	0	25.00	35.00	2.454	2.292	2.359	2.161	8.151	0.014	1.935	0.212	471
pH	0	25.00	35.00	2.450	2.454	2.378	2.240	8.000	0.021	2.060	0.159	710
pH	0	25.00	35.00	2.450	2.464	2.380	2.245	7.990	0.021	2.067	0.156	729
pH	0	25.00	35.00	2.450	2.444	2.377	2.235	8.010	0.020	2.052	0.163	691
TAlk	0	25.00	35.00	2.449	2.453	2.377	2.239	8.000	0.021	2.059	0.159	709
TAlk	0	25.00	35.00	2.451	2.455	2.379	2.241	8.000	0.021	2.061	0.160	710
TAlk	0	25.00	35.00	2.445	2.449	2.373	2.235	8.000	0.021	2.055	0.159	708
TAlk	0	25.00	35.00	2.455	2.458	2.383	2.244	8.000	0.021	2.064	0.160	711
Temperatur	0	25.05	35.00	2.450	2.454	2.378	2.240	8.000	0.021	2.060	0.159	711
Temperatur	0	24.95	35.00	2.450	2.454	2.378	2.240	8.000	0.021	2.060	0.159	708
Salinity	0	25.00	35.01	2.450	2.454	2.378	2.240	8.000	0.021	2.060	0.159	710
Salinity	0	25.00	34.99	2.450	2.454	2.378	2.240	8.000	0.021	2.060	0.159	710

Variable	Error	PCO2
pH	0.01	19
TAlk	0.005	< 2
Temp	0.05	< 2
Sal	0.01	< 1

The second variable to be tested was TAlk where two uncertainty ranges were tested: a best case where TAlk = 0.001mmol/l and a worst case where TAlk = 0.005 mmol/l. The observed uncertainty from the worst case of < 2 μatm on the PCO_2 value shows that the Gran titration based TAlk determination is an almost insignificant source of uncertainty. Similarly with temperature and salinity uncertainties which are outside the expected performance of calibrated CTD devices the induced effect on PCO_2 is on par or less than was the case with TAlk. These results also show that to obtain PCO_2 resolutions of 1μatm or better which are required to monitor interannual PCO_2 changes, it is necessary that TAlk be resolved to within 2 μmol/l, temperature to 0.02°C and salinity to 0.01psu.

2.4 Other Sampling and Analytical Methods

2.4.1 Nutrients

Nitrate

All nitrate analyses were carried out ashore with a standard autoanalyser method (Grasshoff, 1983) on frozen samples collected in the course of each cruise.

Ammonium

Water column ammonium determinations were carried out on board on fresh samples using the standard indo-phenol method (Koroleff, 1983).

Oxygen

Oxygen determinations were carried out on board using a manual Winkler titration procedure whose details can be found in Grasshoff, 1983.

2.4.2 Sediments

Sampling

Sediment vibracores were collected along an offshore transect off the Namibian coast. Approximately 50ml of sediment samples were cored out of the vibracore at 10cm intervals into polythene vials which were frozen at -25°C until ready for analysis. Onshore, the core sub-samples were de-frosted in the sealed vials and amounts of nominally 50gms were weighed and transferred under nitrogen into centrifuge containers. The interstitial waters were separated by centrifuging at 4000 RPM for 20mns and carefully decanted into acid washed tubes ready for NH_4^+ analysis.

Analysis: Ammonium

Interstitial Water Fraction

The ammonium concentrations in the interstitial waters were determined with the same indo-phenol method as was the case for the water column except that the calibration curves were obtained with standards over a concentration range 20 - 100μM. In most instances the interstitial water samples had to be diluted to maintain the absorbance readings in the ideal range of 0.3 - 0.8 AU. The usual care was taken to obtain reagent blanks which were used to correct the standard and sample absorbances.

Adsorbed Fraction

The adsorbed fraction of the NH_4^+ in the sediments was analysed according to the method described by Mackin and Aller, 1984. This method defined adsorbed NH_4^+ as that which is extractable with 2M KCl. The extraction was carried out as a two step procedure to improve the efficiency of the extraction. The adsorbed fraction of the NH_4^+ was measured as the concentration in the KCl using the same indophenol method (Koroleff, 1983).

Chapter 3

3. A Carbonate Stoichiometry Vector Plot

3.1 Background

Conventionally, biogeochemical carbon pumps are mechanisms which drive the carbon fluxes across the permanent oceanic pycnocline against the natural TCO_2 gradient (Volk and Hoeffert, 1985; Longhurst and Harrison, 1989; Maier-Reimer, 1993) One of the most important consequences of the activity of carbon pumps is their impact on the magnitude and direction of the air - sea CO_2 flux (Volk and Hoeffert, 1985; Siegenthaler, 1986). Three principal carbon pumps have been identified, two of which are biologically mediated and a third which is physically driven (Keir, 1993). The two biological pumps comprise the organic carbon pump (C_{Org}) controlled by the photosynthesis - respiration couple (Siegenthaler, 1986; Middelburg et al., 1993), and the inorganic carbon pump (C_{Ing}) which is driven by the deposition and dissolution of mineral carbonates (Broecker and Peng, 1982; Milliman, 1993). The third is a physico-chemical pump, also called the "solubility pump", which is driven by the increased CO2 solubility in cold surface waters and their subduction at high latitudes (Keir, 1993). The two biological pumps can be represented in the form of reversible equations (eqs. 3.1 and 3.2). In each case the forward step depicts the formation of biogenic particles characteristic of euphotic marine environments (Broecker and Peng, 1982; Longhurst and Harrison, 1989; Siegenthaler, 1986). The reverse step depicts the remineralization of these biogenic particles in subsurface and benthic environments (Broecker and Peng, 1982; Middelburg et al., 1993; Milliman, 1993). The depth at which this remineralization - dissolution occurs is a function of such factors as particle size, grazing (Longhurst and Harrison,

1989), aggregate formation (Ittekkot, 1993) and carbonate equilibrium state (Broecker and Peng, 1982).

$$CO_2 + H_2O \underset{\text{<-- Respiration ---------}}{\text{--- Photosynthesis--->}} CH_2O + O_2 \qquad C_{Org} \text{ pump} \qquad \text{eq. 3.1}$$

$$Ca_2^{+} + 2HCO_3^{-} \underset{\text{<---- Dissolution}}{\text{Deposition ->}} CaCO_3 + CO_2 + H_2O \qquad C_{Ing} \text{ Pump} \qquad \text{eq. 3.2}$$

The C_{Ing} pump (eq. 3.2) has a paradoxical influence on marine carbon fluxes. The forward step decreases Total Dissolved Inorganic Carbon (TCO_2) and simultaneously increases PCO_2 (Broecker and Peng, 1982). Similarly, the reverse reaction decreases PCO_2 and increases TCO_2. In contrast, with the C_{Org} pump (through photosynthesis - respiration), changes in TCO_2 and PCO_2 are correlated (Skirrow, 1975). The magnitude and direction of CO_2 fluxes across the air - sea boundary is governed by the PCO_2 gradient with the atmosphere. It is therefore necessary to assess and predict the way in which the C_{Org} and C_{Ing} pumps interact with each other to effect changes to PCO_2. Understanding this interaction is increasingly relevant as remote sensing (Groom and Holligan, 1987) and in situ rate measurements (Holligan et al. 1993) provide a more realistic assessment of the spatial and temporal scales of coccolithophore bloom dynamics on the global carbon cycle (Westbroek et al, 1993). This is apparent in both oceanic (Robertson et al, 1994, Holligan et al., 1993; Townsend et al., 1993) and coastal upwelling environments (Mitchell-Innes and Winter, 1984; Giraudeau et al. 1993) assumed to be dominated by diatoms and flagellates (Hutchings et al. 1995).

Two aspects of the global carbon cycle are driven by the interaction of the two marine biogeochemical pumps. Firstly, the **magnitude** of the total carbon flux ($\Delta TCO_2 = \Delta C_{Org} + \Delta C_{Ing}$) out of the surface layers and into the pelagic, deep or benthic environments. The magnitude of this flux plays a role both in counterbalancing the upwelling of carbon enriched deep waters to the surface (Bolin, 1986; Siegenthaler, 1986; Watson, 1995) and in the long term removal

of carbon from the biosphere through sedimentation (Tsunogai and Noriki, 1991; Milliman, 1993; Middelburg et al., 1993; Watson, 1995). Secondly, and perhaps more importantly in so far as air - sea exchange of CO_2 is concerned, is the ratio or **stoichiometry** (C_{Org}:C_{Ing}) in which these fluxes occur (Tsunogai and Noriki, 1991; Broecker and Peng, 1989; Archer and Maier-Reimer, 1994). This stoichiometric ratio governs the magnitude of the PCO_2 change which accompanies a given change in TCO_2. Predictive assessment of the magnitude of the PCO_2 change arising from changes in the relative magnitudes of the C_{Org} and C_{Ing} pumps within and between oceanic carbon reservoirs is central to both modelling and remote sensing applications within the JGOFS programme.

This study develops a capacity parameter vector model which is used to quantify in a direct way the stoichiometry of the Organic (C_{Org}) and Inorganic (C_{Ing}) carbon pumps. This model introduces a modification which builds on the Deffeys approach (Deffeys, 1965) where the TAlk / TCO_2 ordinate parameters in the latter are replaced with the capacity parameters Total Alkalinity (TAlk) and Total Acidity (TAcy). The vector model provides *inter alia* three useful products:

1: an explicit characterization of the (C_{Org}:C_{Ing}) stoichiometry
2: a graphical relationship between the stoichiometry of carbon addition / removal and PCO_2 change.
3: Assessment of the separate contributions of temperature (solubility pump) and biology (C_{Org} and C_{Ing} pumps) to PCO_2 change.

The required background and definitions for the capacity parameters were provided above in Chapter 2. The following sections make use of those definitions as the basis for the vector plots which describe the stoichiometric relationships between the organic C_{Org} and inorganic C_{Ing} carbon pumps.

3.2 Effects of the addition / removal of carbonate species on TAlk, TAcy and TCO_2.

Capacity and mass parameters change in a simple stoichiometric fashion with the addition / removal of weak and strong acid species (Stumm and Morgan, 1970; Loewenthal and Marais, 1984). For the change in TCO_2:

$$\Delta TCO_2 = \Delta^\circ CO_2 + \Delta^\circ HCO_3^- + \Delta^\circ CO_3^{2-} \qquad \text{eq. 3.3}$$

Where Δ° is the addition (+ve sign) / removal (-ve sign) to or from solution of Δ° mM of species X. For changes in TAlk and TAcy and considering only carbonate and borate weak acid species,

$$\Delta TAlk = 2 * \Delta^\circ CO_3^{2-} + \Delta^\circ HCO_3^- + \Delta^\circ B(OH)_4^- \qquad \text{eq. 3.4}$$

$$\Delta TAcy = 2 * \Delta^\circ CO_2 + \Delta^\circ HCO_3^- + \Delta^\circ B(OH)_3 \qquad \text{eq. 3.5}$$

It should be noted that the above equations and notation (Δ°) reflects the influence on mass and capacity parameters of an external source of weak acids species; it does not reflect changes in the **concentrations** of weak acid species in solution. These can only be determined by introducing equilibrium expressions.

Examination of the expressions (eqs. 3.4 and 3.5) above indicates that TAlk is independent of the addition / removal of CO_2 while TAcy is independent of CO_3^{2-} addition / removal. From a marine biogeochemical standpoint this is important because they are independently driven by the two biogeochemical pumps. The C_{Org} pump which drives CO_2 changes impacts only on TAcy whereas the C_{Ing} pump which drives CO_3^{2-} change impacts only on TAlk. Consequently, these two capacity parameters together provide a direct assessment of the magnitudes of the C_{Org} and C_{Ing} components of the biological pump in the marine environment. This forms the basis for the stoichiometric vector model developed in this study. Though such vector

models have been used in the past (Deffeys, 1965) these did not explicitly separate the effects of the biogeochemical pumps.

3.3 The Deffeys Model Approach

The Deffeys model was originally developed to link intensive parameters, such as pH and CO_3^{2-} to measurable conservative parameters (Deffeys, 1965). In its original form the model was limited to a single component weak acid system (the carbonate subsystem) in water (Deffeys,1965). The two conservative parameters selected (Alkalinity (Alk) and TCO_2) were utilized as ordinates to a vector diagram. The vector model is implemented by plotting the initial and final states (as represented by Alk and TCO_2) before and after a biogeochemical perturbation.

The extension of the Deffeys model to sea water requires that the borate subsystem be included. The alkalinity parameter in the vector diagram becoming TAlk as defined by eq. 3.6. It should be noted that this extension is possible only if the total borate BT remains constant. The two components of the extended Deffeys diagram (TAlk and TCO_2) are algebraically defined as:

$$TAlk \cong \{2^* [CO3\text{-}] + [HCO_3^-]\} + \{[B(OH)_4^-]\} \qquad \text{eq. 3.6}$$

$$TCO_2 = \{[H2CO3]^* + [HCO_3^-] + [CO_3^{2-}]\} \qquad \text{eq. 3.7}$$

Though these parameters are independent in respect of their definitions (TAlk: proton accepting capacity; TCO_2: total dissolved inorganic carbon) they are simultaneously impacted by the principal forcing factor in the C_{Ing} pathway: ie: input or removal of CO_3^{2-}. This mutual dependence on the C_{Ing} pump is central to the problem of using the Deffeys model to interpret in a direct way the C_{Org}:C_{Ing} stoichiometry. To better understand the limitations, it is necessary to review briefly the application of this model to the marine biogeochemical pumps. This is best illustrated by considering two extreme

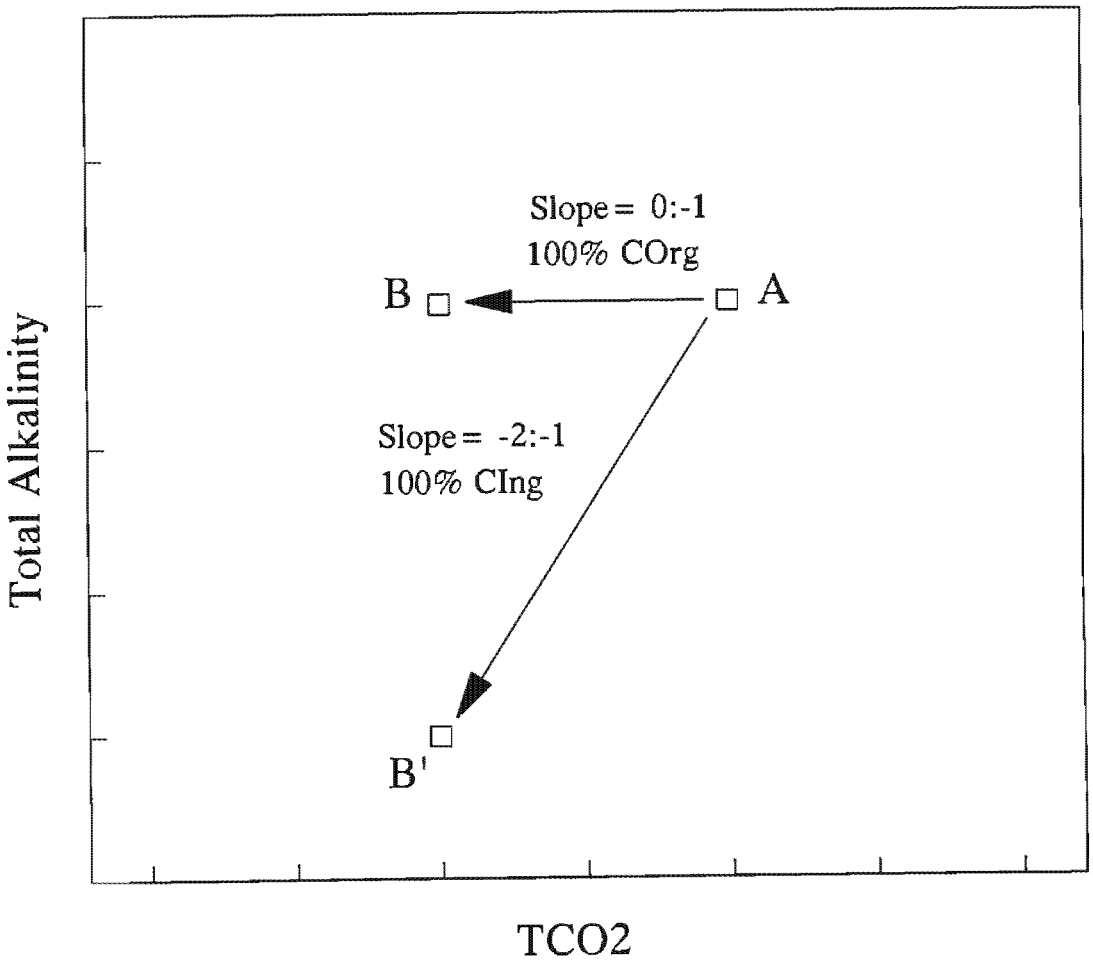

Fig. 3.1: A Deffeys type vector diagram depicting the relationship between the vector slope and the two extremes of the C_{Org} and C_{Ing} stoichiometries. It shows that the C_{Org}:C_{Ing} stoichiometry cannot be predicted directly by the vector slope when TAlk and TCO_2 are used as the cordinates for the vector plot.

perturbations: one in which only the C_{Ing} pump is operative ($\Delta C_{Org} = 0$), and a second in which only the C_{Org} pump is operative ($\Delta C_{Ing} = 0$).

In the first case when only C_{Ing} is operative (C_{Org}=0), one molar unit of carbon (ie: one molar unit of CO_3^{2-}) is removed, then from eqs. 3.6 and 3.7: ΔTCO_2 = -1 and $\Delta TAlk$ = -2 where the signs indicate whether the change is due to input (+) or removal (-). In the extended Deffeys diagram (Fig. 3.1) this change is indicated by the vector AB' with a vector slope -2:-1. In the second case when only C_{Org} is operative ($\Delta C_{Ing} = 0$), if one molar unit of CO_2 is removed by the C_{Org} pump, then from eqs. 3.6 and 3.7: ΔTCO_2 = -1 and $\Delta TAlk = 0$. This change is indicated in the extended Deffeys type diagram (Fig. 3.1) by the vector AB with a vector slope 0:-1.

Comparing the vectorial effects of each individual pump: although the C_{Ing} pump is characterized by the vector slope (-2:-1) and the C_{Org} by the vector slope (0:-1) (other intermediate unit TCO_2 removals would yield end states between B and B' (Fig. 3.1) none of these reflect directly the stoichiometries of the C_{Org}:C_{Ing} pumps. A subsequent calculation is necessary to derive this stoichiometry (Broecker and Peng, 1982).

Two important points arise:

(1): the extended Deffeys plot does not explicitly separate out the spatial or temporal changes arising from C_{Org} and C_{Ing} pumps. That is, a plot of initial and final states in such a diagram does not provide a visual interpretation of the stoichiometry of these two pumps.

(2): Use of the Deffeys diagram in the context of the marine environment as outlined above requires that the alkalinity ordinate parameter be TAlk as defined by eq. 3.6. That is, the alkalinity parameter must include both carbonate and borate subsystems. This is emphasised here because some studies have used the alkalinity parameter as originally defined by Deffeys

where only the carbonate subsystem was considered (Codispoti et al. 1986). This interpretation probably arises for two reasons: firstly, perturbations to the system are only driven by changes to the carbon reservoirs and secondly, Broecker and Peng (1982) for didactic reasons, presented the model in its original form. This subsystem approach to the model has a significant impact of the stoichiometry and manifests itself as an overestimate of the contribution by the C_{Ing} pump.

3.4 Modified Deffeys Approach:

Separation of the effects arising from the two biogeochemical carbon pumps in a vector diagram is attained by replacing the conservative mass parameter TCO_2 in the Deffeys model by the capacity parameter Total Acidity (TAcy). Use of TAcy and TAlk capacity parameters as co-ordinates gives rise to the so called modified Deffeys diagram. This diagram is well known in the context of engineering applications to water conditioning and treatment (Loewenthal and Marais, 1984) as well as in theoretical discussions of the weak acid systems (Stumm and Morgan, 1970).

In terms of the earlier capacity parameter equations (eqs. 3.4 and 3.5), changes in the state of the sea water weak acid system are driven by the addition / removal of CO_2 and or CO_3^{2-} through the C_{Org} and C_{Ing} pumps. These changes can be represented explicitly in a diagram with co-ordinate parameters TAcy and TAlk (Fig. 3.2). Referring to Fig. 3.2, the plot also incorporates a direction format diagram for the vectorial effects of addition / removal of X mM of both CO_2 and CO_3^{2-} into and out of the aqueous phase. Two useful features arise from this:

- Assuming that changes in the state of the sea water weak acid system arise only from the biogenically driven input and output of CO_2 and CO_3^{2-} then

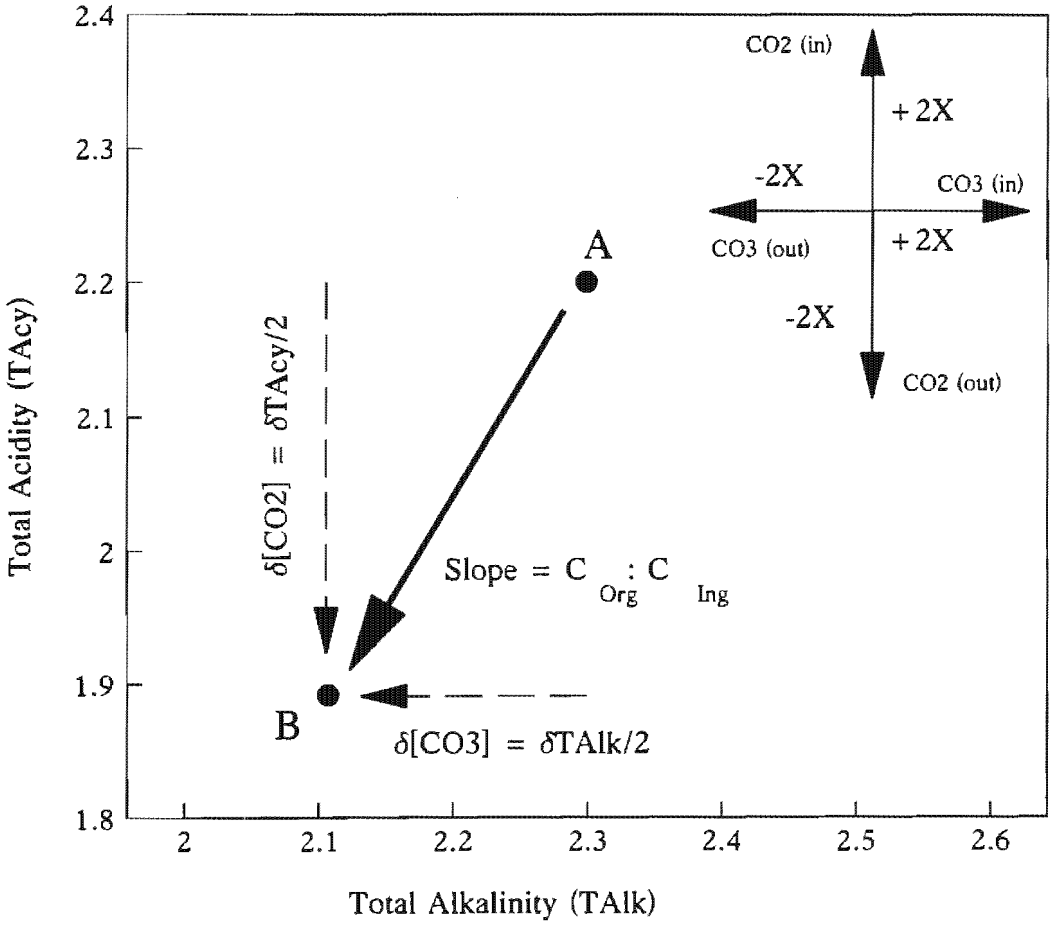

Fig. 3.2: A modified Deffeys plot using TAlk and TAcy as ordinates depicting the vectorial effects addition and removal of CO_2 and CO_3^{2-}. It shows that the effects of the C_{Org} and C_{ing} pumps are explicitely separated. As a result the vector provides a direct indication of both the magnitude and the stoichiometry of the perturbation. Changes in state driven by the C_{Org} pump are reflected by TAcy changes and similarly, changes driven by the C_{Ing} pump are reflected by TAlk changes. By definition the magnitude of the perturbation is half the value of its respective capacity parameter.

from eqs. 3.4 and 3.5, the magnitudes of the addition / removal of these components are reflected as follows:

$$\Delta TAcy = 2 * \Delta^{\circ} CO_2 \qquad \text{eq. 3.8}$$

$$\Delta TAlk = 2 * \Delta^{\circ} CO_3^{2-} \qquad \text{eq. 3.9}$$

Where Δ° X = addition from an external source of Δ° mM of species X.

In this modified approach each pump drives its own vector component making the two pump contributions completely independent of each other. Changes in the magnitude of these components then can be related directly to the input or removal of CO_2 and CO_3^{2-} respectively (Fig. 3.2); ie: $\Delta C_{Org} = \Delta$ TAcy/2 and $\Delta C_{Ing} = \Delta$TAlk/2. The sum of the two vector components gives the change in total dissolved inorganic carbon (TCO_2) concentration:

$$\Delta TCO_2 = \Delta TAcy/2 + \Delta TAlk/2 = \Delta^{\circ} CO_2 + \Delta^{\circ} CO_3^{2-} \qquad \text{eq. 3.10}$$

- The independence of the two capacity parameters used as co-ordinates, as well as the direct relationship between them and the C_{Org} and C_{Ing} carbon pumps, makes it possible to represent graphically the stoichiometry C_{Org}:C_{Ing} by the slope of the vector between the initial and final states (Fig. 3.2).

Summarizing, the first feature above describes the magnitudes of the two carbon pumps and the second, describes the stoichiometry of these pumps via the slope of the vector.

One of the original objectives of this study was to show that the C_{Org}:C_{Ing} stoichiometry is the primary factor controlling PCO_2 variability in the marine environment. The ensuing discussion addresses this objective by establishing

the link between TAcy - TAlk and PCO_2. This is then extended to include temperature effects. This extension allows that the effects of the solubility pump also can be incorporated with the biogeochemical stoichiometry.

3.4.1 Intensive Parameters in Modified Deffeys Plots: PCO_2

Deffeys (1965) showed that vector plots could be usefully applied to graphically represent the relationships between conservative parameters (TAlk and TCO_2) and any other intensive parameters from the aqueous carbonate weak acid system. This arises because the carbonate system is fully characterized by known values for any two system parameters (in this case TAlk and TCO_2) via the mass balance, capacity parameter and equilibrium equations. That is, values for any intensive parameter (in this particular case: PCO_2) can be determined at any point in the diagram. Alternatively, a single value for PCO_2 will plot as a line in the diagram, and a range of PCO_2 values will present as a family of PCO_2 isopleths. The usefulness of these plots is that it is possible to rapidly assess the effects of a given change in state, driven by the addition or removal of carbon, on any intensive variable of interest (eg: PCO_2).

PCO_2 in surface waters governs both the kinetics and the magnitude of the air - sea flux of CO_2 (Siegenthaler, 1986). Changes to PCO_2 in aquatic systems are driven by four processes: the C_{Ing} pump, the C_{Org} pump, the temperature driven solubility pump (Broecker and Peng, 1982; Volk and Hoeffert, 1985; Siegenthaler, 1986) and air - sea exchange. The effects on PCO_2 of perturbations driven simultaneously by one or more of these processes can be quantified explicitly using a modified Deffeys plot in which PCO_2 isopleths have been plotted.

The algebraic relationship between TAcy, TAlk and PCO_2, in the pH range of natural sea water, is formulated using the capacity parameter equations (eqs.

3.4 and 3.5) and equilibrium expressions of the carbonate and borate subsystems (Pytkowicz, 1983). This relationship generates the cubic expression ie: (eq. 3.11):

$$-D(H^+)^3 + (H^+)^2 * (B + C - D*K_B) + (H^+) * (A + B*K_B) + A*K_B = 0 \qquad \text{eq. 3.11}$$

where: $A = 2 * K_1*K_2*K_H*PCO_2$

$B = K_1*K_H*PCO_2$

$C = BT*K_B$

$D = TAlk$

and (H^+) is the activity or concentration of the hydrogen ion as expressed by the particular choice of scale (Culberson, 1981; Dickson, 1992) and K_X is the equilibrium constant on the corresponding scale. This equation can be solved using an iterative procedure. A particular PCO_2 isopleth is then generated as follows: for a given PCO_2 value and a range of TAlk values the corresponding (H^+) concentrations are calculated using eq. 3.11 and the corresponding TAcy values are then determined using the link between this parameter, PCO_2 and (H^+) (eq. 3.12):

$$TAcy = 2* K_H*PCO_2 + K_2*K_H*PCO_2/(H^+) + BT*(H^+)/(K_B + (H^+)) \qquad \text{eq. 3.12}$$

A similar procedure for a number of PCO_2 values yields a family of PCO_2 lines over a range of TAcy and TAlk typical of sea water (Fig. 3.3a,b). It is to be noted that this family of lines was generated using *inter alia* equilibrium equations which incorporate temperature (t), salinity (S) and pressure (P) effects (Skirrow, 1975). The plot shown on Fig. 3.3a is constrained by the conditions: t=10°C, S=35.0 psu, P=1m. It depicts a series PCO_2 isopleths in the range of 200 - 600μatm including the atmospheric pCO_2 equilibrium line (pCO_2 = 356μatm) as a reference.

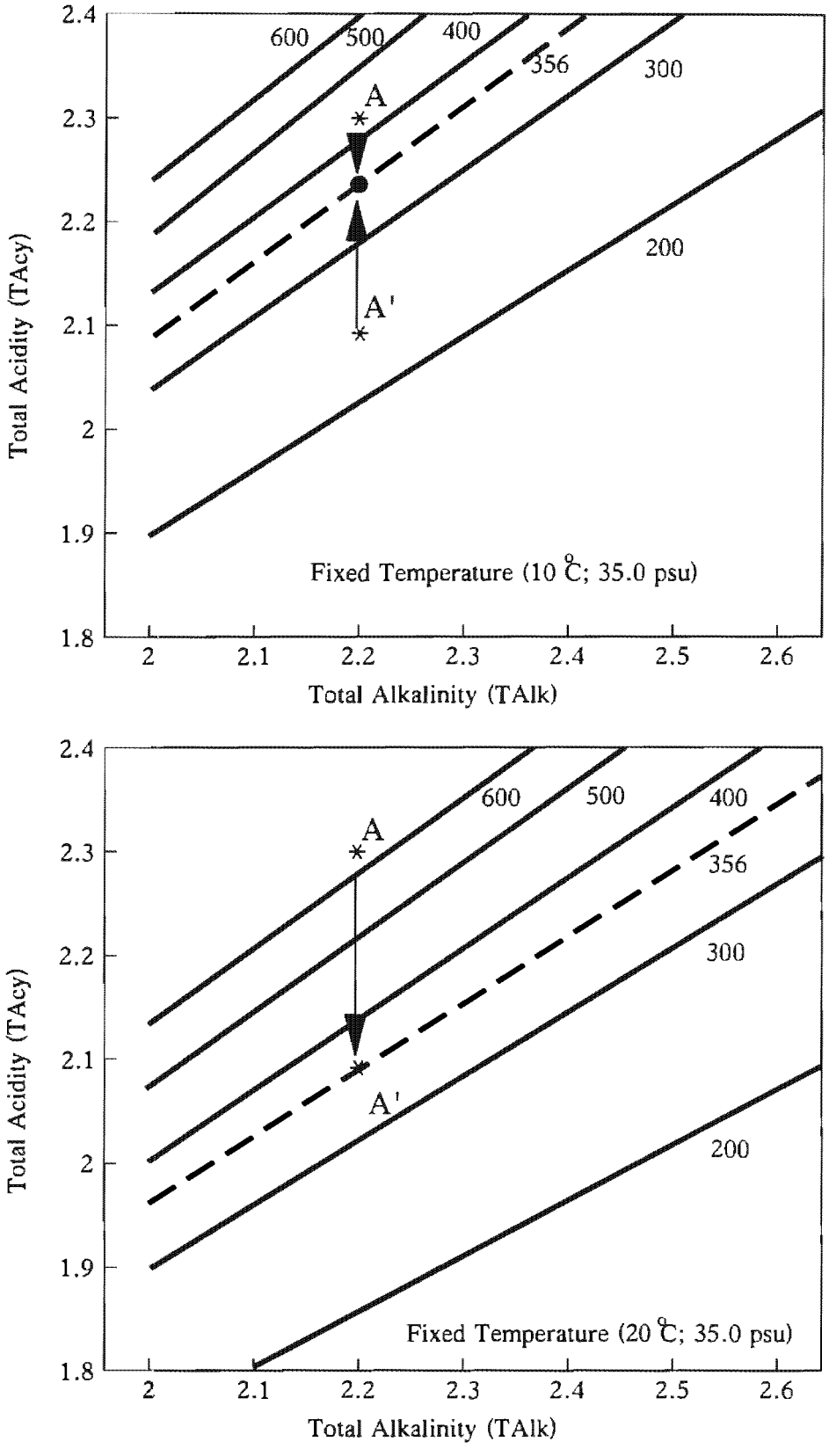

Fig. 3.3a,b: Modified Deffeys plots depicting the relationship between the conservative capacity parameters (TAlk and TAcy) and PCO_2 at two temperatures: (a): 10°C and (b): 20°C. Such plots are useful to establish the realtionship between stoichiometry and PCO_2 change as well as to quantify inter-phase CO_2 fluxes . At each temperature a family of PCO_2 lines is plotted ranging from 200 - 600µatm, including the atmospheric equilibrium line at 356µatm. It shows that the magnitude of the CO_2 change which accompanies atmospheric equilibration (356µatm) can be predicted by the starting and final TAcy values in a fixed temperature regime.

The pCO_2 equilibrium line (pCO_2 = 356 μatm) is particularly useful in assessing inter-phase CO_2 fluxes. For example, consider two sea water types both with TAlk=2.30mM but with one (type A) TAcy=2.30mM and the other (type A') TAcy=2.10mM. The two water types correspond to chemical states where PCO_2 is 440 and 240 μatm respectively (Fig. 3.3a). In the event of water type A being in direct contact with the atmosphere, it would degas until it attained equilibrium between the two phases. This perturbation is given by the vector AB with a -1:0 slope (because ΔTAlk = 0) and a magnitude given by ΔTAcy = 0.07mM. Consequently from eq.(12), the CO_2 perturbation is ΔTAcy/2 = - 0.035mM (-ve sign indicates a loss from the water). Similarly, in the case of water type A' (PCO_2=240 atm), equilibration with the atmosphere will be accompanied by ingassing. The magnitude is given by vector A'B where ΔTAcy/2 = + 0.075mM of CO_2.

The effect of temperature on the relationship between PCO_2, TAcy and TAlk can be shown by re-plotting the same diagram with the physical conditions reset to t=20°C, S=35psu and P=1 (Fig. 3.3b). The initial states of the two water types (A and A') are retained. Comparing the PCO_2 isopleths in Figs. 3.3a and 3.3b, at 10°C and 20°C respectively, the effect of the increase in temperature is to move the isopleths downwards. This arises as a result of the decreased CO_2 solubility (Skirrow, 1975). This change has a practical impact on the phase equilibrium between water types A and A' and the atmosphere. Whereas water type A' at 20°C is now practically in equilibrium with atmospheric pCO_2, the PCO_2 gradient for water type A has increased such that the CO_2 loss in degassing becomes ΔTAcy/2 = - 0.11mM (cf. previous case when it was - 0.035mM at 10°C). It should be noted that because the input or loss of CO_2 across the air - sea boundary occurs with no impact of TAlk, it has the same vectorial effect as the C_{Org} biogeochemical pump.

The two examples above served the didactic purpose of illustrating relationships between PCO_2, capacity variables (TAlk and TAcy), temperature

and simplistic phase interactions. However, the usefulness of vector models to realistic situations is best advanced by considering two examples more specific to the characteristics of upwelling systems based on data from the Benguela System (see Chapters 5 and 6). These examples assume that the necessary corrections for impact of changes in NO_3^- concentrations on TAlk and TAcy have been made.

3.4.2 Application of the Vector Model to Simulated Upwelling Systems

The first, pertains to a sub-surface oceanic environment with fixed physical characteristics (t,S,P) in which both C_{Org} and C_{Ing} pumps are operative. This example is pertinent to changes governed by the biogeochemical history of source (pre-upwelled) waters which feed upwelling areas. The second, pertains to a surface water environment which characterizes changes in state associated with the physical and biogeochemical ageing of post-upwelled waters. Here, the effects of both the C_{Org}- C_{Ing} pumps and temperature are combined in driving PCO_2 changes.

3.4.3 The PCO_2 - C_{Org}:C_{Ing} stoichiometry dynamics of pre-upwelled waters

The importance of the vector model is to both quantify the C_{Ing} and C_{Org} contributions to the overall oceanic carbon pump and, perhaps more importantly, to assess the effects of the stoichiometry of these pumps on PCO_2 in a marine system. For example, upwelling systems are understood and modelled to be oceanic sources of CO_2 to the atmosphere (Watson, 1995). The magnitude of this flux and hence the role of upwelling systems on the global carbon budget, is determined by the PCO_2 of the newly upwelled water. This is governed by the biogeochemical history of the source water. The profound effect of the C_{Org}:C_{Ing} stoichiometric history on the PCO_2 of pre-upwelled waters are best illustrated by example. For this purpose two scenarios are considered, both constrained by the physical conditions t=

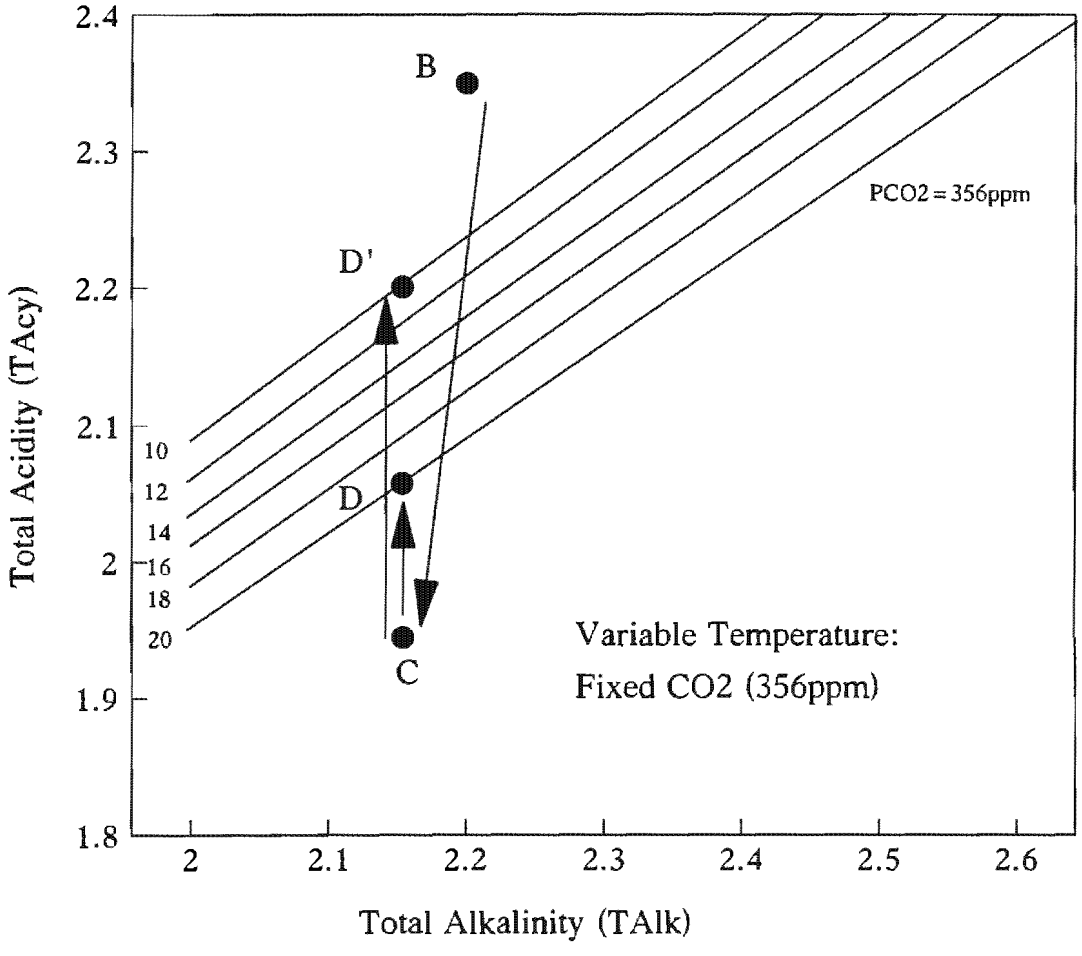

Fig. 3.5: An example of a variable temperature PCO_2 - Modified Deffeys plot. PCO_2 is incorporated under a variable temperature scenario by plotting a family of atmospheric equilibrium lines at different temperatures (10 - 20°C). This is a useful plot in the context of surface waters where both temperature changes and air - sea CO_2 exchange drive CO_2 variability. The example follows the TAcy:TAlk changes of upwelled waters typical of the southern Benguela System and how these changes impact on the atmospheric disequilibrium. BC depicts the impact of the post upwelling bloom pertubation which drives the system from a state above atmospheric equilibrium to one below. BD and BD' reflect the vectors which depict the process whereby atmospheric equilibrium is re-established at 20°C (warmed upwelled waters) or 10°C (if no warming had occured). It shows that in this context warming ameliorates the impact of the biological pump in respect of the CO_2 drawdown.

10°C; S= 35.00psu; P= 1.00m (PCO_2 calculations are all referenced to surface pressure where they determine the magnitude of the flux rate).

The initial state for both stoichiometric scenarios is given by TAlk = 2.20mM and TAcy = 2.10mM. This plots as point A (Fig. 3.4) with PCO_2 = 320 μatm. Water from state A then undergoes either of two biogeochemical perturbations driven by different C_{Org} and C_{Ing} pump stoichiometries. In the first scenario, the perturbation is driven by the C_{Org} pump alone, defined by the magnitude and slope of vector AB. That is an input of CO_2 occurs, as a result of oxidation of organic matter, with no impact on TAlk (a vector slope of 1:0) but an increase in TAcy = + 0.15mM. This results in a concomitant increase in PCO_2 of 180 μatm to a final value of 500 μatm. The magnitude of CO_2 increase is given by ΔTAcy/ 2= +0.075mM which, because ΔTAlk=0, also equals the magnitude of TCO_2 increase. This perturbation, driven only by the C_{Org} pump, is shown to have a significant impact on the final outgassing potential of water type A when it eventually upwells and equilibrates with the atmosphere.

In the second scenario, the perturbation is driven by both the C_{Org} and C_{Ing} pumps to a final state B' in Fig. 3.4. This change is characterized by vector AB' (vector slope 0.75:1) with components ΔTAcy =0.15mM and ΔTAlk =0.2mM (Fig. 3.4) and hence ΔTCO_2=0.175mM. In this scenario, although Δ TCO_2 is larger than the previous case (ΔTCO_2 =0.075mM), it has no impact on PCO_2. These contrasting scenarios emphasise the point that it is the stoichiometry of the C_{Org} and C_{Ing} pumps rather than their sum (ie: ΔTCO_2), which governs the PCO_2 change in oceanic waters.

3.4.4 Combined Effects of Stoichiometry and Temperature on PCO_2 Dynamics in Post - Upwelled Waters.

This section considers the effects of increase in temperature on PCO_2 of post upwelled waters. This increase arises due to sun warming of newly upwelled

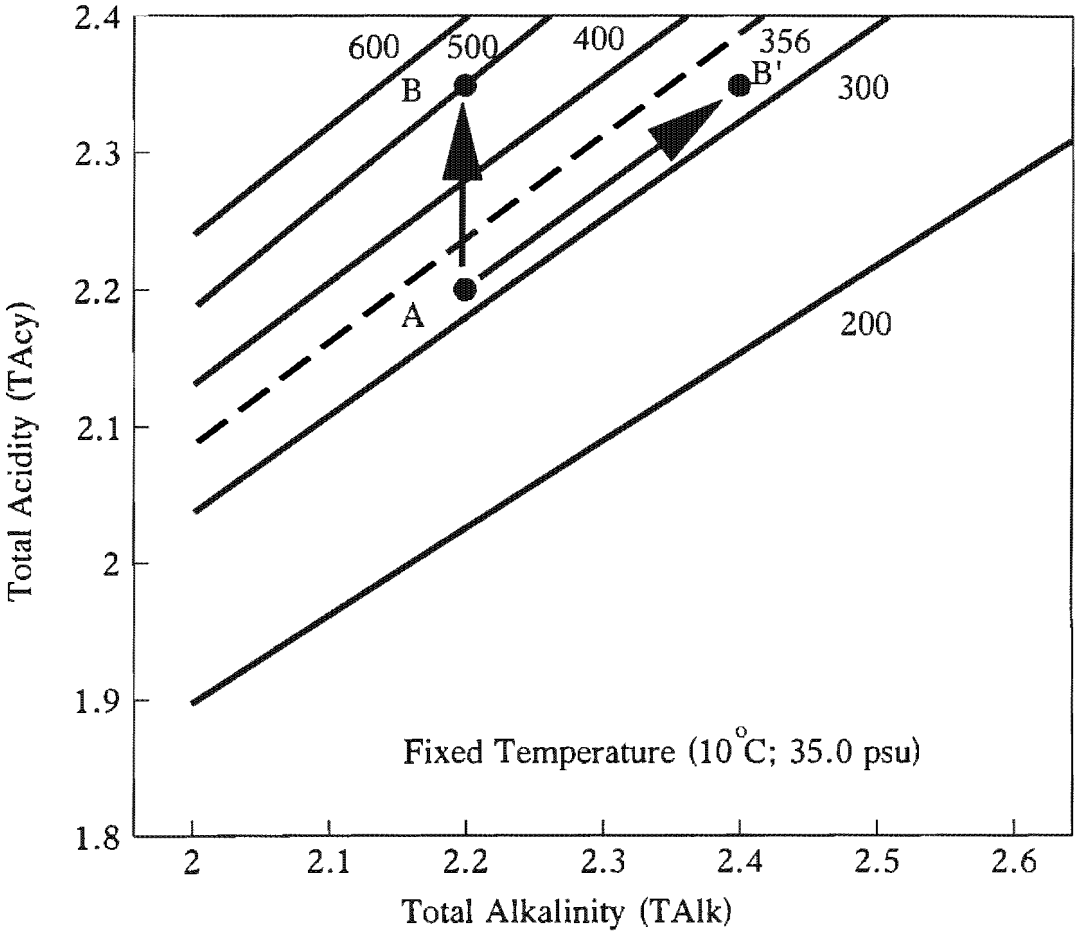

Fig. 3.4: An example of the use of a fixed temperature PCO_2 - Modified Deffeys plot. It depicts two scenarios whereby a sub-surface parcel of water at 10°C (A) undergoes changes of state as a result of two perturbations with stoichiometries AB abd AB'. It shows that although AB' increases the TCO_2 by more than AB its impact on PCO_2 is negligible. This plot re-enforces the view that PCO_2 changes are primarily driven by C_{Org}:C_{Ing} stoichiometry.

waters which outcrop in the surface layer domain and profoundly affects the CO_2 source - sink behaviour of such a system. In coastal upwelling systems such as the Benguela, biological productivity following an upwelling event is able to reduce the PCO_2 of surface waters to values under 200 μatm, well below the atmospheric PCO_2 equilibrium value. Such a situation is expected to result in a significant air - sea CO_2 flux, giving the system a strong CO_2 sink character. However, as is shown below, this expectation is strongly reduced due to effect of warming of the surface layer. These effects are investigated using the stoichiometric vector model in which temperature effects have been incorporated by plotting a family of CO_2 isopleths which represent air - sea CO_2 equilibrium lines at different temperatures (Fig. 3.5). The biogeochemical component of the magnitude of the air - sea CO_2 flux is determined by the PCO_2 gradient across the sea - air interface (Broecker and Peng, 1982; Siegenthaler, 1986). In the short term (seasonal to interannual time scales), the PCO_2 value in atmospheric equilibrium is constant enough to plot it at different temperatures for a range of TAcy and TAlk values (Fig.3.5). In this method, to quantify the magnitude of the CO_2 gain or loss it is only necessary the know the starting TAlk - TAcy state and the position of the atmospheric equilibrium PCO_2 isopleth at the temperature at which equilibrium is reached.

As an example, consider a post upwelled surface layer undergoing a temperature increase from 10°C to 20°C and equilibrating with an atmospheric pCO_2 value of 356 atm (Fig. 3.5). (For continuity, the initial state in this example, point B (Fig. 3.5) corresponds to point B in the first scenario of the previous example shown in Fig. 3.4. This water, initially at 10°C, upwells with a PCO_2 value of 500μatm which is well above the PCO_2 in equilibrium with the atmosphere at this temperature (Fig. 3.5). Referring to Fig. 3.5, a post upwelling phytoplankton bloom now causes a perturbation which changes the water from state B to C with TAlk= 2.15mM and TAcy=1.95mM. This corresponds to a ΔTCO_2 decrease of 0.225mM, a C_{Org}:C_{Ing} pump stoichiometry of 8:1 and a final PCO_2 value well below

atmospheric equilibrium in the temperature range 10-20°C (Fig. 3.5). The CO_2 drawdown potential of an upwelling system at state C is then given by a vector (slope 1:0) linking state C to the PCO_2 equilibrium line at the temperature of the surface layer. The maximum drawdown possible is given by vector CD' which corresponds to the scenario where no warming of the post-upwelled water occurs, ie it remains at 10°C. The magnitude of this vector is ΔTAcy =0.25mM which corresponds to a CO_2 input of ΔTAcy/2 =0.125mM (ie 56% of the carbon removed by the biogeochemical pumps is reintroduced via ingassing from the atmosphere). More realistically, the upwelled waters will warm up in the course of the slow process of equilibrating with the atmosphere to say 20°C. This limits the drawdown (via ingassing) to that given by vector CD. The magnitude of the vector is Δ TAcy=0.1mM which corresponds to a CO_2 input of 0.05mM (ie now only 22% of the carbon removed by the biogeochemical pumps is reintroduced via ingassing from the atmosphere). This application of the vector model to upwelling systems shows that the net effect of biogeochemical and physical forcing is to limit the CO_2 drawdown potential to a fraction of the carbon removed by the biogeochemical pumps.

The above discussion of the biogeochemically and physically driven dynamics of PCO_2 emphasises how the potential of upwelling systems as CO_2 sinks is limited by the decreased CO_2 solubility which accompanies warming of upwelled waters. Only a fraction of the carbon fixed via the biological pumps is replaced by atmospherically derived CO_2. This fraction is likely to be even smaller when the surface remineralization the biogenic carbon component is taken into account. This impact of negative feedback by surface warming on the biogeochemically driven PCO_2 deficit in post upwelled waters will be more significant in tropical areas and under conditions of global warming.

3.5 Nitrate Correction to Total Alkalinity

The underlying assumption thus far in the definitions of Total Alkalinity and Total Acidity used in this study to quantify the carbonate stoichiometry is that only the borate - boric acid weak acid species contribute significantly to carbonate alkalinity - acidity. This assumption is essentially correct in all but this part of the upwelling cycle due to the very minor role played by other weak acid species in most instances. Nitrate is the exception and only at this stage, because its concentration which in pre-upwelled waters is approximately 20μM decreases to zero, as a result of reduction and uptake, within two days and causes the uptake of an equivalent number of protons as shown on equations (2a,b,c).

$NO_3^- + 9H^+ + 8e^- \text{------>} NH_3 + 3H_2O$ eq. 3.13a

$4H_2O + \text{chlorophyll} \text{------->} 2O_2 + 8H^+ + 8e^-$ eq. 3.13b

$NO_3^- + H^+ + H_2O \text{------->} NH_3 + 2O_2$ eq. 3.13c

The first two equations give the main steps associated with nitrate reduction which accompanies photosynthetic requirements of the phytoplankton. The third provides the net stoichiometric relationship from the sum of the two first steps. For the process to occur while maintaining the same ΣCO_2, it must alter both TAlk and TAcy. Normally the change in TAlk and TAcy brought about by this process is insignificant compared to simultaneous changes to carbonate driven changes to the same capacity parameters. In the case of the post-upwelling bloom, as was shown by the preliminary stoichiometry above the ΣCO_2 removal is so dominated by the C_{Org} pathway that the actual change in TAlk is very small. This combined with the fact that the input nitrate concentrations are relatively high (20μM) mean that nitrate reduction will significantly impact the TAlk changes and hence influence the overall stoichiometry of the post upwelling bloom. The correction for this additional mechanism is numerically simple. The stoichiometry from equation (3.13c)

shows that nitrate reduction and proton removal are equimolar and hence the impact on TAlk and TAcy is also equimolar with the total nitrate reduction. The correction to the capacity parameters adds 20µM to the mean TAcy and subtracts the same from TAlk of the Post-upwelling Bloom Water. In so doing it provides new final values which would have been encountered if no nitrate reduction had occurred. A new stoichiometric ratio can now be calculated which is driven only by the C_{Org}:C_{Ing} stoichiometry.

Chapter 4

4. Shelf Scale Physical Oceanographic Processes and their Impact on the Distribution of CO_2 Parameters in the Benguela System

4.1 Background

The interaction of physical oceanographic processes on scales ranging from daily to interannual is thought to be a key factor governing the biogeochemical characteristics and ultimately the CO_2 source - sink behaviour of the Benguela System. Variability in *inter alia* the transport of upwelling events, the frequency of upwelling events, the seasonal persistence of upwelling events and interannual scale El Nino Southern Oscillation (Shannon *et al.*, 1992; Shannon and Nelson, 1996) perturbations all impact on the activity and characteristics of the biological pump. This in turn determines the rates and the magnitudes of present day carbon fluxes.

Although this is the first investigation of the role of physical processes on CO_2 variability in the Benguela System, ecosystem research in the Benguela System (Hutchings *et al.*, 1995) has provided much insight into the interactive role of physical and biogeochemical processes. The dynamics of *inter alia* oxygen, nitrate and more recently ammonium have been shown to be closely coupled to physical processes (Chapman and Shannon, 1987 ; Bailey, 1990; Probyn, 1992 ; Brink *et al.*, 1995; Hutchings *et al.*, 1995). The focus of past biogeochemical work in the Benguela System has been predominantly on oxygen and nitrate because of the fisheries and ecosystem orientation of the objectives (Bailey and Chapman, 1985; Hutchings *et al.*, 1995). Sub-surface hypoxic or anoxic events are an ubiquitous characteristic of the system especially in the northern half where such events can persist over seasonal or

annual time scales (DeDecker, 1970; Chapman and Shannon, 1987). Periodic hypoxic events in the southern Benguela System which are connected with physical dynamics of the system have catastrophic consequences for benthic resources such as rock lobster (Newman and Pollock, 1974). These are closely linked to the occurrence of reduced equatorward wind stress and enhanced stratification which tend to be more frequent in the late summer at the end of the upwelling season (Chapman and Shannon, 1987 ; Bailey, 1990). Research into the relationship between physical oceanography and nitrate variability is driven by the fact that nitrate is a limiting nutrient in the Benguela System (Andrews and Hutchings, 1980; Brown and Hutchings. 1987; Hutchings *et al.*, 1995). Its physical supply rate to the euphotic zone drives and limits phytoplankton new production which in turn provides the free energy to secondary and higher order production including fish resources (Moloney, 1992 ; Hutchings *et al.*, 1995).

The interpretation of the physics behind oxygen and nutrient variability was based on classical Ekman transport view of the Benguela System (Andrews and Hutchings, 1980; Bailey and Chapman, 1985; Bailey, 1990), . Much of this classical view is presently under review (G. Nelson, pers.com). In this study not only are up to date insights incorporated where appropriate, but where possible new ideas based on the carbonate data are postulated. Three of the most important recent advances in understanding of the physical processes in the Benguela System are (Nelson, pers.com) (Shannon and Nelson, 1996):

- the far greater importance of the poleward undercurrent in the long shore transport of upwelled waters within the system
- the role of shelf waves in both cross-shelf and long-shore transport of water
- the clearer understanding of the relative importance of the spatial and temporal scales of variability

These advances and other related insights are now overviewed in more detail with a particular emphasis on the role they may play in driving carbon fluxes in the Benguela System and account for the observed variability in measured carbonate parameters in the water column of the sampled transects.

The physical oceanographic processes in the Benguela System interact with the carbon cycle in three broad ways:

- **Advection: longshore, cross-shelf and vertical**: It provides the mechanisms through which dissolved carbon is supplied to the shelf as SACW, advected along the shelf, upwelled at upwelling cells or transported out of the system: it drives poleward, equatorward and cross shelf transport of carbon.

- **Benthic Boundary Layer (BBL) Turbulence**: In the same way as turbulence and stratification govern the CO_2 fluxes in and out of the surface layer, so BBL turbulence is also likely to play a role in the vertical carbon flux of re-mineralized carbon between the sediments and the overlying water through the benthic boundary layer.

- **Surface Layer (SL) Turbulence - Stratification**: When upwelled water outcrops at the surface, thermal stratification governs the activity of the biological and solubility pumps through its control on phytoplankton bloom dynamics and warming respectively (Pitcher *et al.*, 1991; Probyn. 1992 ; Hutchings *et al.*, 1995; Pitcher *et al.*, 1996). Stratification also governs the rate of CO_2 gas exchange between the surface layer and the overlying atmosphere (air - sea flux) and the underlying sub-surface waters (turbulent diffusion across the thermocline).

Understanding the way these three physical aspects of the Benguela System interact with carbonate biogeochemical processes is central to constraining

the CO_2 sink - source characteristics of the Benguela System. This is the objective of this chapter and it is achieved with the following approach:

- Review state of knowledge in respect of advective and turbulent mixing processes relevant to carbon fluxes.
- Present the physical and biogeochemical oceanographic sections to assess the extent to which present knowledge accounts for the observations.
- Discuss new insights which arise from the data obtained in this study.

4.2 Physical Processes Critical to Carbon Fluxes in the Benguela System

4.2.1 Advection: Longshore and Cross Shelf

In the classical Ekman transport view of upwelling (Neumann and Pierson, 1966) equatorward winds combined with Coriolis force drive a net offshore transport of surface water (Ekman Layer). This has two outcomes:

- it causes a net cross-shelf advection of water integrated over the Ekman friction layer at right angles to the coast. This is replaced by bottom waters which outcrop at the surface through upwelling;
- it also drives equatorward currents.

The first outcome arises as a result of the balance between the frictional and Coriolis terms (Neumann and Pierson, 1966; Smith, 1995). In the southern Hemisphere when the frictional surface is on top, as is the case for surface wind driven layers, the motion is to the left of the driving vector: the equatorward wind. In the case of the benthic boundary layer the frictional surface is inverted, lying at the bottom, and the Coriolis effect is also reversed (Smith, 1995). The net effect is to push the bottom frictional layer water to the right or shorewards in the southern hemisphere. This coupled effect causes

the deficit of water at the coast to be replaced through upwelling of sub-surface waters, which in the Benguela System has always been defined as South Atlantic Central Waters (SACW) (Currie, 1953; Shannon and Nelson, 1996).

In the second case, a barotropic equatorward current arises because of the cross shelf pressure gradient which builds up as a result of the sea slope change created by the advection of surface waters offshore (Neumann and Pierson, 1966; Nelson, 1985; Smith, 1995). In the absence of other advective forcing such as the poleward undercurrent, this geostrophic pressure gradient will drive a barotropic equatorward flow (Smith, 1995). In addition, upwelling will cause isopycnals to tilt upwards towards the coast. If this is sustained over periods longer than the inertial oscillation period, a baroclinic longshore current sets in near to the coast in an equatorward direction.

In terms of the classical view, upwelling would occur along any part of the coast where an equatorward wind stress occurred and generate an equatorward transport of water (Neumann and Pierson, 1966). Early studies in the Benguela which were largely based on the assumptions of the Ekman model proposed a poleward jet located below the outer shelf break as a compensation current for the largely equatorward transport predicted by the model (Currie, 1953; Hart and Currie, 1960). This view of the system predicts that the carbon fluxes would be characterised by two notions:

- the carbonate characteristics of upwelled waters would be largely dominated by the source SACW which because of the relatively rapid cross shelf transit would upwell only slightly modified by localized benthic remineralization.
- the transport of biogenic particulate carbon, resulting from surface biological activity which follows upwelling, would be equatorwards. The downstream deposition and accumulation of biogenic particles would be largely on the equatorward side of upwelling centres (Bailey, 1990).

Past interpretation of biogeochemical dynamics, mostly oxygen and nitrate, in the Benguela System have rested on these two notions. However, the most recent current meter data (Nelson, pers.com.) and biogeochemical evidence (CO_2 in this study) question the accuracy of this view (Shannon and Nelson, 1996). This has led to a complete re-assessment of the nature of advection in the Benguela System and particularly the impact on carbon fluxes (Shannon and Nelson, 1996; Nelson, pres.com.; This study). The following three features characterize the most recent views on advection and its biogeochemical impact in the Benguela System:

Firstly, the bulk of the flow in the Benguela System is polewards rather than equatorward (Shannon and Nelson, 1996). Specifically, calculated meridional transport rates on the shelf (Gordon *et al.*, 1995 in (Shannon and Nelson, 1996) at 27 °S estimate the equatorward and poleward components at 0.7Sv and 1.6Sv respectively. This means that water which outcrops at the upwelling centres is being supplied mainly by a shelf resident poleward moving water mass rather than a cross-shelf supply of SACW. However, a complication arises in respect of linking upwelled water to a poleward flowing water body. The direction of stress for a poleward flow over a fixed benthic friction layer (sediments) is equatorward which, in the southern hemisphere, predicts that the resultant flow is to the left or offshore (Smith, 1995). It has been suggested on the basis of limited data, that in such circumstances upwelling source waters are the intermediate waters overlying the poleward flow (Smith, 1995). This prediction is not consistent with observations in the Benguela System and has been challenged by an alternative mechanism suggested by G. Nelson (pers.com.).

The "Nelson Model" is based on the existence of long wave length longshore and cross-shelf barotropic currents with periods of 3 to 6 days in the southern Benguela System. These are associated with barotropic coastal trapped waves. Of particular significance is the cross-shelf motion which feeds

upwelling in its onshore phase and supresses it in its offshore phase no matter what the wind does to force Ekman transport. This means that upwelling can be fed from the inshore poleward flow rather than it being constrained to a mid water supply based on the offshore flow tendency in the BBL within the poleward flow as discussed by (Smith, 1995).

Secondly, equatorward flow is restricted to the surface layers which originate from aged upwelled waters and a narrow near surface jet located normally above the 300-400m contours (Bang, 1973; Shannon and Nelson, 1996).

Thirdly, the biogeochemical significance of this advection model is that while active phytoplankton blooms and dissolved constituents in the surface layer would be advected equatorward, sedimenting and particularly re-suspended biogenic particles would be largely transported polewards.

The importance of sub-surface advection indicates that physical forcing at the bottom friction layer may play an important role in biogeochemical fluxes. This aspect is now addressed in more detail.

4.2.2 Benthic Boundary Layer (BBL) Turbulence:

The Benthic Boundary Layer (BBL) is probably one of the most ubiquitous but least well understood oceanographic features of the Benguela System and other upwelling systems (Lenz and Trowbridge, 1991; Dingle and Nelson, 1993; Smith, 1995). This applies particularly to the driving mechanisms which sustain it and their role on biogeochemical fluxes in general and CO_2 in particular.

Initial interest in the BBL was stimulated by its role in governing the intensity and extent of low oxygen water in the Benguela System (Dingle and Nelson, 1993). The BBL in the Benguela System is described as a mixed body of

water overlying the sediments with a thickness of no less that 3% of the total water column depth (Dingle and Nelson, 1993) . This value may increase to as much as 10% in the vicinity of shelf breaks where physically driven turbulent mixing is enhanced (Dingle and Nelson, 1993). The most extreme of such excursions is usually found associated with shelf breaks where a "dome" in the isopleths is a consistent feature (Nelson, 1985). This has usually been ascribed to shelf break upwelling (Barange and Pillar, 1992; Summerhayes *et al.*, 1995) but it has been suggested more recently that the "dome" effect reflects enhanced turbulence at the shelf break arising from the semi-diurnal tidal Kelvin wave which propagate along the break (G. Nelson, pers.com). This is one of the physical processes whose role in modulating biogeochemical fluxes has been underestimated and whose specific forcing mechanism is discussed further below in the light of the data from this study.

4.2.3 Surface Layer (SL) Turbulence and Stratification:

The flux of solutes and dissolved gases between two environments separated by a gradient is modelled by the generic expression:

$$F_x = K * \Delta X / \Delta Z \qquad \text{eq. 4.1}$$

where the flux of component X (F_x) is the product of the turbulent exchange coefficient (K_w) and the gradient ($\Delta X / \Delta Z$). In the special case of CO_2 the same expression becomes:

$$F_{CO2} = K_w * \Delta PCO_2 \qquad \text{eq. 4.2}$$

where the CO_2 flux (F_{CO2}) is a function of the turbulent exchange velocity (K_w) and the partial pressure difference (ΔPCO_2) between the surface layer PCO_2 and the atmospheric pCO_2 (Liss and Merlivat, 1986). The expression (eq. 4.2) has physical (K_w) and a biogeochemical (ΔPCO_2) parts both of which are

impacted by wind induced turbulence and stratification driven by solar warming.

The importance of turbulence and stratification dynamics in upwelled waters lies in the control they hold over the vertical carbon fluxes into and out of the surface layer. They play three significant roles which impact on the terms of eq. 4.2:

- they impact on the rates of gas exchange (K_w) between the surface layer and both the overlying atmosphere through the sea surface layer (Liss and Merlivat, 1986; Wanninkhof, 1992)

- they govern phytoplankton bloom dynamics through their impact on, amongst other factors, seeding, cell size, mixing depth, nutrient supply (Hutchings *et al.*, 1995). The relationship between physical forcing through wind driven turbulence and the dynamics of new and regenerated phytoplankton production is also particularly well described by T.A. Probyn in Brink et al., (1995; p109; Fig. 5.2). Phytoplankton bloom dynamics in turn control CO_2 uptake and in doing so, PCO_2 and the short term changes to ΔPCO_2.

- Stratification from sun warming impacts on air - sea CO_2 fluxes through warming of upwelled waters which reduces CO_2 solubility and increases the magnitude of PCO_2 which, in turn, impacts on the biogeochemical part (ΔPCO_2) of the flux expression.

4.2.4 Role of turbulence and stratification on CO_2 dynamics in the surface layer:

Upwelling systems such as the Benguela are characterized by dramatic synoptic scale shifts in the degree of turbulence in the surface layer which characterise "active" and "relaxation" phases of the upwelling cycle (Taunton-

Clark, 1985; Shannon and Nelson, 1996). While turbulence associated with the active phase drives the characteristics and magnitude of new production through its control on phytoplankton seeding and NO_3^- supply (see Chapter 1) most of the physical and biogeochemically driven changes to PCO_2 occur during the "relaxation" phase when stratification begins.

Stabilization of upwelled waters driven by solar heating is a key factor causing the large biomass and highly productive phytoplankton blooms which follow upwelling events (Brown and Hutchings, 1987). These dense phytoplankton blooms (10 - 50 mg Chl_a m^{-3}) bring about dramatic decreases in PCO_2 from the high values of 800 - 1500 μatm which characterize newly upwelled waters to sometimes below 200 μatm (This study). Concurrently, sun warming of the surface layer also decreases the solubility of CO_2 (Weiss, 1974) which increases PCO_2 and reduces the CO_2 drawdown potential of the system (see Chapter 3). Stratification driven by sun warming plays two opposing roles in respect of changes to the magnitude of net CO_2 fluxes between the surface layer and the atmosphere:

- it stimulates phytoplankton production and biomass which decreases PCO_2 in the surface layer and,
- it decreases the solubility of CO_2 which increases the PCO_2.

Stratification in the Benguela System occurs through two mechanisms. Firstly, direct sun warming of upwelled waters can produce a heating rate of 0.5°C / day in a 10m mixed layer (Guastella, 1992). The net solar radiation during the summer in the southern Benguela has been measured at 225Wm^{-2} with values further north being estimated to be slightly higher (Shannon and Nelson, 1996). Secondly, when the upwelling cycle enters a relaxation phase and the equatorward wind stress decreases, the sea surface pressure gradient relaxes through the shoreward flow of surface waters. This surface water is normally warmed ($t > 17°C$) aged upwelled waters which because of its lower density caps the colder ($t < 11°C$) newly upwelled water. An

example of such an occurrence can be found below in the results and discussion from the Olifants River transect. While the former mechanism creates a weakly stratified but stable water column conditions with a weak thermocline, the latter is usually observed as a strongly stratified water column with the thermocline at approximately 10m -20m. Over most of the Benguela System the dominance of one system over another is strongly related to the strength and frequency of upwelling wind events which varies both spatially and seasonally. It should be noted that this variability in the stratification dynamics is to be found within the upwelling area inside the upwelling front. Outside this front in the oceanic system stratification is a permanent feature with surface water temperatures in the range 18 - 20 °C (Nelson, 1985).

The foregoing overview emphasised the role of physical forcing on the biogeochemical part of eq. 4.2. It is now necessary to focus on the role of the same physical forcing on the physical part of the expression (K_w).

4.2.5 The role of physical forcing on CO_2 fluxes across the boundaries of the surface layer.

The surface layer typically has two boundaries (Fig. 4.1):

- the air - sea boundary to the atmosphere and,
- the thermocline boundary to underlying colder waters which are richer in both CO_2 and NO_3^- but lower in both O_2 and DOC.

The physical characteristics of these boundaries govern the gas flux rates into and out of the surface layer. The variability in the resistance of these boundaries to gas and solute fluxes are in turn determined by:

- wind stress (speed) in the case of the air - sea boundary (Liss and Merlivat, 1986; Wanninkhof, 1992) and,

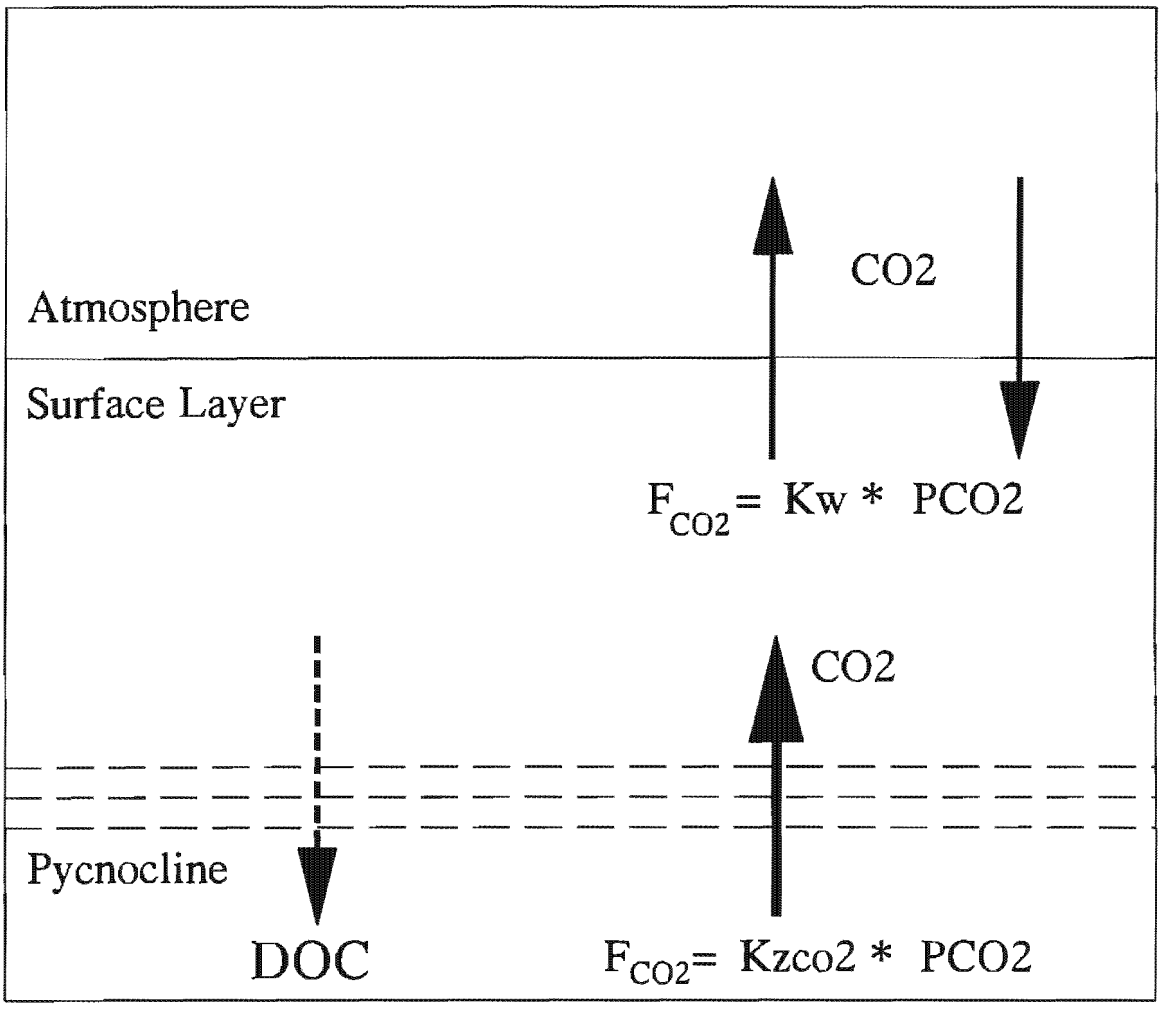

Fig. 4.1: This diagram depicts the two boundaries of the surface layer the fluxes and their driving mechanisms. It shows that CO_2 fluxes across the air - sea boundary are a function of the gradient between atmospheric pCO2 and surface layer PCO_2 as well as the mainly wind driven skin turbulence which is parametrized as the exchange velocity (Kw). The flux across the pycnocline which defines the lower boundary, is a function of the PCO_2 gradient as well as the pycnocline strength which is normally parametrized as the turbulent eddy diffusion coefficient (KzCO2). Modelling of transport across the pycnocline boundary is also of central importance to downward DOC fluxes.

a combination of wind, solar heating and advection which govern thermocline dynamics (Lenz, 1992; Smith, 1995).

Physical Modelling of CO_2 Flux across the Air - Sea Boundary

The modelling of gas transfer flux across the air sea boundary has been the subject of numerous comprehensive studies and reviews (Broecker and Peng, 1982; Liss, 1983; Liss and Merlivat, 1986; Tans *et al.*, 1990; Wanninkhof, 1992; Farmer *et al.*, 1993). Physical forcing of the rate of gas transfer (K_w) across the air - sea interface is driven mainly by surface turbulence which is closely related to wind stress. Although other factors which affect the characteristics of the sea surface layer such as slicks, surfactants and bubbles also play a role in the real value of K_w (Wanninkhof, 1992; Farmer *et al.*, 1993) these have, for the purposes of this study been ignored. The three main approaches to numerically defining K_w range from the highly empirical stagnant layer model (Broecker and Peng, 1982) to the most widely used boundary layer model (Deacon, 1977). The approach adopted in this study for CO_2 is that of the Liss - Merlivat model which is based on the boundary - layer modelling approach (Deacon, 1977) modified to handle changes to surface characteristics at higher wind speeds (Liss and Merlivat, 1986). This approach, which was used in this study, simplifies the temperature dependence of the Schmidt number and provides a solution for 20°C. Although detailed functional relationships exist for the temperature dependence of the Schmidt number (Wanninkhof, 1992), the Liss-Merlivat simplification is close enough to the 18°C atmospheric equilibrium value used in this study. One of the main difficulties in modelling of CO_2 fluxes is that it is difficult to experimentally determine transfer velocity K_w over a range of wind speeds (Broecker and Peng, 1982). The Liss - Merlivat approach models the change in the transfer velocity K_w with wind speed and recognizes three transitions to the relationship each with its own K_w - wind speed (U) relationship:

Sea State	Wind Speed (m/s)	K_w
• smooth surface	< 3.6	0.17U
• rough surface	3.6 - 13.4	2.85U - 9.65
• breaking waves	> 13	5.9U - 49.3

Recent work (Farmer *et al.,* 1993) has shown that this model underestimates K_w at high wind speeds when bubble breaking becomes important. However, over the wide range of conditions which characterize wind driven turbulence in upwelling systems, the Liss - Merlivat model appears to be still adequate. One of the important predictions of this model is the sharp increase in the rate of change of K_w with wind speeds above 3.6m/s (7-8 knots). In respect of gas exchange, it suggests that this speed determines the environmental boundary between calm and windy conditions.

4.2.6 Physical Modelling of the CO2 Flux across the Thermocline Boundary

When upwelled waters stratify, a boundary is set up between the surface layer where most of the CO_2 uptake occurs and the underlying mid or bottom waters where PCO_2 values remain high. Fluxes across the thermocline are governed principally by the strength of the thermocline or, more generally, the pycnocline. The physical factor which best simulates the resistance of the thermocline to the transport of matter or energy across it is the Coefficient of Eddy Diffusion (K_{ed}) (King and Devol, 1979). This is, as with most turbulence coefficients, not simple to measure especially *in situ* when the CO_2 data is being gathered. Some *in situ* measurements have been achieved in the past (Lewis *et al.,* 1984) using turbulence probes but routine acquisition of this type of measurement remains a problem. The approach used in this study is the King and Devol, 1979 use of the thermal diffusion coefficient (K_{Zt}) calculated from net daily average heat flux (Q_t) and the thermocline gradient (dt/dZ) as a proxy for K_{ZCO2}. The main assumption in this approach is that the

magnitude of the unmeasurable K_{ZCO2} can be satisfactorily approximated by the measurable K_{Zt} (King and Devol, 1979). The CO_2 flux is then calculated with the general expression:

$$F = K_{ZCO2} * d(PCO_2/dZ) \qquad \text{eq. 4.3}$$

where the biogeochemical term d(PCO2/dZ) is the PCO_2 gradient across the thermocline as a result of the CO_2 disequilibrium driven by the activity of the biological or solubility pumps in the warmed surface layer. The usefulness of this approach is that it can be extended to model the export flux of DOC, which builds up in the surface layer, into bottom waters.

4.3 Methods: Cruises and sampling

4.3.1 Henties Bay Transect: Northern Benguela Sub-System

The Henties Bay transect was a west bearing sampling line of 6 stations located at latitude 22 25' ^{o}S worked between 16 - 20th March 1992 (Fig.4.2) on the RV Benguela of the Namibian Fisheries Department. The main goals of this cruise were to core the phosphorite rich sediments, investigate potential mechanisms for phosphorite formation (Nathan *et al.*, 1993) and simultaneously to sample the water column for carbonate biogeochemistry (this study) and coccolithophore activity (Giraudeau *et al.*, 1993). Water samples were taken from a General Oceanics CTD-Rosette system which was re-calibrated after the cruise. Sediment vibro-cores were also collected and sampled for the both interstitial and adsorbed NH_4^+. All pH measurements were taken on board (see Chapter 2) and the Total Alkalinity samples were stored for shore analysis.

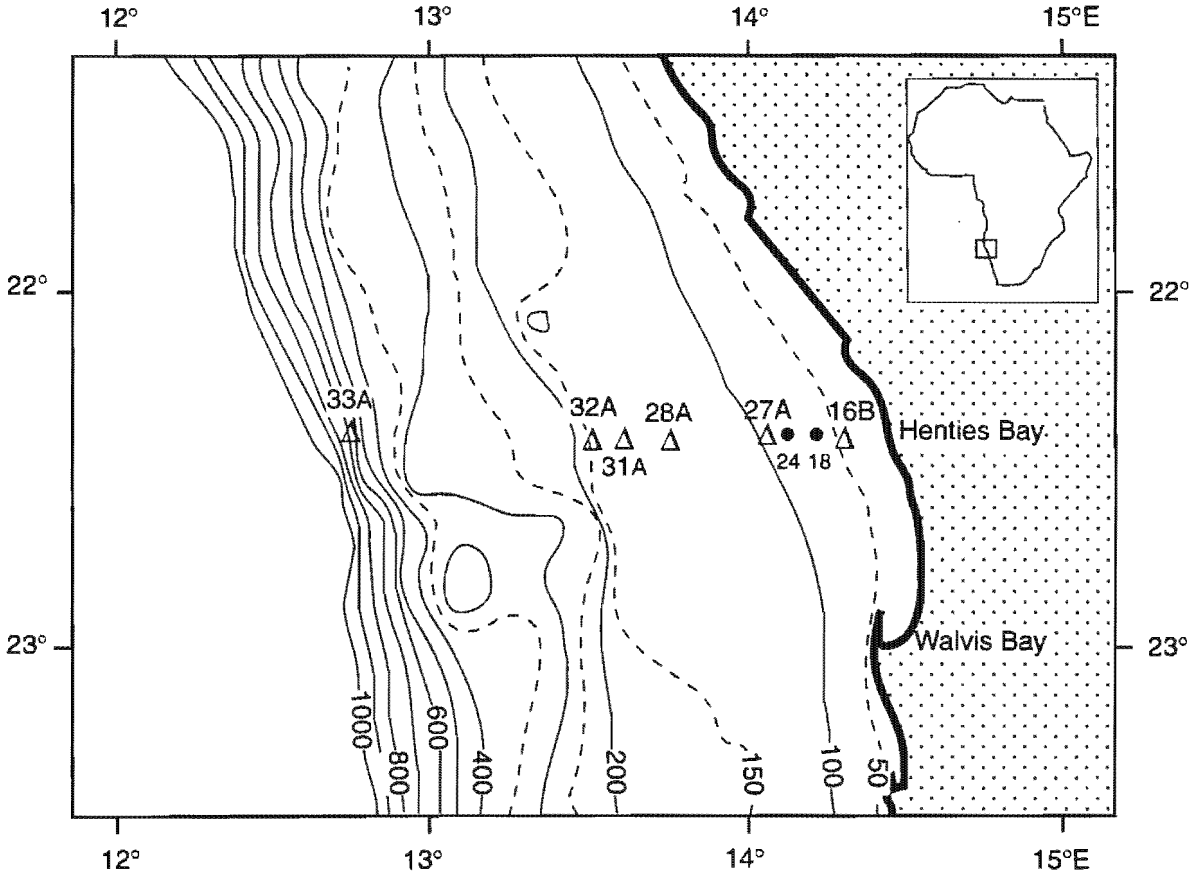

Fig. 4.2: A map showing the station positions from the cross-shelf Henties Bay transect and the bathymetry in the vicinity of the Walvis Bay upwelling centre. Particular note should be made of the station positions relative to the double shelf break profile at 140 and 400m depth. Water column samples were taken at stations 16B, 27A, 28A, 31A, 32A and 33A. Sediment cores were taken at stations 18 and 24. The map was adapted from Bremner, 1981.

The transect was carried out over a part of the Benguela System shelf which is also characterized by a moderately wide (150 km) and straight shelf with a double shelf break at approximately 140 and 400m (Fig.4.2) (Bremner, 1981). Most of the stations (16 - 32) are located over the inner shelf and two 31 and 33 are located over the inner and outer shelf breaks respectively (Fig.4.2). As was discussed above shelf bathymetry is an extremely important determinant of the nature and intensity of physical advection which occur through the whole Benguela System (Shannon and Nelson, 1996).

4.3.2 Hondeklip Bay Transect: Central Benguela Sub-System

The Hondeklip Bay transect was a west bearing line sampled between 16 - 20 June 1993 on the FRS Africana of the Sea Fisheries Research Institute, South Africa with the objective of obtaining a comparative data set for carbonate parameters from the Namaqua region of the Benguela System and to undertake sampling for coccolithophores (Giraudeau and Bailey, 1995). A total of 7 stations were sampled (Fig. 4.3) with specific provision for a set of 3 samples with 5 m spacing within the bottom 20m of the water column to fall within the benthic boundary layer. All analyses were carried out on board during the cruise.

The physiographic factor which most distinguishes the central zone of the Benguela System from its northern and southern counterparts is the width and irregularity of the shelf. The shelf is at its widest in this part of the System stretching up to 180km off the Orange River (Fig. 1.5) and is largely characterized by a single shelf break at about 300m (Fig. 4.3). Its northern boundary is the sharp narrowing of the shelf to 75km to the south of Luderitz (28 °S). The southern boundary is the Olifants Valley where SACW, which dominates biogeochemical characteristics of the southern extremity of the Benguela system, is advected onto the shelf (Dingle and Nelson, 1993).

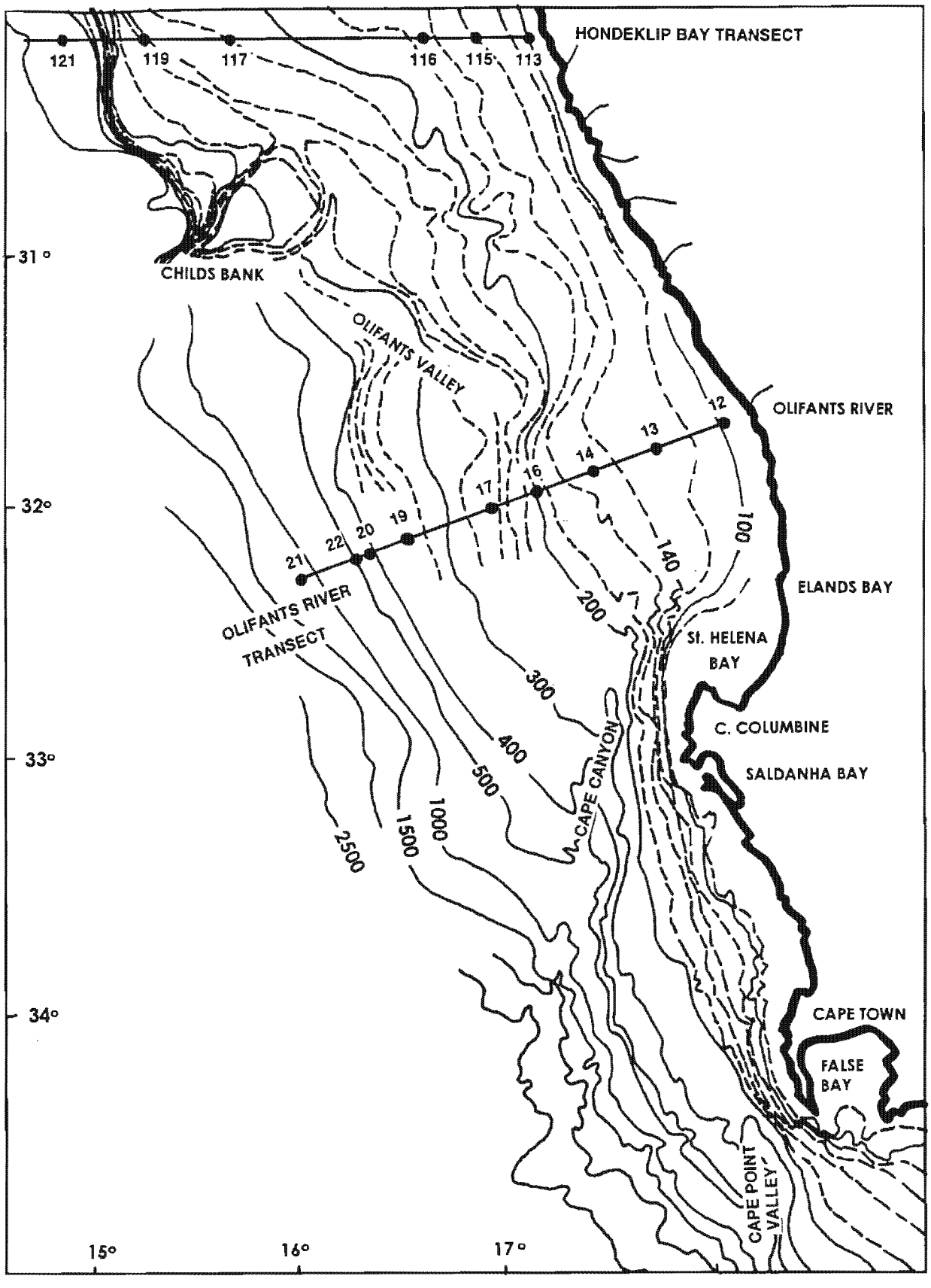

Fig. 4.3: A map showing the station positions from both the Hondeklip Bay and Olifants River transects as well as the bathymetry of the southern half of the Benguela System. The two transects overlie contrasting cross-shelf profiles with a single sharp break at 300m along the Hondeklip bay transect and a less pronounced double break (150m and 400m) along the Olifants River transect. The positions of the transects relative to the upwelling cells should be noted. While the Hondeklip Bay transect is practically within the Namaqua upwelling cell (starting at Hondeklip Bay), the Olifants River transect is 100km north of the Cape Columbine upwelling centre. The Cape Peninsula upwelling centre is located south of Cape Town. The main bathymetric features are Child's Bank, the Olifants Valley, the Cape Canyon and the Cape Point Valley.

4.3.3 Olifants River Transect: Southern Benguela Sub-System

The Olifants River transect was a southwest (247°) bearing line from the coast at 31.5 °S to approximately 600m depth (Fig. 4.3). The transect was sampled in the course of a Plankton Dynamics cruise on the FRS Africana over the period 13/2/91 to 25/2/91, although the data was collected between 13/2/91 and 15/2/91.

The Southern Benguela System can be further divided into two sub-sections, northern *West Coast* and southern *Peninsula* sub-sectors (Fig. 4.3), on the basis of the very different shelf morphologies within the sector. The nomenclature is in keeping with previous usage (Brown *et al.*, 1991). The West Coast sector is the shortest one down to the latitude of Cape Columbine (33 °S) (Fig. 4.3) at which point the shelf morphology changes from a wide shelf with a double break (280 and 500m) to a narrow shelf with a main break at 400m (Fig. 4.3). The latter sector characterizes the Peninsula sector. The Olifants River transect is located in the West Coast sector. In this sector, one lesser shelf break can also be found on the upper shelf (140 - 180m) which is also visible on the transects below. The shelf is cut by two prominent canyons, the Olifants Valley which runs approximately E W at 31.5 °S and the Cape Canyon which runs approximately N - S through the Peninsula sector (Fig. 4.3). All these physiographic features will be shown to play a significant role in both the oceanographic characteristics of the system as well as the carbon fluxes within and through it.

It should be noted that there are differences in the units used to express biogeochemical parameters between the oceanographic cross-shelf sections ($\mu molkg^{-1}$) and those in t - TCO_2 plots (μmol^{-1}: where TCO_2 is expressed as $NTCO_2$ implies a value normalized to a salinity of 35 psu). The reason for this descrepancy is that while it has become normal practice to plot biogeochemical parameter concentrations as ($\mu molkg^{-1}$), the calculation of

fluxes requires that the concentrations be expressed in volumetric terms. The normalization of the concentrations to a fixed reference salinity (35 psu) removes the component of concentration variability linked to salinity changes. All subsequent biogeochemical and modelling chapters use the latter format for concentration.

The contouring of oceanographic sections was done using the kriging method in Surfer for Windows. While the data search and anisotropy aspects of the procedure were optimized as best as possible there are some instances where spurious contouring could not be avoided due to limitations in spatial resolution. These are pointed out in the appropriate instances below.

4.4 Results and Discussion

Because of the simplicity of the Ekman model it is often tempting to view a zonal section across the shelf of an upwelling system as a spatial representation of the temporal evolution of an upwelling cycle. However recent work has emphasised the importance of longshore flow through the system so that upwelling systems need to be interpreted more as a 3 dimensional systems. The ensuing spatial physical and biogeochemical sections are zonal cross sections of the Benguela System such that each transect spans the shelf within each of the 3 sectors proposed above. The use of NO_3^- and O_2 biogeochemical transects is in support of the interpretation provided by the carbonate parameters. They are an independent test of the oceanographic consistency of the carbonate data.

4.4.1 Henties Bay Transect: Northern Benguela System

Wind Regime

The Henties Bay transect is located between the two most important centres of upwelling inducing cyclonic wind stress curl in the Benguela System : Cape Frio (CF) at 18 °S and Luderitz (LZ) at 27 °S (Shannon and Nelson,

1996). There is also an upwelling centre immediately to the south of the transect off Walvis Bay (23°S) (Fig. 4.2) (Lutjeharms and Valentine. 1987 ; Shannon and Nelson, 1996). Equatorward winds in this part of the Benguela System are not as sensitive to seasonal variability as in the southern Benguela System. Typically, at these sites (CF and LZ) winds range between moderate-high to high -very high and in the mid sector, where the transect was sampled, the range is low-moderate to moderate-high (Boyd, 1987). This period of the year (March) corresponds to the austral late summer - autumn season which at this latitude is characterized by low - moderate equatorward wind regimes (Boyd, 1987; Shannon and Nelson, 1996). The wind record for the month of March 1992, taken from the lighthouse at Pelican Point, Walvis Bay is shown on (Fig. 4.4) and depicts the variability in the equatorward wind component.

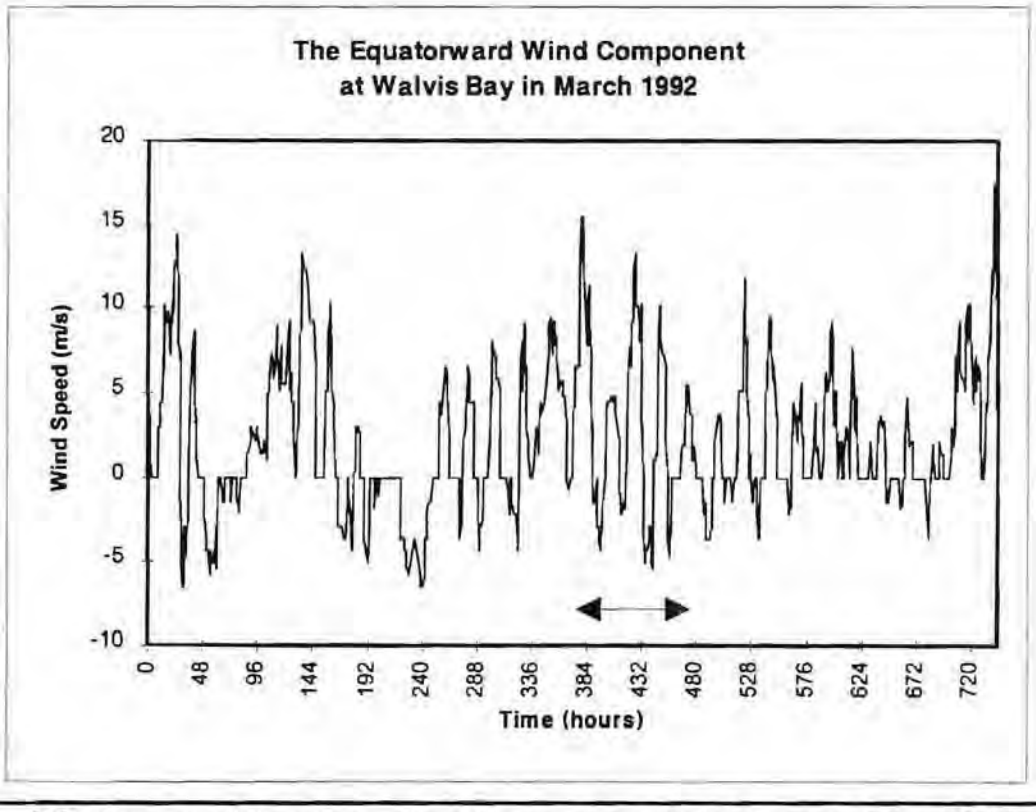

Fig. 4.4: A one month long time series of the equatorward wind component from Walvis Bay in March 1992. The wind pattern is characterised by diurnal reversals which occur over a shorter period than the local inertial oscillation period and do not therefore result in upwelling. The period over which the samples were collected is marked by the double arrow.

The strongest features of this wind record are its diurnal signal over the whole month and its strength in the period immediately preceding the cruise (Fig. 4.4). The equatorward component peaks in the afternoon period but for most night time periods, especially during the cruise it is characterized by poleward reversals (Fig. 4.4). It is clear from this record that the wind field is strongly modulated by the diurnal heating and cooling of the arid Namib desert abutting on the coast. Because the period of the diurnal wind variability is shorter than the inertial oscillation period for this latitude (~32hrs) it is predicted that the equatorward wind field did not result in upwelling.

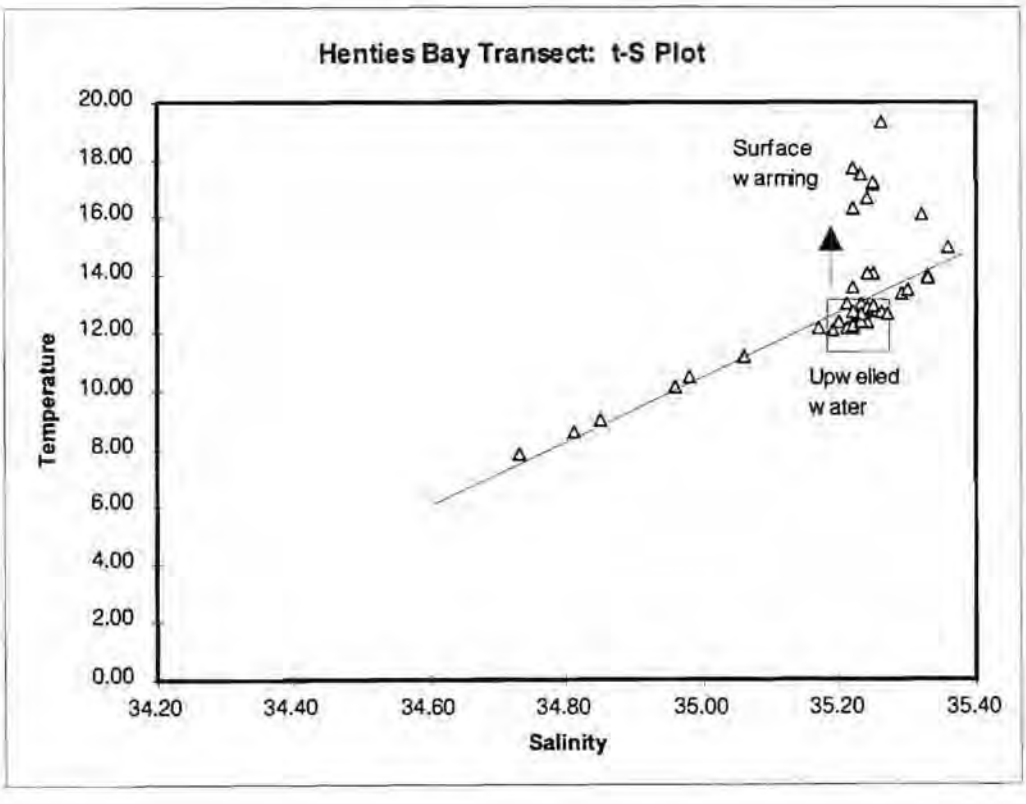

Fig 4.5: A t - S plot using the data from the Henties Bay transect. It shows that most of the points coincide with the line which characterises the t - S properties of South Atlantic Central Water (SACW). It also shows that most of the shelf resident SACW was defined by $11^{\circ}C < t < 13^{\circ}C$; $35.2 < S < 35.3$. The effects of sun warming of upwelled waters is shown by the points lying above the SACW trend.

Physical Characteristics: Temperature and Salinity

The t-S plot shows that the water sampled in this section has its origin in the linear part of the t-S characteristics of South East Atlantic waters (6°C - 16°C, 34.60 - 35.50) which define South Atlantic Central Water (SACW) (Fig. 4.5). Most of the samples were taken on the shelf where the salinity range is typical of the upper end of the SACW t - S range (S: 35.20 - 35.40) (Fig. 4.5). Some of the data which lie above the main linear relationship (fitted by eye) represent aged upwelled waters. In upwelling systems evaporation rates are very low (Guastella, 1992) thus, during the ageing process the temperature may increase with solar heating but the salinity remains unchanged. This makes salinity a suitable conservative variable with which to characterize waters in upwelling systems. This sector of the northern Benguela shelf is largely characterized by upwelled water with a t-S range of 35.20 - 35.25 which upwell with temperature in the range 12 - 13 °C and subsequently warm up to 17 - 19 °C at the surface. This concurs with historical data from this sector of the Benguela System (Shannon, 1985) and indicates that SACW is being upwelled onto the shelf from a depth of 150-200m.

Physical Sections: Advection, Stratification and BBL turbulence

The temperature and salinity sections (Figs. 4.6a,b) are representative of typical water column physical characteristics in the central Namibian sector of the Benguela System. The temperature section (Fig. 4.6a) shows that the system was in a relaxation state, characterized by a stratified upper water column (< 30m) with a particularly strong thermocline close to shore. Under upwelling conditions newly upwelled water (t < 13°C S ~ 35.25) would normally outcrop.

The observed relaxation state could then be explained in two ways:

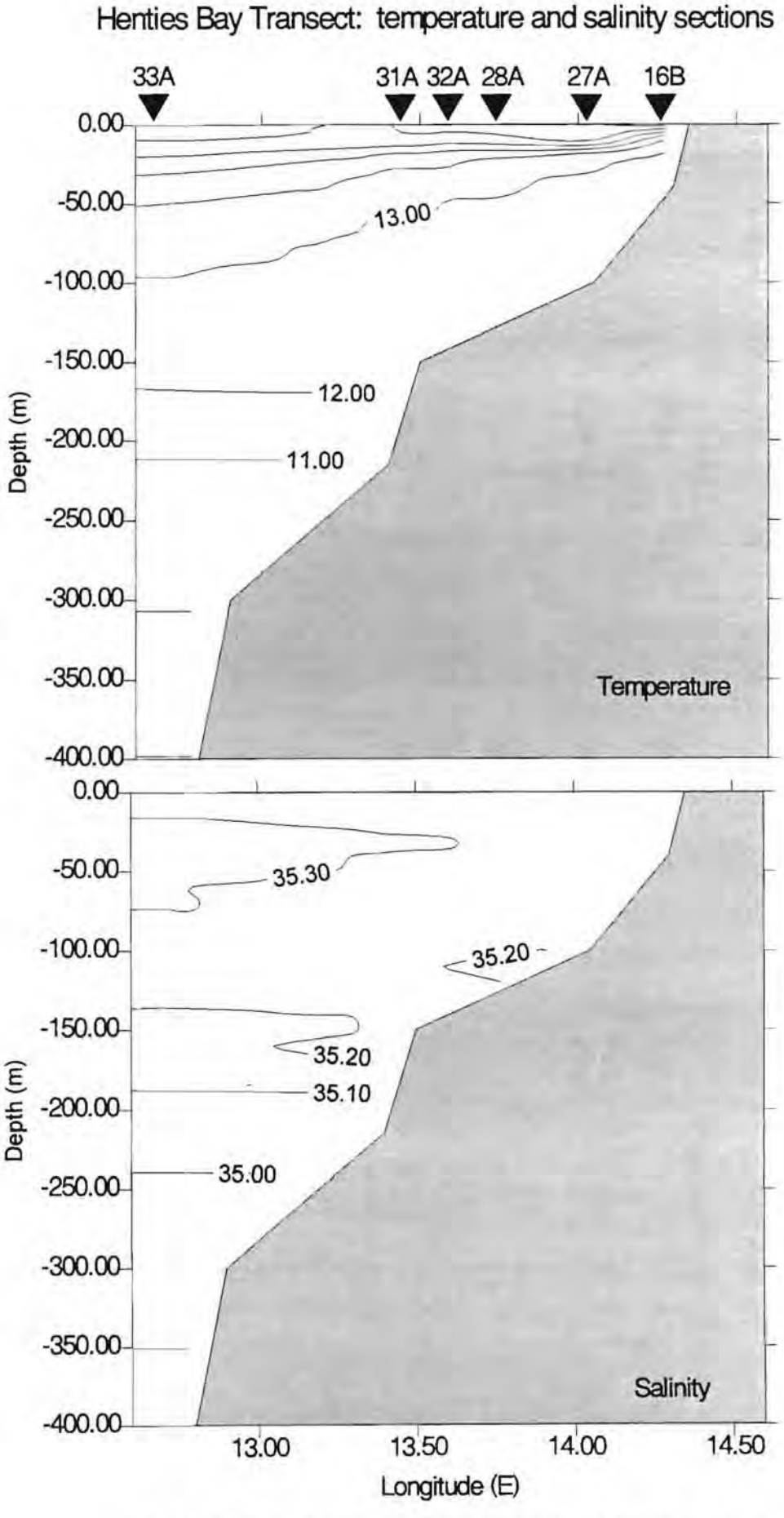

Fig. 4.6a,b: Temperature and Salinity sections plotted with data from the Henties Bay transect. The station positions are marked along the top axis They show that shelf waters which upwell in the vicinity of the Walvis Bay a temperature of 12-13oC and salinity 35.20 psu. The intense stratification along the inshore area is indicative of no active upwelling.

- The equatorward wind stress is modulated by a strong diurnal sea - land breeze signal. The diurnal equatorward wind reversals which occur at a higher frequency than the inertial oscillation frequency (~32hrs) do not induce upwelling (G. Nelson, pers.com.). However it should be noted that the land - sea wind reversals diminish offshore so it is possible that upwelling could occur at distances of more than 50 km offshore (G. Nelson pers.com.).

- The sampling area is approximately 60km on the equatorward side of the closest upwelling centre of Walvis Bay (Fig. 4.2). The surface water represents therefore warmed aged upwelled water from the Walvis upwell cell which is advected equatorward. The salinity (Fig. 4.6b) which over the entire surface layer ($Z < 20m$) has a range 35.22 - 35.26 support an upwelled origin for the surface water.

Given the geographic location of the transect and present insight of poleward flow characteristics in the Benguela System (Shannon and Nelson, 1996), it is hypothesized that the bulk of the subsurface (> 20m) water covered by the transect (S: 35.20 - 35.25) would have originated from a site to the north of the transect. There, it would have been advected from the slope region onto the inner shelf and entrained into the poleward shelf flow. Current meter data from this area shows that there is a net poleward transport but that seasonal flow reversals are also evident (G. Nelson, pers.com.). Poleward longshore advection as the main supply route for upwelled waters, as opposed to a more classical Ekman transport driven cross-shelf flow is supported by the presence of fine-grained sediments on the central Namibian shelf (R. Johnson pers.com.). It was suggested that the accumulation of diatomaceous ooze on the inner shelf was only compatible with a very reduced (25%) bottom friction linked to Ekman driven cross shelf flow (R. Johnson pers.com.). By deduction, long shore transport associated with the poleward undercurrent must play a more important role in respect of the

supply of water which gets upwelled. This is a strong factor supporting the notion that the Walvis Bay upwelling cell is largely supplied with water which is advected onto the shelf at Cape Frio from where it is transported polewards. When this water comes within the zone of influence of an upwelling centre, such as Walvis Bay it is then upwelled to the surface where it outcrops.

Similarly, surface waters could either be equatorward moving aged upwelled waters originating from the Walvis Bay cell (Bailey, 1990) or poleward moving Angola surface waters (Boyd, 1987). The southward intrusion of saline and warm surface waters from Angola into the central Namibian shelf is a periodic occurrence in the late summer - early autumn coinciding with the reduction of equatorward wind stress (Boyd, 1987). The core of saline water found on the western end of the salinity section in the depth range 20 - 80m extending as far as the inner shelf break is probably the only evidence for a poleward intrusion of Angola water.

Biogeochemical Sections: Carbon (TCO_2 and PCO_2), Oxygen and Nitrate

The TCO_2, PCO_2 , O_2 and NO_3^- sections have two significant features (Figs. 4.7a,b and 4.8a,b):

- the extremes in their vertical structure and,
- the separation of the BBL concentration maxima into two discrete bodies of water each coinciding with a shelf break zone.

The highest dissolved carbon values (TCO_2: > 2.25 $\mu molKg^{-1}$; PCO_2 > 900 μatm) are found in the benthic boundary layer, the mid water range is (TCO_2: 2.20 - 2.25 $\mu molKg^{-1}$; PCO_2: 600 - 900μatm) and the surface waters (TCO_2: < 2.20 $\mu molKg^{-1}$; PCO_2: < 600μatm)(Fig. 4.7a,b). Similarly, in the case of oxygen distribution an inversely correlated vertical structure is

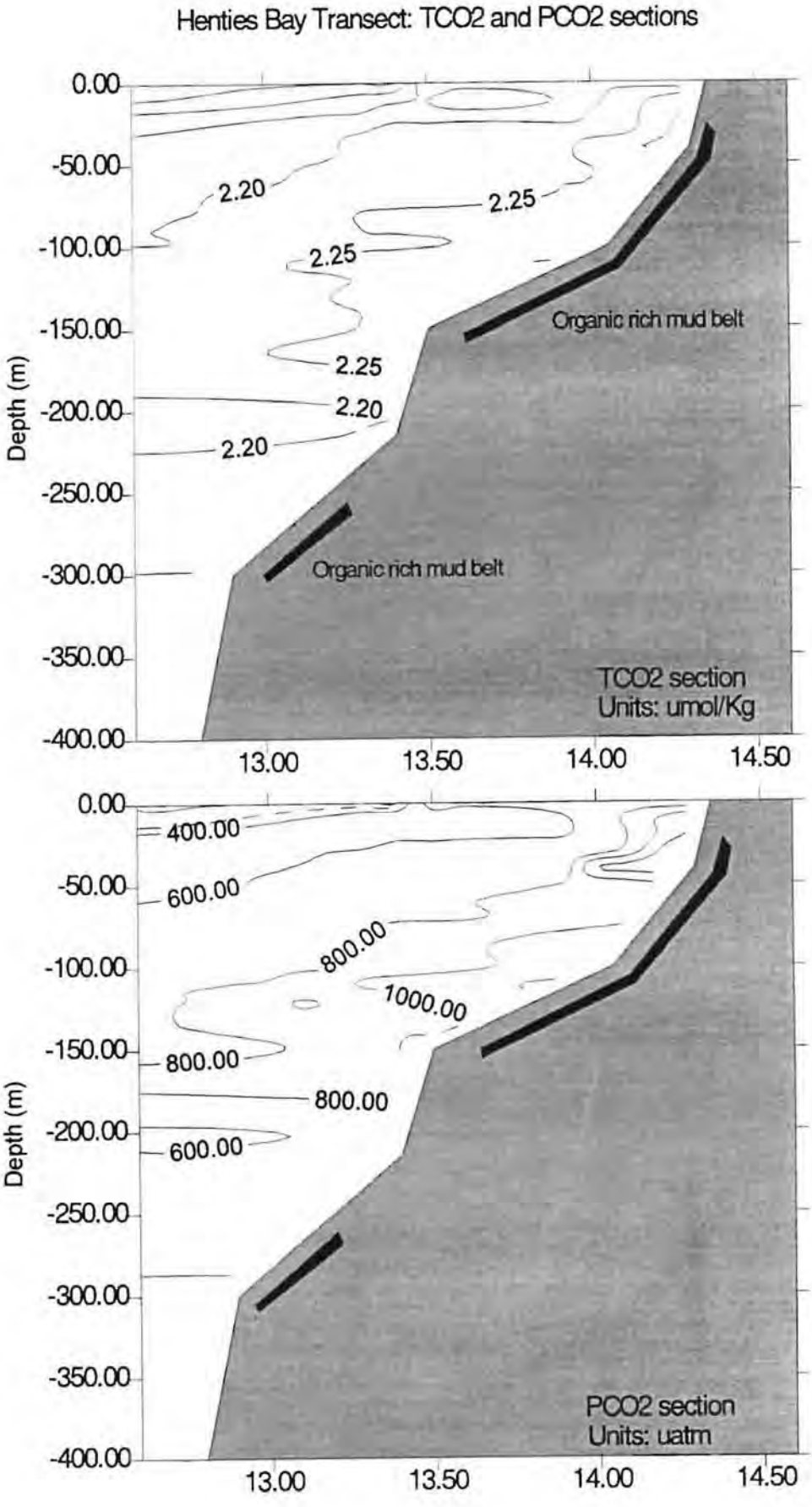

Fig. 4.7a,b: TCO2 and PCO2 sections from the Henties Bay transect. The location of the organic rich mud belts which underlie the transect are shown to be located on shelf segments above the slope breaks. It can be seen that the highest PCO2 values (> 1000 uatm) are associated with remineralization from the inner shelf mud belt. It can be seen from station positions marked on Fig. 4.6a that there was not enough spatial resolution to show the same high PCO2 with the mud belt on the outer shelf.

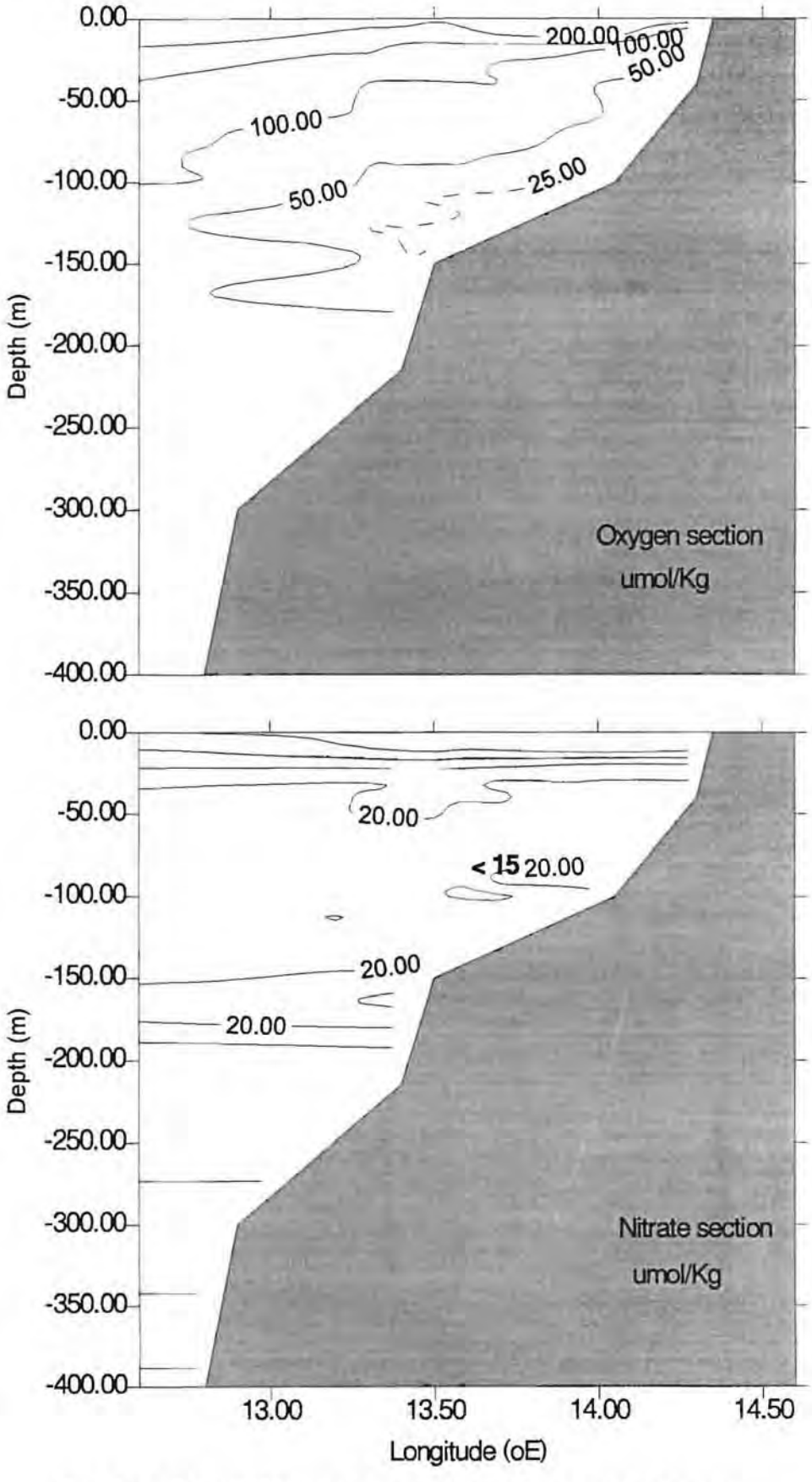

Fig. 4.8a,b: O2 and NO3 sections from the Henties Bay transect. The main feature to note is the coincidence of lowest O2 < 25umol/Kg abd NO3 < 15umol/Kg concentrations with the elevated PCO2 values (Fig. 4.7b). Benthic remineralization is the common driving process and is making use of both O2 and NO3 as electron acceptors.

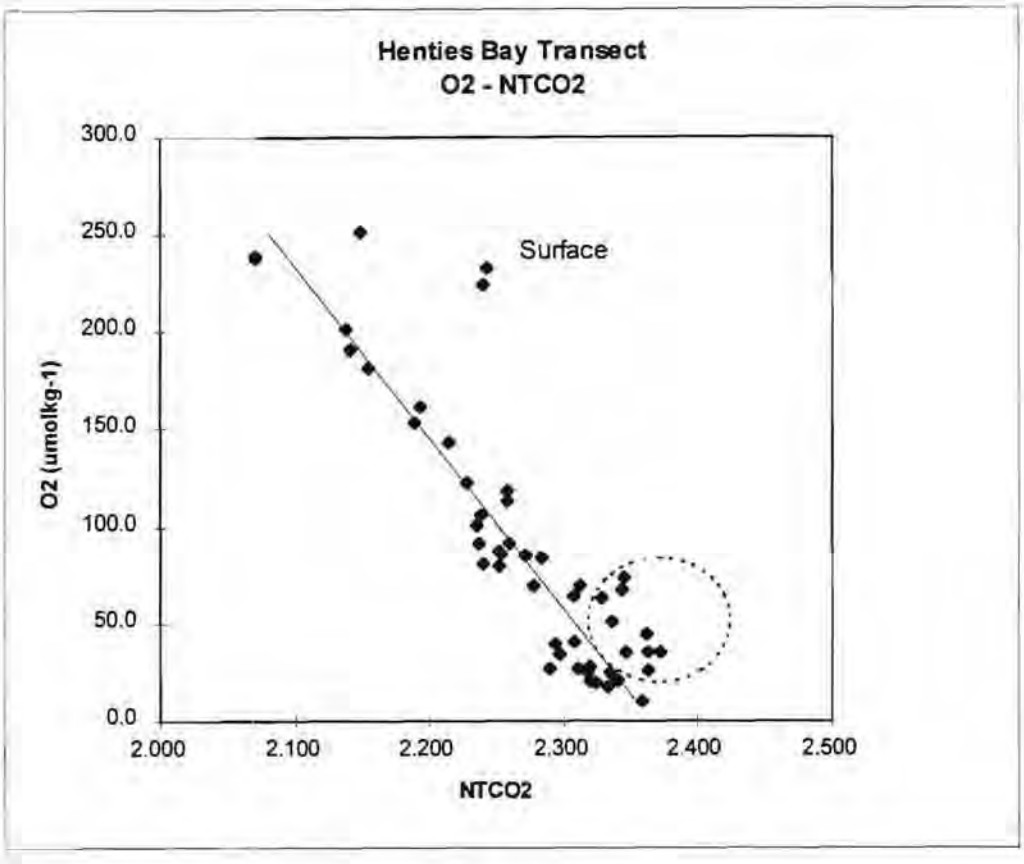

Fig. 4.8c: A scatter plot depicting the relationship between O_2 and $NTCO_2$ (TCO_2 normalized to 35 psu) for data collected along the Henties bay transect. This plot is used to clarify the relationship between TCO2 and O2 changes which are not clearly represented in the transect sections (Figs. 4.7a and 4.8a). It shows that most of the points lie close to the trend line which closely reflects the -1:1 O_2:TCO_2 stoichiometry typical of aerobic systems. There are limited excursions of data points reflecting increases in TCO_2 without the concomitant reduction in O_2 (circled). These are likely to be due to CO_2 inputs driven by oxidation pathways using electron acceptors other than oxygen. On the basis of the observed evidence for de-nitrification in the mid to lower water column (Fig. 4.8b) it is very likely that NO_3^- is the most likely alternative electron acceptor. The reduction of mid water NO_3^- by 5 - 10 $\mu molkg^{-1}$ would result in the release of 7.5 - 15 $\mu molkg^{-1}$ of CO_2 which accounts for most of the observed excursions. Additional CO_2 inputs could originate from SO_4^{2-} reduction in the sediments.

observed with values of O_2 < 50μmolKg^{-1} within the BBL and O_2 > 150 μmolKg^{-1} in the surface layer (Fig. 4.8a,c). The nitrate section shows the same vertical change with values NO_3 < 5 μmolKg^{-1} at the surface but while bottom values reach a peak of 31 μmolKg^{-1} over the outer shelf break, the concentrations in the inner shelf BBL decrease to NO_3 < 20 μmolKg^{-1} (Fig. 4.8b). This de-nitrification, which has been observed in the past in the same system (Chapman and Shannon, 1985), occurs when NO_3^- becomes the preferential electron acceptor after oxygen concentrations are reduced to a level which allow denitrifying bacteria to become active (Fenchel and Blackburn, 1979).

The vertical biogeochemical water column gradient is in sharp contrast to the more homogeneous physical characteristics, particularly salinity, of the shelf water column and the biogeochemical characteristics of pre-formed SACW. SACW with the t,S characteristics of that which is found on the Namibian shelf (t , S) can be identified on the outer shelf in the depth range 80 - 130m with TCO_2 and PCO_2 characteristics in the range 2.20 -2.21 μmolKg^{-1} and PCO_2 625 - 650 μatm respectively (Fig. 4.7a,b). The main factor affecting the changes to the biogeochemical parameters is the activity of the biological pump and how it interacts with the physical dynamics.

The biogeochemical sections and data show that there is a zone of enhanced TCO_2 2.26 - 2.31 μmolKg^{-1}; PCO_2 > 1000 μatm (not contoured on Fig. 4.7a,b) in the BBL closely linked to the inner shelf (25 -150m) (Fig. 4.7a,b). Similarly, low O_2 concentrations (O_2 < 25μmolKg^{-1}) can also be seen to coincide with the same spatial scale. This is in good agreement with historical observations across the Namibian shelf which indicate that bodies of water with low oxygen concentrations (< 1ml/l) are consistently associated with discrete sites across the shelf (Chapman and Shannon, 1985). These discrete sites (marked on Fig. 4.7b) coincide with bands of sediment which are relatively enriched with particulate organic carbon (Rogers and Bremner, 1991). Here, not only does enhanced acumulation of POC occur but re-mineralization as

well which leads to spatially constrained increase in TCO_2 and decreased O_2 concentrations. The inner shelf zone (Z < 150m) of this transect coincides with a wide stretch of organic rich diatomaceous muds: see Fig. 4.27 from (Bremner, 1983). The spatial resolution of the stations was not sufficient to clearly resolve the boundaries of all these transitions. This is shown by the fact that though the same sediment map for the Namibian shelf predicts there to be a second zone of POC accumulation at 260-300m depth along the transect, its impact was not resolved by the station spacing. This result emphasises the need to define sampling scales to the needs of the processes being studied. The mechanisms by which the discrete accumulation of POC occurs in the sediment are hypothesised and discussed in detail below.

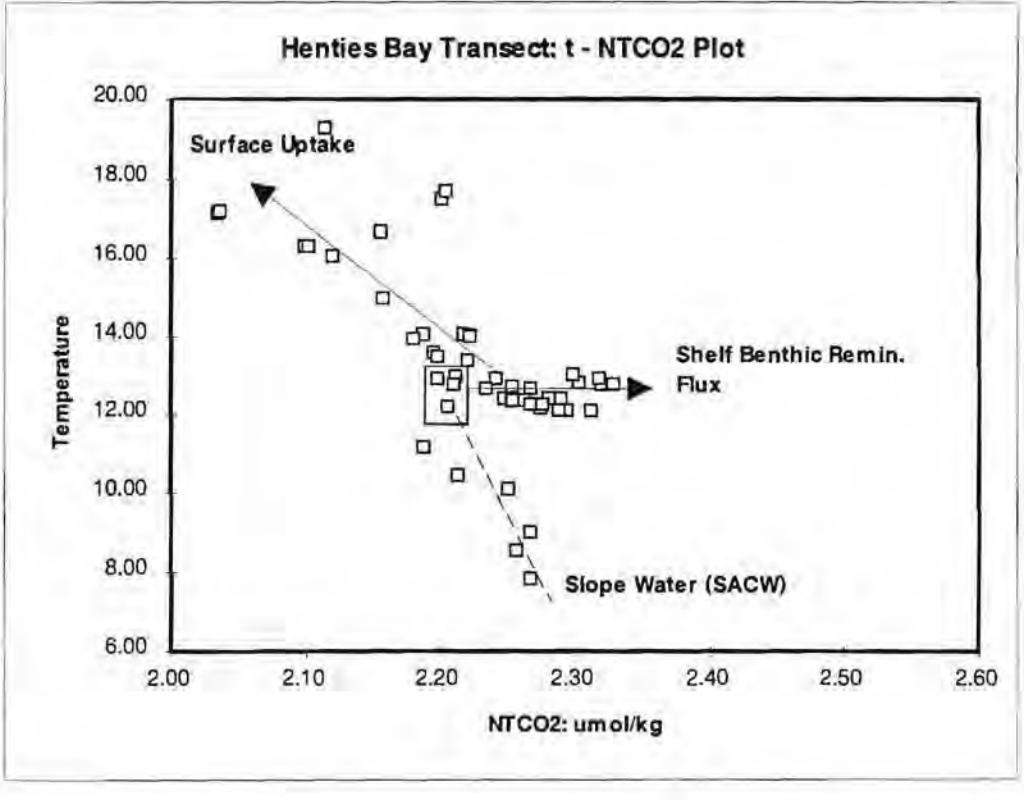

Fig. 4.9: A t - $NTCO_2$ plot of the data from the Henties Bay transect. NTCO2 refers to the TCO_2 concentration ($\mu molKg^{-1}$) normalized to a salinity of 35.00 psu. It shows that virgin SACW in this part of the Benguela System is characterised by $2.19 < NTCO_2 < 2.21$ $\mu molKg^{-1}$ which is significantly modified by benthic remineralization in the inner shelf (NTCO2 > $2.30\mu molKg^{-1}$) prior to upwelling. Surface warming as well as uptake and degassing of CO_2 to the atmosphere reduces the values to ~ $2.05\mu molKg^{-1}$ which is close to atmospheric equilibrium. The characteristics of slope water are also shown.

Physical - Biogeochemical Relationships:

One of the most useful ways to elucidate the relative magnitudes of the changes driven by both physical and biogeochemical forcing is to plot them through appropriate independent variables. Such a plot, of temperature and $NTCO_2$ (Fig. 4.9), describes the relative magnitudes of surface and benthic processes which modify the TCO_2 and temperature characteristics of SACW during its sub-surface shelf advection upwelling and subsequent ageing. Temperature is more useful, in this case, than salinity because it also reflects surface residence through its response to sun warming. TCO_2 on the other hand is independent of temperature whereas PCO_2 is not (see Chapter 3). The impact of the benthic remineralization flux enhanced by BBL turbulence on poleward flowing SACW is shown by the shift in TCO_2 values within the 12 - 13 ^{o}C temperature range. Virgin SACW TCO_2 values (2.20 - 2.21 $\mu molKg^{-1}$) increase sharply to a range of 2.30 - 2.35 $\mu molKg^{-1}$ (Fig.4.9). The long term impact of surface productivity and the loss of CO_2 across the air - sea boundary is given by the vector linking the t - TCO_2 block for the inner shelf waters to a range of TCO_2 values which decrease with increasing temperature.

4.4.2 Hondeklip Bay Transect: Central Benguela Sub-System

Wind Regime

The equatorward wind regime begins to acquire a stronger seasonal signal compared to the northern Benguela System, with very light winds in the winter moderate - high strength in the spring and late summer and high - very high strength in mid summer (Boyd, 1987). The period when the study was undertaken mid-June 1993, coincided with the period during which a light wind regime was predicted (Boyd, 1987).

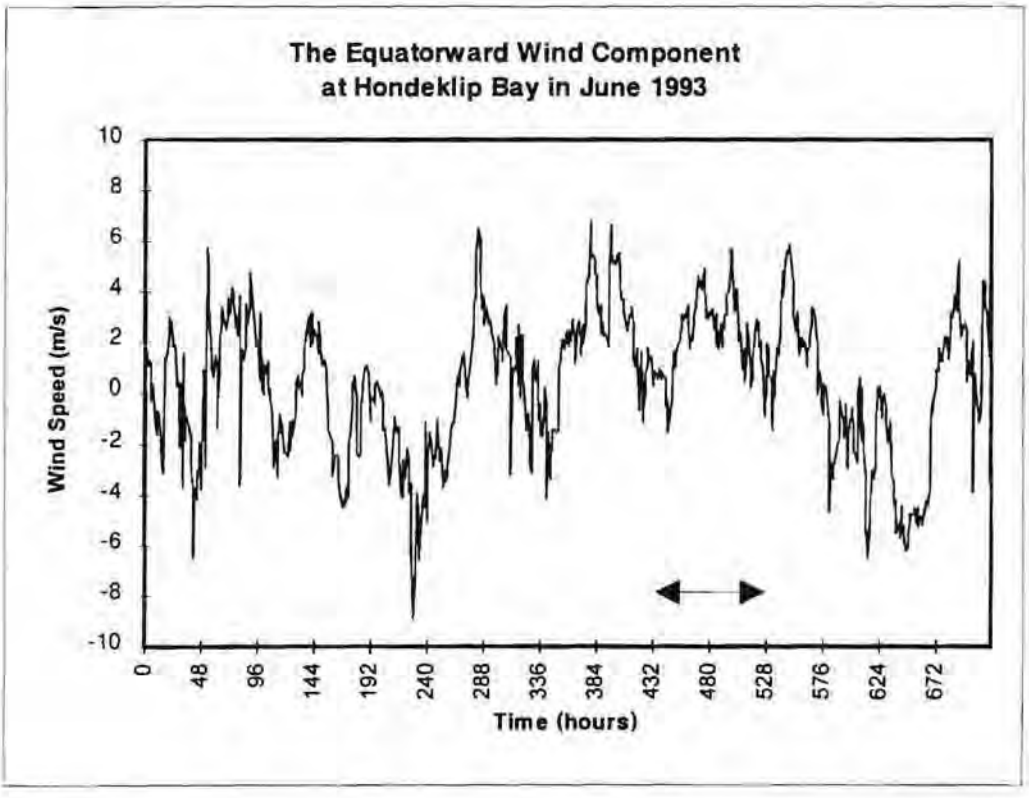

Fig. 4.10: A one month long time series of the equatorward wind component from Hondeklip Bay in June 1993. The period over which the transect was sampled is marked with the double arrow. Each interval corresponds to 2 days (48 hours). Sampling coincided with the end of a 4 day active upwelling cycle which should be reflected by the physical and biogeochemical sections.

The wind history for the two weeks preceding the study is somewhat at odds with this average expression of wind variability and shows that an almost summer-like 3-4 day equatorward wind cycle dominated the system (Fig. 4.10). This is indicative of the degree of variability in such a system where interannual variability plays an important role in both the strength and seasonality of the winds. The length of these periods exceeded the inertial oscillation period of about 24 hours for this latitude with the result that upwelling could be expected.

Physical Characteristics: Temperature and Salinity.

The t-S plot shows that most of the water sampled in the Hondeklip Bay transect had its origin in SACW which spans the linear part of the t-S plot for

the south east Atlantic Ocean (6 - 16°C ; 34.60- 35.60) (Shannon, 1985). Samples cover practically the whole range (Fig. 4.11) although waters which outcrop are restricted to the range (10 - 11°C; 34.80 - 35.00). There is some evidence for warming of previously upwelled waters (S: 34.80 35.00) shown as a series of points lying on the warmer side of the SACW t-S line (Fig. 4.11). The deeper samples from the transect reached into the core of Antarctic Intermediate Water shown as a salinity minimum (S < 34.40) and the deepest sample reached the core of what is likely to be a mixture of NADW and CDW which is typically found in the eastern Cape Basin (Reid, 1989). The t-S characteristics of shelf water differ markedly between the Henties Bay and Hondeklip Bay transects. This suggests that the SACW which supplies upwelled water to the Hondeklip Bay area originates from a different source to that which was sampled in the Henties Bay transect.

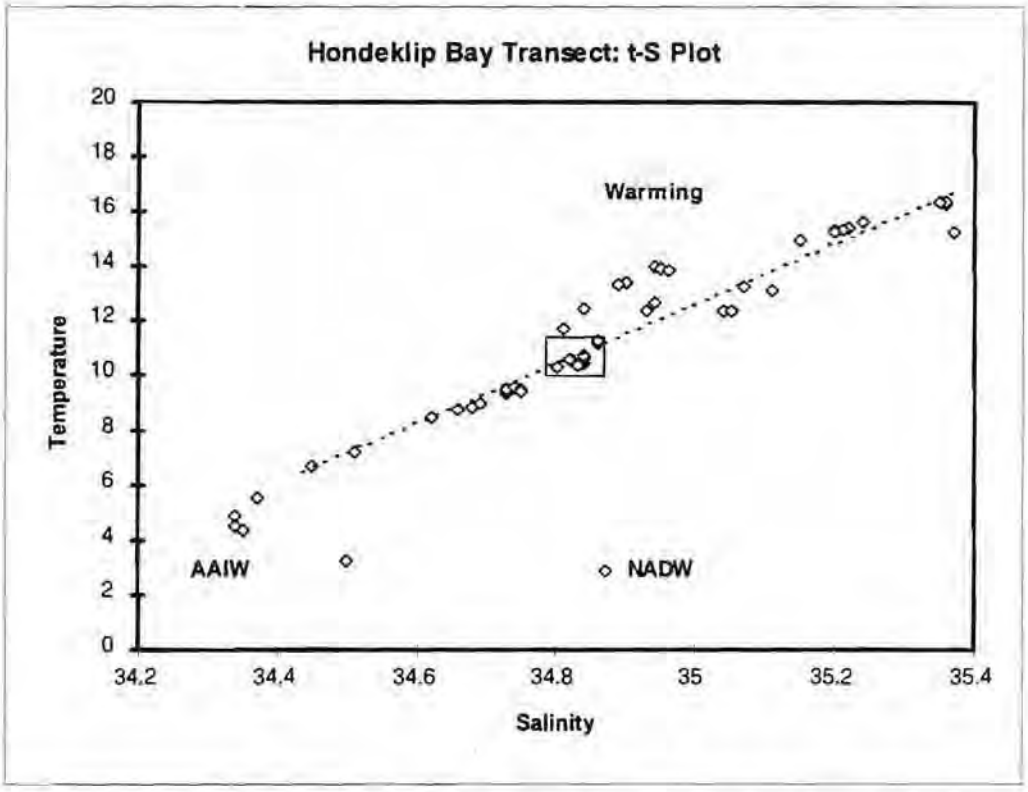

Fig. 4.11: A t - S plot of the data from the Hondeklip Bay transect. It shows That the inner shelf water which upwells at the Namaqua upwelling cell is physically characterised by 10 < t < 11°C ; 34.8 < S < 34.9 which is also part of the t - S continuum which defines SACW. The extent of warming is reduced to 14°C due to the sampling period coinciding with the austral winter. Also shown are the cores of Antarctic Intermediate Water (AAIW) and North Atlantic Deep Water (NADW).

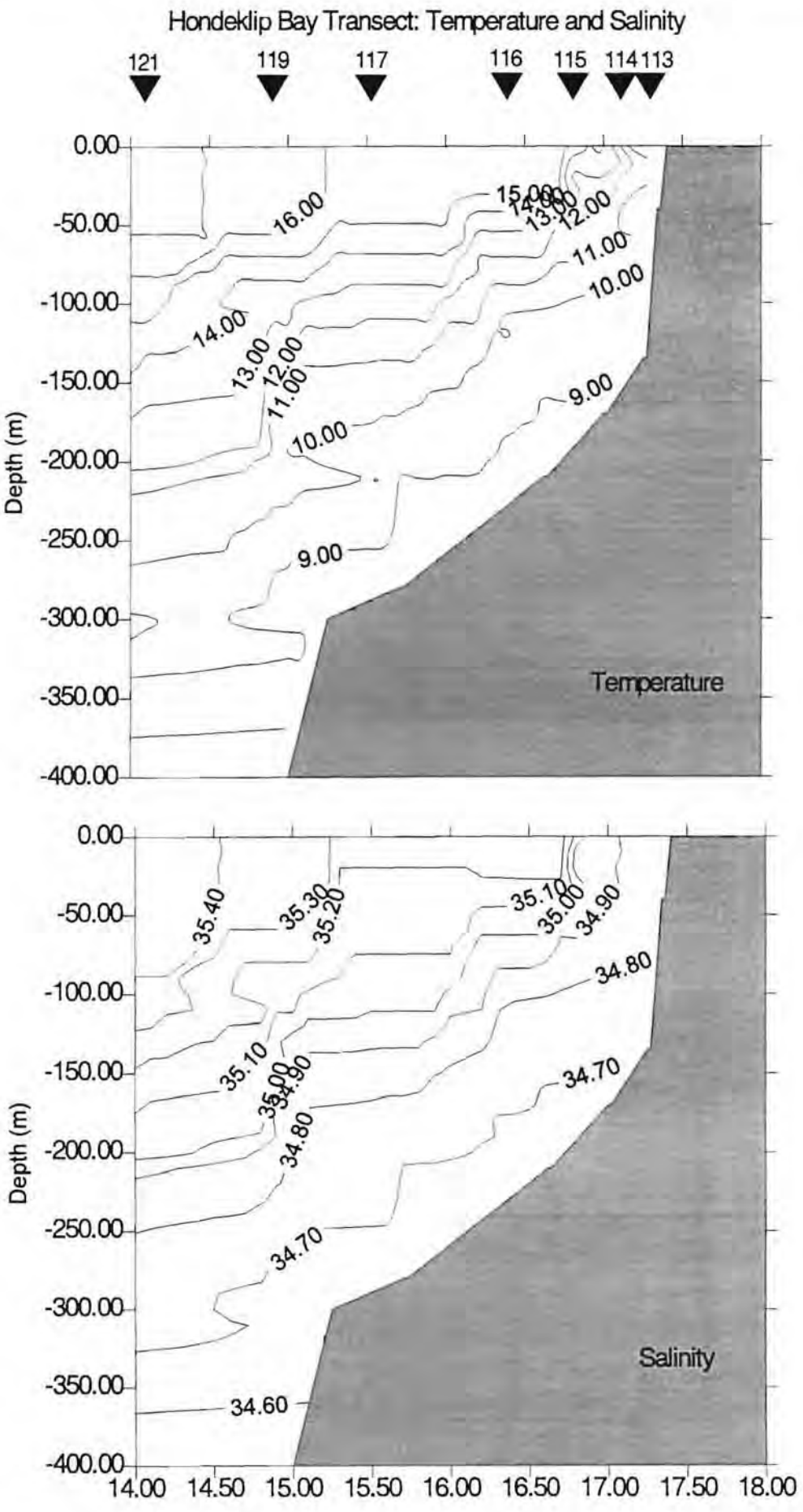

Fig. 4.12a,b: Temperature and salinity sections plotted with data from the Hondeklip Bay transect. The station positions are marked along the top of the temperature plot. The main features include, isopleths indicate that there was active upwelling (11oC outcroping), the upwelling front t < 11oC, the oceanic front S = 35.00psu in the upper 50m and the step in the isopleths at the shelf break.

Physical Sections: Advection, Stratification and BBL Turbulence

The slopes of the isopleths in the temperature and salinity sections confirm the predictions above that the system was in an "active" phase of upwelling (Fig. 4.12a,b). Outcropping of the t < 11°C and S = 34.85 isopleths (Fig. 4.12a,b) occurs at the stations 113 and 114 closest to shore. This type of pressure gradient would normally, in terms of Ekman theory, drive an equatorward current (Neumann and Pierson, 1966). As with the Namibian shelf, current meter measurements confirm that poleward flow drives advection throughout most of the subsurface water column in this central zone of the Benguela system. In this scenario is expected that the surface layer would be entrained in the general equatorward flow of the Ekman layer. Furthermore an equatorward baroclinic jet should be located as a narrow band beyond the shelf break in the depth range 300-400m where the isotherms and isohalines steepen (14 -15 °E).

The sharp upturn of the isopleths in the upper 40m across the transect is indicative of wind driven mixing which occurs due the weak thermal stratification of the system in the Austral winter. Of particular significance to the carbon flux is the well mixed water column at station 113 which overlies a shelf zone with intense carbon re-mineralisation. Upwelling intensity is clearly highest close to shore but the lack of stratification would be expected to sustain large CO_2 fluxes into the atmosphere from the newly upwelled water while at the same time inhibiting photoautotrophic activity within the zone bounded by the upwelling front.

Two frontal (temperature and salinity) structures can be seen close to the main upwelling cell on the eastern end (Fig. 4.12a,b) . The thermal front separates the newest upwelled water (t < 12°C) from the warmer aged counterpart from earlier events (12 -17 °C). The salinity front separates upwelled SACW water from warmer and more saline oceanic water (S > 35.00). It is likely that most of the CO_2 exchange occurs within the salinity

front which marks the western boundary of the upwelling system at the time the transect was sampled. In the winter when the strength and persistence of equatorward wind stress decreases there is a shoreward shift of the oceanic front.

At all the stations, samples were taken in the vicinity of what was expected to be the benthic boundary layer. These were at 5, 10 and 15 m off the bottom and in all of them both the t and S values support the existence of a BBL at least 15m thick. The shelf break dome is not well resolved because of station spacing but it can be partly seen as a steepening of the isopleths at the shelf break. This is supported by the biogeochemical sections below.

Biogeochemical Sections: Carbon (TCO_2 and PCO_2), Oxygen and Nitrate

The three features of oceanographic significance in the biogeochemical sections along the Hondeklip Bay transect (Fig. 4.13a,b and 4.14a,b) are:

- as was the case in the Namibian transect, there exists a strong vertical gradient between the surface layer and the benthic boundary layer.
- there is only one major benthic boundary layer "dome" associated with the single shelf break at 300m.
- the highest TCO_2 / PCO_2 values of the whole data set are located close to shore - these are the values which characterize upwelled waters in at Hondeklip Bay.

The surface layer is characterized by TCO_2 values which range from < 2.10 $\mu molKg^{-1}$ outside the upwelling front to the extremely high values of 2.20 - 2.40 $\mu molKg^{-1}$ and single values of over 2.5 $\mu molKg^{-1}$ within the front (Fig. 4.13a). As expected, PCO2 values mimic TCO2 with a range from near atmospheric equilibrium for aged upwelled waters (~350 μatm) to the unusually high inshore values exceeding 3000μatm (Fig. 4.13b). As a result of the active upwelling stage during which sampling started, these high

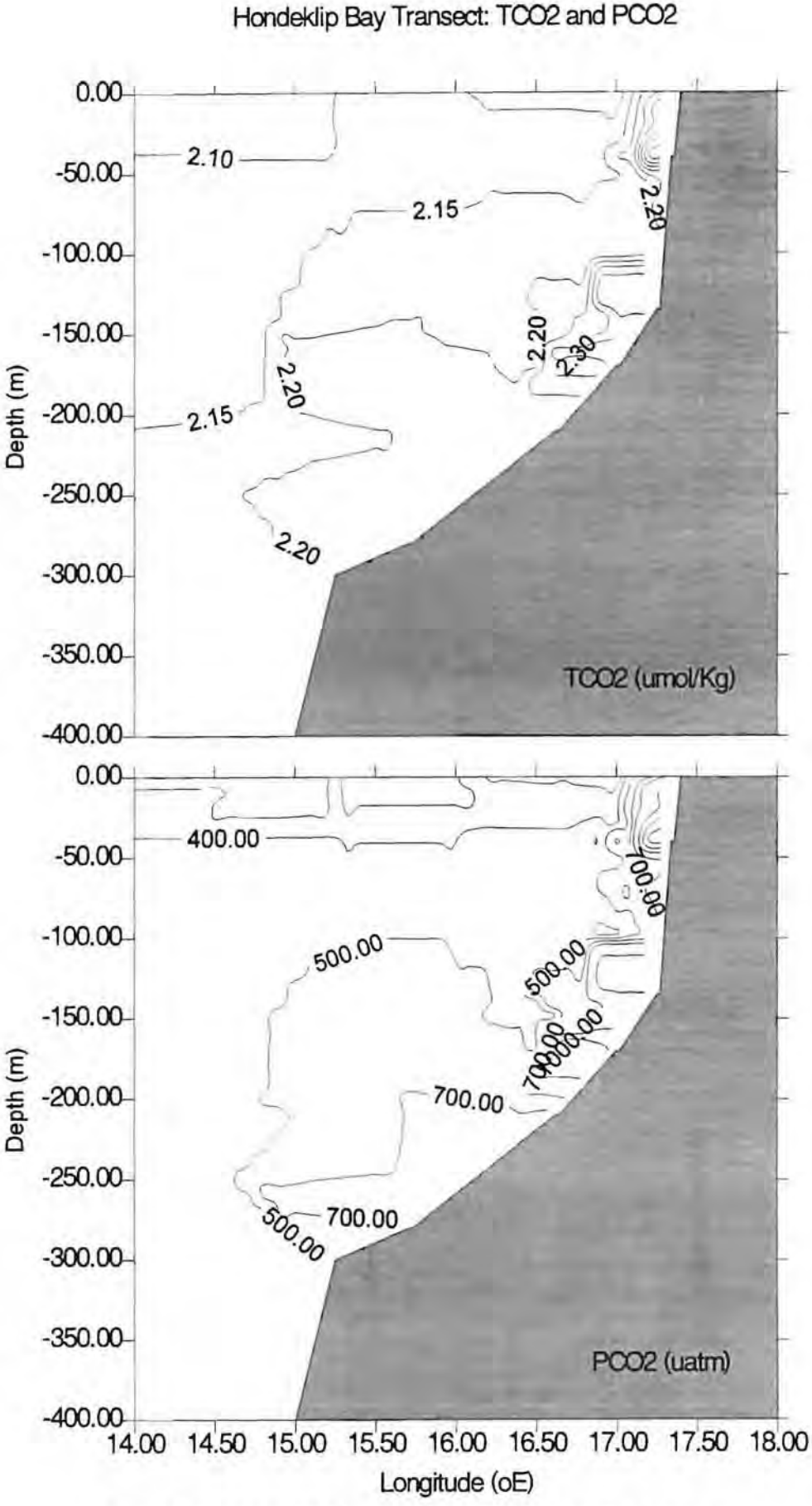

Fig. 4.13a,b: TCO2 and PCO2 sections from the Hondeklip Bay transect. The intense gradients off the sediments in two zones of the shelf (120-200m and 0 - 80m) indicate that benthic remineralization is an important modifier of shelf based SACW. The PCO2 values are the highest recorded in the system with 3000uatm upwelling to the surface in the very narrow inshore zone (station 113). The waters outside the oceanic front are close to equilibrium with the atmosphere. Both plots show the "dome" effect in the zone above the shelf break.

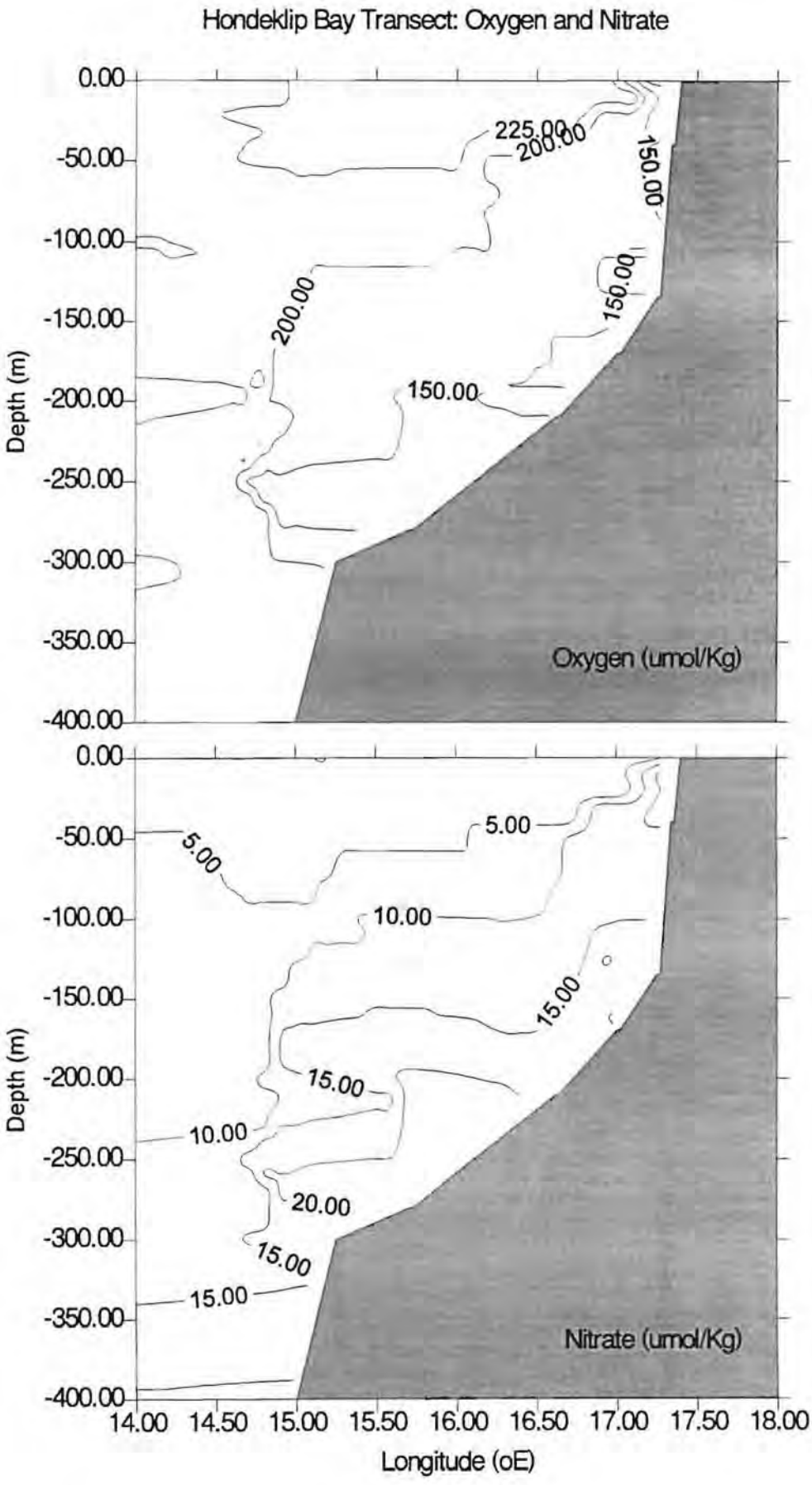

Fig. 4.14a,b: Oxygen and nitrate sections from the Hondeklip Bay transect. The water column distributions are very similar in character to the CO2 variables. Oxygen concentrations in the BBL are not as low as were observed in the Henties Bay transect which makes it more likely that nitrification will occur. This is supported by the elevated [NO3] > 20umol/Kg above the shelf break.

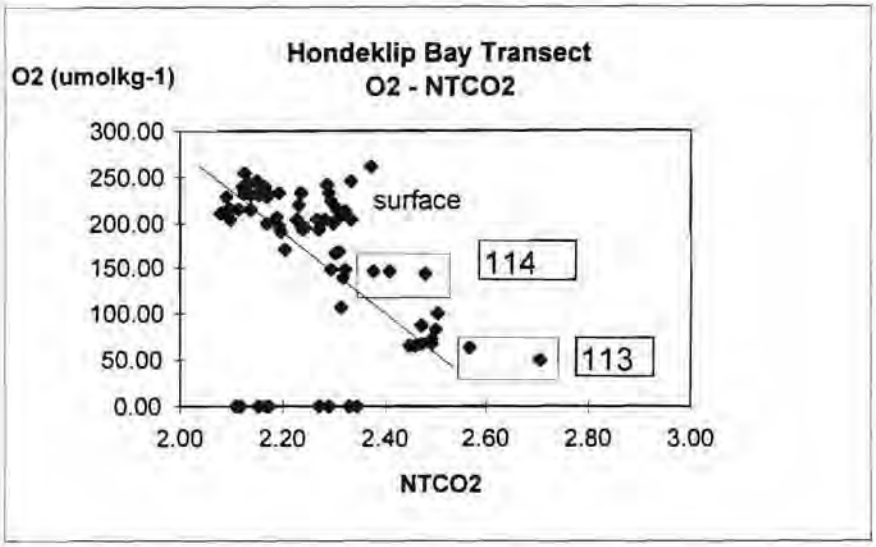

Fig. 4.14c: Scatter plot depicting the relationship between O_2 and $NTCO_2$ (TCO_2 normalized to 35 psu) for the data collected along the Hondeklip bay transect. This plot clarifies the relationship between TCO2 and O2 which is not completely resolved by the contouring in Figs. 4.13a and 4.14a. It shows that most of the points lie closely along a trend line which depicts the overall stoichiometry between O_2 and TCO_2 driven by the couple of aerobic respiration and photosynthesis. There are however three excursions corresponding to the bottom values from stations 113 (lower rectangle) and 114 (upper rectangle) as well as the spread of surface values. The sub-surface (113 and 114) excursions from the trend line indicate that close to the sediment - water boundary there is a de-coupling in the "global" stoichiometry of TCO_2 - O_2 which it is suggested is driven by the impact of the anaerobically (SO_4^{2-} - HS^- couple) driven CO_2 flux. The presence and elevated activity of sulphate reducing bacteria in this part of the Benguela System has been extensively recorded by G. Bailey (Pers.Com.) of the Sea Fisheries Research Institute. Such a process would increase the TCO_2 value of the overlying waters without changing the O_2 concentrations in the same stoichiometry are is expected from aerobically driven respiration. This explains why some of the highest PCO_2 values recorded in the Benguela System can coexist with non-zero O_2 concentrations. The spread of values at the surface is suggested to be linked to the asymmetry in the gas exchange rates between CO_2 and O_2 where the rate of the latter is approximately 10 times larger than that for CO_2. At the top end of the trend line the samples are in equilibrium with the atmosphere. The points on the X axis correspond to samples for which no O_2 values exist.

values outcropped within the upwelling front. These values indicate that surface waters are being upwelled from a reservoir of modified SACW located very close inshore where the highest PCO_2 values are located (Fig. 4.13b). This is strong support for the "Nelson model" whereby the source of upwelled waters is the biogeochemically enriched poleward undercurrent rather than the intermediate waters as suggested by Smith 1995. As was the case in the Henties Bay transect the most significant biogeochemical enrichments of the sub-surface waters occurred in sections of the shelf where organic rich sediments accumulated. The prediction from the BBL-PCO_2 sections that there should be two accumulation patches (PCO_2 > 1000μatm) (one at 100-180m and a second Z < 50m), is borne out by sediment geochemical data (Birch, 1975).

Oxygen and nitrate values (Fig. 4.14a,b) reflect the same system status, with aged waters outside the front (low NO_3^-; high O_2) and a reciprocal status within the front (NO_3^- ~ 20μM/Kg O_2 ~ 100μM/Kg). The existence of relatively high O2 concentrations with correspondingly high TCO2 increases suggests that the bulk of the CO2 addition may be driven by benthic anaerobic respiration (Fig. 4.14c).

The variability of TCO_2 and PCO_2 values across the shelf in the vicinity of the BBL highlights the role played by varying magnitudes of both the benthic remineralization flux and the physical turbulent mixing. In the vicinity of the shelf break the distortion of the isopleths indicates that this is the region of highest physically forced BBL turbulent mixing. The thickness of the BBL as reflected by the > 500μatm isopleth is ~ 150m (~ 50% of the water column depth) which contrasts sharply with a BBL of less than 50 metres closer inshore (Fig. 4.13b). In the inshore region where the depth range < 150m the PCO_2 values in the BBL increase sharply to ~2500μatm between 50 - 200m and over 6500μatm at the benthic interface inshore of 50m depth. The two bottom values (6500 and 4500μatm) at station 113 are the highest PCO_2

values recorded in the Benguela System. The existence of this gradient is indicative of the magnitude of the biogeochemical flux rate which exceeds the physical mixing rate.

Physical - Biogeochemical relationships

The relationship between physical and biogeochemical forcing over the whole shelf transect is, as with the northern Benguela Sub- System , best shown using the relationship between temperature and normalized TCO2 (Fig. 4.15). The data are distributed along two main vectors:

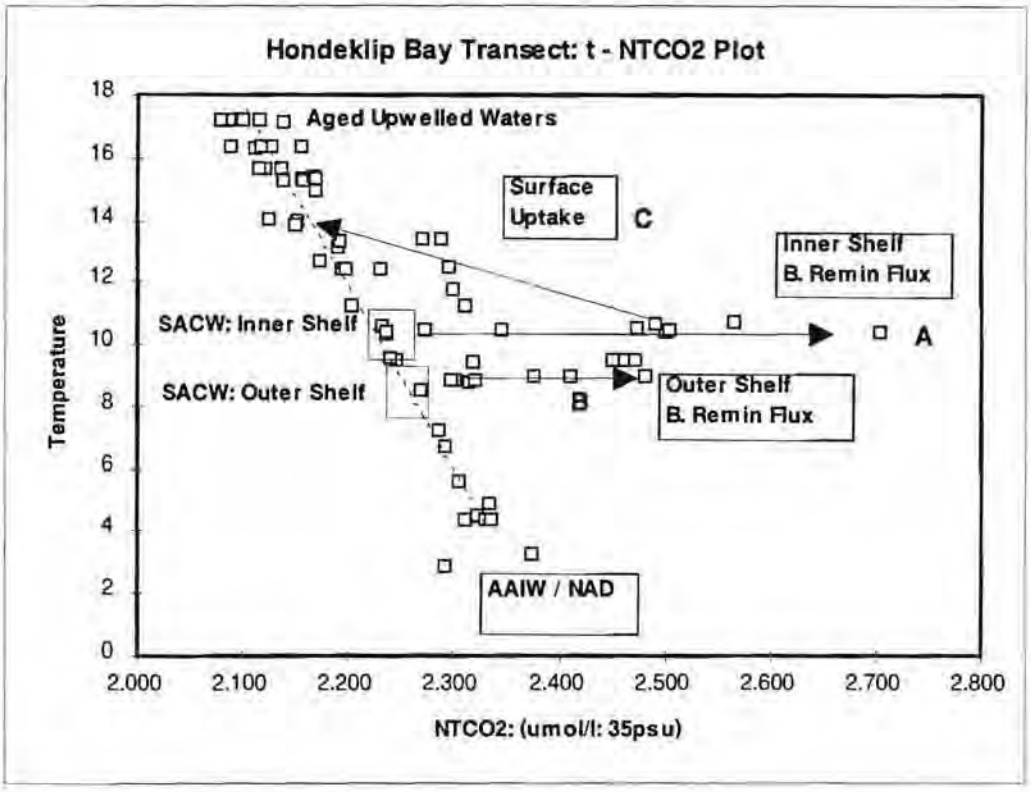

Fig. 4.15: A t - $NTCO_2$ plot using data obtained from the Hondeklip Bay transect. As before TCO_2 values are normalised to salinity of 35.00 psu. The plot shows general t - $NTCO_2$ relationship which characterises SE Atlantic waters (dotted line) from surface to intermediate (AAIW / NADW) depths as well as the shelf based processes (vectors A, B and C) which modify these. See text below for more details.

- a vector with a negative slope which was fitted by eye includes all data outside the benthic boundary layer or influenced by it. SACW freshly upwelled onto the shelf is depicted by a block characterized by the ranges (10-11°C in the inner shelf Z < 150m and 8-9°C on the outer shelf Z: 150-300m). At the top (low TCO_2 , warm waters) are the surface layer data points representing aged upwelled waters whose TCO_2 has been reduced through the activity of the biological pump and degassing across the air - sea boundary. At the lower end (high TCO_2 ; low temperature) are the intermediate and deep water masses from AAIW to CDW/NADW.
- the horizontal vectors (A and B) represents the interactive impact of BBL turbulent mixing and the benthic biogeochemical flux. The points are constrained by the temperature range of SACW on the shelf where Z < 300m. The points on the colder range (t~9 °C) represent the impact of turbulence in the vicinity of the shelf break which increases the TCO_2 from 2.20μmolKg^{-1} to 2.45-2.47 μmolKg^{-1} (Fig. 4.15). The points on the warmer vector (t = 10 - 11°C) represent those from the inner shelf (Z < 150m) where TCO_2 increases from 2.20 μmolKg^{-1} to 2.47 - 2.50 μmolKg^{-1} and at station 113 to the extreme of 2.70 μmolKg^{-1} (Fig.4.15).

Water which upwells at Hondeklip Bay has, through a history of poleward advection, BBL turbulence and benthic remineralization flux, the characteristics given by vector B (Fig.4.15). Through a combination of warming which reduces the solubility of CO_2 and primary production activity which drives the biological pump, the TCO_2 reduces to the range TCO_2 2.05 - 2.15 μmolKg^{-1} which characterises aged upwelled water. This change is depicted by the vector C (Fig. 4.15).

4.4.3 Olifants River Transect: Southern Benguela System

Wind Regime

The wind characteristics of this sector of the Benguela System are more distinctly seasonal than their northern counterparts (Boyd, 1987). Upwelling inducing equatorward winds drive this sector of the Benguela System in the spring - summer period between September and March. This period is characterized by high-very high equatorward wind stress whereas, in contrast, the winter (May - July) is characterized by weak northerly - westerly winds (Boyd, 1987). The transect was sampled in the month of February when the system is expected to be in the late stage of the summer high - very high equatorward wind stress (Boyd, 1987). The wind history in the period immediately preceding the transect can be seen on (Fig. 4.16) which depicts the variability in the upwelling inducing equatorward wind component over the entire month of February 1991 when the samples were taken.

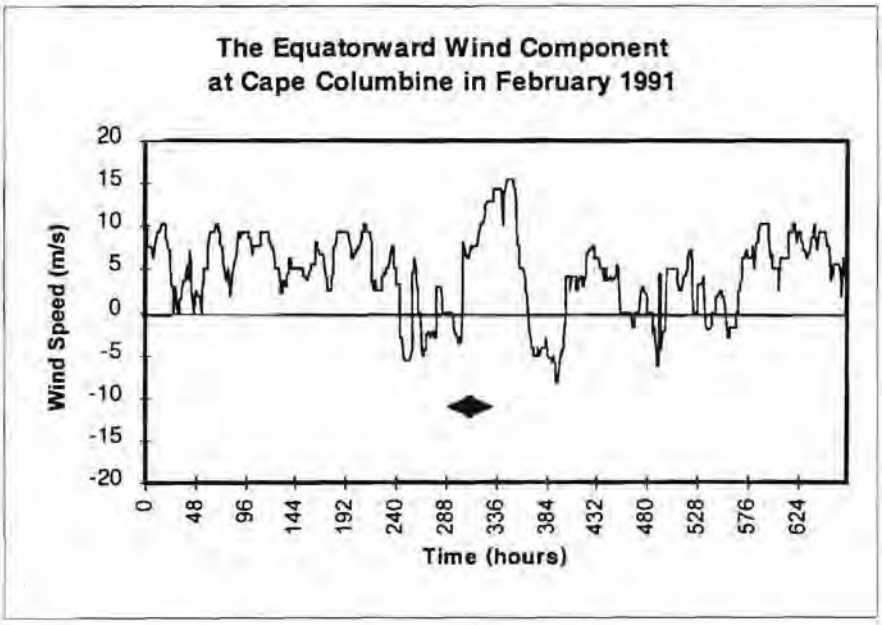

Fig. 4.16: A month long time series of the equatorward wind component from Cape Columbine which was taken to be a suitable proxy for the wind history of the zone covered by the Olifants River transect. The transect was sampled from 13/2/91 to 15/2/91 in the early stages of the cruise. It shows that the sampling occurred at the end of a "relaxation" period of the upwelling cycle which had in turn been preceded by 8 days of equatorward wind.

On the basis of the wind history it is predicted that the physical and biogeochemical characteristics of the transect should be consistent with the relaxation phase of an upwelling cycle: a sub-surface cross shelf density gradient shown as isotherms and isohalines shoaling towards the coast and a stratified surface layer. Biogeochemically this should provide for the existence of a surface post - upwelling phytoplankton bloom and a concomitant drop in PCO_2 values from those which characterize newly upwelled water in this sector.

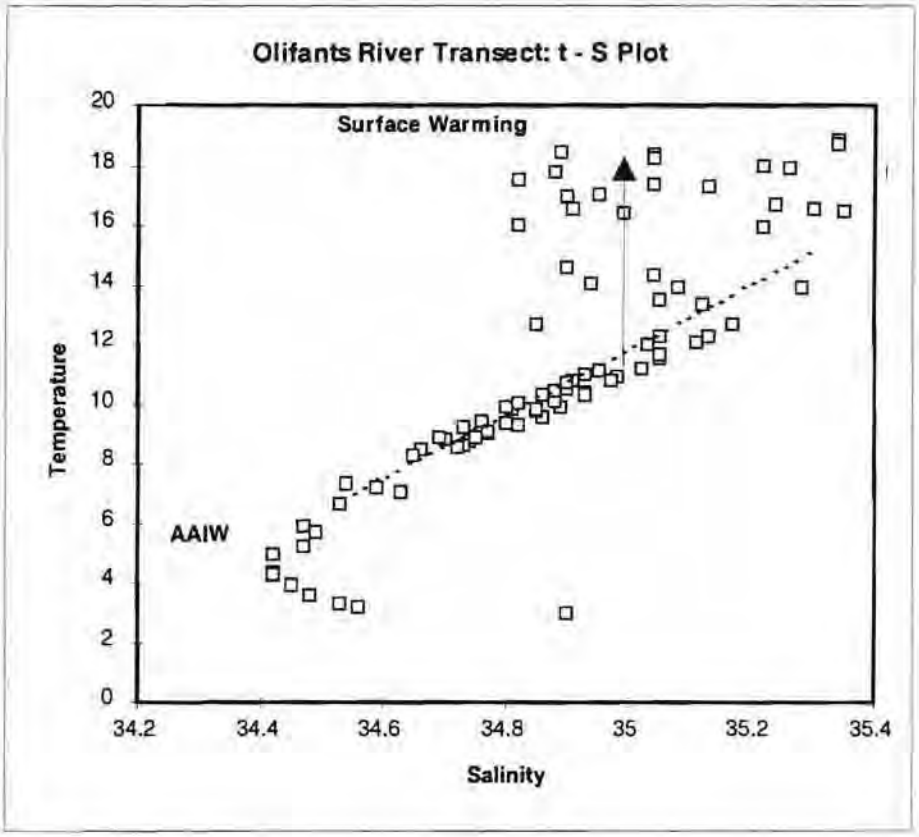

Fig. 4.17: A t - S plot of data taken from the Olifants River transect. It shows that the bulk of the points lie on the overall SACW trend line. Water upwells at Cape Columbine with physical characteristics defined by $9 < t < 11^{\circ}C$; $34.8 < S < 34.9$. The plots shows the effect of surface warming which alters the temperature without significantly changing the salinity. The warm waters with salinity above 35.0 lie outside the oceanic front.

Physical Characteristics: Temperature and Salinity

The t - S characteristics of the data collected from the transect (Fig. 4.17) show that as with the previous transects most of the water on the shelf had its origin in the linear section of the t-S plot which characterizes SACW for the SE Atlantic Ocean (Reid, 1989). The deeper samples reached well into the core of AAIW depicted as a salinity minimum in the range 34.4 - 34.6 and the very deepest sample reached the core of CDW / NADW also found in the Cape Basin (Reid, 1989). The greatest concentration of samples is in the range 34.70 - 35.00. There is evidence for the presence of warmed (t > 12°C) aged upwelled water which still retain their original salinities. The group with the highest salinities are shown below to be part of the equatorward jet which is a permanent feature in this part of the Benguela System (Shannon and Nelson, 1996). In most respects the physical (t-S) characteristics of this sector of the Benguela System appear to be almost identical to the previously discussed for the Hondeklip Bay transect. However, biogeochemically, the two sectors will be shown below to contrast sharply.

Physical Sections: Advection, Stratification and BBL turbulence

The temperature and salinity sections of the Olifants River transect are shown on (Fig. 4.18a,b) . The first noticeable feature is that the surface layer (Z<50m) was, as predicted from the wind record, stratified with an intense thermocline in the near shore Station 12 (from 18°C at 8m to 10°C at 25m). The estimated mid-summer warming rate of the surface 20m is about 0.5 °C d^{-1} (Guastella, 1992). Given that the relaxation phase was only 3 days old and that the temperature of upwelled water in that vicinity is approximately 10°C, the surface water overlying the thermocline (t> 17°C) is clearly too warm to be aged upwelled water from the immediately past upwelling event.

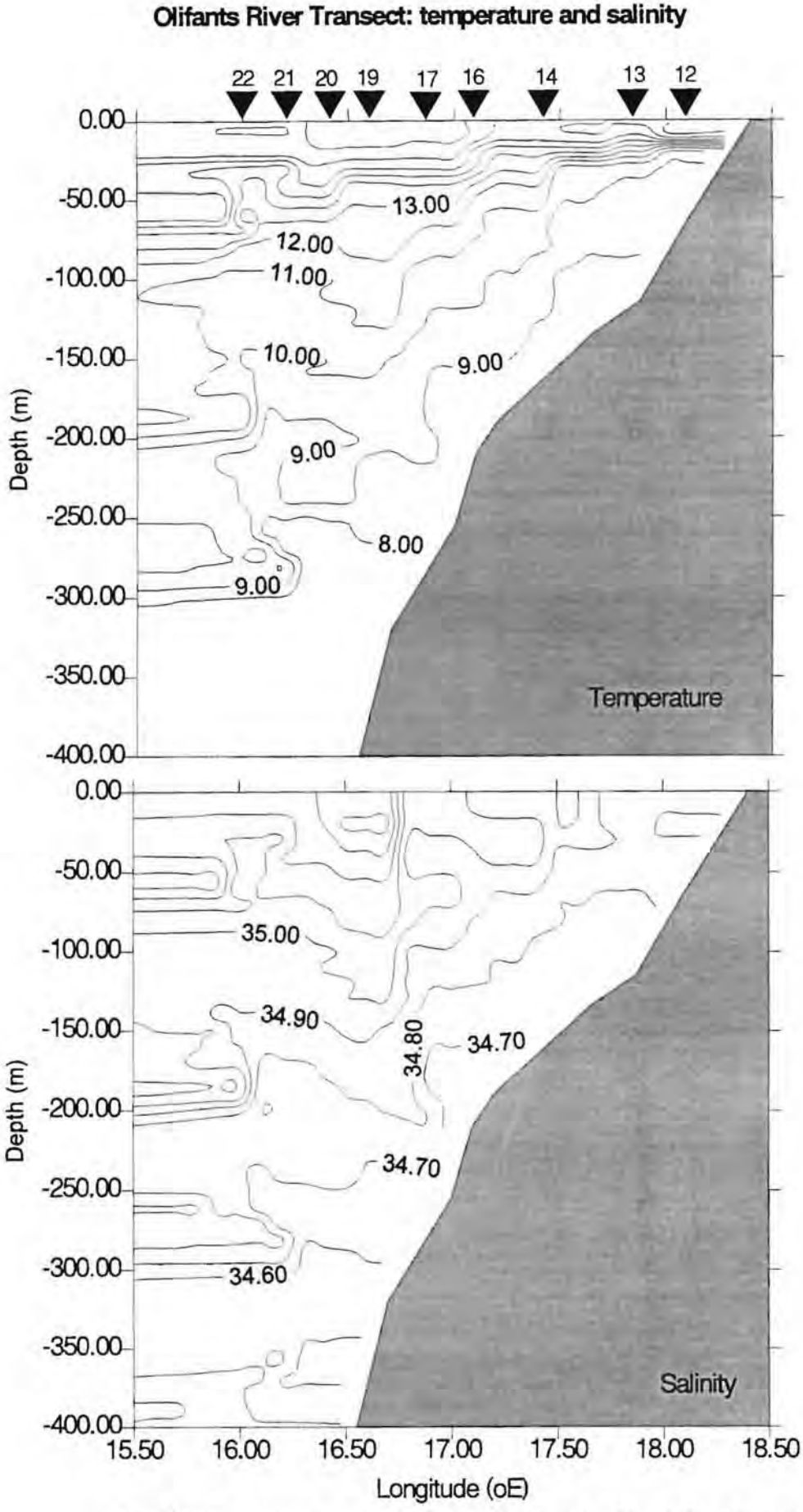

Fig. 4.18a,b: Temperature and salinity sections from the Olifants River transect. The station positions are marked along the top of the temperature section. The most significant features are: the "dome" over the outer shelf break at 400m, the oceanic front (S=35.00) in the upper 50m and the intense thermal stratification in the inner shelf zone (Z < 120m).

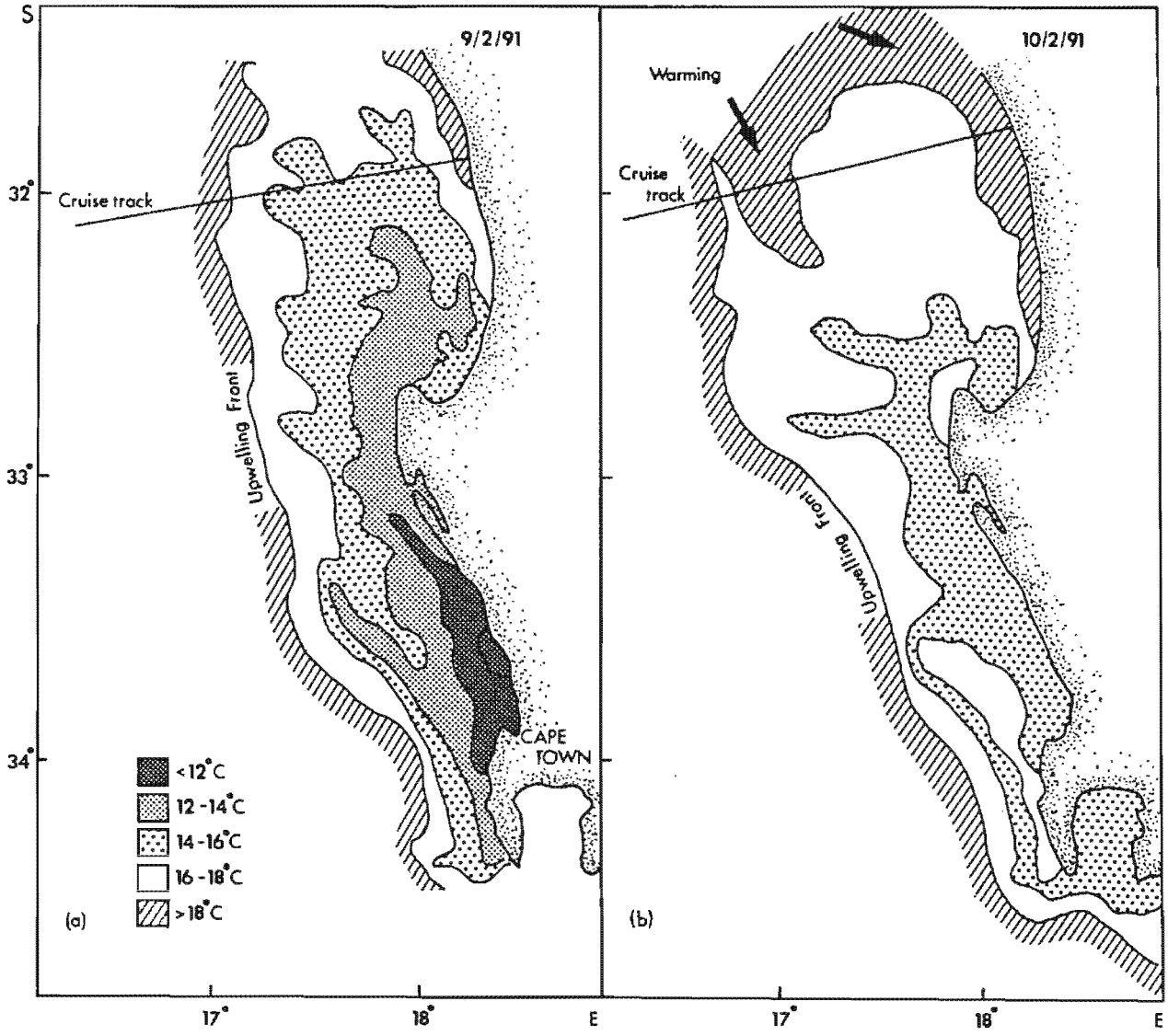

Fig. 4.19: Diagrams made from NOAA infra-red images of the southern sector of the Benguela System on two consecutive days which preceeded the Olifants River transect by 3 days. On the 9/2/91 which was at the end of an upwelling period there is an extensive tongue of upwelled water where t < 16°C and the upwelling front is clearly visible. According to the wind record (Fig. 4.16) the winds reversed on the 10/2/91. On the same day a rapidly poleward advancing front of warm > 18°C surface water can be seen to be filling the area from the north. This warm layer of aged upwelled water flows over and caps the newly upwelled water resulting in the strong thermocline shown on Fig. 4.18. The speed of this flow is also significant at an estimated 0.65m/s.

It is more likely that this water was advected in as part of the compensation to the upwelling surface slope which accompanies the relaxation of the equatorward wind stress. The advection of this warm water which induced a rapid stabilization of the surface layer can be clearly seen in the sequence of drawings taken from NOAA infrared images (Fig. 4.19) At the end of the period of sustained equatorward winds on the 9/2/91 the transect was dominated by a tongue of cool water developed from the equatorward advection of upwelled water from the Cape Columbine upwelling cell. As soon as the equatorward wind stress terminated, the same area was rapidly (< 1 day) filled with warm water (t > 18°C) being advected polewards at the surface. This water, because of its lower density, caps the cooler newly upwelled waters inducing advectively controlled stratification (Fig. 4.18a). It is also clearly of upwelled origin because its salinity (34.82 - 34.95 is indistinguishable from the subsurface and cooler waters (Fig. 4.18b). It is therefore likely to be aged upwelled water but at least two weeks old. The advection of aged warmed water destroys the sharp temperature front which often separates new and aged upwelled waters but the sharp salinity front which separates upwelled from oceanic surface waters can still be clearly seen between stations 16 - 19 and particularly between stations 17 - 19 (Fig. 4.18a,b). This physical dynamic has three important biogeochemical implications particularly in respect of CO_2 fluxes:

- the warm water provides enhanced seeding potential of newly upwelled waters because it retains the residual biomass of its own bloom.
- the turbulent shear between the two layers transports both carbon and nitrogen into this highly stratified environment.
- the strong thermocline reduces the CO_2 flux rate from the underlying CO_2 rich waters into the surface layer. This increases the potential from the post bloom PCO_2 disequilibrium between the surface layer and the atmosphere above and the sub-surface water below to be corrected through ingassing from the atmosphere.

As with both the northern and central sectors the cross shelf pressure gradient represented by the isotherms and isohalines (Fig. 4.18a,b) would under classical Ekman interpretation result in an equatorward barotropic current over most of the shelf (Neumann and Pierson, 1966). However, the southern Benguela is the sector in which the poleward sub-surface flow is not only strongest but least susceptible to seasonal scale reversals (Nelson, pers.com.). It is expected that most of the water column was being advected polewards. In the instance when the transect was sampled this also applied to the surface layer which in the "relaxation" phase of the wind cycle brings aged upwelled waters polewards over the newly upwelled waters.

The cross shelf gradient is broken by a "dome" perturbation located in the vicinity of the deep shelf break region at 500m (Fig. 4.18a,b). This feature is, as before, attributed to turbulent mixing linked to the interaction of one or more advective mechanisms. This interaction results in the development of a benthic boundary layer (see Further Discussion below) whose thickness is a function of the degree of turbulent mixing. The magnitude of this feature compared to transects in the central and northern sectors is indicative of the increased turbulence within the southern Benguela System at the time of the transect.

Biogeochemical Sections: Carbon (TCO_2 and PCO_2), Oxygen and Nitrate

The biogeochemical sections from the Olifants River transect show that this sector of the Benguela System is similar to the two previous sections from the perspective of spatial variability: it shows surface carbon and nitrogen uptake and oxygen production and the enhanced, although comparatively much smaller, input, particularly of carbon, through the dynamics of the BBL turbulent mixing (Figs. 4.20a,b and 4.21a,b). What is noticeably different is that the extremes differ. Both the surface TCO_2 and PCO_2 minima (PCO_2 < 200µatm ; TCO_2 < 1.95 $\mu molKg^{-1}$) and benthic maxima (PCO_2 > 800µatm; TCO_2 > 2.20) are also the lowest recorded in this study (Fig. 4.20a,b). In the

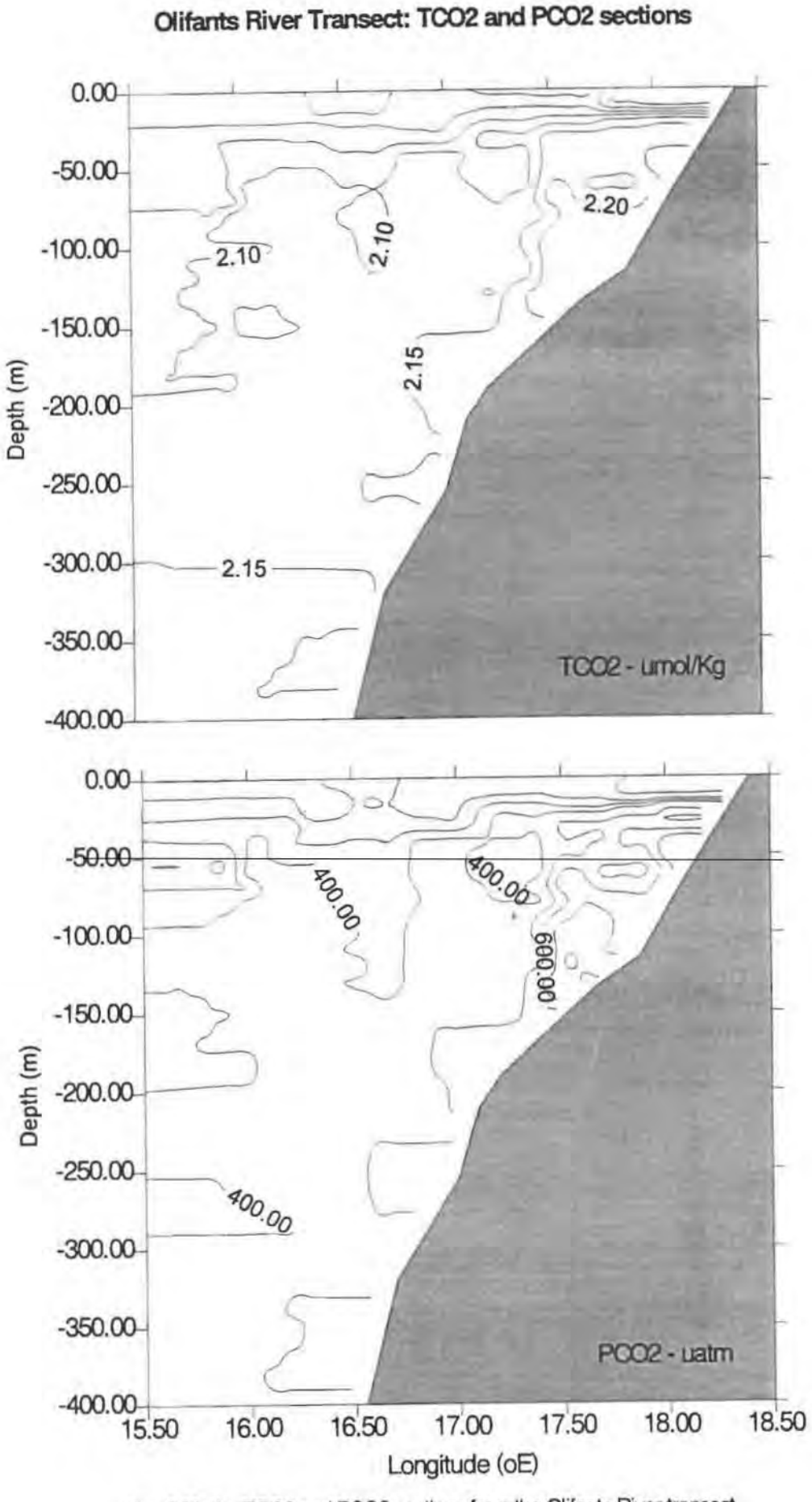

Fig. 4.20a,b: TCO2 and PCO2 sections from the Olifants River transect. These plots show that in the southern end of the Benguela System the impact of benthic remineralization is less pronounced than in earlier sections. The distribution of CO2 parameters is largely governed by physical processes except in the iiner shelf zone where benthic PCO2 increases to 800uatm and surface values drop to below 200uatm.

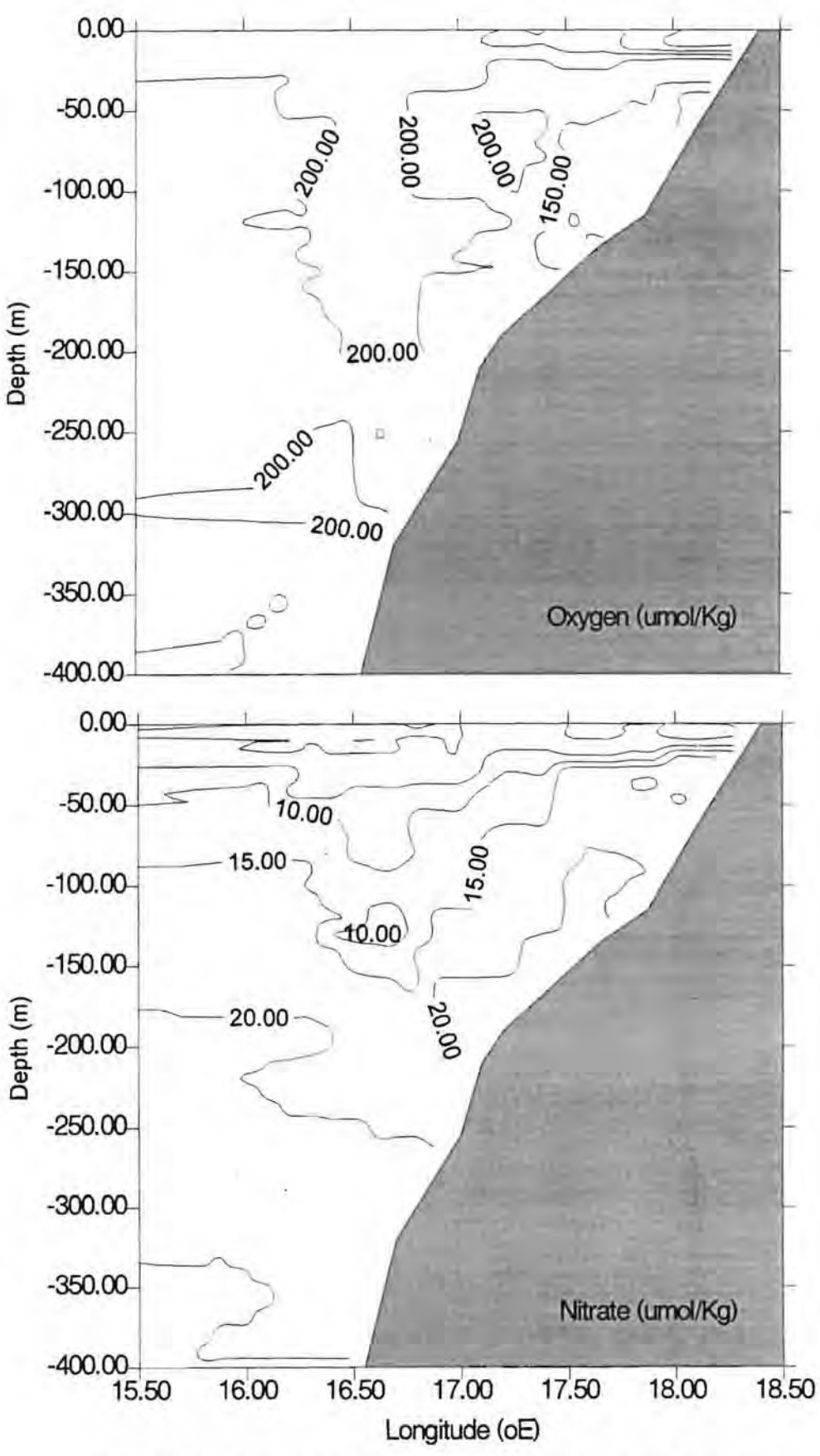

Fig. 4.21a,b: Oxygen and nitrate sections form the Olifants River transect. These sections confirm the same physical features depicted earlier. They also emphasise the position of the equatorward jet as a deep penetration of well oxygenated water as well as the elevated NO3 concentrations in the BBL above 200m due to nitrification of remineralized ammonium.

case of nitrate the spatial variability is very similar particularly to the Hondeklip Bay transect (Fig. 4.21b cf. Fig. 4.14b). The NO_3^- section is useful in identifying the zones of enhanced BBL mixing and it shows that the benthic remineralization flux coupled with nitrification impacts on the NO_3^- concentration in the overlying water in the inner shelf (Z < 200m). The NO_3^- concentrations above the 200m shelf break increase from the background SACW values of ~ 15 - 20 $\mu molKg^{-1}$ to over 20 $\mu molKg^{-1}$. The overall range of NO_3^- concentrations is similar to that in the Hondeklip Bay transect.

The lower BBL TCO_2 / PCO_2 enrichments in this transect compared to both the Henties bay and Hondeklip Bay transects suggests that *inter alia* two potential processes play a role:

- Lower annual new production rates which provide in the case of the Olifants River transect, low accumulation potential of POC in the sediments. The role of biogeochemically driven forcing is quantitatively addressed in the final Chapter 7 as part of the model predictions.
- Turbulent mixing energy in the BBL is high enough to resuspend the biogenic particles and transport them off the shelf. In this case the remineralization will not occur in an area where it can feedback to upwelling waters. This would keep the PCO_2 values of upwelling shelf waters closer to that of SACW (450-600 μatm) and lower the degassing rates of newly upwelled waters. The role of the physically driven explanation is further discussed below in the context of BBL turbulence.

Physical - Biogeochemical Relationships:

The relationship between physical and biogeochemical variability is once again summarized by the t - TCO_2 relationship (Fig. 4.22). It supports the conclusions above that in this sector benthic remineralization flux plays a relatively smaller role in adding carbonate species to upwelled waters and that exceptional surface stratification dynamics result in the lowest TCO_2 in

the Benguela System (Fig. 4.19). Most of the data lie on a trend vector (fitted by eye) which links surface resident warm (t > 14°C) aged upwelled waters whose PCO_2 is close to atmospheric equilibrium to deep AAIW and CDW waters.

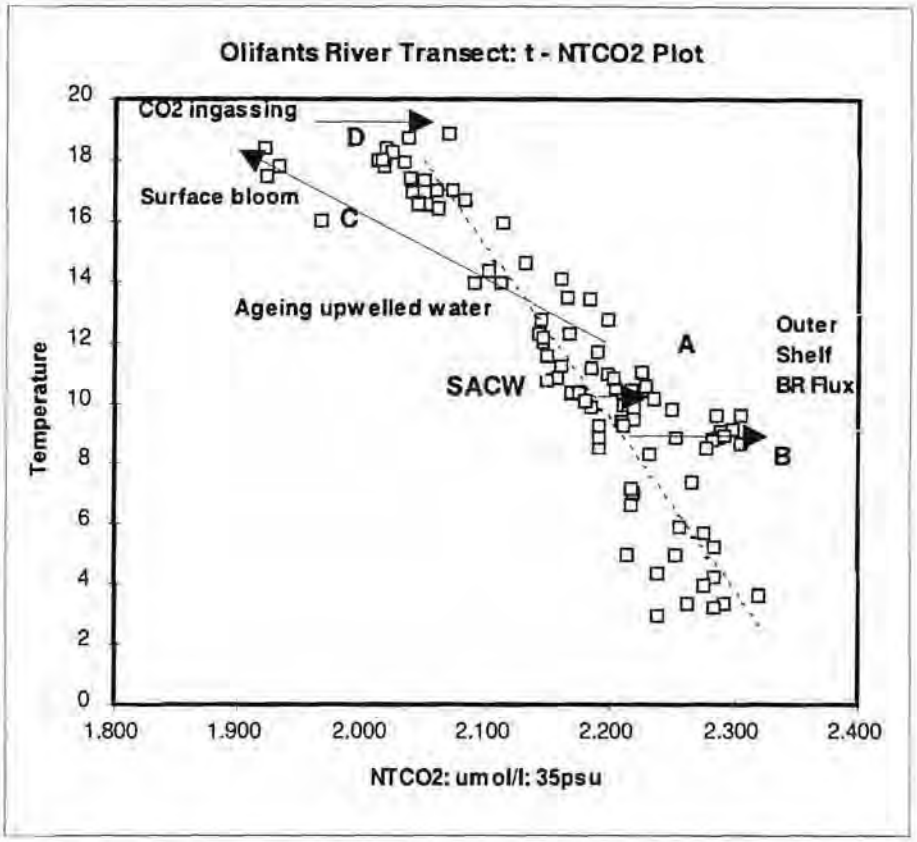

Fig 4.22: A t - $NTCO_2$ plot using data from the Olifants River transect. It shows the overall SACW trend (dashed line) linking AAIW / NADW on the low t and high NTCO2 to the surface waters where the converse applies. It shows that the degree of impact which benthic remineralization (vectors A and B for the inner and outer shelf areas respectively) has on the characteristics of SACW on the shelf is the smallest of all 3 transects. This is especially so for the inner shelf waters from where upwelled waters are sourced. In contrast, the magnitude of surface uptake on $NTCO_2$ by the post upwelling bloom (vector C) is the largest of the 3 transects and provides for a potential CO_2 ingassing flux given by vector D.

This trend vector is identical to the one from the Hondeklip Bay transect which suggests that it may be a general property of waters from the SE Atlantic. The small group of points in the temperature range 8-10°C which have slightly higher TCO_2 (TCO_2 > 2200 $\mu molKg^{-1}$) than the main trend line are the only evidence for the impact of a benthic carbon flux. This increase of approximately 100 $\mu molKg^{-1}$ is small compared to the equivalent changes of

400μmolKg^{-1} and 300 μmolKg^{-1} from the Hondeklip Bay and Henties Bay transect transects respectively.

In almost all aspects the results depicted in the plots and cross-shelf sections are consistent with existing ideas on the advective and turbulent mixing characteristics in the Benguela System. Of these, the most important one is:

- that TCO_2 and PCO_2 values of waters which outcrop upwelling centres are consistent with their being supplied with water out of the poleward undercurrent flowing along the inner shelf. This lends strong support to the "Nelson model " which predicts that long period cross-shelf currents associated with shelf waves overcome the tendency of the poleward undercurrent to flow offshore.

Two questions are of particular interest arise from careful analysis of the data.:

- If the upwelling centres are being supplied with water from the shelf based poleward flow then why are the physical and carbonate characteristics not consistent with a general poleward flow from Namibia to the Cape Peninsula ? Is it possible that water is being advected onto and off the shelf at a few propitious sites along the Benguela System ?
- While the physical and carbonate cross-shelf sections, where the "dome" effect is seen, support the notion that it is driven by some distinct physical process connected to shelf break regions, neither provide positive support for the shelf break upwelling (Barange and Pillar, 1992) or benthic turbulence hypotheses (Nelson, pers.com.). The question which remains is; is there any other means to provide support for one or other hypothesis ?

4.5 Further Discussion: New Insights

4.5.1 The "Gate" hypothesis

The "gate" hypothesis is a view on the advective water flows through the Benguela System which attempts to address the inconsistencies between the observations from this study and the notion that a poleward undercurrent connects the northern and southern extremeties of the Benguela System (Shannon and Nelson, 1996). The rationale for this conceptual model is that there is strong biogeochemical evidence (Fig. 4.23) that each of these transects has a unique source of SACW. If t - TCO_2 characteristics of sub-surface inner shelf waters from all 3 transects are plotted together, they form recognizable clusters which differentiate them on either temperature or TCO_2 criteria (Fig. 4.23).

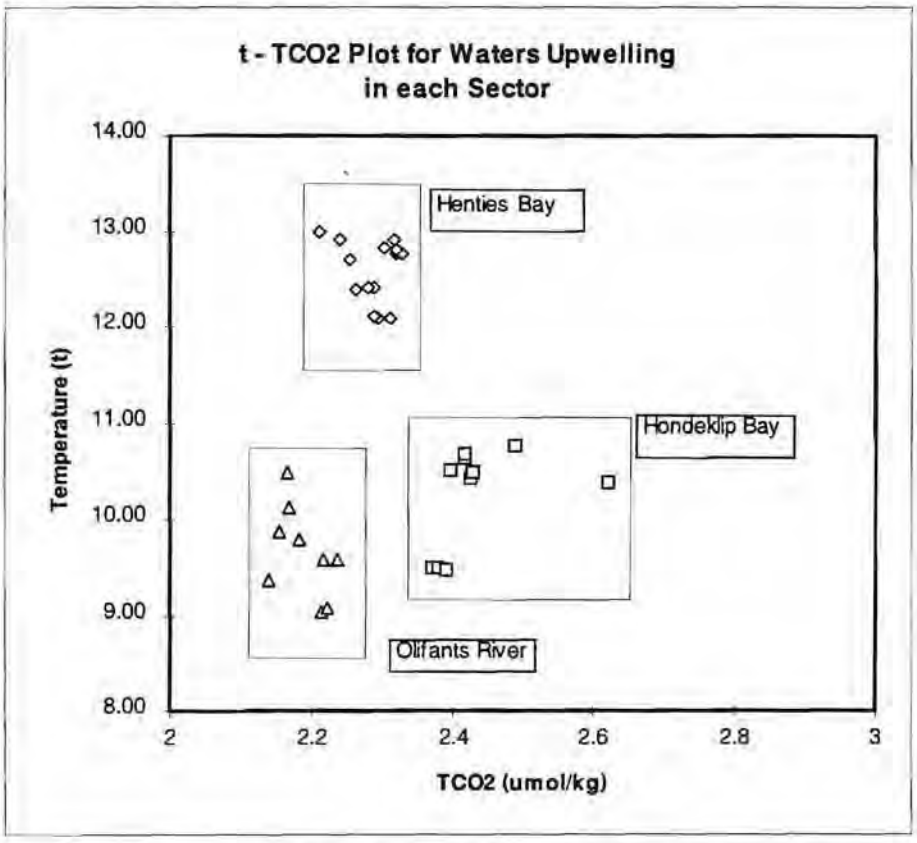

Fig. 4.23: A t - TCO_2 plot using sub-surface inner shelf water (ISW) data from all 3 transects. It shows that they form distinct clusters which are the basis for the "gate" hypothesis suggesting that the Benguela System can be divided into 3 sectors each of which has a distinct supply of SACW. (see text below for more details).

This plot shows that:

- Inner shelf water (ISW) from the Henties Bay transect cannot be the source of inner shelf water at the Hondeklip Bay transect because, even though as might be expected, TCO_2 in the latter is higher, the temperature difference is not consistent with a poleward link between the two sectors. The same applies to the salinity characteristics which are 35.25 psu in the northern sector and 34.75 - 34.85 in the central sector. Given that the Luderitz upwelling area is a site of very strong and persistent equatorward wind stress it is hypothesised that it forms the "gate" between the northern and central sectors of the Benguela System. SACW which upwells in the central sector is advected onto the shelf in the vicinity of Luderitz. To maintain continuity, northern sector inner shelf waters are advected offshore. It is tempting to link this potential offshore advection with that identified by Agenbag and Shannon, 1988 in the vicinity of Meob Bay (25 ^{o}S). The link between the offshore displacement located by remote sensing (Agenbag and Shannon, 1988) and a concomitant sub-surface advection is something which should be explored further.
- Even though there is only a minor difference in their temperatures the inner shelf waters at both the Hondeklip Bay (central sector) and Olifants River (southern sector) transects differ visibly in their TCO_2 ranges. The magnitude of TCO_2 of ISW at the Olifants River transect (2.15 - 2.25μM) is lower than that which was measured the Hondeklip Bay transect (2.4 - 2.5μM). This is not consistent with a poleward flow link between the central and southern sectors. This result suggests that inner shelf water in the central sector as measured at Hondeklip Bay flows off the shelf to the north of the Olifants River transect. This is in good agreement with the observation by Dingle and Nelson, 1993 that the Olifants Valley is a conduit for the inflow of "new" relatively cold and fresh SACW. This inflow floods the inner shelf in the southern Benguela System and characterises the waters which outcrop at both Cape Columbine and Cape Peninsula. This predicts that the outflow of central sector inner shelf water must be somewhere to the south of Child's Bank.

In terms of this conceptual model, the Benguela System is divided into three sectors: a northern sector extending from 18°S to 27°S , a central sector extending from 27 °S to 32°S and a southern sector from 32 °S to the Cape Peninsula 34oS (Fig. 4.24). The northern boundaries of each sector are the zones where an inflow of "new" SACW is advected from the slope and onto the shelf where it gets entrained into the general poleward flow. Each of these "gate" sites (Cape Frio (18 °S) , Luderitz (27 °S), Olifants Valley (32 °S) has three physical and environmental characteristics which are not shared with any other upwelling cells;

- they are characterized by varying periods of particularly strong equatorward wind stress. The persistence of this situation varies, with the southern Benguela System having a stronger seasonal scale variability (Boyd, 1987).
- they are sites where the shelf narrows.
- within the constraints of seasonal variability, they are centres of maximum cyclonic wind stress curl (Shannon and Nelson, 1996).

Cross shelf advection acts as a "gate" inhibiting the poleward undercurrent from the upstream (north side) sector from moving southwards into another sector. It is hypothesised that the upstream poleward current is forced westwards and advects off the shelf to maintain flow continuity as compensation for the volume which is advected shorewards. This conceptual model predicts that while an upwelling cell at the "gate" site upwells virgin SACW, all other upwelling sites polewards but still within the same sector upwell SACW modified by the nature and magnitude of the benthic remineralization flux characteristic of that sector of the shelf. This heterogeneity in the biogeochemical characteristics of upwelled waters induced by the oceanographic constraints of shelf advection is predicted to have a major modulating effect in the CO_2 fluxes between the Benguela System and the atmosphere.

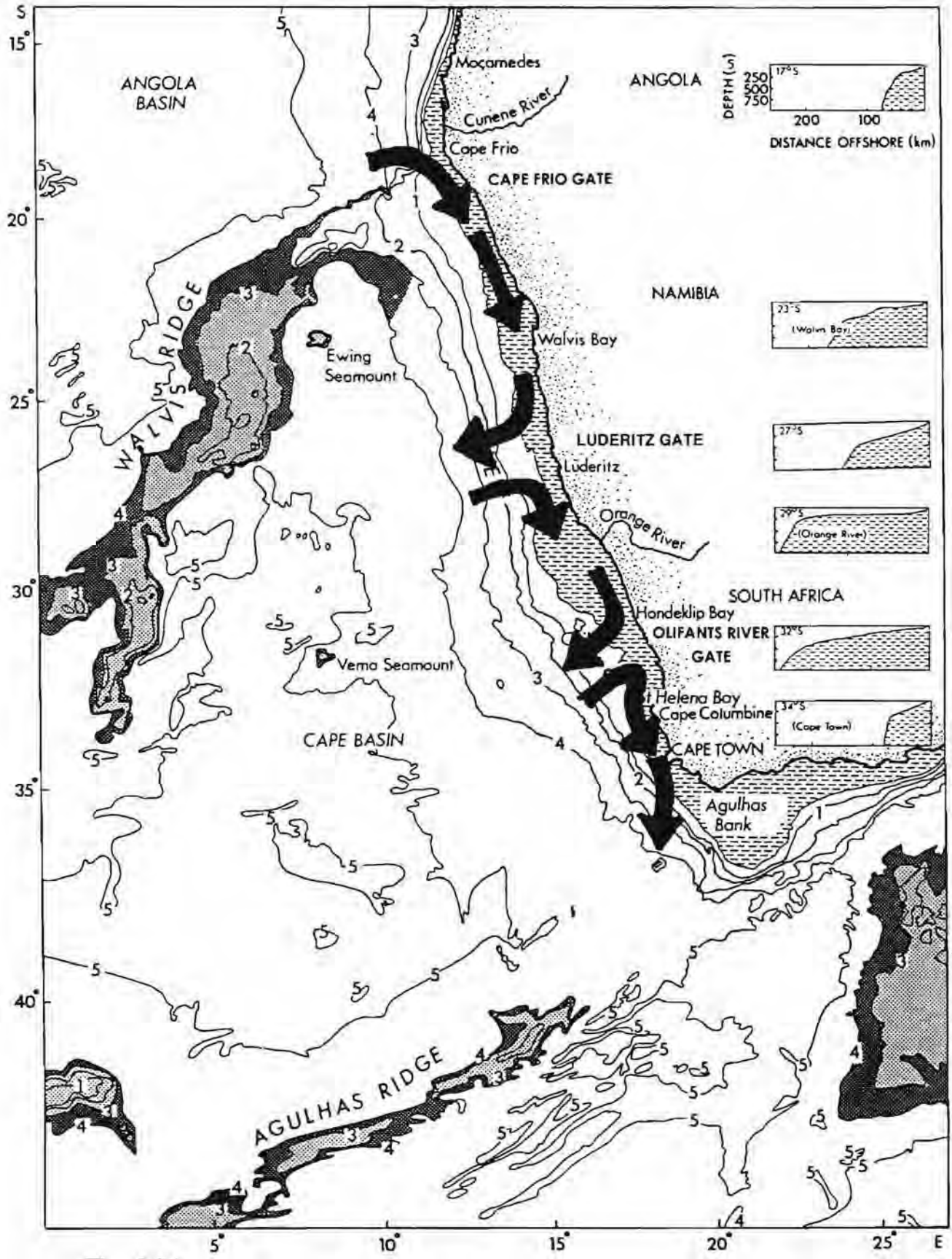

Fig. 4.24: A map of the geography of the Benguela System showing the location of the sub-surface inflows of South Atlantic Central Water (SACW) from the slope and onto the shelf which define the three "gate" sites. The three "gate" sites are Cape Frio at the northern boundary, Luderitz, separating the northern and central sectors and Olifants River, separating the central and southern sectors. To the north of each inflow there is a corresponding outflow of modified SACW from the shelf to the slope. In the southern sector the outflow is through the southern boundary of the system to the south of the Cape Peninsula. Each sector has two upwelling centres: Cape Frio and Walvis Bay in the northern sector, Luderitz and Namaqua (Hondeklip Bay) in the central sector and Cape Columbine and Cape Peninsula (Cape Town) in the southern sector.

To summarise:

- The long term transport of carbon is polewards. In this context the widely used terminology for biogenic carbon transport "downstream" should mean polewards and not equatorward as it is still used (Bailey, 1990).

- Upwelling does not occur through cross shelf advection of SACW from 300-400m to the surface creating a coast wide ribbon of upwelled waters. Instead, SACW outcrops at specific upwelling centres in first two steps of a 4 step upwelling cycle which is best described with a conceptual model (Fig. 4.25). This diagram depicts the 3 sector Benguela System with its "gates" located at the northern boundary of each sector. The upwelling cycle is as follows:

  Step 1: At each of the three "Gate" sites, shelf width minima and favorable wind characteristics (Shannon and Nelson, 1996) result in a flux of SACW (F_{SACW}) onto the shelf and polewards along both the inner (F_{ISW}) and outer (F_{OSW}) shelf. Immediately to the north of each "gate" site (not shown for Cape Frio) there is a corresponding offshore flow which compensates for the onshore advection at that "gate". The combined effect of this cross shelf shear is the formation of an environmental barrier, a "gate" which divides the Benguela System into 3 recognizable sectors (Fig. 4.24, 4.25).
  Step 2: In the vicinity of each of the six main upwelling centres poleward flowing inner shelf water (F_{ISW}) upwells and outcrops at the surface through flux (F_{UPW}). The "gate" boundaries of the system are such that the six upwelling centres are located in such a way that there are two per sector: Cape Frio (CF) and Walvis Bay (WB) in the northern sector, Luderitz (LZ) and Namaqua (NQ) in the central sector, Cape Columbine and Cape Peninsula (CP) in the southern sector. Cape Frio (CF), Luderitz (LZ) and Cape Columbine (CC) cells are close to the "gate" sites. The

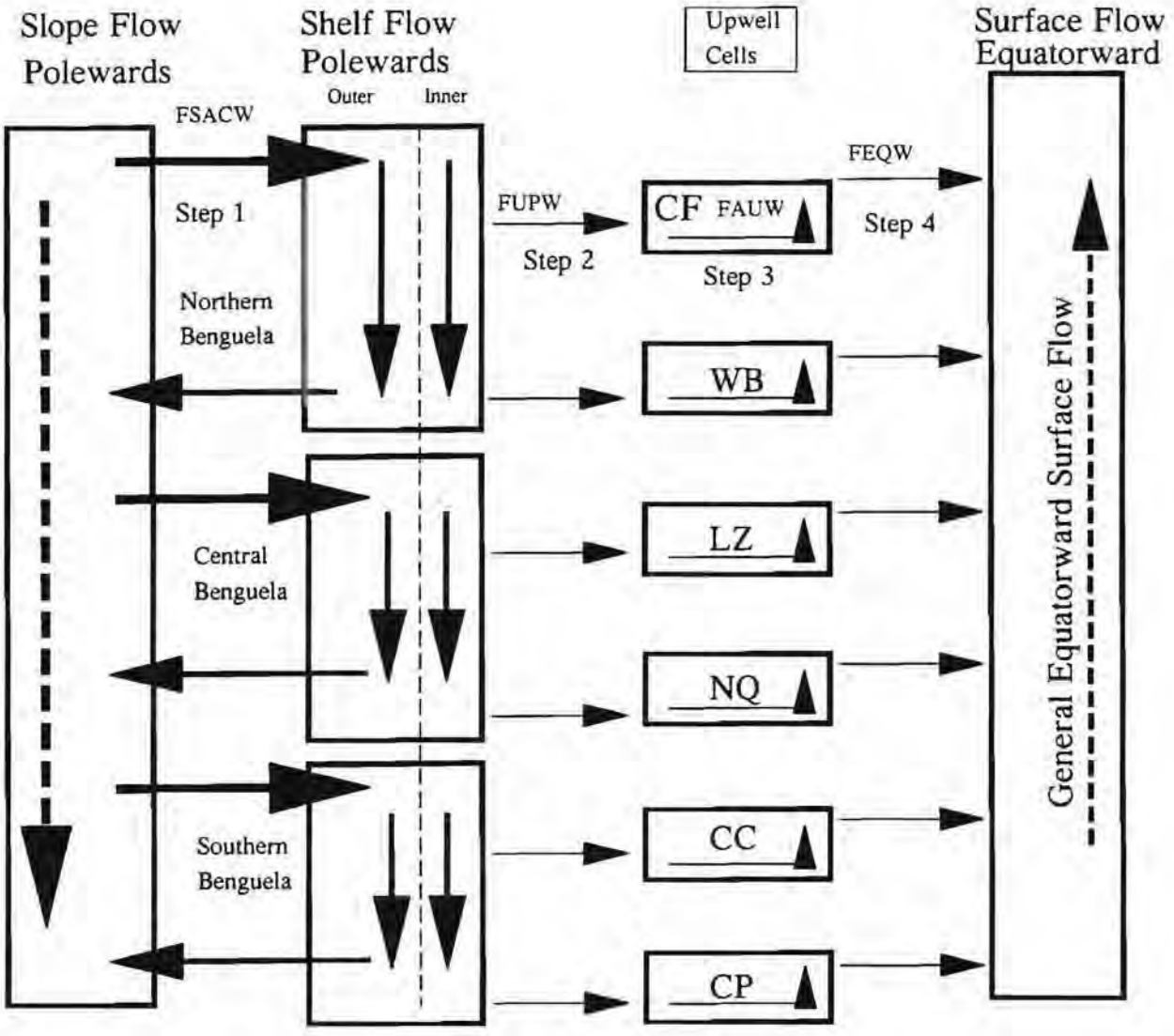

Fig. 4.25: The conceptual model of the Benguela System as formulated in terms of the "Gate Hypothesis" (see Chapter 4) which forms the basis for the advective fluxes of carbon to be quantified with the box model. It shows that South Atlantic Central Water (SACW) is advected to the surface in two steps. In step 1 it is advected onto the shelf from the slope as a flux FSACW at one of 3 "gates" which mark the northern boundary of each sector (northern, central and southern Benguela). On the shelf SACW is entrained onto the poleward flow of Inner Shelf Water (ISW) from where, in the vicinity of one of the 6 upwelling centres, it is advected to the surface in step 2 as a flux of newly upwelled water (FUPW). The surface part of the upwelling cycle is also composed of 2 steps. Step 3 is the physical and biogeochemical ageing of upwelled water as a flux FAUW associated with each upwelling centre. Aged upwelled water is finally entrained into the surface equatorward flux (FEQW) as step 4. To the north of each "gate" there is a compensatory offshore flux.

remainder of the upwelling centres Walvis Bay (WB), Namaqua (NQ) and Cape Peninsula (CP) are located downstream of their respective "gate" sites.

Step 3: Within each upwelling centre upwelled water ages physically and biogeochemically with a flux (F_{AUW}) which corresponds to the warming water within the upwelling front.

Step 4: Aged upwelled water is entrained into the general equatorward surface flow to which it contributes a flux (F_{EQW}). This corresponds to the water body confined by the oceanic front. It should be noted that for continuity $F_{UPW} = F_{AUW} = F_{EQW}$. These fluxes are quantified in the modelling stage addressed in Chapter 7.

The implications of this stepped upwelling cycle for carbonate chemistry and carbon fluxes are:

- Water which outcrops at the "gate" upwelling cells is virgin SACW but in all other instances it is modified in the course of poleward advection along the inner shelf shelf through the effects of benthic remineralization flux. Therefore the activity of the biological pump and its impact of CO_2 fluxes at a particular upwelling cell will depend on its distance downstream from the "gate" and on the benthic remineralization flux in the sector.
- The detrital carbon flux arising from the activity of the biological carbon pump in the vicinity of upwelling centres is likely to be mostly transported polewards (poleward undercurrent) or shorewards (cross shelf component of upwelling).
- The detrital carbon resuspended from the sediments is not expected to be transported between sectors but offshore where in all likelihood it gets deposited on the slope. This predicts there to be accumulation of particulate organic and inorganic carbon on the slope in the latitude ranges of 26-28°S, 33-34°S and at the bottom end of the Cape Point Valley (Fig.4.24)

- It is intriguing to conjecture that these advectively driven outflow sites could provide an important route for the supply of "free energy" in the form of biogenic carbon generated by inner shelf production to deep sea (slope) food chains.

These "gate" sites are not suggested to be permanent or impermeable features because the intensity of their main forcing factor, the wind, is known to be highly variable on synoptic, seasonal and interannual scales. Relaxation of the persistence of equatorward wind stress either by the ENSO or seasonal effects could open the "gate" and allow poleward transport between sectors. This may be the explanation for the occasional intrusion of very low O_2 waters from the Central Sector into the Southern Benguela System with catastrophic consequences for benthic biota (Newman and Pollock, 1974; Bailey and Chapman, 1985; Bailey, 1990). The generation of hypoxic or high PCO_2 waters is closely related to benthic boundary layer processes which are now addressed in some detail.

4.5.2 Benthic Boundary Layer (BBL) Turbulence

The aim of this discussion is to explore the relationship between BBL turbulence and sediment - water flux of particulate and dissolved biogeochemical components. This is done using a conceptual model whose predictions are verified by the distribution of biogenic sediments on the shelf in both the northern (Bremner, 1983) and southern Benguela System (Birch, 1975).

The biogeochemical importance of BBL turbulence is two fold:

- It enhances the flux of re-mineralized dissolved biogeochemical components into the water column. The benthic remineralization flux is

particularly important for CO_2 because of the impact it has on the PCO_2 of waters which outcrop.

- If BBL turbulence is high enough such as in shelf break zones, it is predicted to resuspend biogenic and lithogenic sediment particles. This process of spatially heterogeneous erosion and accumulation thereby governs the distribution of the geochemical and geophysical character of the sediments. This has an additional feedback effect: if the biogenic organic particles which settle in the sediments are eroded from parts of the shelf, it is predicted that the benthic re-mineralization flux in those same areas will be reduced.

While a full mechanistic understanding of BBL turbulence remains a long term objective, two physical forcing mechanisms are thought to play a particularly important role in generating the turbulence which sustains the BBL (G. Nelson, pers.com.):

- Semi-diurnal tidal Kelvin waves which propagate along the shelf edge.
- Poleward undercurrent which characterises sub-surface flow in the Benguela.

The biogeochemical consequences of BBL turbulence at shelf breaks are summarised as a conceptual model (Fig. 4.26) whose predictions are then tested against existing water column and sediment physical and geochemical data from the northern and the southern Benguela System.

4.5.3 BBL turbulence conceptual model:

The model shows two degrees of turbulence as reflected by the thickness of the BBL. At the shelf breaks the isopleth which defines the upper boundary of the BBL is distorted into a "dome" as a result of mixing from a predicted enhanced turbulent energy in the vicinity. This is consistent with the

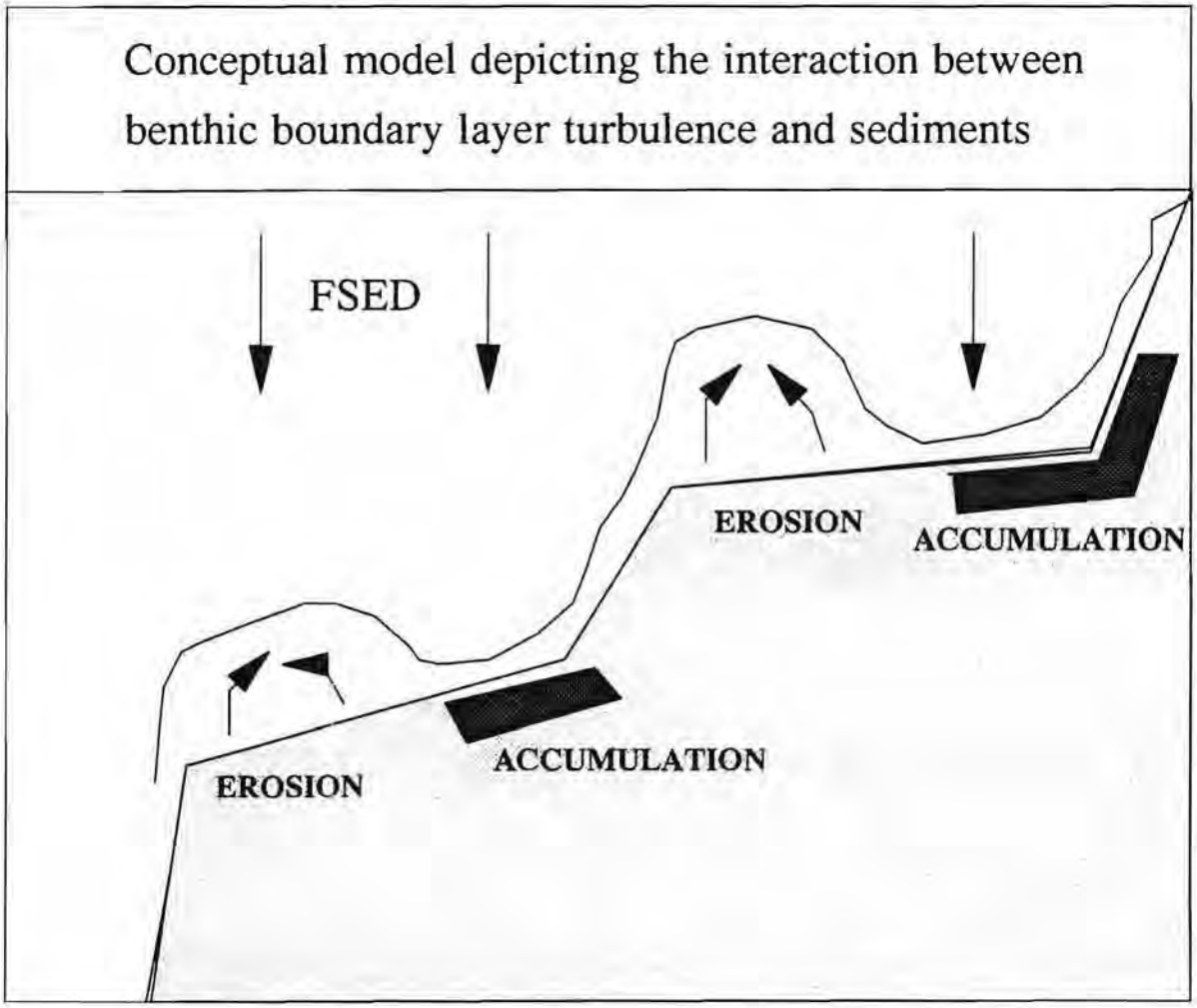

Fig. 4.26: A conceptual model of showing the relationship between the areas of erosion linked to enhanced turbulence at the shelf breaks and the intermediate zones of reduced turbulence where biogenic detritus accumulates. The enhanced turbulence at shelf breaks manifests itself through a thickening of the benthic boundary layer. This conceptual model is designed to correspond to the observed distribution of organic carbon on the shelf of the northern sector (Fig. 4.27).

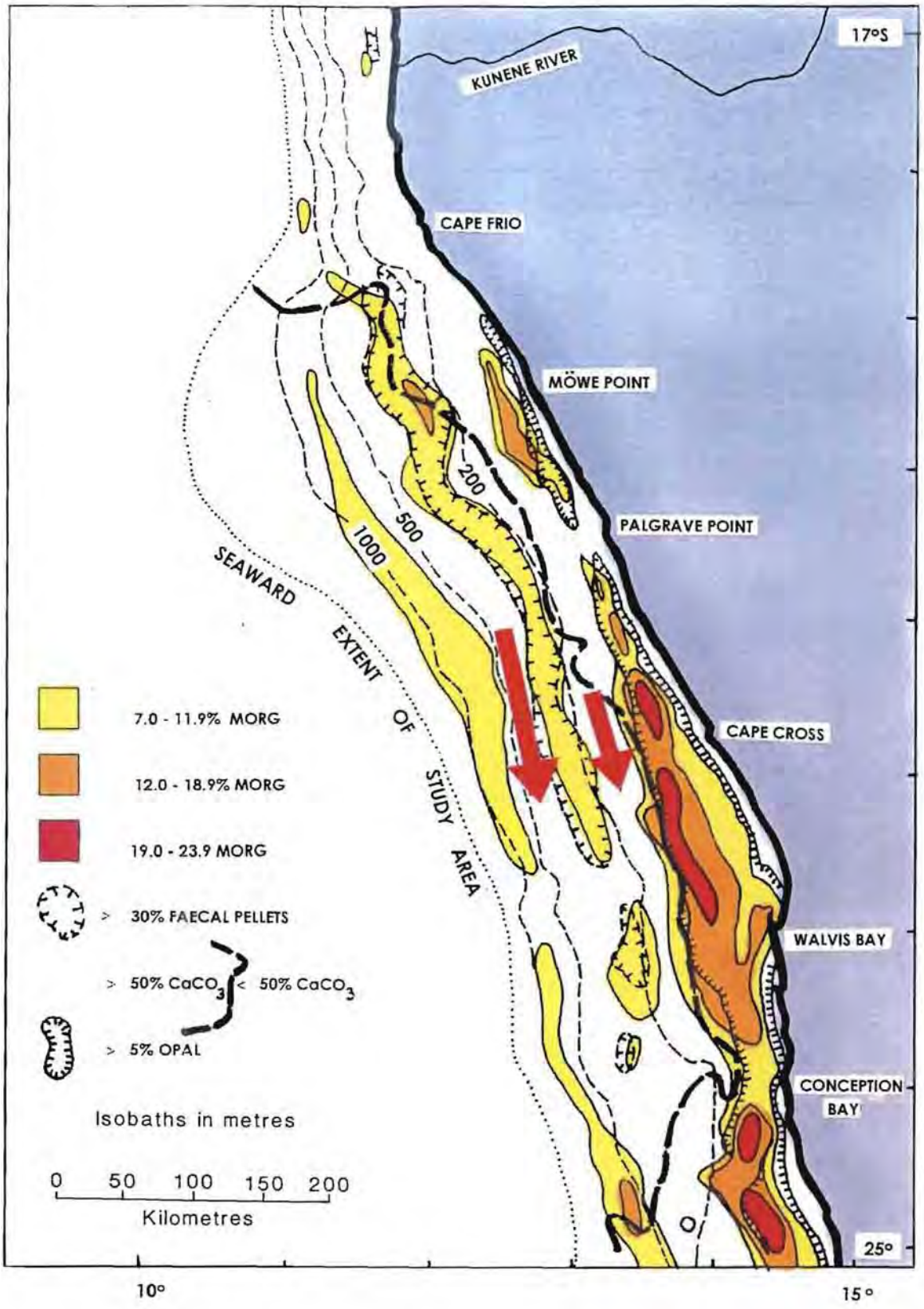

Fig. 4.27: A map of the distribution of organic matter on the shelf of the northern sector. It shows how areas of elevated organic carbon are concentrated along longshore bands separated by corresponding belts depleted in organic matter. These depleted belts correspond spatially to the location of the two main shelf breaks along much of the northern sector. The arrows indicate the axes of enhanced turbulence where erosion is suggested to be the dominant physical process. Organic matter which sediments out in these erosion belts is suggested to be either deposited laterally or tranported off the shelf onto the slope at the exit site to the north of the Luderitz "gate". This sediment map was adapted from Bremner, 1983.

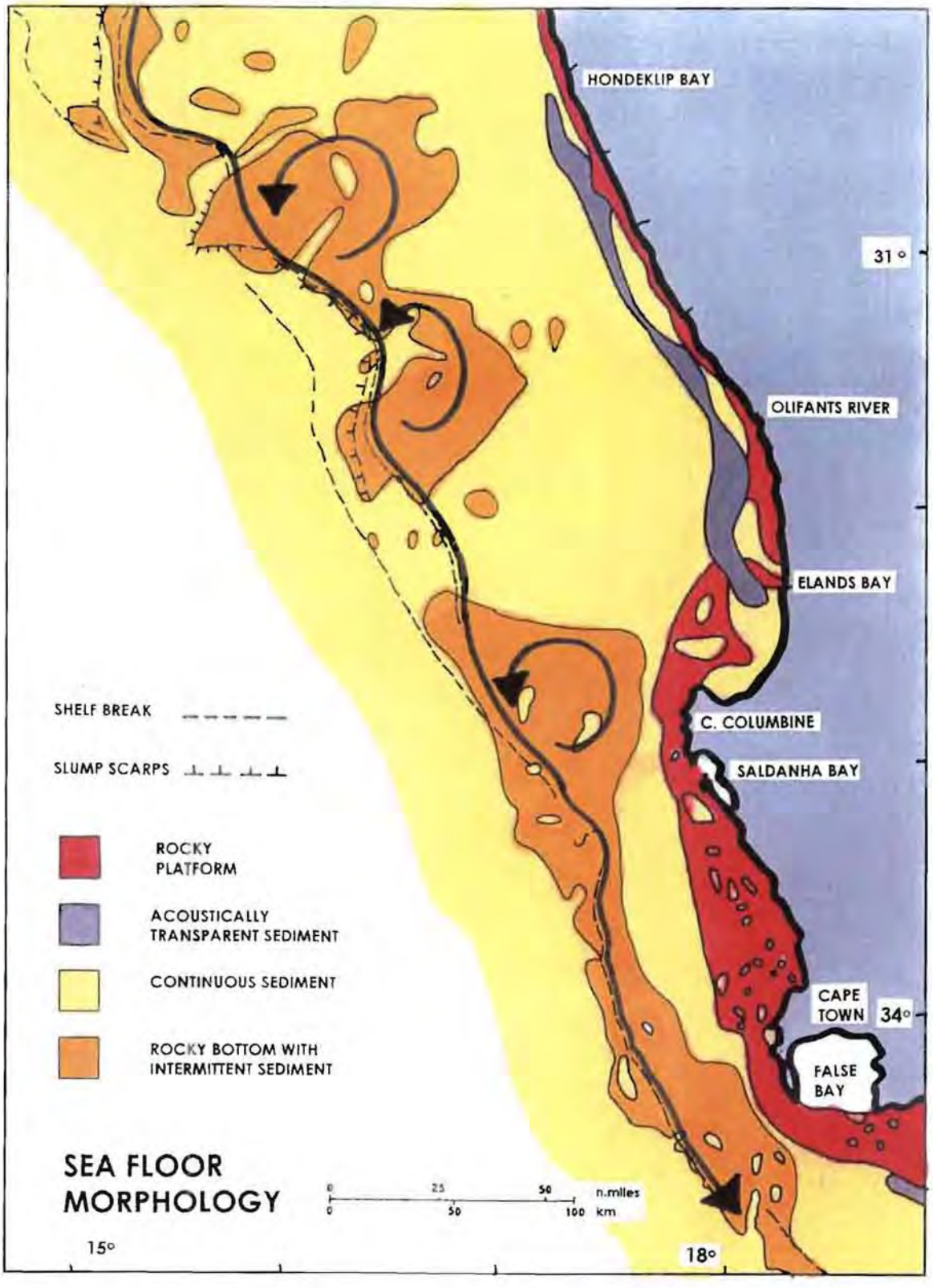

Fig. 4.28: A map of sediment morphology from the southern end of the Benguela System south of 30°S. It is used to suggest that it provides further support for the robustness of the notion that the shelf breaks are zones of enhanced turbulent energy which is reflected by the sediment morphology. This map shows that the belt of rocky bottom with intermittent sediment is located, as was the case in the northern sector, imediately above the shelf break. The long arrow indicates the axis of enhanced turbulence and likely poleward transport of biogenic detritus. The three areas where the belt widens (Child Bank, Olifants River Valley and Cape Canyon) are thought to lead to turbulent eddy shedding which spreads the turbulent energy wider. This map was adapted from Birch, 1975.

Chapter 5

5. Shelf Scale Biogeochemical Processes I: Benthic Remineralization

5.1 Background

The sub-surface part of South Atlantic Central Water (SACW) upwelling in the Benguela System is suggested to be two step process: firstly, SACW is advected from the slope region onto the shelf through one of three "gates" and secondly, once on the shelf, it gets entrained in a general sub-surface poleward flow (Chapter 4). The water which outcrops at upwelling centres is derived from this poleward flow along the inner shelf domain. Therefore, the biogeochemical characteristics of waters which outcrop at one of 6 major upwelling cells is a function of not only the SACW source water but also the distance which the particular cell lies poleward of the "gate".

Globally, marine shelf areas (Z < 200m) have two salient biogeochemical characteristics:

- A large proportion (30-100%) of the particulate carbon export flux reaches the sediments (Middelburg *et al.*, 1993). This focuses most of the remineralization flux on the benthic environment as opposed to the water column remineralization which characterises the deep ocean.
- The greatest turnover of organic matter. Such systems occupy 9% of the ocean surface area but account for 83% of the carbon remineralization and 87% of the burial (Middelburg *et al.*, 1993).

The fact that the Benguela System fits these two characteristics was clearly shown with the biogeochemical transects discussed in the context of the oceanographic processes (Chapter 4: Results and Discussion). The PCO_2 and TCO_2 transects from all three sectors share two common characteristics:

- They all have a vertical gradient which intensifies close to the BBL. This feature is consistent with the first general property of shelf sediments: most of the particulate carbon export flux reaches the sediments thus suggesting that the bulk of the remineralization occurs in the sediments and benthic boundary layer.
- the vertical biogeochemical gradients are largest in the sub-surface water column overlying the sediments with the highest organic carbon concentrations. This feature is consistent with the second general property of shelf sediments: fast burial and remineralization rates.
-

This potential relationship between sediment composition and remineralization rates makes it necessary to briefly review sediment characteristics in the Benguela System.

The spatial distribution of geophysical and biogeochemical characteristics of sediments in the Benguela System were overviewed most recently by Rogers and Bremner, 1991. Most of the biogeochemical characteristics (organic carbon and $CaCO_3$) (Figs. 8 and 10 in Rogers and Bremner, 1991) were obtained from the detailed studies of Bremner, 1983 in the northern sector and Birch, 1975 for the central and southern sectors. The following features are evident:

Organic carbon is constrained in two main zones:

- The spatially most extensive sediment deposits of high organic carbon are found spanning virtually the whole length of the northern sector (18-27°S). Although the whole shelf in this sector is characterized by high organic

carbon content (> 2%) the highest values can be seen to be spread along longshore bands. While a potential mechanism to account for this spatial banding has already been discussed (see Chapter 4) it should be noted that the highest organic carbon values are to be found in the diatomaceous muds located on the landward side of the inner shelf break. These muds which have an average thickness of 5m have built up since the holocene sea level transgression (R. Dingle, pers.com.).

- The northern and central sectors are clearly separated by a zone of low organic carbon spatially associated with the Luderitz upwelling zone which was used to physically define the boundary of the two sectors (see Chapter 4)
- In the central and southern Benguela sectors the high POC deposits are spatially constrained along a narrow inshore ribbon which widens slightly at the southern range. This deposit where values lie mostly in the range (2-5%) organic carbon is spatially coherent with a narrow belt of terrigenous muds originating from the Orange River. While this does not imply that the organic carbon is of terrigenous origin it does indicate that it is a zone where physical turbulence conditions are suitable for the accumulation of fine particulates which include planktonic detritus. The remainder mid and outer shelf of the Central and Southern sectors are characterized by low organic carbon (< 2%).

The spatial distribution of inorganic carbon ($CaCO_3$) (Fig. 10 in Rogers and Bremner, 1991) has the following characteristics:

- Overall it is the inverse of the organic counterpart. The highest concentrations (> 50%) are located on the outer shelf although both in the Northern and Central sectors this range extends well onto the inner shelf.
- The lowest concentrations (0-5%) are along a narrow inshore belt which extends over the whole Benguela System. It should be noted that lower inshore concentrations do not necessarily imply reduced inputs rather, the $CaCO_3$ is "diluted" by a significant input of terrigenous material from the

Kunene, Orange and Olifants rivers which is advected polewards by the sub-surface flow.

- While there is evidence for zonal variability linked to upwelling centres such as Cape Frio, Luderitz and the Southern Benguela this is not as complete as was the case for the organic carbon where clear breaks occurred. The difference in the concentrations and distribution of the two sediment carbon components is indicative of differences in the temporal preservation of organic carbon and $CaCO_3$. This is addressed in further detail below.

One of the most important new insights into dynamics of the Benguela System is the importance of longshore poleward advection as opposed to the classical Ekman cross shelf view (Chapter 4) for the supply of water to upwelling centres. The significance of this view to understanding of the biogeochemical fluxes and their impact on PCO_2 within the Benguela System have already been alluded to (Chapter 4) and in this section the theme is developed in greater detail.

Vertical fluxes are the product of a physical turbulent mixing term (KZx) and a biogeochemical gradient term (dCx/dZ). The variability in the magnitude and biogeochemical biogochemical consequences of the physical term in the BBL has been highlighted through observed changes to the thickness of the BBL and cross shelf variations in the sediment particle sizes and biogeochemical composition (Chapter 4). In this section I address the benthic remineralization processes which govern the biogeochemical gradients.

Significant changes are consistently observed in the pre-formed biogeochemical properties of SACW from between its advection onto the shelf and the point when it outcrops at an upwelling centre in the Benguela System. In all instances there are differences in both the magnitudes and the stoichiometries of these changes in respect of CO_2, nitrogen (NO_3^- and NH_4^+) and to a lesser extent CO_3^{2-}. Each of the stoichiometric relationships (C_{Org} :

C_{Ing} and C:N) has a certain but predictable impact on the PCO_2. The benthic remineralization flux which governs the change in the chemical characteristics of sub-surface shelf domain waters is driven by a complex interaction of physico - biogeochemical processes of which include *inter alia*:

- characteristics of the pelagic flux (magnitude and stoichiometry)
- relative rates of biogeochemical pathways (oxic/anoxic oxidation, dissolution)
- nature of biogeochemical utilization of N (nitrification - denitrification)

particle - water phase equilibria of charged chemical species (adsorption of NH_4^+)

- turbulence - particle interactions (particle accumulation / erosion, mixing)

The net cumulative effect of these processes not only governs the characteristics of the sediments, but also the benthic flux of dissolved products of diagenesis. In the case of carbon, stoichiometric characteristics of this flux are also thought to determine the CO_2 source - sink characteristics of the system.

The objectives of this section are:

- to highlight the important but previously underestimated interactive role of sediment and benthic boundary layer (BBL) processes in driving the observed biogeochemical changes in carbon and nitrogen in shelf domain waters and, .
- to constrain the relationship between PCO_2 and the remineralization stoichiometries C_{Org} : C_{Ing} and C_{Org} : NO_3^-. Of particular interest are the mechanisms which give rise to the stoichiometric disequilibria and their impact on PCO_2 variability and the source - sink nature of the system.

5.2 Methods

The results presented below have two constraints:

- the focus of the interpretation is largely spatially limited to the inner shelf region (Z < 100m), the origin of the water which outcrops at the upwelling cells.
- the focus of the results and discussion in this section is on stoichiometric relationships, the mechanisms underlying them and the biogeochemical inputs (average carbon and nitrogen parameter concentrations) for the box model in Chapter 7. The spatial variability of the biogeochemical parameters (PCO_2 , TCO_2, O_2 and NO_3^-,) has been addressed in the context of the oceanographic characteristics of the Benguela System (Chapter 4).

The results are set out by sector and as far as possible the same structure is applied to each of the three sectors. Within each sector there are two upwelling cells (see Chapter 4). Field data only exists for three of the upwelling cells, one from each sector (Walvis Bay in the northern sector; Namaqua in the central sector; Cape Columbine in the southern sector). For each of these upwelling centres the stoichiometric relationships are established in two formats:

- the whole data set from a particular site is used to depict stoichiometric relationships (C_{Org} : C_{Ing} and C:N). The stoichiometry shown in these plots is the global value which includes both surface and sub-surface waters.
- for the box modelling stage it is necessary that water types which mark critical stages of the upwelling cycle are identified and have their biogeochemical characteristics defined. These are represented in table format where the magnitude and stoichiometry of the changes are shown. The C_{Org}: C_{Ing} stoichiometric relationships for these box model input data are also graphically depicted as (TAcy-TAlk) vector plots where the impact

of both perturbation magnitude and stoichiometry on PCO_2 can be best seen (see Chapter 3 for the theory).

For those upwelling centres where field data was not collected (Cape Frio in the northern sector; Luderitz in the central sector and Cape Peninsula in the southern sector) the biogeochemical characteristics to be used for the box model were defined as follows: both Cape Frio and Luderitz are at the "gate" sites for the waters which fill the northern and central sector shelves. The characteristics of the water which outcrops at these sites are therefore defined as unmodified SACW whose biogeochemical properties were obtained from samples within the SACW core from the same sector. The Cape Peninsula upwelling cell is very close to the Cape Columbine centre in a system where remineralization is weakest. Its biogeochemical characteristics are therefore set by the characteristics of waters which upwell at Cape Columbine. The extent to which these assumptions influence the model predictions will be evaluated in the modelling stage through a sensitivity analysis.

5.3 Results and Discussion

5.3.1 Northern Sector: Henties Bay Transect

In the northern sector SACW is hypothesised to be advected onto the shelf along the northern boundary adjacent to Cape Frio where a fraction of the water outcrops but the bulk is advected polewards over the shelf (see Further Discussion in Chapter 4). Because of the biogeochemical modifications which accompany this process the water is redefined from SACW to Northern Sector Shelf Water (NS-SW). Of particular interest to modelling fluxes at upwelling cells are waters which flow polewards along the inner shelf (Z < 100m) and get entrained in the wind driven upwelling. This water is termed NS - Inner Shelf Water (NS -ISW).

Carbon Remineralization Flux and Stoichiometry

The C_{Org} : C_{Ing} stoichiometry of the data from the Henties Bay transect is shown in Fig. (5.1) which depicts a NTAcy - NTAlk, (Total Acidity and Total Alkalinity normalized to S = 35.00), plot (see Chapter 3).

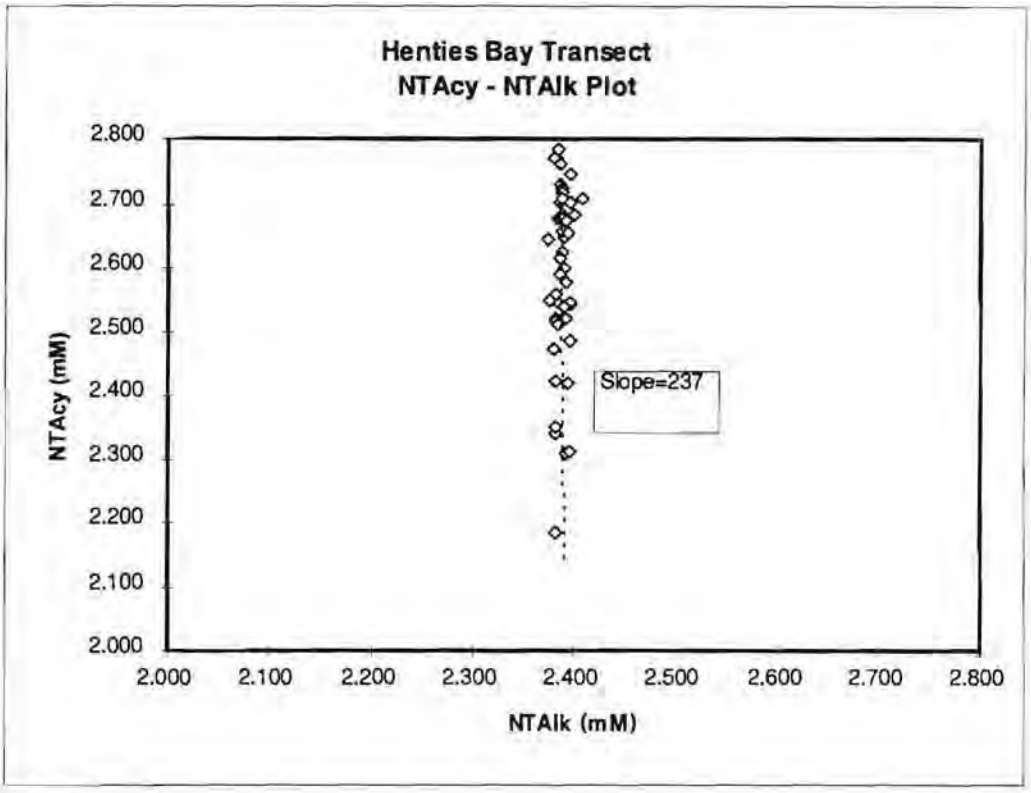

Fig. 5.1: A plot of all individual Total Acidity and Total Alkalinity data from the Henties Bay transect. It shows (slope = 237) that the addition or uptake of carbonate plays an insignificant role in the carbon cycle of the northern sector. Carbon fluxes are driven by photosynthesis and oxidation.

The axes have been scaled so that they span the same magnitude range and the slope reflects stoichiometry in a direct way The plot which includes all sub-surface and surface data, shows that changes in state to the carbonate system in the northern Benguela sector are almost completely driven by organic carbon pathways (photosynthesis and respiration couple). This is numerically supported by the calculated mean of the TAlk values (2.388± 0.006 mM) which spans a very narrow range. The slope of the line is calculated using a geometric mean (GM) functional regression technique

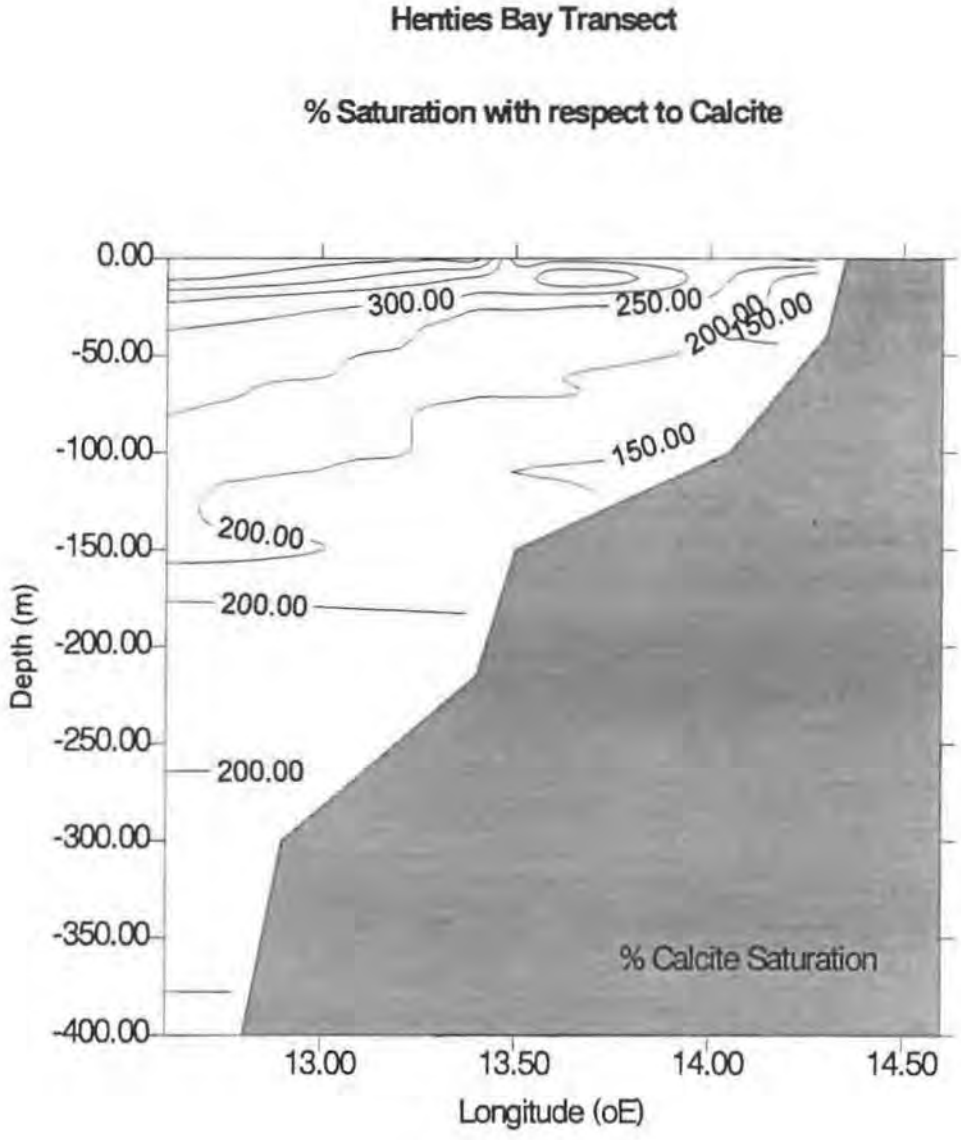

Fig. 5.2: A section showing the degree of saturation (%) of carbonate with respect to calcite. It shows that, despite the high PCO2 values (see Fig. 4.7 b) in the benthic boundary layer, the water column is supersaturated with respect to calcite.

(Ricker, 1984) which gives the value 237 or, practically a nil contribution from (NTAlk. The upper points represent sub-surface waters most impacted by benthic remineralization and the lower points those waters most impacted by surface productivity and or degassing to the atmosphere. SACW advected into the northern sector has a mean NTAcy value of 2519 μM which is close to the mid point of the span of the data.

The lack of evidence for CO_3^{2-} dissolution was unexpected given the high PCO_2 values (see Fig. 4.7b) in the BBL which should decrease the saturation levels. However, a plot of CO_3^{2-} saturation with respect to calcite (Fig. 5.2) confirms that nowhere is the system undersaturated with respect to the form of $CaCO_3$ (calcite) which makes up the structure of coccoliths (Honjo, 1976; Milliman, 1993). This probably also accounts for the fact that Namibian shelf sediments are not only rich in organic carbon but in $CaCO_3$ as well (see Fig. 4.27). Along the outer shelf coccolithophore $CaCO_3$ may make up more than 50% of the sediment mass (Giraudeau, pers.com.). It should be noted that the sub-surface waters with lowest super saturation were predictably located over the shelf areas where the highest concentrations of organic rich sediment are found. This reinforces the view of the role played by benthic remineralization in carbon fluxes where, if $CaCO_3$ dissolution was to occur, it would be in those areas.

Carbon : Nitrogen Remineralization Flux and Stoichiometry

The relationship between ΔCO_2 and ΔNO_3^- variability in the waters sampled along the Henties Bay transect is depicted in Fig. 5.3 which plots NTAcy and NO3-. Changes to CO_2 are related to NTAcy through $\Delta CO_2 = \Delta NTAcy/2$ (Chapter 3). The plot provides an unexpectedly weak relationship between these two parameters which are theoretically linked through the Redfield ratio (C:N ~ 6.6; or in the NTAcy format of the plot $\Delta NTAcy: \Delta NO_3^- \sim 13.2$) which is plotted as a line through the data. Particle adsorption together with

denitrification are proposed as the two mechanisms underlying the observed C:N remineralization disequilibrium.

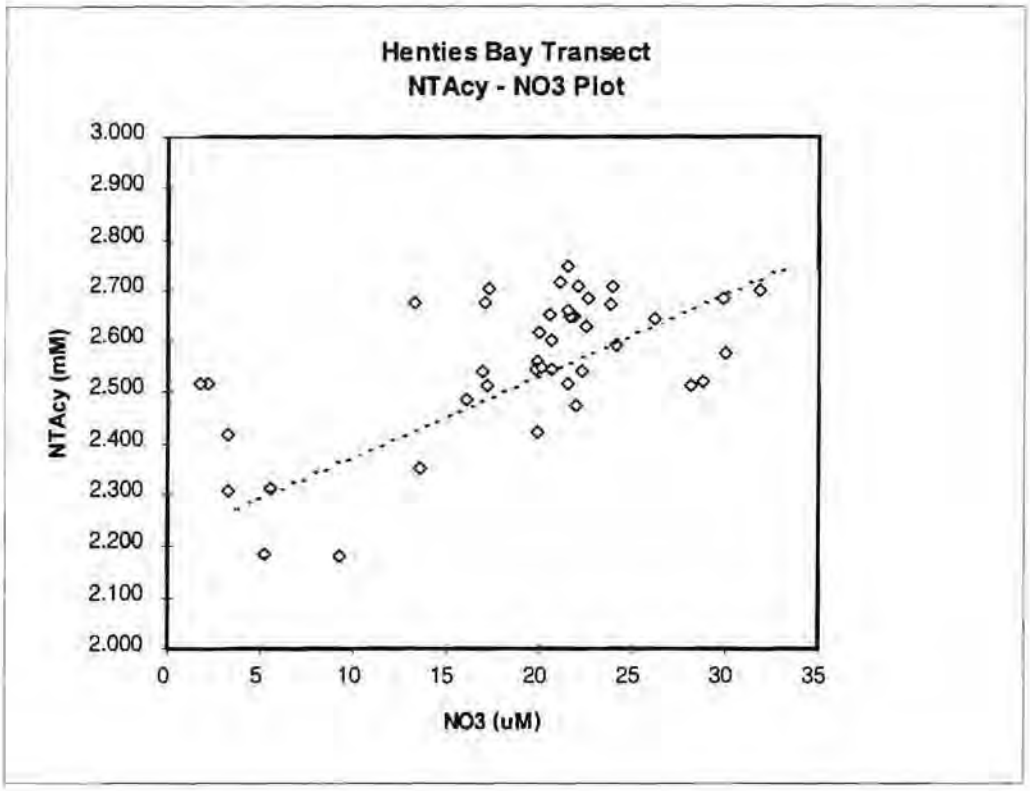

Fig. 5.3: A plot of Total Acidity and Nitrate normalized to a common salinity of 35 psu using data from the Henties Bay transect. It shows that the points have a weak fit to the line which defines the Redfield ratio (6.6). The reason for this is a combination of denitrification of new NO_3^- and adsorption of NH_4^+ in the sediments (see Further Discussion).

The effectiveness of the particle adsorption mechanism is best illustrated using a data set of adsorbed and pore water NH_4^+ taken from two sediment cores (B1/18 and B1/24)) collected in the course of the same transect (see Fig. 4.2 in Methods section of Chapter 4 for location). Both cores were taken from the organic rich muds from the inner shelf domain where NS-ISW acquires its characteristics (Fig. 5.4). It can be seen that in both cases, but particularly for core B1/18, the pore water (Fig.5.4 a) NH_4^+ profiles mimic the adsorbed fraction (Fig.5.4b) closely, suggesting that an equilibrium existed for NH_4^+ between the two phases. What is particularly useful about these data is the calculation of the mass balance between the two phases. Despite the fact that the pore water NH_4^+ concentrations are very large (480 - 580μM

close to the top), it was calculated (using an average 21% w/w water content) that 92-94% of the NH_4^+ in this environment is adsorbed onto the solid phase.

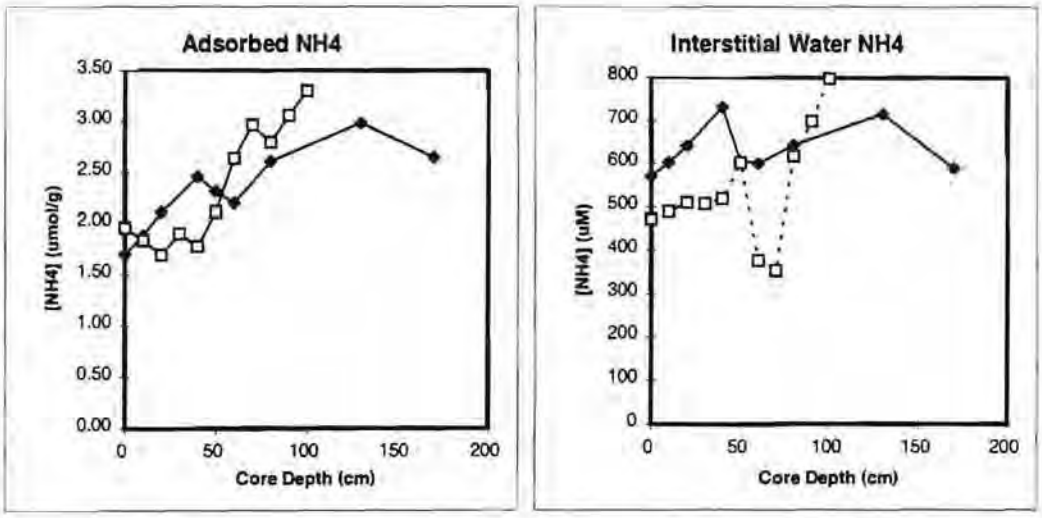

Fig. 5.4: Two plots showing the adsorbed (left) and pore water (right) concentrations of NH_4^+ from two cores B1/18 (solid line), B1/24 (dashed line) taken during the Henties Bay transect. The plots show that pore water and adsorbed NH_4^+ concentrations appear to be well correlated particularly in the case of core B1/18. (See Fig. 4.2 for locations).

The overall relationship between adsorbed and pore water NH_4^+ is depicted on the scatter plot (Fig.5.5) which includes the least squares regression line linking them together ($Y = 4.354 * X - 0.367$; $r^2 = 0.67$).

Comparative data from other sediment environments show that this is the steepest slope emphasising that in this system particle adsorption is a particularly relevant biogeochemical mechanism. This results in the observed values of about 1.8 μmol adsorbed NH_4^+ /g of the solid fraction close to the sediment - water boundary.

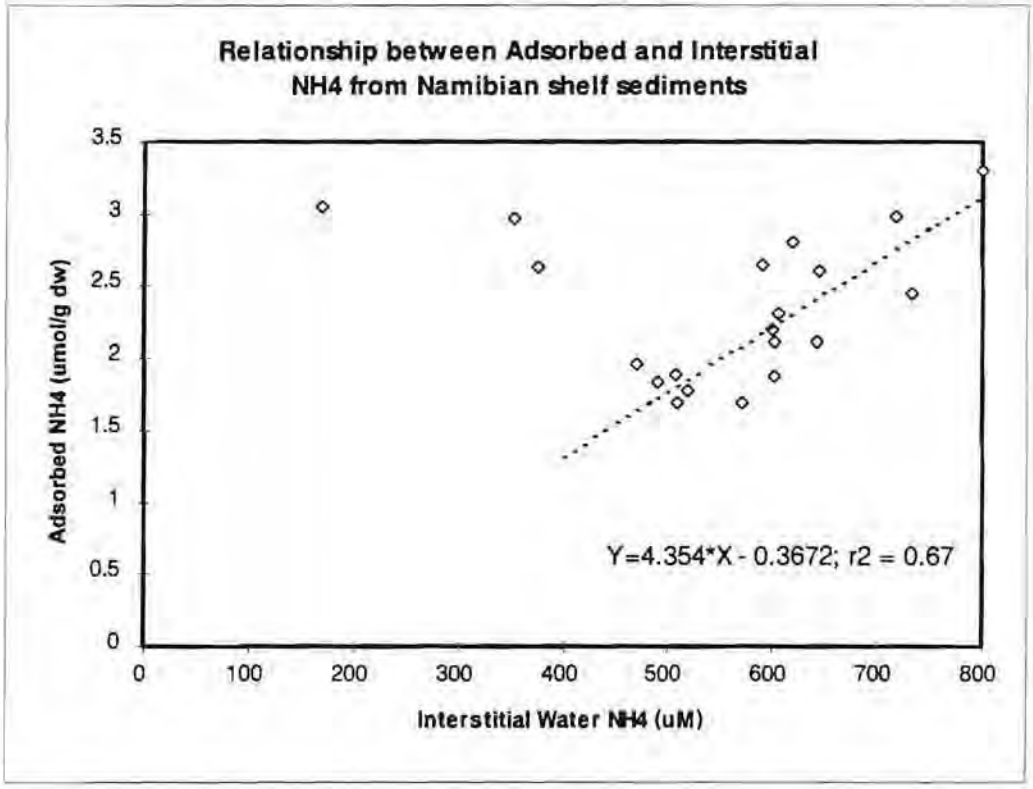

Fig. 5.5: A scatter plot of the adsorbed and pore water NH_4^+ concentrations from the Henties Bay transect. It confirms that there is a significant correlation between the two variables which suggests that adsorption is an important mechanism regulating free NH_4^+ in the benthic environment.

Box Model Input Data

The carbonate and nitrate characteristics of NS - ISW which outcrops at the Walvis Bay upwelling cell are constrained by physical properties: depth Z < 100m and t < 12.80 °C (obtained from stations 16 and 27). These waters overlie the inner and outer edges of the organic rich diatomaceous muds (see Fig. 4.27). The average carbonate parameter and nitrate concentrations in the sub-surface domain at each of the stations are also shown in Table 5.1 as NS - ISW1 (16) and NS - ISW2 (27).

Northern Benguela Sector: Henties Bay Transect

Carbonate and Nitrate Parameter Concentrations
Units: umol/l; Normalized to S = 35.00psu

Sub-Surface Domain

Water	Station	Depth	NTALK	NTACY	NTCO2	PCO2	NO3
NS-SACW	33	98.7	2383	2519	2239	626	21.57
NS-ISW1	16	10.5-37.3	2384	2762	2360	1466	
NS-ISW2	27	51.8-91.2	2388	2670	2317	1020	21.45
NS-ISW			2386	2716	2339	1243	21.450
NS-ISW (NO3 Corr)			2386	2716			
Change			3	197	100	617	-0.12
CO2 addition				99			
CO3 addition			2				
COrg:CIng Stoichiometry			66				
NO3 addition							-0.12
C:N Stoichiometry							-820.83

Table 5.1: Summary of the average biogeochemical (carbon and nitrogen) characteristics of "new" South Atlantic Central Water prior to it being advected onto the shelf of the northern sector (NS-SACW) and the biogeochemically modified SACW on the inner shelf (NS-ISW) and sampled during the Henties Bay transect. The table also shows the net calculated additions of CO_2, CO_3^{2-} and NO_3^- as well as their stoichiometry.

The integrated value was then divided by the depth of integration to provide the average values used for stations 16 and 27 (Table 5.1). The values for stations 16 and 27 were averaged to provide a final uncorrected value for pre-upwelled NS - ISW. Although the NO_3^- change (-0.12μM) is small, the correction step to the carbonate parameters (NTAcy and NTAlk) is included for consistency and to emphasise its role (see Chapter 3). The ΔCO_2 and ΔCO_3^{2-} additions which are linked to (TAcy/2 and (TAlk/2 respectively are shown and used to calculate the C_{Org}: C_{Ing} stoichiometric ratio of 66 in the benthic remineralization flux.

The most noticeable points are:

- as was suggested by the NTAcy-NTAlk general data plot (Fig. 5.1) the impact of inorganic carbon (C_{Ing}) remineralization in the sub-surface domain is minimal (3 μM).
- most of the modification of biogeochemical properties between NS-SACW and NS - ISW is driven by the oxidative remineralization of organic carbon into CO_2 which modifies NTAcy only.
- in respect of CO_2 fluxes, PCO_2 increases by ~100% between the point when NS-SACW (626μatm) is advected onto the shelf and the time when it reaches the vicinity of the mid-Namibian Inner Shelf as NS-ISW (1243μatm) at the Henties Bay transect.
- whereas NTAcy increases between the two end-members, NO_3^- remains largely unchanged registering a small (-0.12μM) but perhaps not significant decrease (there was no NO_3^- data for station 16). This is reflected by the large and negative value for the $\Delta CO_2 : \Delta NO_3^-$ stoichiometry of -820.83.

The stoichiometry and magnitude of the perturbation to the carbonate system as measured by the averaged data in Table 5.1 is graphically depicted by a vector plot (Fig. 5.6). It makes use of NTAcy and NTAlk to independently quantify the contributions by organic and inorganic carbon remineralization pathways. It depicts the relationship between the C_{Org} and C_{Ing} perturbations and their impact on PCO_2. The two end-members (NS-SACW and NS - ISW) are plotted using their respective NTAcy and NTAlk co-ordinates super-imposed on a family of PCO_2 lines all plotted at a constant temperature of 12.5 °C which characterises waters which upwell in the northern sector (Fig. 5.6). This visually confirms the earlier observation that the inorganic carbon remineralization pathway plays little or no role in this change. PCO_2 change in this system is wholly controlled by the oxidation of organic carbon into CO_2. The numerical magnitude of the NTAcy change driven by CO_2 addition is given on Table (5.1) ΔTAcy = 197μM. This corresponds to a CO_2 addition of 99μM and a $C_{Org} : C_{Ing}$ stoichiometry of 66. This value is smaller than that

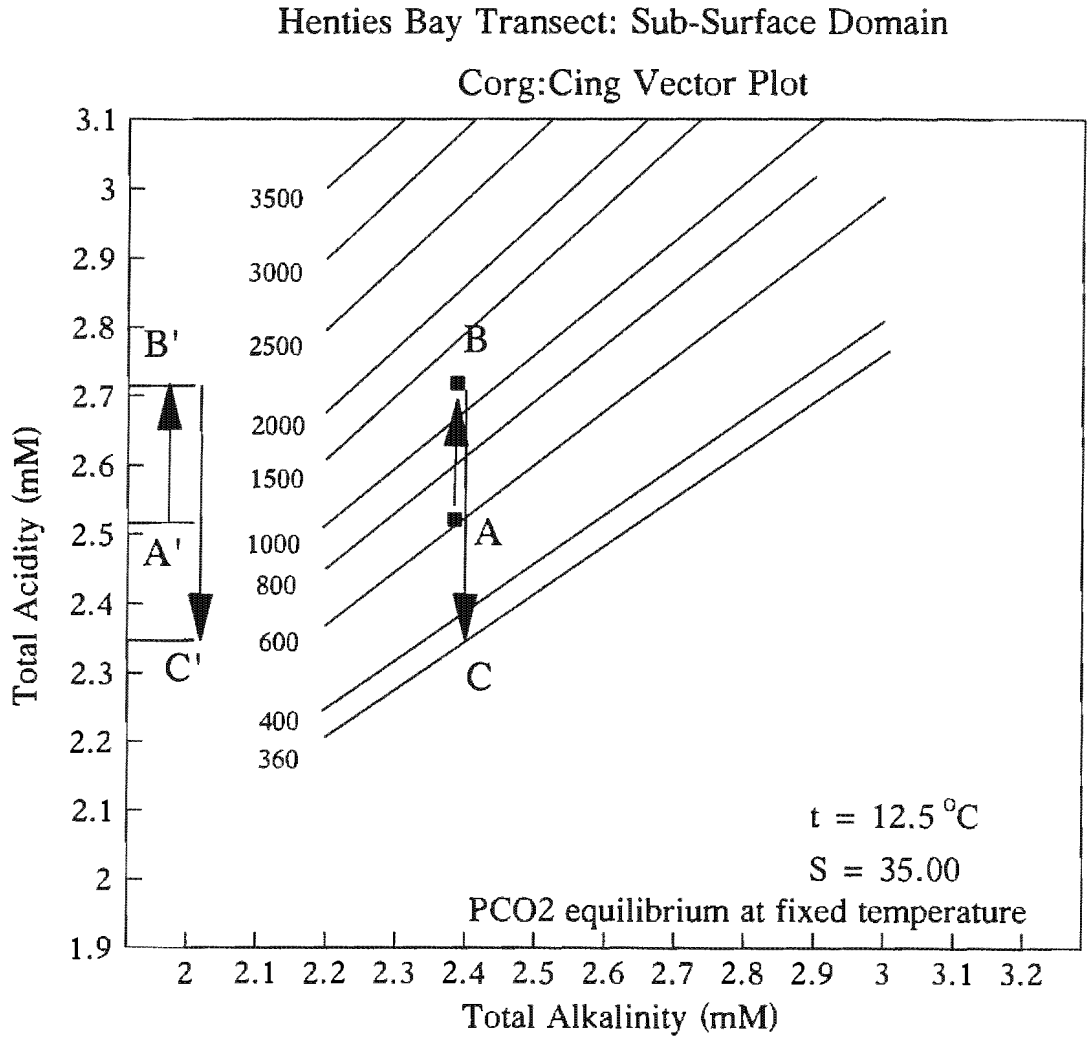

Fig. 5.6: A Total Acidity - Total Alkalinity vector plot showing the magnitude of the changes brought about by the organic (C_{Org}) and inorganic carbon (C_{Ing}) remineralization in the northern sector. The characteristic values for the end - members (NS-SACW (A) and NS-ISW(B)) were obtained from Table 5.1. Also plotted are the PCO_2 lines computed for a temperature of 12.5°C which is typical of SACW in the northern sector. The plot confirms that carbon remineralization fluxes are almost completely governed by oxidation of organic carbon (C_{Org} pathway). (see text for further details).

which was calculated using the whole data set (237) but both support the view that C_{Ing} is an insignificant contributor to the carbon remineralization flux.

The ΔTAcy between the upper value of the NS - ISW (B) and the atmospheric PCO_2 equilibrium line (C) provides the potential magnitude of the CO_2 degassing process in the context of an abiotic "Strangelove Ocean". The numerical value is given by the vector component (B'C') (ΔNTAcy = 360μM; ΔCO_2 = 180μM). In reality, this degassing scenario is ameliorated by the surface productivity.

The averaged input data for the box model (Table 5.1) also reflects the combined effect of both carbon and nitrogen remineralization mechanisms as shown by the change in NO_3^- characteristics between off the shelf NS-SACW and the biogeochemically modified NS - ISW (Table 5.1). While the re-mineralized CO_2 flux contributed 99μM to the ΔTCO_2, the NO_3^- concentration decreased by 0.12 μM. Had the NO_3^- increased by the amount predicted by the Redfield ratio (6.6) its concentration in NS-ISW would have to be (21.57 + 15.00 = 36.57μM). The measured C:N stoichiometry (ΔCO_2 : ΔNO_3^- = -820.8) confirms that remineralized NO_3^- makes no net contribution to the pre-formed characteristics of waters upwelling in the vicinity. The mechanistic basis for these stoichiometric disequilibria is addressed in the discussion below.

5.3.2 Central Sector (CS): Hondeklip Bay Transect

Carbon Remineralization Flux and Stoichiometry

The overall C_{Org} : C_{Ing} stoichiometry of the biogeochemical data from the Hondeklip Bay transect is depicted in Fig. 5.7.

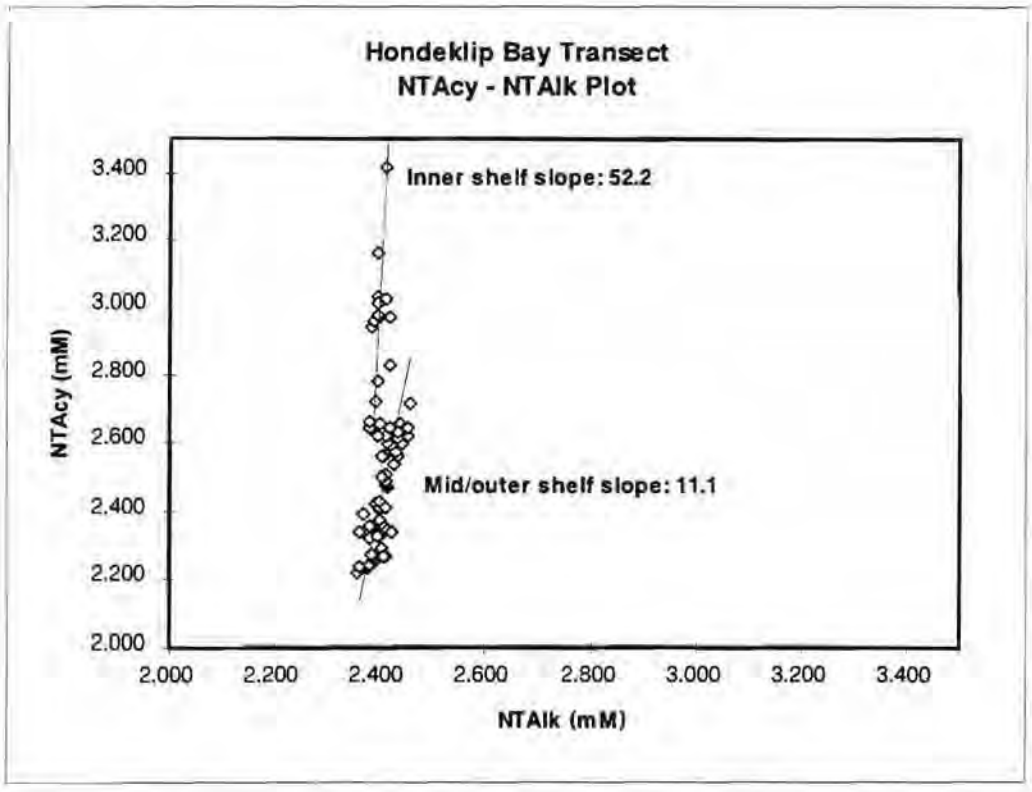

Fig. 5.7: A plot of all individual Total Acidity and Total Alkalinity data from the Hondeklip Bay transect. It shows that similarly to the northern sector changes in the chemical state of the carbonate system are largely driven by the organic carbon mechanisms (C_{Org} : C_{Ing} - 52:1 and 11:1 in inner and outer shelf respectively) with the inorganic carbon uptake and dissolution making a minor impact. There is a noticeable stoichiometric difference between inner shelf and mid/outer shelf samples with the C_{Ing} pathway making a relatively larger contribution in the mid/outer shelf.

As was the case for the transect in the northern sector, the central sector is also almost exclusively driven by the photosynthetic - respiration couple which impacts only on ΔNTAcy. It is clear however that the overall span of variation is larger than was the case for the northern sector. The top NTAcy values from the inshore station 113 reach 3.40 (cf. 2.70 for the northern sector) which is expected to be reflected in much higher PCO_2 values. The lowest values close to 2.20 are similar to those on the Henties Bay transect and in both cases reflect surface samples close to atmospheric PCO_2 equilibrium. As was the case in the northern sector, NTAlk variability was insignificant compared to NTAcy in the overall carbon fluxes which is reflected by the overall trend slopes of the scatter plot (Fig. 5.7). Although there is an overall steep slope of 52.21, the data set can be even visually divided into

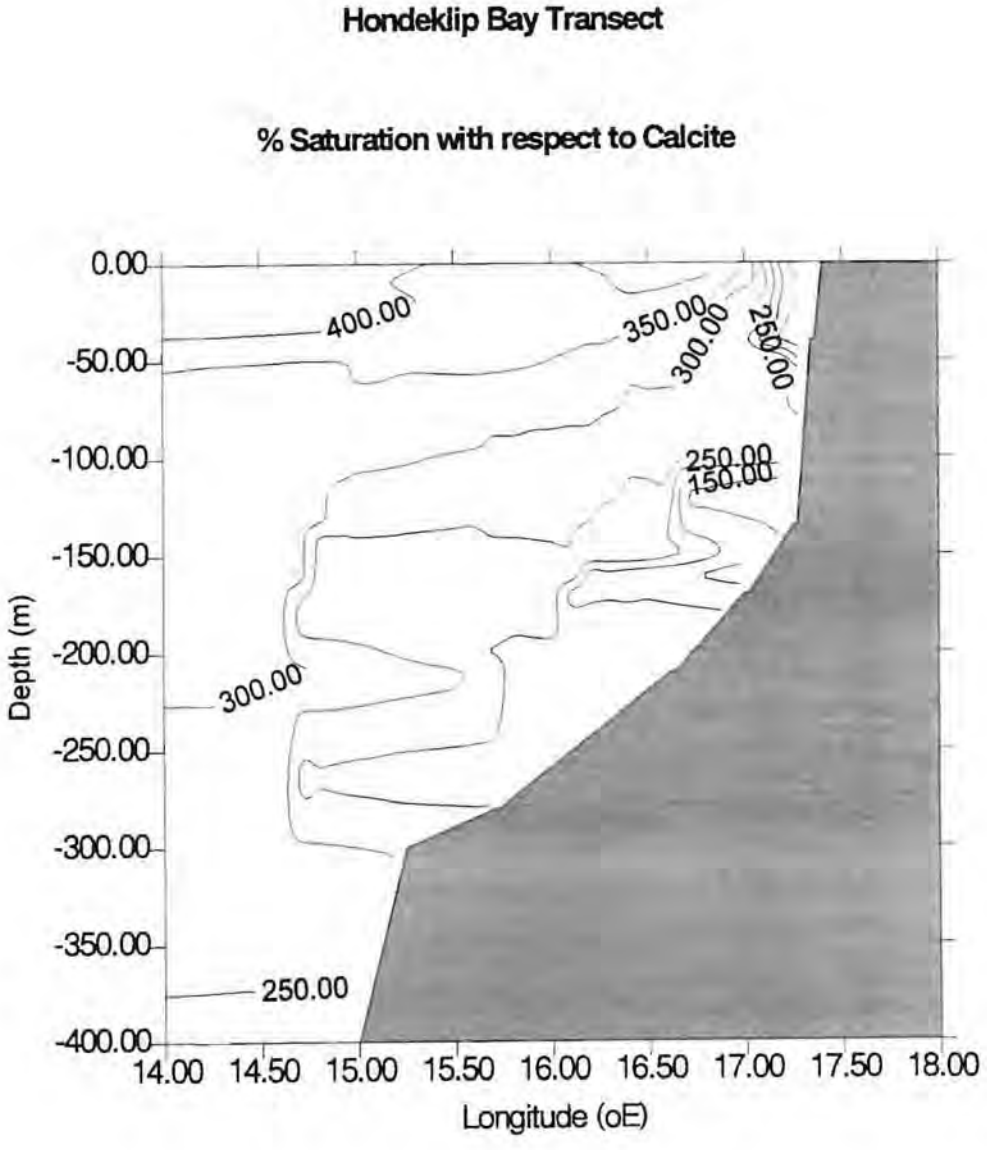

Fig. 5.8: A cross-shelf section showing the degree of saturation (%) in the water column with respect to calcite. It shows that apart from a very narrow inshore area of 10km the shelf water column is supersaturated.

two stoichiometric groups. The larger part of the data set where NTAcy values are < 2.70mM which characterises most of the shelf water except the narrow inshore belt, has a slope of 11.14 indicating that the water column is reflecting some activity of both uptake and remineralization of $CaCO_3$. The second group of data points in the higher range of NTAcy which come from the two inshore stations where the slope is 240 reflect no significant $CaCO_3$ uptake or dissolution. The overall mean NTAlk of 2.404± 0.021 mM shows a wider range than the Henties Bay transect samples which reflects the increased $CaCO_3$ uptake - remineralization activity.

The minor effect of CO_3^{2-} dissolution on TAlk is explained, as was the case in the northern sector, by the fact that over most of the transect the water column was super-saturated in respect of calcite (Fig. 5.8). Given this result it is surprising that the mid and outer shelf data indicate a significant $CaCO_3$ remineralization. This may be accounted for by the fact that sediment $CaCO_3$ may have a significant component of aragonite which is more soluble than calcite (Broecker and Peng, 1982; Milliman, 1993). The CO_3^{2-} (calcite) saturation data indicates that only the water column at the inner most station and the bottom sample from the adjacent station were undersaturated. In spite of this the data from the same location was shown above to have no indication of $CaCO_3$ dissolution activity. This indicates that there is little $CaCO_3$ deposition in the otherwise very productive inshore belt. As was the case for the northern sector the variability of CO_3^{2-} saturation with respect to calcite is driven by changes in CO_2 rather than by the addition or removal of CO_3^{2-}.

Carbon : Nitrogen Remineralization Flux and Stoichiometry

The overall relationship of TAcy and NO_3^- for the Hondeklip Bay transect is depicted in Fig. 5.9 where the Redfield ratio (Rr) slope has also been super-imposed.

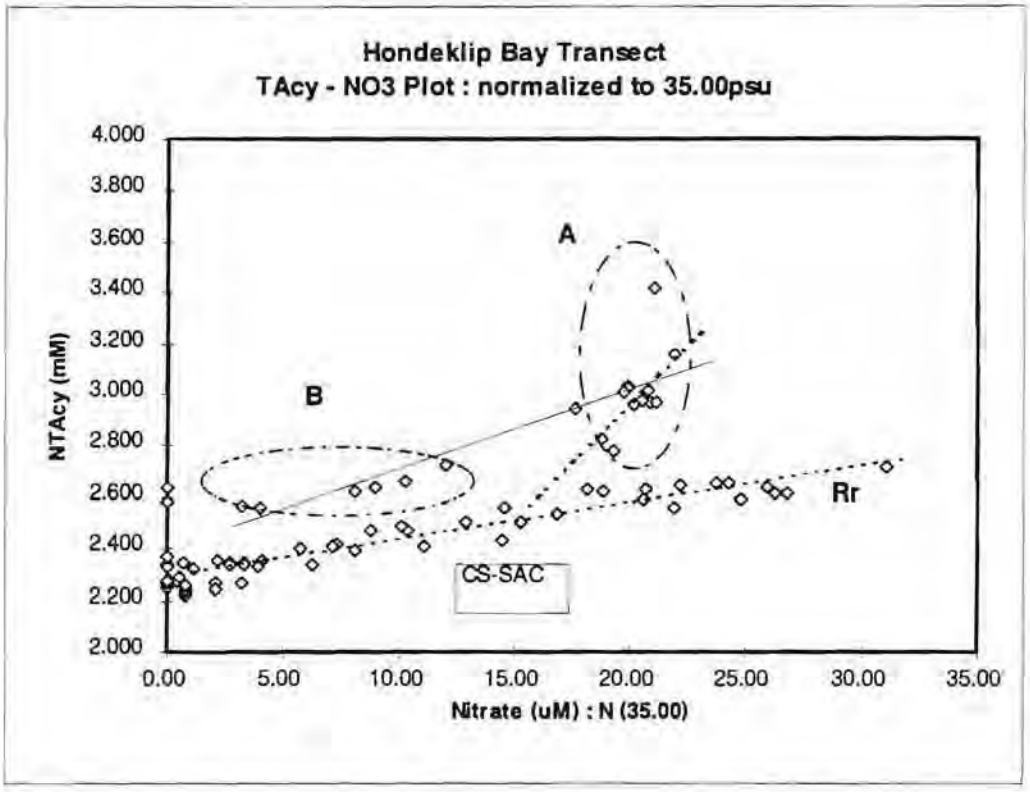

Fig. 5.9: A plot of Total Acidity and NO_3^- concentrations, normalized to 35 psu, from the Hondeklip Bay transect. It shows the extent to which C:N uptake and remineralization dynamics deviate from the Redfield ratio given by the dashed line. Most of the data points do follow the Redfield ratio except those grouped into areas A and B. The samples from these groups come from the inshore stations where upwelling and its consequences were most evident (see text). The dashed line linking SACW to A (CS-ISW) indicates the general C:N stoichiometry of remineralization (~ 40) and the line linking B to A is the stoichiometry of surface uptake (~ 13).

In sharp contrast to the northern sector where the relationship was weak, in the central sector, the majority of data points fall close to the stoichiometry predicted by the Redfield ratio (6.6). These data indicate that de-nitrification is not a significant biogeochemical process mediating the NO_3^- variability in most of the central sector. The interesting exception is a part of the data (group A) where TAcy increases sharply with little concomitant input of NO_3^-. These data correspond to those in the inshore belt central sector inner shelf water (CS-ISW) where a significant C:N disequilibrium is induced by local biogeochemical processes. It is suggested that the driving mechanism behind this group of anomalous observations is again, the adsorption of remineralized NH_4^+ by benthic biogenic and lithogenic particles (Berner, 1976;

Boatman and Murray, 1982; Mackin and Aller, 1984). With this mechanism, remineralized CO_2 is released into the BBL at a rate which is a function of the pore water - BBL gradient and turbulent diffusion increasing the TAcy while NH_4^+ is retained in the sediment and BBL. NH_4^+ measurements of the subsurface waters at stations 113 and 114 showed (unpublished data) that its concentrations are low ($< 2\mu M$ even in the BBL thus contributing little to correcting the C:N disequilibrium.

The second group of anomalous data points (group B) is linked to group A by a line whose slope is the stoichiometry which characterises the surface utilization of upwelled NO_3^- and CO_2 also within the upwelling front. This predicted CO_2:NO_3^- stoichiometry of 13 is confirmed later when the box model data is defined for the surface layer domain.

Box Model Input Data

The box model input data for the carbonate parameters which incorporate the biogeochemical characteristics discussed above are presented in Table 5.2. The biogeochemical characteristics of central sector South Atlantic Central Water (CS-SACW) which is advected onto the shelf in the central sector were taken as shown from two slope stations where the (t,S) core was sampled at 306 and 204m which were in both cases at least 200m off the BBL. These values reflect CS-SACW unmodified by the benthic remineralization flux, an assumption which is supported by the relatively low PCO_2 of $458\mu atm$. The biogeochemical characteristics of CS-ISW which upwells at the Namaqua upwell cell were obtained from the subsurface values at the two inshore stations (113 and 114). In the case of station 113 where the water column was filled to the surface with newly upwelled water, the depth integration to calculate the average was taken from the surface. The overall average for the carbonate parameters in CS-ISW is, as before, calculated from the individual station values. The individual values for NTAcy and NTAlk were

corrected for the 6.41μM NO_3^- addition from which the magnitudes of the parameters concentration changes, CO_2 and CO_3^{2-} additions and

Central Benguela Sector: Hondeklip Bay Transect

Carbonate and Nitrate Parameter Concentrations
Units: umol/l; Normalized to S = 35.00psu

Sub-Surface Domain

Water	Station	Depth	NTALK	NTACY	NTCO2	PCO2	NO3
CS-SACW	121/119	306/204	2413	2480	2234	458	13.67
CS-ISW1	113	1-34	2398	3058	2516	3445	20.51
CS-ISW2	114	113-123	2388	2957	2461	2496	19.64
CS-ISW			2393	3008	2489	2971	20.08
CS-ISW(NO3 Corr)			2399	3001			
Change			-14	521	255	2513	6.41
CO2 addition				261			
CO3 addition			-7				
COrg:CIng Stoichiometry				-38			
NO3 addition:							6.41
C:N Stoichiometry							40.68

Table 5.2: Summary of the average biogeochemical (carbon and nitrogen) characteristics of "new" South Atlantic Central Water prior to it being advected onto the shelf of the central sector (CS-SACW) and the biogeochemically modified SACW on the inner shelf (CS-ISW) and sampled during the Hondeklip Bay transect. The table also shows the net calculated additions of CO_2, CO_3^{2-} and NO_3^- as well as their stoichiometry.

stoichiometry were derived. The only potentially problematic aspect of the carbonate parameter changes between CS-SACW and CS-ISW is the small decrease in NTAlk (-9μM). The reason for this change is unknown but is hypothesised to be due to a combination of the change in one or more proton acceptors which have not been accounted for and to a much lesser extent, experimental error. The impact of this change in the overall CO_2 biogeochemistry is, however, very small and will for the modelling purposes be ignored. The most significant comparative difference between the data set from the northern and central sectors is that the CO_2 addition into shelf based CS-ISW is 167% higher (264μM cf. 99μM) in the latter. This difference in the impact of the benthic remineralization flux is reflected in the PCO_2 values

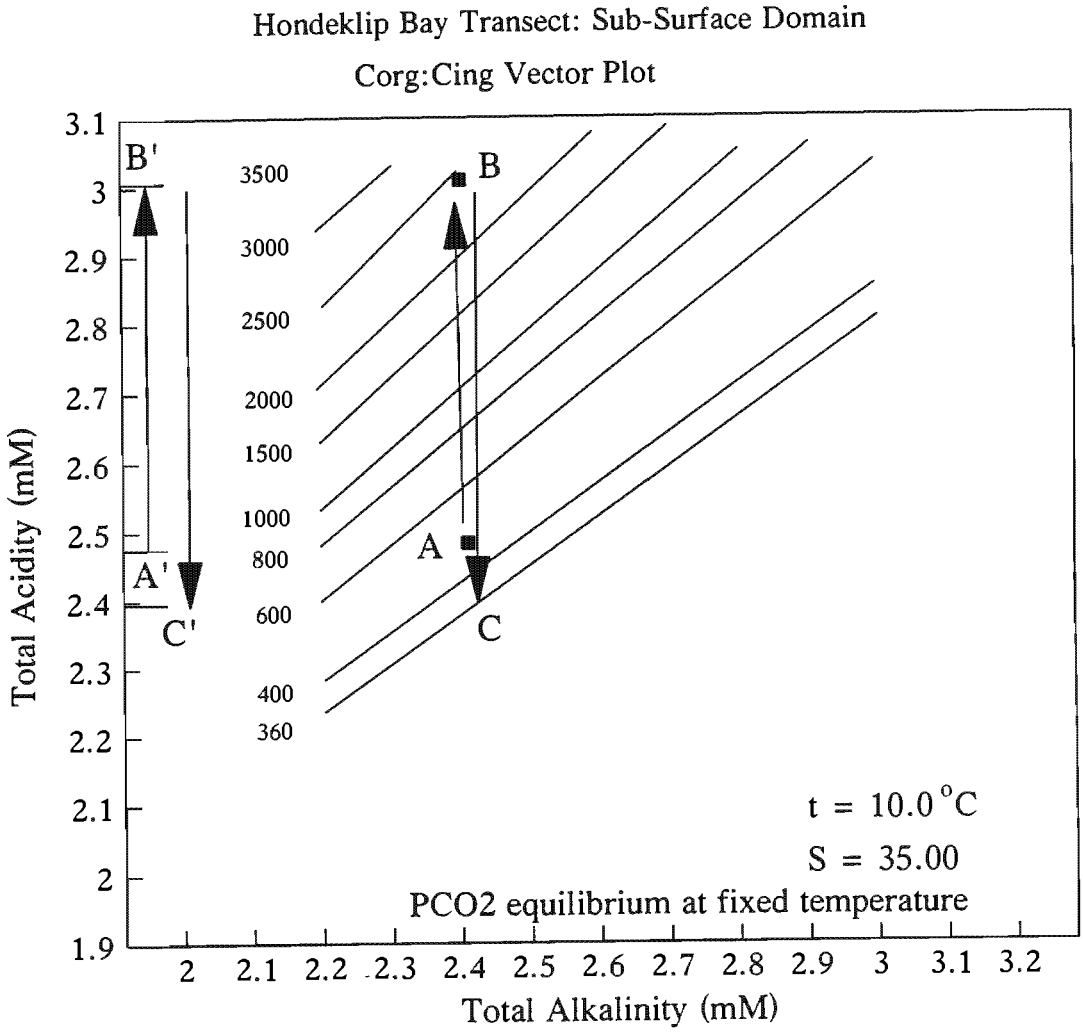

Fig. 5.10: A Total Acidity - Total Alkalinity vector plot showing the magnitude of the changes brought about by the organic (C_{Org}) and inorganic carbon (C_{Ing}) remineralization in the central sector. The characteristic values for the end - members (CS-SACW (A) and CS-ISW(B)) were obtained from Table 5.2. Also plotted are the PCO_2 lines computed for a temperature of 10°C which is typical of SACW in the central sector. The plot confirms that carbon remineralization fluxes are almost completely governed by oxidation of organic carbon (C_{Org} pathway). (see text for further details).

which in the central sector increase by 2513μatm compared to 617 μatm in the northern Sector. The C_{Org} : C_{Ing} stoichiometry is large (-56) (negative sign due to the apparent decrease in TAlk) quantitatively confirming the minimal role of CO_3^{2-} input through dissolution of biogenic $CaCO_3$ along the inshore belt.

The magnitude and stoichiometry of NTAcy and NTAlk additions are graphically depicted on Fig. 5.10. The plotted positions of the capacity parameters are superimposed on a family of PCO_2 lines calculated for a temperature of 10°C and salinity 35psu which characterised waters upwelling at the Namaqua upwelling cell. The CO_2 addition into CS-ISW arising from the benthic flux is given by the NTAcy/2 vector component. The lack of any CO_3^{2-} addition which would have decreased the vector slope means that the CO_2 addition maximizes its impact on PCO_2.

The ΔTAcy between the upper value of the ISW (B) and the atmospheric PCO_2 equilibrium line (C) provides the potential magnitude of the CO_2 degassing process in an abiotic "Strangelove Ocean". The numerical value is given by the vector component (B'C') (ΔNTAcy = 617μM; ΔCO_2 = 309μM). As before, this degassing scenario is ameliorated by the mediation of surface productivity.

5.3.3 Southern Sector (SS): Olifants River Transect

Carbon Remineralization Flux and Stoichiometry

The overall C_{Org}:C_{Ing} stoichiometry for the data collected along the Olifants River transect is depicted on Fig. 5.11 where the NTAcy and NTAlk values are plotted together. As was the case for the previous two data sets from the

northern and central Benguela sectors it indicates that carbonate biogeochemistry and fluxes within this sector is wholly driven by CO_2 input - output and, in contrast, CO_3^{2-} plays a minimal role. The slope of the functional regression (17.22) confirms the visual interpretation.

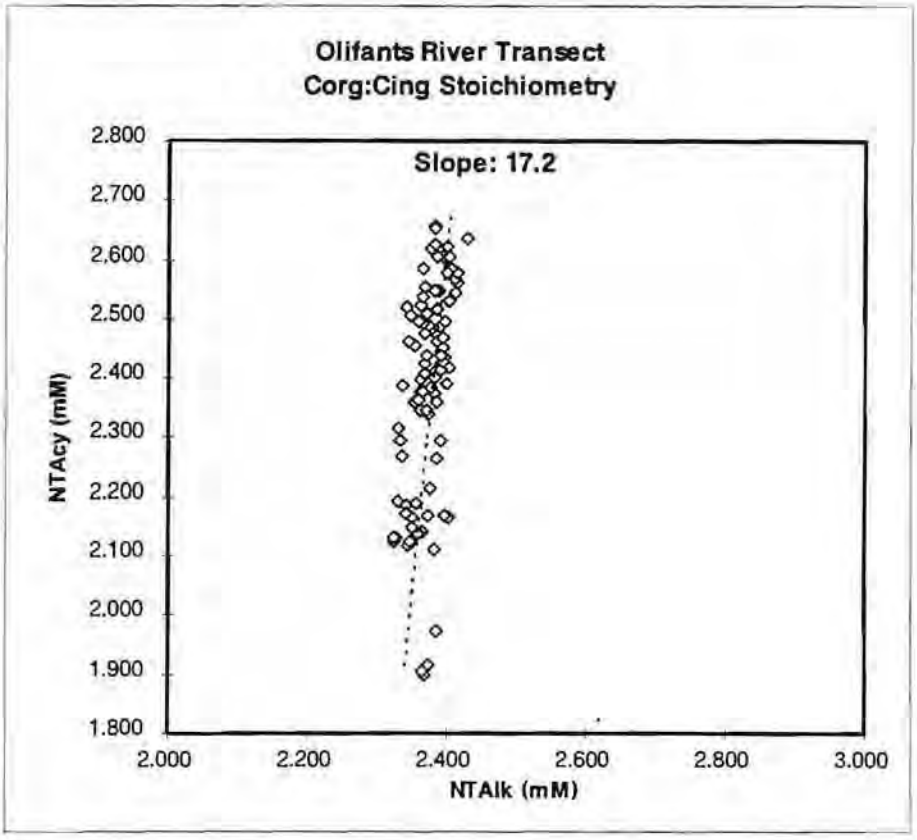

Fig. 5.11: A plot of all individual Total Acidity and Total Alkalinity data from the Olifants River transect. It shows that similarly to the northern and central sectors, changes in the chemical state of the carbonate system are largely driven by the organic carbon mechanisms ($C_{Org} : C_{Ing}$ ~ 17) with the inorganic carbon uptake and dissolution making a minor impact. There are no significant cross-shelf differences. (see text for further details)

This is the smallest average slope in all three sectors (cf: 237 in the northern sector; 52.21 in the central sector). It indicates that the data in the southern Benguela sector are consistent with a small but measurable level of $CaCO_3$ uptake - remineralization. The distribution of data points shows that the magnitude of the CO_2 input is the lowest of all three sectors. The highest value is 2640μM compared to 2710 and 3400μM for the Henties Bay and Hondeklip Bay transects respectively. In contrast, this data set also produced

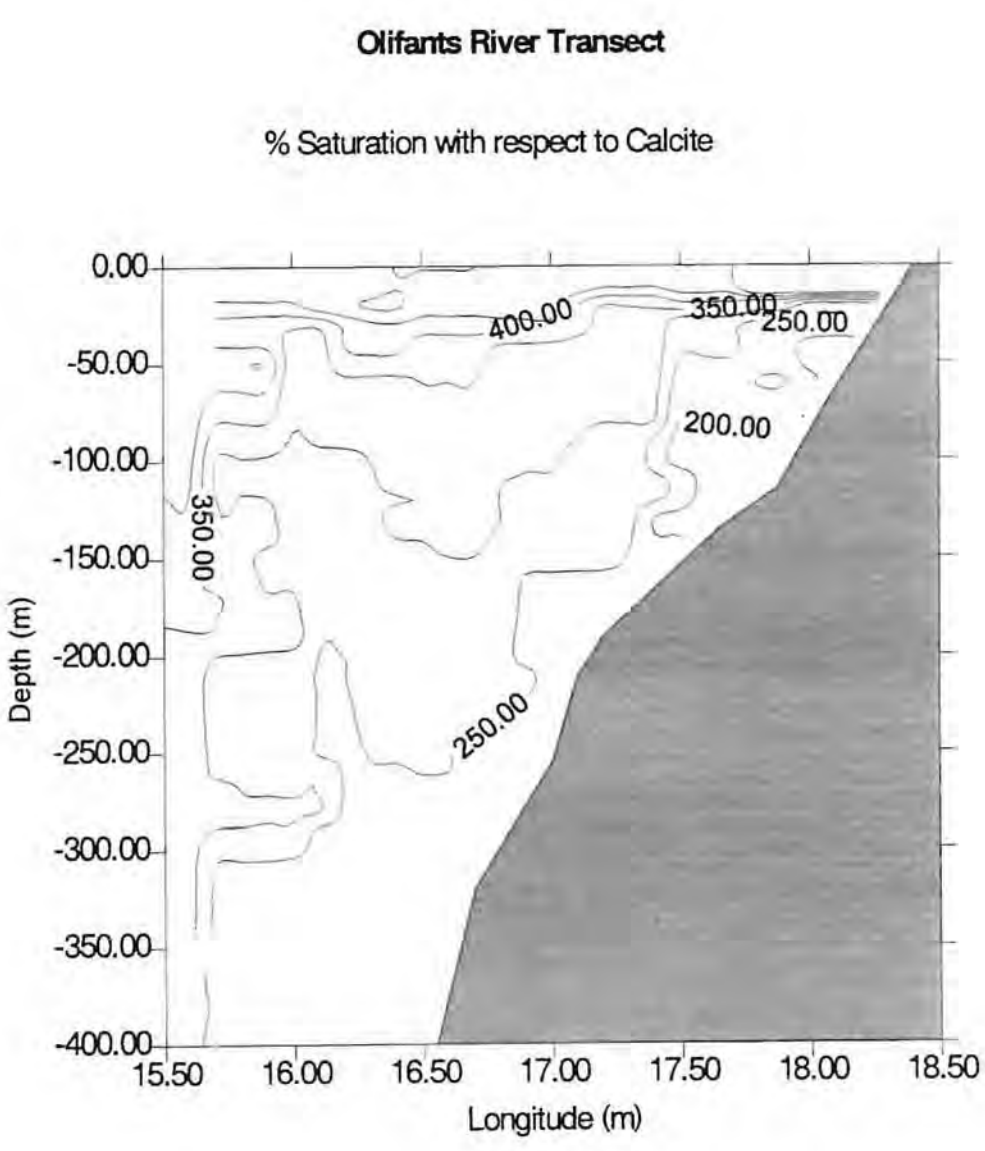

Fig. 5.12: A cross-shelf section from the Olifants River transect showing the degree of saturation (%) with respect to calcite. It shows that the whole water column was supersaturated.

the lowest NTAcy values of all 3 sectors. The mean NTAlk is 2.374±0.023 whose range is similar to that in the central sector. The minimal impact of the C_{lng} pathway in this sector is supported by the CO_3^{2-} super saturation levels which characterised the whole transect (Fig. 5.12) which shows that the water column is never undersaturated with respect to calcite. The lowest levels of super saturation are found closely associated with the BBL in the inshore area which is also where sediment organic matter is concentrated and hence where CO_2 remineralization is highest. As with the northern and central sectors CO_3^{2-} saturation with respect to calcite is driven by CO_2 input and its impact on pH which shifts the carbonate species equilibria.

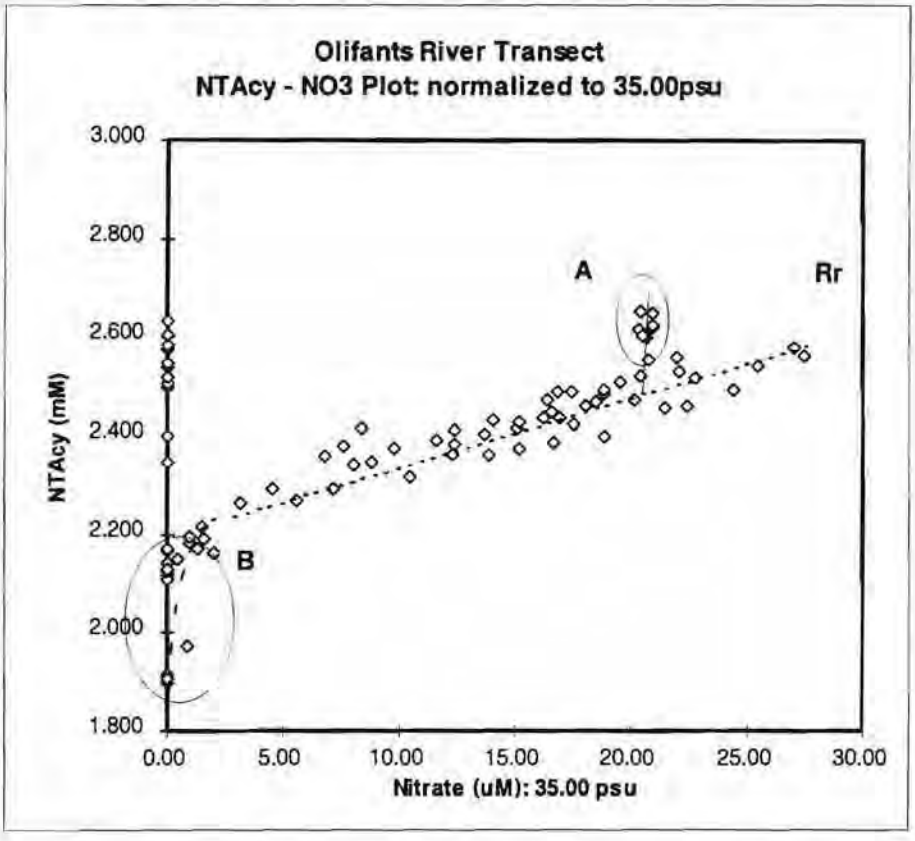

Fig. 5.13: A plot of Total Acidity and NO_3^- concentrations, normalized to 35 psu, from the Hondeklip Bay transect. It shows the extent to which C:N uptake and remineralization dynamics deviate from the Redfield ratio given by the dashed line. Most of the data points do follow the Redfield ratio except those grouped into areas A and B. The samples in group A represent those from the inner shelf where the input of CO_2 from the benthic remineralization flux was not accompanied by a stoichiometric amount of NO_3^-. Similarly, group B are surface samples where CO_2 was taken up without a stoichiometric NO_3^- component. This implies that NO_3^- remineralization and re-use, possibly as NH_4^+ was a dominant mechanism in the surface post upwelling bloom.

Carbon : Nitrogen Remineralization Flux and Stoichiometry

The plot depicting the stoichiometry between NTAcy and NO_3^- is shown in Fig. 5.13. It shows that, as was the case with the central sector but in contrast with the northern sector, most of the data fall onto a line which models the Redfield Ratio (6.6). This indicates that over most of this sector's water column, where redox levels are normal (aerobic) nitrification is occurring closely correlated to CO_2 production by benthic remineralization. As with the central sector samples this relationship breaks down in the vicinity of the surface and some parts of the benthic boundary. This disequilibrium is characterized by two groups of data (Fig. 5.13). Group A is indicative of a zone (inshore) where remineralized CO_2 is being mixed into the BBL and overlying water column without a concommittant flux of NO_3^-. As was the case earlier, it is suggested that this disequilibrium is driven by the same NH_4^+ adsorption mechanism operating in the organic rich inshore sediments. Here the lower redox conditions suppress the rates of nitrification of remineralized NH_4^+ which retains it in the adsorbed form within the sediment zone. The second group (group B) from the surface domain, is in the low NO_3^- end of the plot. Here, a sharp decrease in TAcy occurs even though NO_3^- is low or zero. This disequilibrium which occurred in the surface layer domain is caused by the uptake of CO_2 occurring where recycled NH_4^+ is the only nitrogen resource. This process will be addressed in detail in the context of the surface layer biogeochemistry (Chapter 6).

Box Model Input Data

The depth averaged box model input data is shown on Table (5.3) which is structured in an identical way to the previous cases. As before, the biogeochemical characteristics of southern Benguela South Atlantic Central Water (SS-SACW) which upwells onto the shelf through the Olifants Canyon (Dingle and Nelson, 1993) were obtained from slope stations where the

samples were located over 400m from the BBL. The low PCO_2 (415 μatm cf. 458 μatm in the central sector) confirms that the core of SACW on the slope is free of any BBL impact.

Southern Benguela Sector: Olifants River Transect

Carbonate Parameter Concentrations
Units: umol/l Normalized to S=35.00psu

Sub-Surface Domain

Water	Station	Depth	NTALK	NTACY	NTCO2	PCO2	NO3
SS-SACW	20/21	150-286	2389	2435	2200	415	18.48
SS-ISW1	12	30.7-62.5	2378	2612	2283	755	19.88
SS-ISW2	13	41.7-81.7	2377	2526	2240	557	18.55
SS-ISW			2378	2569	2262	656	18.73
SS-ISW (NO3 Corr)			2378	2569			
Change			-11	134	62	241	0.25
CO2 addition				67			
CO3 addition			-6				
COrg:CIng Stoichiometry				-12			
NO3 addition							0.25
C:N Stoichiometry							268

Table 5.3: Summary of the average biogeochemical (carbon and nitrogen) characteristics of "new" South Atlantic Central Water prior to it being advected onto the shelf of the southern sector (SS-SACW) and the biogeochemically modified SACW on the inner shelf (SS-ISW) and sampled during the Olifants River transect. The table also shows the net calculated additions of CO_2, CO_3^{2-} and NO_3^- as well as their stoichiometry.

The carbonate parameter concentrations of inner shelf water (SS-ISW) which upwells at the Cape Columbine upwelling cell are defined by the average values from the sub-thermocline water column at the two inshore stations (12 and 13). The overall change in each parameter as well as the CO_2 and CO_3^{2-} additions were calculated in the same way as before. The magnitude of the CO_2 addition (67μM) confirms the earlier observation that in the Southern Benguela the impact of the benthic remineralization flux is the smallest relative to the northern (99μM) and central (264μM) sectors. The calculated CO_3^{2-} addition was again negative by a small amount of 6μM which as was explained earlier is ascribed to a combination of unquantified minor proton

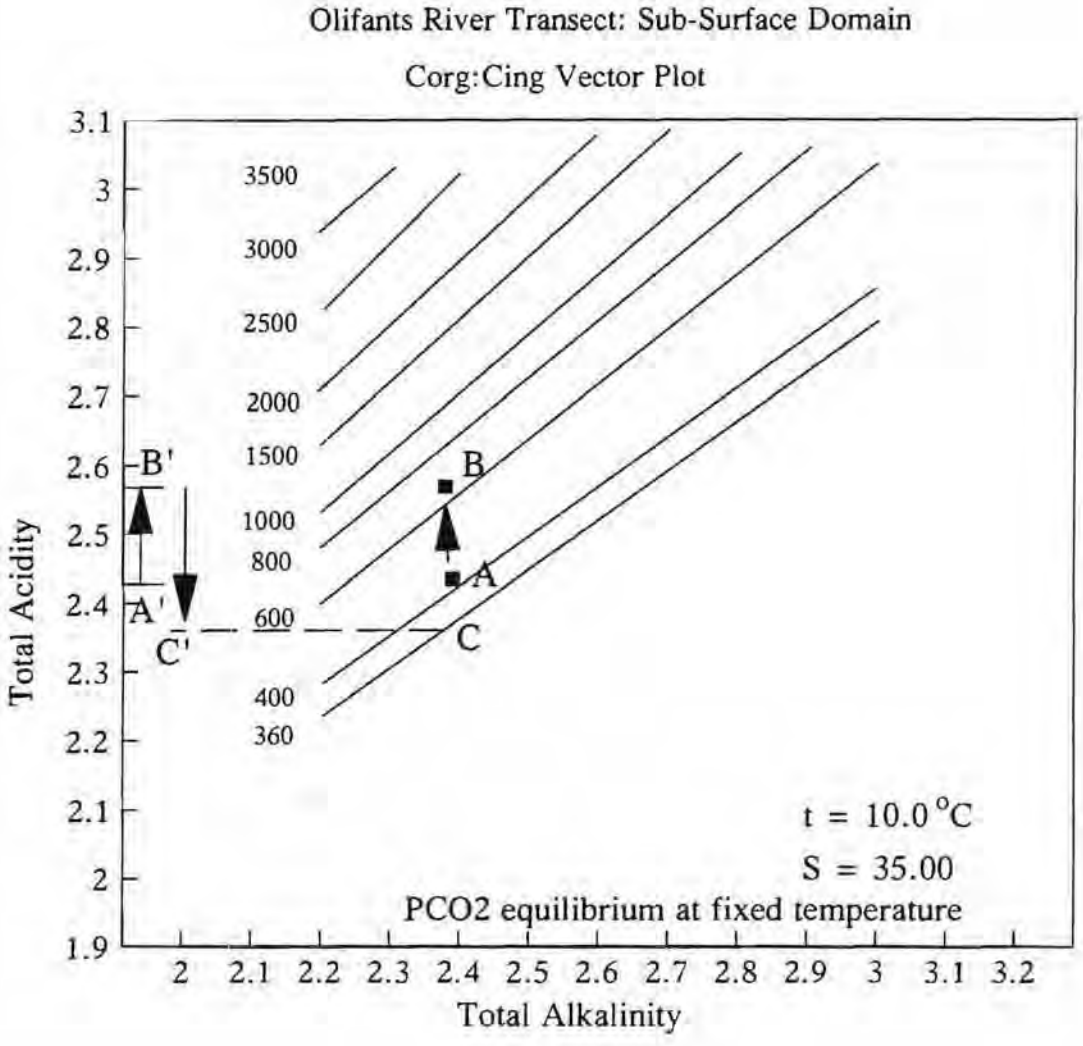

Fig. 5.14: A Total Acidity - Total Alkalinity vector plot showing the magnitude of the changes brought about by the organic (C_{Org}) and inorganic carbon (C_{Ing}) remineralization in the southern sector. The characteristic values for the end - members (CS-SACW (A) and CS-ISW(B)) were obtained from Table 5.3. Also plotted are the PCO_2 lines computed for a temperature of 10°C which is typical of SACW in the central sector. The plot confirms that carbon remineralization fluxes are almost completely governed by oxidation of organic carbon (C_{Org} pathway). (see text for further details). The most notable contrast to other sectors is the much smaller magnitude of the remineralization vector A-B. It suggests that in this sector benthic remineralization is much less important as a modifying factor on SACW.

acceptors and analytical error. This only induces a small 0.25% uncertainty to the final results and can therefore be ignored. The calculated C_{Org} : C_{Ing} stoichiometry, though negative, is consistent with the slope of the regression for the whole data set (Fig.5.11) in that it supports a minimal role for C_{Ing} remineralization. The relationship between the magnitude and stoichiometry of the perturbation of the carbonate capacity parameters in the southern sector and PCO_2 is graphically depicted on Fig. 5.14. As before the PCO_2 lines were calculated at the temperature closest to that which characterises upwelled water (10°C). The plot emphasises the earlier observation that the perturbation driven by the benthic remineralization flux is small. The ΔTAcy between the upper value of the ISW (B) and the atmospheric PCO_2 equilibrium line (C) provides the minimum potential magnitude of the CO_2 degassing process in an abiotic "Strangelove Ocean". The numerical value is given by the vector component (B'C') (ΔNTAcy = 199μM; ΔCO_2 = 100μM. In reality, this degassing scenario is modified by surface warming which increases it and simultaneously reduced by surface productivity. Given the small magnitude of the degassing potential, these data point to this sector as being the one where surface productivity has the greatest potential of inducing a CO_2 flux from the atmosphere into the surface layer. That is, ISW is being upwelled with relatively high NO_3^- concentrations and relatively low PCO_2.

5.4 Further Discussion

Three features characterise the carbon and nitrogen remineralization fluxes in the sub-thermocline Benguela System:

- Importance of benthic rather than water column remineralization fluxes.
- The dominance of C_{Org} remineralization and the negligible role of C_{Ing} pathway of $CaCO_3$ dissolution.

- The strong C:N disequilibrium of the benthic remineralization flux which is >> Redfield ratio.

These characteristics combine to varying extents in each of the three sectors to provide the biogeochemical characteristics (CO_2 and NO_3^-) of newly upwelled waters at each of the individual upwelling cells. The net effect is that they not only govern the PCO_2 of waters which outcrop at the upwelling cells but also the extent to which surface production is able create a CO_2 drawdown. This ultimately determines the rate and direction of the synoptic - seasonal - interannual CO_2 flux across the air - sea boundary. The ensuing discussion provides a detailed descriptive view of each of the most important remineralization mechanisms driving biogeochemical change. The coherence of proposed mechanisms is tested through its consistency with the data sets. These mechanisms form the conceptual framework to the numerical box model which is used to constrain the source - sink character of the Benguela System (Chapter 7).

The mechanisms are addressed in two broad categories:

- those which govern the C_{Org} :C_{Ing} remineralization stoichiometry
- those which govern the C_{Org} :N (NO_3^-) stoichiometry

5.4.1 Remineralization of Organic Carbon

In keeping with its focus on marine resources, past and present interest on sub-surface remineralization in the Benguela System has concentrated largely on two main areas:

- the spatial and temporal incidence of hypoxic waters which impact on the distribution and mortality of living resources (Newman and Pollock, 1974).

- preformed nutrient (NO_3^-) enhancement of upwelled waters on the shelf which increases the potential for surface production (Bailey. 1987 ; Bailey, 1990).

In both cases the sampling has largely focused on oceanographic conditions which led to those biogeochemical changes to develop as well as their advection. Explicit *in situ* rate measurements of electron acceptor uptake have been limited to SO_4^{2-} at a few sites in the southern and central sectors (Bailey, pers.com.). These type of measurement are important in respect of constraining the magnitudes and variability of individual metabolic pathways. However, they are thought to underestimate total CO_2 metabolism because in most instances two or more electron acceptor oxidation pathways occur simultaneously (Middelburg *et al.,* 1993). This become particularly relevant when addressing the difficult question of whether overall oxidation rates of organic matter differ significantly between aerobic and anaerobic environments (Middelburg *et al.,* 1993). This issue is pertinent in shelf systems such as the Benguela where rates are high and both types of redox environment co-exist spatially or temporally.

This issue also links up to one of the ongoing debates of the organic biogeochemical field (Middelburg *et al.,* 1993) : are enhanced burial rates (accumulation) linked to differential kinetics of aerobic or anaerobic oxidation or simply to high particle fluxes from the overlying productive surface layer . The first view has been criticised on the basis that most anaerobic respiration is measured by the loss of the SO_4^{2-} electron acceptor (Middelburg *et al.,* 1993). Exclusion of the potentially more important methanogenesis could underestimate the overall benthic remineralization rates. *In situ* measurements of total respiration have not been able to find any significant differences in the kinetic rates of the two oxidative remineralization pathways . In contrast, it has been observed that the remineralization rate constant is proportional to the square of the accumulation rate .

Past work in the Benguela System has shown that benthic remineralization of detrital organic matter plays an important role in altering the characteristics of upwelled waters (Bailey. 1987). This results in the observed benthic - pelagic coupling feedback mechanism . This suggests that benthic areas with the highest rates of input of pelagic organic material are also where highest rates of oxygen consumption and nitrogen remineralization are found (Middelburg *et al.,* 1993).

The water column transects (see Chapter 4) which were sampled in this study strongly support the hypothesis that the flux of remineralized CO_2 is driven by the input flux of detrital material rather than any kinetic rate differences between aerobic and anaerobic systems. All transects show the same consistent characteristics (Figs. 4.7, 4.13 and 4.20):

- enhanced concentrations of TCO_2 and PCO_2 within the BBL which supports the hypothesis that remineralization is primarily occurring in the benthic environment and,
- where increased concentrations occur as a result of benthic remineralization they are located without exception over sediments with highest organic carbon content. The spatial location of the organic rich sediments are indicated in the PCO_2 section from the Henties Bay transect (Fig. 4.7).

The Henties Bay transect showed the lowest oxygen concentrations in the BBL (O_2 < 50 μM some of the values < 20 μM) compared to both Hondeklip Bay and Olifants transects (O_2 50-100μM in the BBL) (Figs. 4.7, 4.13 and 4.20). In contrast, the largest input of CO_2 into the BBL through benthic remineralization was recorded in the inshore station of the Hondeklip Bay transect (PCO_2 2500-3000 μatm ; single bottom values as high as 6500 μatm). The Henties Bay transect PCO_2 gradient into the BBL was in the same order of magnitude (PCO_2 1200-1500 μatm) with the values in the Olifants River transect being the lowest (PCO_2 ~ 800 μatm). The area with

the lowest redox status (O_2 < 20μM in the northern sector) did not correspond to the expected highest PCO_2 values. These results suggest that the relationship between the remineralized CO_2 flux into the BBL was not correlated to the redox status of the system and furthermore it appeared to have been insensitive to the organic content of the sediment. The exclusion of these two factors leaves the input detrital particle flux rate as the untested but most likely factor which governs the remineralization rate of CO_2.

One possible hypothesis is that remineralization rate is driven by the input rate of fresh planktonic detritus high in protein, carbohydrates and lipids rather than condensed humic materials . Such a hypothesis would account for why the remineralization rates do not appear to correlate to the organic content of sediments. A system where detrital organic matter is rapidly condensed into more heterotrophic resistant "humic material" would simultaneously increase burial rates and decrease remineralization rates. This process would be assisted by accelerated sedimentation rates driven by aggregate formation around fast sinking aeolian lithogenic particles (Ittekkot, 1993). This would still be consistent with the view that enhanced CO_2 production is linked to areas of high productivity where the period of sedimentation is short and decoupled from factors such as sediment organic content and redox environments.

This conclusion, which needs to be tested in a direct way, emphasises the importance of benthic remineralization as the process which not only determines CO_2 content of upwelled waters in the Benguela System but in doing so also controls the redox status. High burial rates of POC along the Benguela inner shelf, reflected by high sediment POC, are not the result of low redox conditions but rather the two factors are concomitantly the result of high input flux rates. This indicates that sedimentation rates and mechanisms are a critical sampling component to any future carbon flux study in the Benguela System. Interestingly, this is also the most neglected type of sampling in the past 20 years of intensive work in the system.

5.4.2 Remineralization of Calcium Carbonate:

The C_{Org} :C_{Ing} stoichiometric relationships for all three transects suggest that the remineralization of $CaCO_3$ through dissolution was an insignificant factor in the overall carbon flux in the Benguela System shelf (Figs. 5.1, 5.7 and 5.11). The main reason for this was provided by the transect data which showed that super saturation in respect of calcite was a consistent feature of the water column in all three transects (Fig. 5.2, 5.8 and 5.12). The only exception was the most inshore station (113) of the Hondeklip Bay transect where the very high remineralization rates of CO_2 lowered the pH sufficiently to decrease the CO_3^{2-} concentration to below saturation. This exception is probably not significant enough to alter the prediction that in the Benguela System $CaCO_3$ is accumulating in the sediments at rates close to its surface production in the form of coccolithophores (Giraudeau *et al.*, 1993; Giraudeau and Bailey, 1995) and sub-surface production of both pelagic and benthic foraminifera .

This is strongly supported by the $CaCO_3$ distribution in the sediments of the Benguela System (Rogers and Bremner, 1991). $CaCO_3$ makes up the largest reservoir of carbon in the sediments but unfortunately because of the methodological exclusion of the < 63μ fraction (Giraudeau, pers.com.) it was not possible to separate the relative contributions of coccolithophores and foraminifera. It is particularly the contribution of the former which is of interest because their role in the carbon fluxes within the Benguela System are so poorly understood. The only qualitative description of the distribution of coccolithophores in the sediments of the Benguela System was provided by Giraudeau, 1992. In this study, which excluded the > 63μ fraction and hence any comparison with abundance of foraminifera, it was shown that coccolith

abundance increased with depth. It is estimated that coccoliths contribute ca. 50% of total carbonates in the outer shelf (Giraudeau, pers.com.).

Based on the results from this study and the carbon characteristics of the long term reservoir in the sediments it is suggested that the $C_{Org} : C_{Ing}$ stoichiometry of remineralization in the Benguela System is large (> 20) reflecting a small (< 5%) contribution from $CaCO_3$ dissolution.

5.4.3 C:N Remineralization Stoichiometry and Pathways

Ammonium NH_4^+ is the final metabolic product from the oxidative remineralization of organic nitrogen by heterotrophic activity in both aerobic and anaerobic environments (Fenchel and Blackburn, 1979). In sediments where surface derived organic matter accumulates rapidly, such as in shelf systems, the remineralization of organic nitrogen can lead to high concentrations of NH_4^+ and CO_2. The remineralized components are expected to be released into the overlying BBL in a similar stoichiometric ratio as the source biogenic material. However, one of the most unexpected biogeochemical results from the sub-surface water column data in the Benguela System was the strong C:N disequilibrium in the remineralization flux of CO_2 and NO_3^- (Tables 5.1, 5.2 and 5.3). This disequilibrium or de-coupling in the stoichiometry of the remineralization of carbon and nitrogen, where the nitrogen flux is stoichiometrically small, is characterized by a C:N ratio much larger than that which is predicted by the Redfield ratio. The average values obtained from the depth averaged data summarized in Tables 5.1 to 5.3. These show that the disequilibrium was largest in the data from the northern sector (C:N -820) where the NO_3^- addition was infact negative, followed by the southern (C:N = 268) and the central sectors (C:N = 41). These stoichiometric values are both very high and variable. In a system as dynamic as the Benguela it is expected that the magnitudes will vary widely in space and time but on the basis of these results it is predicted that the

observations from cross-shelf water column sections depicted earlier (see Results and Discussion). In the intermediate zone the BBL is much shallower reflecting lower turbulent mixing energy. For the purposes of this conceptual model there is no spatial bias in respect of the input flux (F_{SED}) of sedimenting biogenic and lithogenic particles.

Under the elevated turbulence conditions predicted for the shelf break zones, fine particles of biogenic and lithogenic origin get resuspended and transported both shorewards and polewards driven by the two main advective forcing factors. In the process, particles can either be transported longshore and off the shelf at the "gate" exit sites or cross-shelf into the less turbulent zones (Fig. 4.26). In the latter case, particles may get re-deposited in the calmer intermediate zones where they accumulate. The combined effect of these mechanisms is predicted to give rise to alternating long shore bands of sediments either high or low in organic carbon and / or finest lithogenic particles such as clays and silt.

The predictions of this model are borne out by both sedimentological and water column biogeochemical parameters. A map depicting the distribution of % particulate organic matter (POM) (in this case POC = POM / 1.8) in the sediments of the Namibian shelf (Bremner, 1983) shows the predicted long shore bands very clearly (Fig. 4.27) . The longitudinal zones with the lower % POM coincide with the two shelf break zones (140 and 400m) which characterize that sector of the Benguela System (see Fig. 4.27). The biogenic carbon deposited on the sediments from the overlying high surface productivity is being continuously eroded from the shelf break zones and accumulating in the intermediate zones. These sediments have the two characteristics which are predicted by the BBL turbulence model: the alternating bands and the longshore spread. Two other aspects of this part of the system add to the internal consistency of this model:

- it was predicted that enhanced BBL turbulence at the shelf breaks would erode biogenic particles to an extent which would decrease the benthic

remineralization flux associated with them. This is confirmed by the section (Fig.4.7b). It shows the elevated values of PCO_2 arising from the benthic remineralization flux into the BBL across the Namibian shelf to be located where organic rich sediment accumulate and not where turbulence driven erosion occurs at the shelf breaks.

- a plot of the meridional boundaries of the organic rich Namibian sediments shows that the northern limit is Cape Frio and the southern limit is to the north of Luderitz as predicted by the "gate" hypothesis. It is suggested that the organic rich sediments are being transported offshore to the north of the Luderitz "gate" rather than polewards into the central Benguela Sub-System.

Similarly, in the southern Benguela (Birch, 1975) a sediment map depicting the distribution of physical characteristics (Fig. 4.28) shows that the shelf area immediately above the shelf break at 400 m has been so completely eroded that only bare rock remains. The intermediate zones, including the slope, by contrast, are covered with acoustically transparent sediments ie: fine ooze. Besides confirming the presence and effects of enhanced shelf break turbulence, this case also indicates that the degree of turbulence in the southern Benguela System is higher than that in Namibia.

Perhaps one of the most significant predictions of the combined role of BBL turbulence and poleward advection is that both dissolved and re-suspended particulate carbon are being transported polewards. Thus, in northern Benguela System the shelf sediments high in organic and inorganic carbon are suggested to originate from the downstream effects of Cape Frio and Walvis Bay productivity and to a lesser extent the equatorward overflow of surface production from the Luderitz upwelling cell (Bailey, 1990). The second prediction is that because of the combined effects of resuspension and a southern boundary outflow, extensive carbon deposition should be observed on the slope at the latitudes of the "gates".

stoichiometry will be always much larger than the Redfield ratio. This non - Redfield benthic remineralization stoichiometry has significant implications for the CO_2 source - sink character of the Benguela System. The CO_2 drawdown potential of newly upwelled waters is primarily governed by the NO_3^- flux which, coupled to the Redfield ratio of C:N (~6.6) which characterizes phytoplankton uptake, determines the theoretical maximum carbon export flux (Eppley and Peterson, 1979). Any disequilibrium in the benthic flux of remineralized CO_2 and NO_3^- / NH_4^+ where the stoichiometry is greater than the Redfield ratio will reduce the potential of the surface productivity to create a CO_2 deficit and generate a CO_2 drawdown flux.

There are three possible explanations for the observations:

- A substantial proportion of the DIN pool comprises remineralized NH_4^+ which has not been oxidized (nitrification) to NO_3^-. That is, calculating the C:N ratio on the basis of NO_3^- alone may underestimate the DIN component.
- Denitrification of NO_3^- in the low redox environment of the BBL causes loss of most of the NH_4^+ which is nitrified.
- Adsorption of remineralized NH_4^+ onto lithogenic and biogenic particles in the sediment and BBL "chokes" the NH_4^+ flux out of the sediments.

The **first explanation** is based on a simple view that if the bulk of the remineralization is in the form of NH_4^+, a stoichiometry based solely on NO_3^- will produce an apparently large C:N disequilibrium. Data obtained simultaneously from the transects in the Central and Southern sectors (unpublished data; SFRI archives) showed that the NH_4^+ concentrations, even within the BBL, never rose above 2μM and were mostly below 1μM. No NH_4^+ samples were taken on the Henties Bay transect but an extensive historical data set covering 59 stations along the length of the northern sector shelf (SNECA, 1985, 1986) provides a similar outlook: NH_4^+ is a very minor component (< 5%) of the DIN pool in upwelling waters even in the BBL over the organic rich diatomaceous ooze. The NH_4^+ remineralization flux is not

translating into a sufficiently large increase in the DIN concentration of the BBL so as to maintain the stoichiometric integrity of the benthic C and N flux. On this basis the first option is discounted as a significant factor.

With the **second explanation**, the NH_4^+ released from the sediments either through a diffusive flux or resuspension, is nitrified (Fenchel and Blackburn, 1979) and subsequently in the context of the low redox conditions prevalent particularly on the Namibian shelf, it is lost as N_2 through kinetically controlled dissimilative nitrate reduction or denitrification (Fenchel and Blackburn, 1979). Denitrification is a well known phenomenon, particularly in the northern sector where low redox conditions characterise the water column below the thermocline and preformed NO_3^- concentrations can be reduced by up to 50% (Chapman and Shannon, 1985). This was apparent in the NO_3^- section from the Henties Bay transect (see Fig. 4.8 b) which showed a decrease in the NO_3^- concentration close to the BBL to < 15μM. While it is understandable that NO_3^- advected onto the shelf as SACW might be denitrified in the low redox conditions of the northern sector shelf, it is less obvious how the same could happen to NH_4^+ generated by the benthic remineralization flux. Denitrification of the remineralized NH_4^+ requires an intermediate oxidation or nitrification step whose redox and temperature requirements are not consistent with the BBL environment in the northern sector (Fenchel and Blackburn, 1979). In contrast, for the Central and Southern sectors where O_2 concentrations are higher (O_2 > 50(M), increases in nitrate concentrations are normally observed between virgin SACW and newly upwelled water (Bailey and Chapman, 1987). This is consistent with nitrification being a dominant mechanism through which remineralized NH_4^+ is oxidized to NO_3^- to modify the pre-formed characteristics of upwelled waters. This increase in NO_3^- is also well documented especially in the Southern Benguela where NO_3^- 15-18μM in SACW can, especially along the inshore belt, increase to 20-25μM in newly upwelled waters (Bailey, 1979). In this study, the same was observed in the central sector where NO_3^- increased from ~14 to ~ 20μM (Table 5.2). In these more consistently aerobic conditions, the denitrification

step is suppressed (Fenchel and Blackburn, 1979). While the second option cannot be completely discounted it is thought that the key mechanism is provided by a third.

The third option, adsorption, arises because of the weaknesses in the biochemical mechanisms to account for the total remineralized NH_4^+ budget. While NH_4^+ adsorption in sediments is a well described process (Mackin and Aller, 1984) its role in modulating nitrogen fluxes, particularly in upwelling systems has been underestimated. The question is asked, to what extent is the C:N disequilibrium of the benthic remineralization flux driven by de-nitrification and or sediment particle adsorption ?

5.4.4 NH_4^+ Adsorption Model

Nitrogen is remineralized as NH_4^+ which has a strong electrophilic affinity for negatively charged sites of organic functional groups and clay minerals. At the pH of natural sea water most organic functional sites are ionized by the loss of the associated protons. That is in most cases the pK is < pH. This has led to the observation that in the presence of organic matter most particulates in the sea are negatively changed as a result of a ubiquitous coating of organic matter. This increases the availability of sites for positively charged ions such as NH_4^+ to adsorb on to and develop a Langmuir type of inter phase equilibria (Mackin and Aller, 1984). Such an equilibrium relationship was clearly reflected in the core profiles (Fig. 5.4) and the regression linking the adsorbed and pore water NH_4^+ concentrations from the organic rich inshore mud belt on the Namibian shelf (Fig. 5.5). The slope of the regression which reflects an adsorption coefficient (ml/g), is not only among the largest in the literature (Mackin and Aller, 1984) but the magnitudes of adsorbed and pore water NH_4^+ concentrations are the highest recorded for a benthic system away from anthropogenic inputs.

The fact that under these conditions of high NH_4^+ concentrations in both solid and aqueous phases of sediments little or no NH_4^+ increase is observed in the BBL can be attributed to:

Dissolved NH_4^+ flux out of the sediments due to resuspension being rapidly scavenged by the sedimenting or re-suspended particle flux and re-deposited onto the sediment or transported as bed-load.

Most of the NH_4^+ remineralization occurs in organic rich sediments where surface derived flux of planktonic detritus is large. This flux adsorbs most of the upward NH_4^+ flux and in doing so provides a "pump" by which nitrogen is retained in a relatively small closed cycle between the sediments and the BBL. This mechanism is suggested to be the main throttle of the N remineralization flux and hence the primary cause for the disequilibrium of the C:N remineralization flux. This mechanism predicts that C:N ratios of sediment POM should be < Redfield ratio. The fact that this is not always observed is suggested to be due to *inter alia* two problems:

- the methodological one of both acification and washing resulting in the leaching of most of the labile fraction of both NH_4^+ and amino acids.
- the transport of the particulates across and off the shelf.

The de-coupling of the carbon and nitrogen remineralization cycles in the benthic environment is conceptually depicted in Fig.(5.15) with a view to explaining the observations presented above. Organic carbon and nitrogen are deposited onto the sediments in the form of a detrital pelagic flux (1). Benthic oxidative - remineralization (aerobic or anaerobic) produces CO_2 and NH_4^+ as its metabolite products (2). Whereas CO_2 equilibrates with the concentrations in the overlying BBL, NH_4^+ follows an adsorption equilibrium pathway which modulates its free form concentration in pore waters (3). The pore water NH_4^+ lost from the sediments through turbulent diffusion follows one of two pathways depending on the redox condition in the BBL: it can be nitrified to NO_3^- and add to the existing NO_3^- in the water (4a) or alternatively,

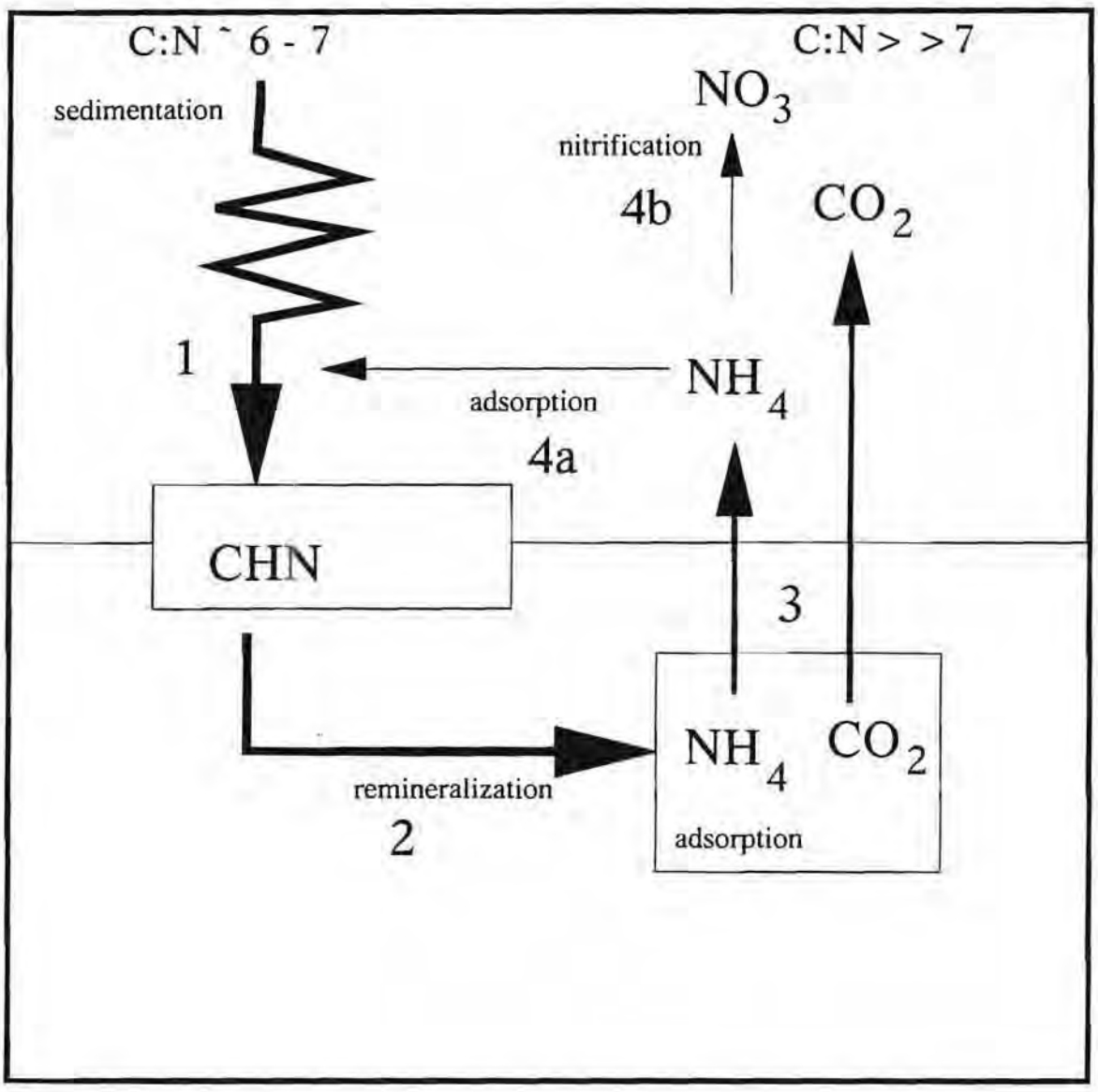

Fig. 5.15: Depicts a simplified conceptual model of the key steps in the benthic NH_4^+ adsorption mechanism. The biogenic sedimentation flux settles on the sediment with a C:N ratio which is still close to the original phytoplankton (1). Benthic oxidative remineralization (2) metabolizes the organic matter to its terminal CO_2 and NH_4^+ components. The elevated concentrations of both CO_2 and NH_4^+ in the interstitial water drives a benthic flux (3). However, NH_4^+ adsorbs onto both biogenic and lithogenic particles which results in the decoupling of their remineralization stoichiometry. The resulting benthic flux has a stoichiometry >> 6 -7 which characterized the input material. The NH_4^+ which is released into the benthic boundary layer can either be re-adsorbed onto the sedimentation flux or nitrified to NO_3^- and upwelled.

it can be adsorbed by the sedimenting pelagic detrital flux and returned to the sediment (4b). It is predicted that shelf areas where the sedimenting particulate flux is large (Namibian inner shelf) the combination of low redox conditions and flux of fresh particulates will drive the benthic nitrogen cycle mainly along pathway 4b. Where the sedimenting particle flux is lower and the system is more persistently aerobic (Southern and Central sectors) the N cycle will be a combination of 4a and 4b. It is further predicted that sediments mainly driven by 4b should have a lower C:N ratio than those driven by 4a and 4b.

This NH_4^+ adsorption mechanism coupled to the advectively driven offshore transport of biogenic particles postulated in Chapter 4, provides an intriguing possible mechanism for the supply of both carbon and nitrogen to deep sea food chain on the slope. The addition of the nitrogen component lends further support to the notion that the exit sites to the north of the "gates" should be prime areas where the deep sea food chain obtains its input from surface inshore production.

Chapter 6

6. Shelf Scale Biogeochemical Processes II: Surface Layer Uptake and Export

6.1 Background

After benthic remineralization which provides the pre-formed PCO_2 and NO_3^- characteristics of shelf waters which outcrop at upwelling centres in the Benguela System, surface productivity is the next major mediator of carbon and nitrogen biogeochemistry within the upwelling cycle. It drives changes to the PCO_2 of upwelled waters which in turn, and depending on whether PCO_2 drops to below or above atmospheric equilibrium, determines the magnitude and direction of CO_2 fluxes across the air -sea boundary.

The short and long term CO_2 flux between upwelled waters and the atmosphere depends largely on 4 main biogeochemical factors:

- the PCO_2 of upwelled waters which outcrop at the surface.
- the rate at which surface based NO_3^- driven new primary production reduces PCO_2 through photosynthesis.
- the surface warming rate which reduces CO_2 solubility and increases PCO_2.
- efficiency with which particulate organic carbon (POC), particulate inorganic carbon (PIC) and dissolved organic carbon (POC) are exported into deep or benthic environments.

While the first factor has been addressed (see Chapter 5), the second and third factors are the subject of this part of the study. The fourth factor, which requires direct measurement of the carbon export flux (sediment traps and DOC gradients) is the only one for which practically no data exists in the Benguela System. It is addressed with the carbon box modelling part of this

study (Chapter 7) where its predictions in respect of export fluxes are tested against the best alternative proxy variables.

Phytoplankton dynamics are defined by *inter alia* such characteristics as seeding, productivity rates, new versus regenerated production, cell size, biomass, formation of aggregates and nannofossil activity all of which are governed to a large extent by physical turbulence levels (Pitcher *et al.*, 1992; Brink *et al.*, 1995; Hutchings *et al.*, 1995). The interaction of these factors on time scale of hours to seasons drives the activity of the biological pump which then governs the net CO_2 source - sink character of the system. The net biogeochemical expression of how these ecological factors interact is provided by the way in which they alter the bulk chemical properties of newly upwelled waters. These are measured as changes to the concentrations of bulk parameters (CO_2 and NO_3^-) and their stoichiometry (C:N and $C_{Org} : C_{Ing}$). These bulk property changes parametrize the underlying complex ecological and physical interactions in a way which they can be incorporated into biogeochemical models. Two stoichiometric relationships have a particular bearing on PCO_2 change by phytoplankton activity:

- The net time integrated C:N (Redfield) Ratio which governs the "gearing " between C and N.
- The C_{Org}:C_{Ing} stoichiometry which governs the relationship between PCO_2 and TCO_2 change (see Chapter 3).

6.1.1 C:N Stoichiometric Disequilibrium in the Surface Layer

The importance of a C:N disequilibrium in the uptake of CO_2 and NO_3^- in the surface layer lies in both its ecological significance as well as in the fact that it is the only way to offset the C:N disequilibrium induced by the benthic remineralization flux (see Chapter 5). Much of the interpretation and modelling of carbon uptake and remineralization in the ocean in relation to nitrogen (NO_3) is governed by the long standing notion that the two are

stoichiometrically related through the robust Redfield Ratio (C:N) of 6.6 (Redfield *et al.,* 1963). The most widely used expression of the elemental stoichiometry in plankton is:

$$H_3PO_4 + 16HNO_3 + 106CO_2 + 122H_2O = (CH_2O)_{106}(NH_3)_{16}\,H_3PO_4 + 138O_2$$

which represents the approximate elemental ratios in photosynthesis in the forward reaction and aerobic respiration of the same organic matter in the reverse reaction (Redfield *et al.,* 1963). The perceived robustness of this relationship led to the more recent models through which carbon export flux could be related to new production which is in turn governed by the pre-formed NO_3^- supply rate (Eppley and Peterson, 1979). That is:

Carbon Export Flux = New Production = NO_3^- flux * Redfield Ratio

However, recent field work (Sambrotto *et al.,* 1993) and review of historical experimental data (Banse, 1994) has raised questions about the robustness of the Redfield ratio. Non-Redfield stoichiometry in the surface layer domain was addressed by Sambrotto *et al.,* 1993 for both shelf (Bearing Sea, Gerlache Strait) and open ocean (eastern North Atlantic) marine systems. In all cases it was found that the relative uptake of dissolved CO_2 (ΔTCO_2) and nitrogen (NO_3^-) was larger (> 7) than the Redfield ratio. The conclusion was that nitrogen was being recycled to fix additional CO_2 into POC which contributed to a larger POC flux out of the surface layer. The implication of this conclusion was that the use of the Redfield ratio would significantly underestimate new carbon production from NO_3^- and hence the role of phytoplankton as atmospheric CO_2 sinks. While there is little dispute that such C:N disequilibria occur in the bulk concentrations of TCO_2 and NO_3^- (Sambrotto *et al.,* 1993; Banse, 1994), disagreements have arisen as to the mechanism and its consequences (Toggweiler, 1993; Banse, 1994). Sambrotto *et al.* 1993 arrived at their conclusions by interpreting that phytoplankton cell material enriched in nitrogen (protein) (C:N < 4) was

preferentially recycled leaving behind a flux of relatively nitrogen depleted POM (C:N > 8). Such a model leads to the conclusion that the recycling of NO_3^- as NH_4^+ acts as an enhancement to the carbon pump and over time leads to the observed C:N disequilibrium where the temporally integrated uptake ratios of CO_2 and NO_3^- are large C:N > 8. The main counter to this argument incorporates the much neglected and usually not well constrained role of DOC (Toggweiler, 1993). This view is based on the lack of consistent evidence that non - Redfield stoichiometries occur in sinking particles within or below the surface layer (Copin-Montegut and Copin-Montegut, 1983; Altabet and Francois, 1994; Anderson and Sarmiento, 1994). It was suggested that the alternative explanation for the C:N disequilibrium in changes to bulk CO_2 and NO_3^- concentrations was through the production of a nitrogen deficient pool of DOM (Toggweiler, 1993; Williams, 1995). This fraction remains in the surface layer where a labile fraction is heterotrophically oxidised to CO_2 which partly offsets the "benefit" of non Redfield C:N stoichiometry as an additional CO_2 sink (Sondergaard and Middelboe, 1995; Williams, 1995). A review of two mesocosm experiments conducted in 1960 and 1962 (Banse, 1994) where TCO_2 and NO_3^- concentration changes were monitored over a period of days concurs with the Sambrotto *et al.*, 1993 view that the Redfield ratio is not a useful predictor of export carbon production. However, the data and conclusions also appear to lend support the DOC mechanism proposed by Toggweiler, 1993 and supported by Williams, 1995 to account for the apparent C:N disequilibrium in the uptake of TCO_2 and NO_3^-. The importance of this consensus is that it established the basis for the link between observed C:N stoichiometric disequilibrium in the uptake of CO_2 and NO_3^- and DOC production. This relationship forms the basis for modelling of the DOC fluxes in the Benguela System (see Chapter 7) and its mechanistic basis will be developed further below.

In upwelling systems such as the Benguela surface productivity is limited by the nitrogen (NO_3^-) load of newly upwelled waters (Andrews and Hutchings, 1980; Brown and Hutchings, 1987 ; Probyn, 1992). In such instances the

amount of carbon (CO_2) which can fixed through photosynthesis is theoretically limited by the NO_3^- flux.

6.1.2 Carbon Stoichiometry (C_{Org}:C_{Ing})

Based on the importance of $CaCO_3$ as a constituent of shelf sediments in the Benguela System, it could be expected that the system be characterised by elevated coccolithophore activity (Giraudeau, 1992). As a consequence, the C_{Org} : C_{Ing} stoichiometry could be an important factor in the biogeochemical modelling of CO_2 fluxes. The known aspects of coccolithophore activity in the Benguela System were reviewed earlier (Chapter 1) and all indications are that they are not a significant factor in carbon export fluxes from the surface layer.

In this part of the study the stoichiometric relationships from field samples in the Benguela System are investigated using the vector plots developed earlier (see Chapter 3). The value of such a stoichiometric approach is that it not only quantifies the C_{Org} : C_{Ing} relationships both numerically and visually but it also provides the independent magnitudes of the C_{Org} and C_{Ing} components and their relationship with PCO_2 (see Chapter 3).

The objectives of this section are to quantify the magnitude of these stoichiometries in all 3 sectors of the Benguela System, propose plausible mechanisms to account for their existence and to discuss their ecological significance.

6.2 Methods

The results presented below characterise the carbon and nitrogen parameters values of each of the *two end members* in the surface domain of the upwelling cycle at each of the six main upwelling centres in the Benguela

System. In terms of the 4 step upwelling cycle described earlier it deals with changes in step 3 (see Fig. 4.25): that is, the ageing of newly upwelled water. In terms of the box model there are two end members to be characterized:

- *Newly upwelled water (UPW)*: the biogeochemical characteristics of waters which outcrop at upwelling centre X through the flux (F_{UPW}: Fig. 4.25) are sourced from poleward flowing inner shelf waters (ISW) located in the vicinity of the same upwelling centre. Biogeochemical modification was shown earlier to be a function of their poleward advection period over the organic rich sediments which lie predominantly along the inner shelf (see Chapter 5). The characteristics of these waters were defined earlier in the context of sub-surface remineralization.

- *Aged upwelled waters* (AUW): are upwelled waters which have been physically and biogeochemically modified or matured through warming and phytoplankton activity respectively (see Chapter 4). It is in the course of this change that the biggest part of the CO_2 change occurs. Age of waters at this stage of the upwelling cycle can be assessed through either the temperature increase (warming rate of 0.5 - 1 $^{\circ}C$ / day) (Guastella, 1992) or the NO_3^- concentration decrease from its source water value. The latter occurs as a result of the phytoplankton activity which follows an upwelling event (Brown and Hutchings, 1987a). In the Benguela System there exists a good relationship between temperature and NO_3^- concentration which is depicted on Fig. 6.1. Despite the spread of the data ($r^2 = 0.72$) it provides a useful insight into the bulk physical and biogeochemical ageing of upwelled waters:

On average, the phytoplankton bloom which follows an upwelling event uses up the advected NO_3^- at a rate which reduces it to zero by the time the temperature reaches the range of 13-16$^{\circ}C$ (Fig. 6.1). Given that the warming rate is ~0.5 /day (Guastella. 1992) and the temperature of newly upwelled

waters 10°C this constrains the period of the primary bloom to a range of 6 - 12 days.

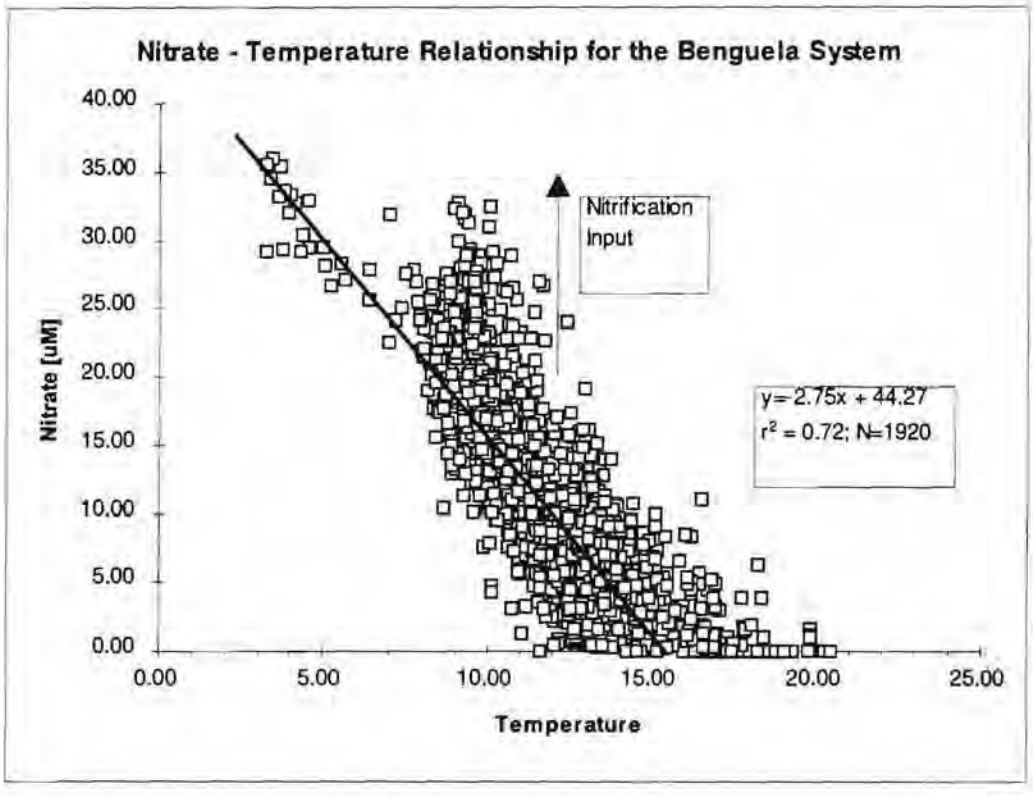

Fig. 6.1: A plot of a historical data set of nitrate concentration (μM) and temperature from the Benguela System obtained from the SADCO data base, Stellenbosch, South Africa. It shows that a good relationship exists between these two variables. It also shows that by the time upwelled waters have aged to a temperature of 13 - 15°C the NO_3^- concentration is zero. The statistical intercept of the temperature axis is 16.1°C .

This is good agreement with the observed bloom cycles of 6 - 10 days (Brown and Hutchings, 1987b) but, for calculation purposes the period of ageing of upwelled waters was taken conservatively to be 14 days. The magnitude of the perturbations at each upwelling centre which drive biogeochemical change in CO_2 and NO_3^- are the focus of these results.

The end member (UPW and AUW) biogeochemical characteristics averaging approach to define the perturbations in upwelling centres is a necessity due to the spatial rather than temporal orientation of the sampling. Each transect (see Chapter 4: Methods) cuts through an upwelling centre and includes

waters at different sub-surface and surface stages of the upwelling cycle. The data depict the temporally integrated (bulk type) biogeochemical change which upwelled water undergo during the main stages of the cycle. This approach is well suited for the box modelling strategy adopted in this study which models scenarios rather than dynamics.

The biogeochemical results below have the following common features:

- The average values which characterize the end members of the upwelling cycle in the surface domain were obtained through the same depth integration approach used earlier in the sub-surface domain.
- All the values are normalized to a salinity of 35 psu
- Changes to the magnitudes of normalized carbonate capacity parameters Total Alkalinity (NTAlk) and Total Acidity (NTAcy) in AUW have been corrected for the impact of NO_3^- removal (see Chapter 3).
- The net CO_2 uptake by surface blooms was obtained by correcting the total CO_2 decrease for the simultaneous loss of CO_2 through degassing to the atmosphere using the Liss - Merlivat approach (Liss and Merlivat, 1986). In all instances the calculation used average *in situ* winds over a 2 week period preceding the sampling and the total flux was also calculated over 14 days.

As was the case earlier in the sub-surface domain examples (Chapter 5) actual field data only exist for 3 of the 6 upwelling centres, one in each sector (Walvis Bay, Namaqua and Cape Columbine). For the remaining 3 (Cape Frio, Luderitz and Cape Peninsula) the model input data is synthesised using the following two rules:

- Cape Frio and Luderitz are at the "gate" sites for the northern and central sectors respectively where no poleward advection over the inner shelf has occurred. The characteristics of newly upwelled water at these two centres are therefore given by those of unmodified SACW. The Cape

Peninsula upwelling cell is located poleward of the gate site of the Southern sector. However, in this sector, especially south of Cape Columbine where sediment organic carbon levels are low (Birch, 1975), benthic remineralization is thought to be reduced and for the purposes of this study the biogeochemical characteristics of newly upwelled water are the same as those for Cape Columbine.

- The extent to which carbon is impacted at the sites for which no data exists is determined by the NO_3^- concentration of the appropriate SACW and the C:N and C_{Org}: C_{Ing} stoichiometries at the sites within the same sector for which data exists. For example, the ΔCO_2 and ΔCO_3^{2-} changes at the Cape Frio upwelling cell will be driven by the NO_3^- concentrations, C:N and C_{Org} : C_{Ing} stoichiometries of the Walvis Bay cell.

6.3 Results and Discussion

6.3.1 Walvis Bay Upwelling Cell (Northern Benguela)

Carbon Fluxes and C_{Org} : C_{Ing} Stoichiometry

The biogeochemical parameter changes which were measured between upwelling source water for the Walvis Bay upwelling cell WB-ISW and aged upwelled water (WB-AUW) sampled along the inner section (stations 16 and 27) of the Henties Bay transect are shown in Table (6.1). These values include the NO_3^- which is required for the corrections to NTAlk and NTAcy as well as to calculate the C:N stoichiometry. The carbonate and NO_3^- characteristics of the source water WB-ISW were defined previously in the context of the benthic remineralization flux which determined its pre-formed character (see Chapter 5). The warmed (17 - 19°C) surface layer was in this instance approximately 10m thick in the inner shelf (stations 16 and 17). This value is less than the usual "standard" Benguela System mixed layer depth of

Northern Benguela Sector: Henties Bay Transect

Carbonate and Nitrate Parameter Concentrations
Units: umol/l; Normalized to S = 35.00psu

Surface Layer Domain

Water	Station	NTALK	NTACY	NTCO2	PCO2	NO3
WB-ISW		2386	2716	2339	1243	21.450
WB-AUW1	16	2382	2341	2150	486	***
WB-AUW2	27	2390	2516	2241	738	1.98
WB-AUW		2386	2429	2196	612	1.980
WB-AUW (NO3 Corr)		2367	2448			
Gross Change		-19	-268	-143	-631	-19.47
Gross CO2 addition:			-134			
CO3 addition:		-10				
CO2 degassing: Liss-Merlivat (18oC, 35, 25m, 4.57m/s, 14days 927uatm)			9			
CO2 addition (Air-Sea Corr)			-125			
CO3 addition:		-10				
COrg:CIng Stoichiometry		13				
NO3 addition:						-19.47
C:N Stoichiometry						6.42

Table 6.1: This table summarizes the biogeochemical (carbon and NO_3^-) characteristics of waters upwelling and ageing at the Walvis Bay upwelling centre. The characteristics of newly upwelled water are obtained from those of the Inner Shelf Water (ISW) (see also Chapter 5) and those of aged upwelled water (AUW) were averaged from warm surface waters at stations 16 and 27 of the Henties Bay transect. The table shows not only the concentrations of carbon and nitrogen parameters but also the changes between the two surface end-members and the stoichiometry of this change. (see text)

25 - 30m (Waldron, 1996). The depth integrated averages for stations 16 and 27 are shown as WB-AUW1 and 2 respectively. The "binned" value for WB-AUW = (AUW1 + AUW2) / 2 provides the average for aged upwelled waters in the surface domain in the vicinity of the Walvis Bay upwell cell. The NTAlk and NTAcy values were corrected for the impact of NO_3^- removal (WB-AUW (NO_3^- Corr) which as was shown earlier (see Chapter 3) has the effect of creating an apparent increase in NTAlk and decrease in NTAcy by equimolar amounts. These parameters were accordingly adjusted to reverse this effect. The magnitude of the changes in the carbonate capacity parameters and NO_3^- concentrations as well as the negative additions (uptake) of CO_2

(NTAcy/2) and CO_3^{2-} (NTAlk/2) in the ageing of upwelled waters were shown (Table 6.1).

The magnitudes of the initial changes (negative gross addition) include the combined effects of *phytoplankton uptake* and *CO_2 degassing* to the atmosphere. To quantify the phytoplankton uptake it is necessary to correct for the early CO_2 degassing effect. This was done using the Liss-Merlivat model (Liss and Merlivat, 1986; Wanninkhof, 1992). The CO_2 flux across the air - sea boundary is given by the product of the wind driven turbulent diffusion coefficient (K_w) (see Chapter 4) and the biogeochemically driven PCO_2 gradient. The CO_2 flux was calculated using a K_w value based on a mean wind speed of 4.57m/s (average for the 2 weeks preceding the sampling), and an average PCO_2 gradient value of 927μatm (average of WB-ISW (PCO_2 = 1243μatm) and WB-AUW (PCO_2 = 612μatm). The magnitude of the CO_2 loss through degassing was calculated to be 9 μM assuming a "typical" 25m thick surface mixed layer and an ageing or degassing period of 14 days. The corrected CO_2 decrease linked to phytoplankton uptake was then calculated as 125μM, and a $C_{Org} : C_{Ing}$ stoichiometry of 13. This final ΔCO_2 value was also used to derive the C:N stoichiometry (C:N = 6.42) of the phytoplankton driven biogeochemical change to the surface layer.

The following features should be noted (Table 6.1):

- although PCO_2 decreased by ~50% to (612μatm) relative to the source water (1243μatm), it remained well above atmospheric equilibrium (360μatm) with only 10% of the NO_3^- remaining. Part of this effect is due to the concomitant warming of the surface layer. The system therefore remained a significant source of CO_2 to the atmosphere even after the main phytoplankton bloom.
- there was a significant decrease (19 μM) in NTAlk concomitant to the photosynthesis and degassing driven decrease in NTAcy (268μM)

resulting in the C_{Org}:C_{Ing} stoichiometry of 14. When the ΔNTAcy is corrected for the degassing loss of 9μM of CO_2 (ΔNTAcy = 18μM) the resulting phytoplankton driven C_{Org}:C_{Ing} stoichiometry changes to 13 (Table 6.1).

- The C:N stoichiometry of CO_2 and NO_3^- uptake 6.42 was close to the Redfield ratio of 6.6.

The small but significant decrease in NTAlk is somewhat problematic because although coccolithophores were found to be present, predominantly in the surface layer of the two inner stations (16 and 27), they had a relatively low standing stock (< $400*10^3$ cells / l) (Giraudeau *et al.*, 1993). Given existing data on coccolith $CaCO_3$ content (Fernandez *et al.*, 1993) this standing stock could not account for the observed NTAlk change. There are three possible explanations for the observed decrease in NTAlk:

- The analytical precision of the Gran titration was lower than the estimated error of 1μM for this study.
- The sampled *Emiliania huxleyi* was the remnants of a much larger bloom
- Other proton acceptors may be present in variable concentrations which have not been incorporated into the calculation of the magnitude of NTAlk.

The first option is the least likely one because 1μM is the maximum estimated error of the Gran titration procedure based on sequential standards (see Chapter 2). It is more likely that one or both remaining options play a role. Such questions should become part of any future field programme as although the differences are small for the purposes of this study they would be significant for any interannual monitoring.

The magnitude and stoichiometry of the perturbation to the carbonate system in the surface domain of the Walvis Bay upwelling cell is graphically depicted using the vector plot approach (Fig. 6.2). It visually confirms that the stoichiometry of the change (vector AB) is primarily driven by photosynthetic

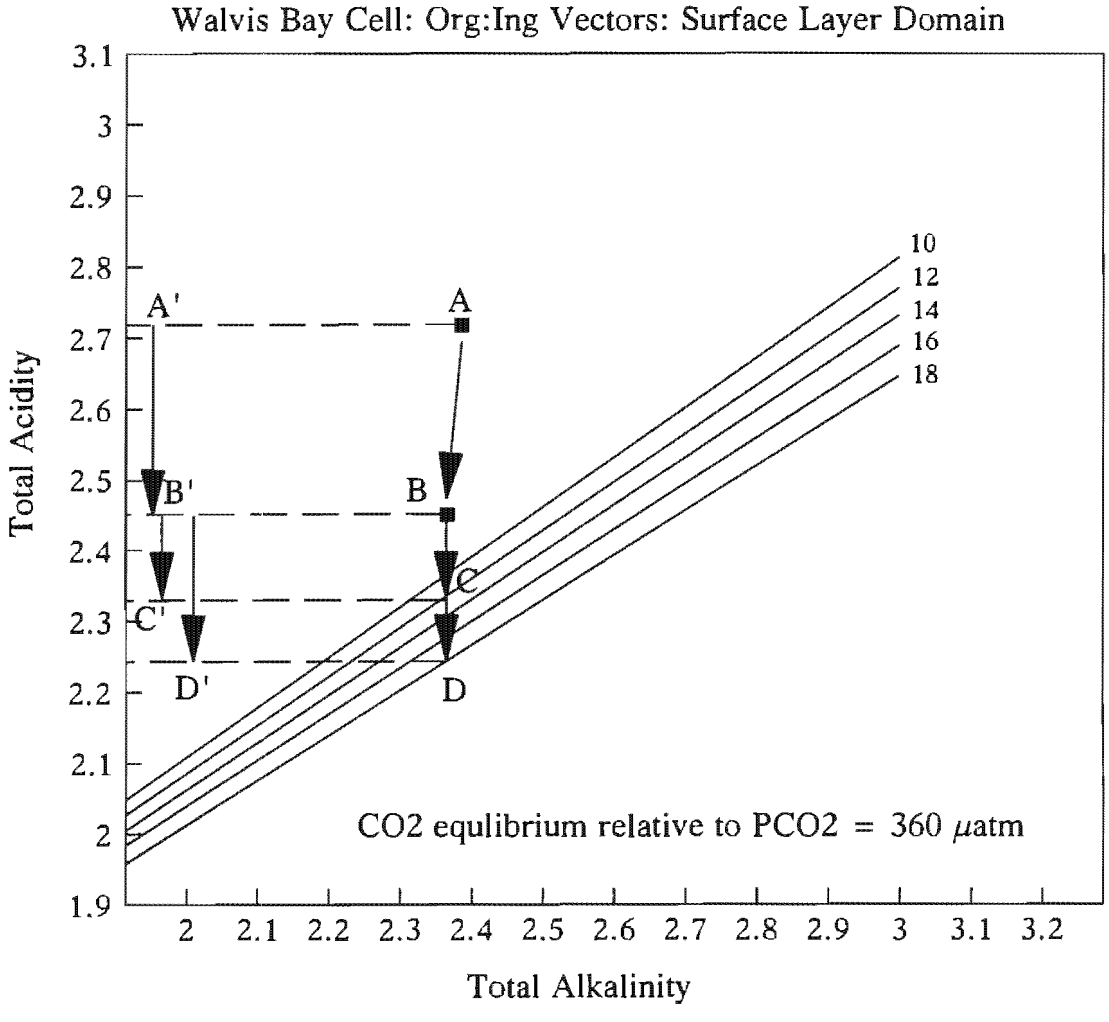

Fig. 6.2: A Total Acidity - Total Alkalinity vector plot depicting the changes brought about by the organic ($_{COrg}$) and inorganic (C_{Ing}) carbon pumps to newly upwelled waters in the vicinity of the Walvis Bay upwelling cell. It shows that carbon uptake is largely driven by photosynthesis with the C_{Ing} pathway making a minor impact (C_{Org} : C_{Ing} stoichiometry 13 from Table 6.1). Also plotted are a family of lines which define the atmospheric equilibrium PCO_2 over a range of temperatures which typify those found between newly upwelled and aged upwelled waters. Such a combined plot allows rapid visualization of whether the particular surface stage of the upwelling cycle is ingassing or outgassing CO_2. In this case it can be seen that the post bloom TAcy (B) is well above the atmospheric equilibrium of newly upwelled water (C: 12.5°C) and even more so for aged upwelled water (D: 18°C). The total post bloom CO_2 degassing potential is then given by vector B'D'.

carbon fixation and CO_2 degassing which impacts only on NTAcy. The degassing component is too small to be resolved in the plot. The magnitude of the photosynthesis driven CO_2 uptake is given by vector component A'B' (where $\Delta CO_2 = \Delta TAcy / 2$). Depicted on the vector plot are also the atmospheric PCO_2 equilibrium lines for $PCO_2 = 360\mu atm$ over a range of temperatures which characterise the warming range of newly upwelled water to aged upwelled water. As was explained earlier warming reduces the CO_2 solubility (increasing PCO_2) which graphically translates to a lowering of the isopleths on the vector plot. The magnitude of the degassing component (CO_2 loss up to atmospheric equilibrium) if no warming occurred is given by vector component B'C' which joins state B to the 12°C PCO_2 isopleth (Fig. 6.1). When the warming effect is incorporated the magnitude of the vector component increases to B'D' corresponding to the 18°C isopleth. The ΔCO_2 value is again given by NTAcy/2 and the flux is calculated assuming a mean mixed layer of 25m which is more typical than the 10m found when the transect was sampled.

C:N Stoichiometry

The C:N stoichiometry of 6.42 (Table 6.1) which characterized the CO_2 and NO_3^- decrease driven by phytoplankton uptake was very close to that which is predicted by the Redfield ratio of 6.6. The ratio was calculated using the ΔCO_2 (125μM) value corrected for the loss of CO_2 to the atmosphere in the course of "ageing" of the water column and the concommittant NO_3^- decrease (19.47μM). The NO_3^- uptake by phytoplankton did not reduce concentrations to zero at the inshore stations which means that there was still some scope for further reduction in PCO_2 which would limit the overall magnitude of the CO_2 outgassing. Based on the measured stoichiometry of 6.42, this additional CO_2 uptake would, however, only lower NTAcy by about 25 μM which is not enough to turn the direction of the CO_2 flux. This issue will be addressed in the modelling in Chapter 7. The persistence of residual NO_3^- is

consistent with other observations based on NO_3^- distribution in surface waters along the Namibian shelf (Probyn, 1988).

6.3.2 Cape Frio Upwell Cell (Northern Sector)

Carbon Fluxes and C_{Org} : C_{Ing} Stoichiometry

As was explained earlier (see Chapter 4) there is no field data to constrain the Cape Frio upwell cell carbonate system. The underlying assumption, based on the "gate" hypothesis, is that because SACW is advected onto the shelf at that latitude, it will upwell at Cape Frio with the same biogeochemical characteristics.

Northern Benguela Sector: Cape Frio Upwell Cell: Simulated Data

Carbonate and Nitrate Parameter Concentrations: Model data
Units: umol/l; Normalized to S = 35.00psu

Surface Layer Domain

Water	Station	Depth	Temp	NTALK	NTACY	NTCO2	PCO2	NO3
CF-ISW			12.8	2383	2519	2239	626	21.570
CF-AUW			18	2383	2217	2087	335	0.000
CF-AUW (NO3 Corr)				2362	2239			
Gross Change				-21	-280	-152	-291	-21.57
Gross CO2 addition:					-140			
CO3 addition:				-11				
CO2 degassing: Liss-Merlivat (13oC, 35.25, 25m, 4.57m/s, 493uatm)					-2			
CO2 addition (Air-Sea Corr)					-138			
CO3 addition:				-11				
COrg:CIng Stoichiometry				13				
NO3 addition:								-21.57
C:N Stoichiometry								6.42

Table 6.2: This table summarizes the biogeochemical (carbon and NO_3^-) characteristics of waters upwelling and ageing at the Cape Frio upwelling centre. As there were no data collected from this upwelling centre all the parameter values had to be calculated on the basis of: characteristics of newly upwelled water (CF-UPW) are obtained from those of South Atlantic Central Water (see also Chapter 5) and those of aged upwelled water (AUW) were calculated from the NO_3^- concentration and C:N stoichiometry at Walvis Bay assuming that: 1) the NO_3^- is reduced to zero; and 2) that TAlk. does not change. The table shows not only the concentrations of carbon and nitrogen parameters but also the changes between the two surface end-members and the stoichiometry of this change. (see text)

That is, the biogeochemical character of SACW will not be changed as a result of benthic fluxes which modify NB-SACW into WB-ISW in the mid - northern sector. At this stage there is no evidence to test whether this assumption is correct. With the input characteristics being constrained by NB-SACW subsequent changes, driven by surface phytoplankton activity, are modelled assuming similar C:N (6.42) and C_{Org}:C_{Ing} (13) stoichiometries as those observed for the Walvis Bay system. The results are shown on Table (6.2) which defines the carbonate and NO_3^- changes which characterize the predicted carbon fluxes at the Cape Frio upwelling cell. The most notable feature is that the final PCO_2 (335μatm) value for CF-AUW is below the atmospheric equilibrium value of 360 μatm. This is in contrast to the Walvis Bay cell (Table 6.1) where the final predicted PCO_2 was > 600μatm.

C:N Stoichiometry

The C:N stoichiometry for the Cape Frio system is assumed for these box-modelling purposes to be identical to that which characterized the Walvis Bay upwell cell that is, 6.42. This figure was used to calculate the decrease in NTAcy which would follow the utilization of the NO_3^- in upwelled NB-SACW to predict the final PCO_2 of aged upwelled waters off Cape Frio.

6.3.3 Namaqua Upwelling Cell (Central Sector)

Carbon Fluxes and C_{Org} : C_{Ing} Stoichiometry

The changes to the carbonate and NO_3^- bulk water parameters brought about by surface productivity in the vicinity of the Namaqua upwell cell are summarized in Table 6.3 where the method to obtain the values was identical to that described for the Walvis Bay upwell cell. The biogeochemical properties of newly upwelled waters were obtained from NQ-ISW whose characteristics were calculated earlier (see Chapter 5). The biogeochemical characteristics of aged upwelled waters (NQ-AUW) were physically

constrained by t > 13°C; S = 34.88. The samples were taken at the end of an active phase of the upwelling cycle (see Chapter 4) as a result of which, the whole water column at station 113 was filled with newly upwelled NQ-UPW.

Central Benguela Sector: Namaqua Upwelling Cell: Hondeklip Bay Transect

Carbonate and Nitrate Parameter Concentrations
Units: umol/l; Normalized to S = 35.00psu

Surface Layer Domain

Water	Station	NTALK	NTACY	NTCO2	PCO2	NO3
NQ-UPW		2404	3007	2489	2971	20.08
NQ-AUW	114	2409	2578	2281	707	4.81
NQ-AUW (NO3 Corr)		2394	2593			
Gross Change		-10	-414	-208	-2971	-15.27
Gross CO2 addition:			-207			
CO3 addition:		-5				
CO2 degassing: Liss-Merlivat (14oC,35,25m,3.29m/s;14days;1893uatm)			4			
CO2 addition (corrected)			-203			
CO3 addition:		-5				
COrg:CIng Stoichiometry		41				
NO3 addition						-15.27
C:N Stoichiometry						13.31

Table 6.3: This table summarizes the biogeochemical (carbon and NO_3^-) characteristics of waters upwelling and ageing at the Namaqua upwelling centre. The characteristics of newly upwelled water (UPW) are obtained from those of the Inner Shelf Water (ISW) (see also Chapter 5) and those of aged upwelled water (AUW) were averaged from warm surface waters at stations 14 of the Hondeklip Bay transect. The table shows not only the concentrations of carbon and nitrogen parameters but also the changes between the two surface end-members and the stoichiometry of this change. (see text)

This freshly upwelled water is characterized by the highest PCO_2 values recorded in the Benguela System (PCO_2: 2500 - 3000μatm). It was only at station 114 located within the upwelling front that a recognizable surface layer of warmed aged upwelled water (PCO_2 < 1000μatm) with a thickness of 10m had formed whose biogeochemical characteristics were used to define NQ-AUW. The much lower NO_3^- value (4.81μM) in the surface layer supports the view (Fig. 6.1) that the chosen surface water was indeed ageing upwelled

water whose NO_3^- has decreased by 15.27μM relative to newly upwelled waters (Table 6.3). This change to the NO_3^- concentration was used to make the necessary correction to the capacity parameters (NTAlk, NTAcy).

As was the case with the Henties Bay transect on the Namibian shelf the bulk of the biogeochemical impact on the carbonate system is through the photosynthetic uptake of CO_2 which decreases the NTAcy value by 414 μM after the NO_3^- correction (Table 6.3). In contrast, ΔNTAlk is small (10μM after the NO_3^- correction). Once again the problem arises as to the cause of this small but significant decrease in NTAlk. Coincidentally, and as was the case for the Henties Bay transect, a bloom of coccolithophores was identified and counted in the vicinity of the inshore stations (Giraudeau and Bailey, 1995). This population, with a low standing stock of $200*10^3$ cells/l (Giraudeau and Bailey, 1995) was also dominated by *Emiliania huxleyi* in the same order of magnitude as the one located along the Henties Bay transect ($300*10^3$ cells/ l). The maximum predicted impact of such a bloom on NTAlk is no more than 2μM which leaves at best 7μM unaccounted for. The presence or loss of unknown proton acceptors cannot be ruled out but for modelling purposes it is ignored.

The gross CO_2 and CO_3^{2-} changes (removal) of 207 and 5 μM respectively include, in the case of CO_2, the combined effects of *photosynthetic uptake* and *degassing* to the atmosphere. The atmospheric loss component was calculated as before using the Liss-Merlivat model (Liss and Merlivat, 1986; Wanninkhof, 1992). The CO_2 flux was calculated with a PCO_2 gradient of 1839 (average of 2971 and 707 μatm), an average wind speed of 3.29 m/s over a 14 day period. The accumulated CO_2 loss over this period was calculated to be 4μM which constrains the photosynthetically driven CO_2 uptake to 203μM. The C_{Org}:C_{Ing} stoichiometry was calculated from the corrected ΔCO_2 and ΔCO_3^{2-} as 41 which is clear indication that C_{Ing} played a minimal role in surface domain biogeochemistry. This confirms the fact that despite the presence in the water of the coccolithophorid *Emiliania huxleyi*,

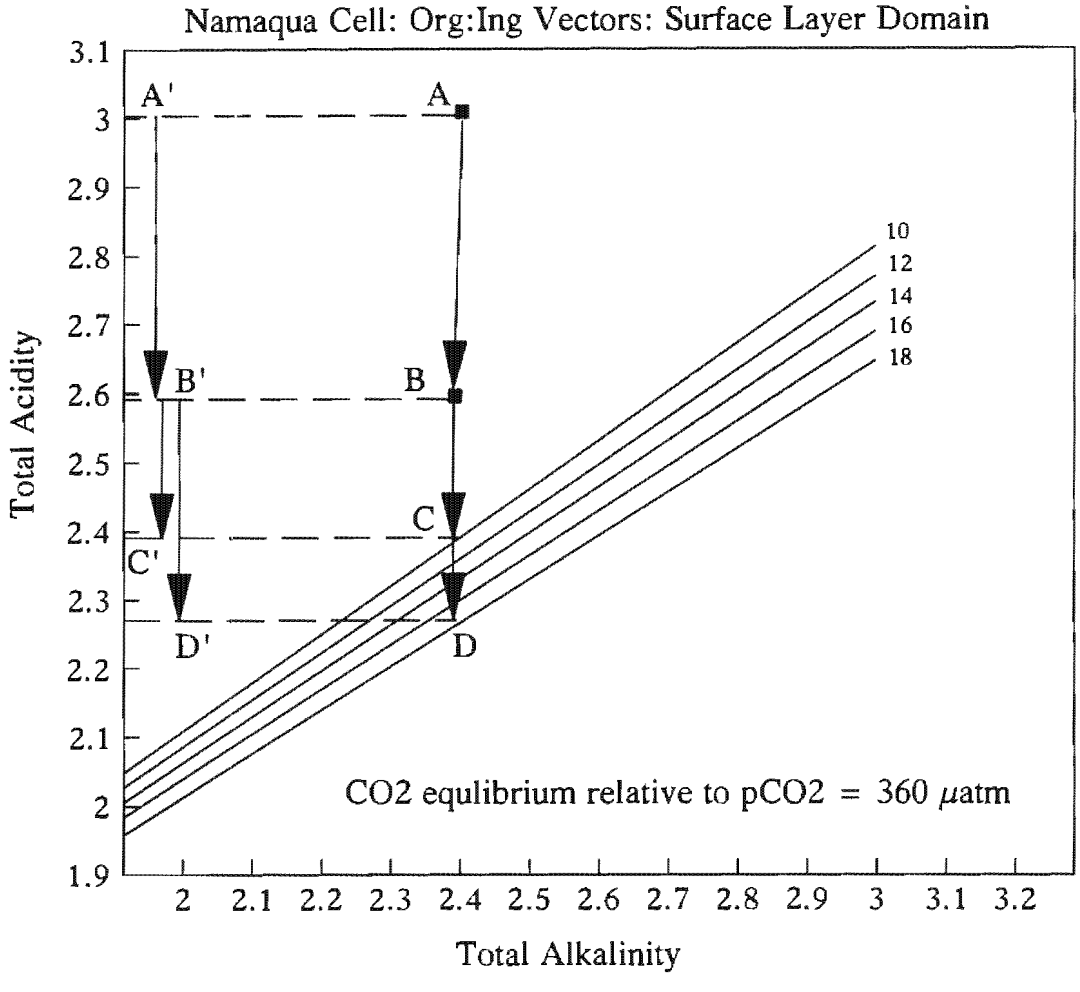

Fig. 6.3: A Total Acidity - Total Alkalinity vector plot depicting the changes brought about by the organic (C_{Org}) and inorganic (C_{Ing}) carbon pumps to newly upwelled waters in the vicinity of the Namaqua upwelling cell. It shows that carbon uptake is largely driven by photosynthesis with the C_{Ing} pathway making a minor impact (C_{Org} : C_{Ing} stoichiometry 41 from Table 6.3). Also plotted are a family of lines which define the atmospheric equilibrium PCO_2 over a range of temperatures which typify those found between newly upwelled and aged upwelled waters. Such a combined plot allows rapid visualization of whether the particular surface stage of the upwelling cycle is ingassing or outgassing CO_2. In this case it can be seen that the post bloom TAcy (B) is well above the atmospheric equilibrium of newly upwelled water (C: 10°C) and even more so for aged upwelled water (D: 18°C). The total post bloom CO_2 degassing potential is then given by vector B'D'.

the perturbation to the carbonate chemical system was driven largely by photosysnthesis.

The stoichiometry of the change in state of the carbonate system is graphically depicted using the vector plot (Fig. 6.3). The slope of the vector AB reflects the stoichiometry of the C_{Org}:C_{Ing} pathways and the magnitude of the photosynthetically removed CO_2 is given by the vector component A'B' where $\Delta CO_2 = \Delta NTAcy/2$. The further scope for long term degassing of CO_2 to the atmosphere is given by vectors BC and BD. Vector BC defines the degassing under the sampling conditions which coincided with the austral winter when insolation rates are relatively low. The magnitude of the vector (B'C') is given by the NTAcy change from state B to the PCO_2 isopleth at 14°C. With the onset of summer this surface water would warm up to the typical temperature of 18°C inducing further degassing to the appropriate isopleth given by vector BD and vector component B'D' (Fig. 6.3). For modelling purposes the surface equilibration temperature was taken to be 18°C.

C:N Stoichiometry

The C:N stoichiometry for the uptake of CO_2 and NO_3^- in the course of surface ageing of newly upwelled waters is given in Table 6.3 as 13.30. This is an unexpectedly large number close to double that which is predicted by the Redfield ratio. It accounts for the observation that although the NO_3^- decreased by a smaller amount (15.27μM) relative to that in the Henties Bay transect (19.47μM) the PCO_2 decrease was 3.7 times larger. This might raise the question as to whether the correction made for the loss of CO_2 through degassing was realistic. However, it is thought that in view of the fact that the degassing loss is constrained using actual wind data over a realistic time period of 14 days that the error margin on the estimate is small. Even if the loss was doubled the impact on the C:N ratio would be small. It is suggested that the explanation lies, as was suggested by Sambrotto *et al.*,1993, in the

fact that upwelled NO_3^- was being remineralized as NH_4^+ in the surface layer which could then sustain further photosynthesis and CO_2 uptake. This stoichiometry was apparent in the NTAcy - NO_3^- plot shown in the previous section using the full data set from the Hondeklip Bay transect (Fig. 5.8).

6.3.4 Luderitz Upwell Cell (Central Sector)

Carbon Fluxes and C_{Org} : C_{Ing} Stoichiometry

There was no carbonate and nitrogen field data for the Luderitz upwell cell and as a result it is treated in the same way as Cape Frio. Because its position coincides with the entrance "gate" for CB-SACW the biogeochemical characteristics of upwelled waters at Luderitz are taken to be those of CB-SACW. The biogeochemical characteristics are summarized on Table (6.4).

Central Benguela Sector: Luderitz Upwell Cell: Synthetic Data

Carbonate and Nitrate Parametar Concentrations: Model data
Units: umol/l; Normalized to S = 35.00psu

Surface Layer Domain

Water	Station	Depth	Temp	NTALK	NTACY	NTCO2	PCO2	NO3
LZ-UPW			10	2413	2480	2234	458	13.670
LZ-AUW			18	2413	2237	2102	324	0.000
LZ-AUW (NO3 Corr)				2403	2223			
Gross Change				-10	-257	-132	-134	-13.67
Gross CO2 addition:					-129			
CO3 addition:				-5				
CO2 degassing: Liss-Merlivat (13oC, 35.25, 25m, 6.5m/s, 409uatm)					3			
CO2 addition (Air-Sea Corr)					-126			
CO3 addition:				-5				
COrg:CIng Stoichiometry				41				
NO3 addition:								-13.67
C:N Stoichiometry								13.30

Table 6.4: This table summarizes the biogeochemical (carbon and NO_3^-) characteristics of waters upwelling and ageing at the Luderitz upwelling centre. As there were no data collected from this upwelling centre all the parameter values had to be calculated on the basis of: characteristics of newly upwelled water (LZ-UPW) are obtained from those of South Atlantic Central Water (see also Chapter 5) and those of aged upwelled water (AUW) were calculated from the NO_3^- concentration and C:N stoichiometry at Namaqua (NQ) assuming that: 1) the NO_3^- is reduced to zero; and 2) that TAlk. does not change. The table shows not only the concentrations of carbon and nitrogen parameters but also the changes between the two surface end-members and the stoichiometry of this change. (see text)

The magnitude of the changes to the carbonate characteristics are driven by the magnitude of the NO_3^- concentration (13.67μM) , the C:N ratio (13.30) and C_{Org} : C_{Ing} (41) stoichiometry all obtained from the Namaqua upwell cell (Table 6.4). As was the case in Cape Frio, because the NTAcy and NTAlk concentrations are unmodified by the input of CO_2 from benthic remineralization the magnitude of CO_2 removal was sufficient to lower the PCO_2 to below atmospheric equilibrium. The Luderitz upwell cell is therefore a potential net CO_2 sink and its contribution to the overall CO_2 budget in the Benguela System is addressed in the context of the box model (Chapter 7).

C:N Stoichiometry

The C:N ratio of CO_2 and NO_3^- uptake in this part of the system is provided by that which was measured in the Namaqua upwell cell (13.30).

6.3.5 Cape Columbine Upwelling Cell (Southern Sector)

Carbon Fluxes and C_{Org} : C_{Ing} Stoichiometry

The changes to the carbonate parameter and NO_3^- concentrations between newly upwelled (CC-UPW) and aged upwelled waters (CC-AUW) sampled in the Olifants River transect are summarized in Table 6.5. The calculation of depth integrated concentrations follows the same rules as were detailed for the previous examples. The carbonate characteristics of newly upwelled water (UPW) supplied from CC-ISW were obtained from the section dealing with sub-surface properties (Chapter 5). The samples were taken relatively close to the Olifants Valley "gate" through which the Southern Benguela is supplied with upwelled water (see Fig. 4.24). It is therefore expected that, in contrast to the water from the Henties Bay and Hondeklip Bay transects, which were located at least 300km poleward of the "gates", these should reflect much lower NTAcy and PCO_2 enrichments. The data confirm this as the NTAcy and PCO_2 values for CC-ISW which upwells at Cape Columbine

Southern Benguela Sector: Cape Columbine Upwelling Cell: Olifants River Transect

Carbonate Parameter Concentrations
Units: umol/l Normalized to S = 35.00psu

Surface Layer Domain

Water	Station	NTALK	NTACY	NTCO2	PCO2	NO3
CC-UPW		2378	2569	2262	656	18.73
CC-AUW1	12	2372	1907	1927	170	0
CC-AUW2	13	2374	1939	1945	171	0.44
CC-AUW		2373	1923	1936	170.5	0.22
CC-AUW (NO3 Corr)		2354	1942			
Gross Change:		-23	-627	-326	-485.5	-18.51
Gross CO2 addition			-314			
CO3 addition		-12				
CO2 degassing: Liss-Merlivat (18oC,35,25m,6.03m/s;14days;508uatm			6			
CO2 addition (Air -Sea corr)			-307			
CO3 addition:		-12				
COrg:CInq Stoichiometry		27				
NO3 addition:						-18.51
C:N Stoichiometry						16.61

Table 6.5: This table summarizes the biogeochemical (carbon and NO_3^-) characteristics of waters upwelling and ageing at the Cape Columbine upwelling centre. The characteristics of newly upwelled water (UPW) are obtained from those of the Inner Shelf Water (ISW) (see also Chapter 5) and those of aged upwelled water (AUW) were averaged from warm surface waters at stations 14 of the Olifants River transect. The table shows not only the concentrations of carbon and nitrogen parameters but also the changes between the two surface end-members and the stoichiometry of this change. (see text)

are 2569μM and 656μatm respectively. The biogeochemical characteristics of aged upwelled waters (CC-AUW) were taken from stations 12 and 13 located in the inshore region (see Fig. 4.3) where PCO_2 had dropped to the lowest values measured in the Benguela System (170μatm). As was the case with the earlier transects after the NO_3^- corrections there is an unexpectedly large residual in the ΔNTAlk (-23μM). Again this points to the effect of either an unaccounted for proton acceptor or an underestimated effect of coccolithophore activity. The magnitude of the CO_2 decrease driven by phytoplankton activity (corrected for CO_2 degassing) is 314μM which is the largest change in all three sampled transects. The PCO_2 values in CC-AUW

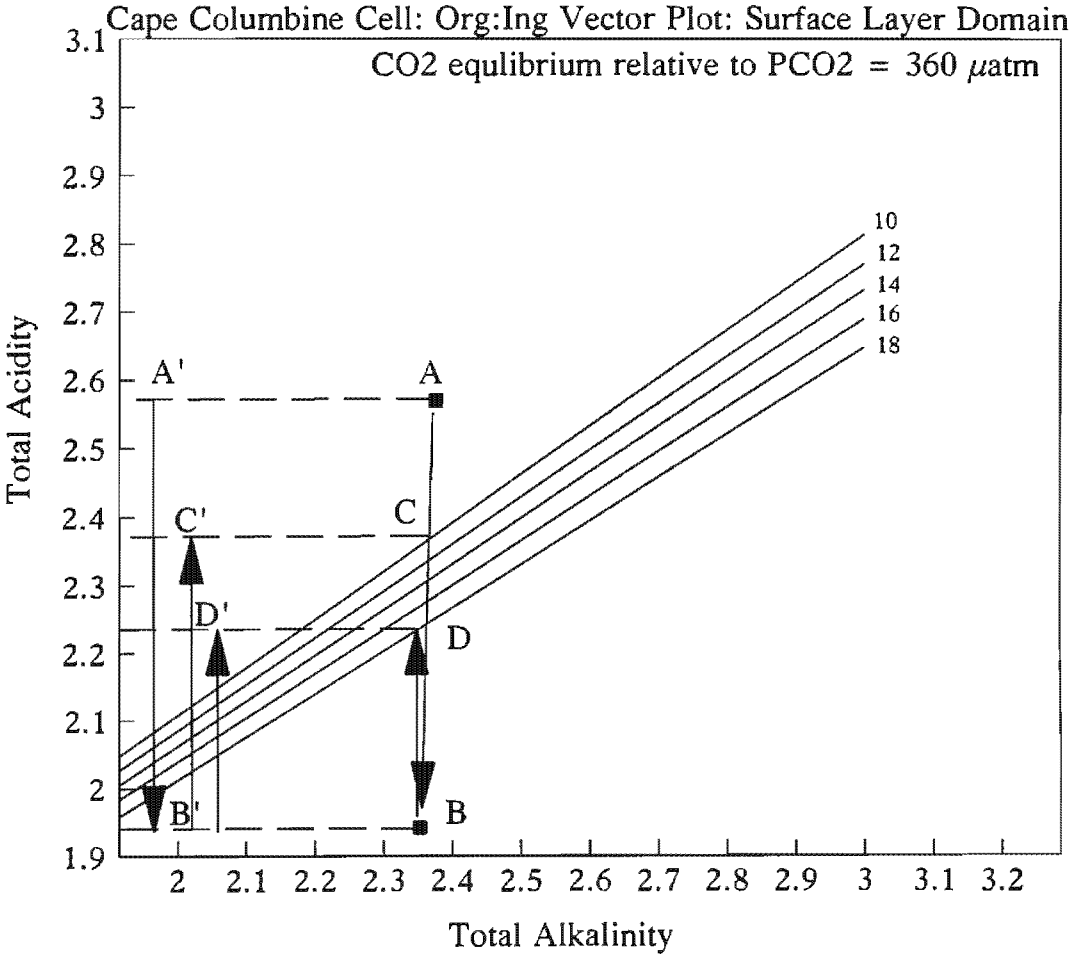

Fig. 6.4: A Total Acidity - Total Alkalinity vector plot depicting the changes brought about by the organic (C_{Org}) and inorganic (C_{Ing}) carbon pumps to newly upwelled waters in the vicinity of the Cape Columbine upwelling cell. It shows that carbon uptake is largely driven by photosynthesis with the C_{Ing} pathway making a minor impact (C_{Org} : C_{Ing} stoichiometry 27 from Table 6.5). Also plotted are a family of lines which define the atmospheric equilibrium PCO_2 over a range of temperatures which typify those found between newly upwelled and aged upwelled waters. Such a combined plot allows rapid visualization of whether the particular surface stage of the upwelling cycle is ingassing or outgassing CO_2. In this case, in contrast to other examples, it can be seen that the post bloom TAcy (B) is well below the atmospheric PCO_2 equilibrium line. The CO_2 ingassing potential relative to newly upwelled water is given by the vector B'C' which links the final post-bloom state B to the 10°C equilibrium line. This ingassing potential is however reduced by the warming of newly upwelled waters to 18°C which then reduces the theoretical scope for ingassing to vector B'D'.

are the lowest recorded in the Benguela System but it should be noted that the sampled area supported one of largest blooms recorded in this system where chlorophyll$_a$ concentrations reached 50μg/l (Probyn, pers.com.). It appears from these data that there exists a southward trend of increasing magnitude of CO_2 removal for relatively small difference in NO_3^- concentrations. The factor which appears to be driving this meridional effect is the C:N ratio which also increases polewards from 6.42 in the northern sector, 13.30 in the central sector to 16.61 in the southern sector.

The stoichiometry and magnitudes of the changes of ΔCO_2 and ΔCO_3^{2-} are graphically depicted on a NTAcy - NTAlk vector plot (Fig. 6.4). It confirms the observation that, like all other parts of the Benguela System, carbon fluxes are dominated by the photosynthetically driven CO_2 uptake. The main difference is the visual depiction of the way in which the phytoplankton driven perturbation (vector AB) reduces the NTAcy to well below all the atmospheric PCO_2 equilibrium lines. Here the magnitude of ingassing or CO_2 drawdown is given by the vector BC which links the final state B to the PCO_2 equilibrium isopleth at 18°C (state C) (Fig. 6.4). It clearly shows how the warming process through its impact on CO_2 solubility reduces the drawdown potential from the isopleth which characterizes newly upwelled waters (10°C) to aged upwelled waters at 18°C. The magnitudes of these vector changes are again depicted by the NTAcy vector components where $\Delta CO_2 = \Delta NTAcy /2$.

C:N Stoichiometry

The C:N stoichiometry which characterizes the concommittant decrease of CO_2 and NO_3^- is calculated to be 16.61 after the CO_2 degassing component has been accounted for. This is the highest ratio in the system (cf. 6.42 and 13.31 in the northern and central sectors respectively) and would be consistent with a system where nitrogen recycling as opposed to only new nitrogen drives CO_2 uptake by phytoplankton. This high C:N stoichiometric

ratio in combination with a relatively low impact of sub-surface remineralization are the critical factors which turn the Southern sector into a CO_2 sink.

6.3.6 Cape Peninsula Upwelling Cell (Southern Sector)

Carbon Fluxes and C_{Org} : C_{Ing} Stoichiometry

As was the case with both the Cape Frio and Luderitz upwelling cells no samples were taken for the Cape Peninsula upwelling centre. This upwelling cell is however well away, polewards, of the Olifants River valley "gate" site. The input characteristics for this upwelling cell were taken to be identical to those of the Cape Columbine centre with the justification that in this sector the shelf is narrow and the areas of organic carbon accumulation on the inner shelf are spatially very restricted, especially south of Cape Columbine (Birch, 1975). There are two possible explanations for the low organic carbon build up in the southern sector sediments:

- Current meter records indicate that in the southern Benguela System the poleward flow is both strong and more persistent than the northerly sectors (G. Nelson, pers.com.). In terms of the conceptual model put forward in Chapter 4, this would increase the BBL turbulence and lead to erosion of biogenic particles which have lowest densities.
- The flux of biogenic carbon from surface production in the southern sector is low. This will be addressed in the modelling Chapter 7.

The key assumption is, however, that the biogeochemical input and ageing characteristics at the Cape Peninsula upwelling cell are identical to those of Cape Columbine. The calculated biogeochemical characteristics of newly upwelled and aged upwelled water for the Cape Peninsula upwelling centre are given in Table 6.5. This assumption, like the previous ones, should be tested in any future carbon related work in this system.

Southern Benguela Sector: Cape Peninsula Upwell Cell: Synthetic Data

Carbonate and Nitrate Parameter Concentrations: Model data
Units: umol/l; Normalized to S = 35.00psu

Surface Layer Domain

Water	Station	Temp	NTALK	NTACY	NTCO2	PCO2	NO3
CP-UPW		10	2378	2569	2262	656	18.730
CP-AUW		18	2375	1919	1936	174	0.000
CP-AUW (NO3 Corr)			2356	1938			
Gross Change			-22	-650	-326	-482	-18.73
Gross CO2 addition:				-325			
CO3 addition:			-11				
CO2 degassing: Liss-Merlivat (13oC, 35.25, 10m, 4.62m/s, 927uatm)				-14			
CO2 addition (Air-Sea Corr)				-311			
CO3 addition:			-11				
COrg:CIng Stoichiometry			27				
NO3 addition:							-18.73
C:N Stoichiometry							16.61

Table 6.6: This table summarizes the biogeochemical (carbon and NO_3^-) characteristics of waters upwelling and ageing at the Cape Peninsula upwelling centre. As there were no data collected from this upwelling centre all the parameter values had to be calculated on the basis of: characteristics of newly upwelled water (CP-UPW) are obtained from those of ISW at Cape Columbineand those of aged upwelled water (AUW) were calculated from the NO_3^- concentration and C:N stoichiometry at Cape Columbine assuming that: 1) the NO_3^- is reduced to zero; and 2) that TAlk. does not change. The table shows not only the concentrations of carbon and nitrogen parameters but also the changes between the two surface end-members and the stoichiometry of this change. (see text)

C:N Stoichiometry

The C:N stoichiometry and its impact in this sector are identical to those which defined the biogeochemical characteristics of the Cape Columbine upwelling cell. The further implications of these results are now discussed in more detail.

6.4 Further Discussion:

One of the salient aspects of the data sets presented above was that, in contrast to open ocean upwelling systems (Murray *et al.*, 1994; Watson,

1995), surface PCO_2 values in the Benguela System can, in many instances, drop below atmospheric equilibrium ($PCO_2 < 360\mu atm$). This challenges the notion that, because waters which outcrop at upwelling centres are high in PCO_2 upwelling areas are CO_2 sources to the atmosphere (Watson, 1995). Coastal upwelling systems such as the Benguela System appear not to follow the rule established from open ocean systems. It is suggested that the main reason for the difference is that in open ocean upwelling systems there is usually incomplete utilization of upwelled NO_3^- which limits the scope for the CO_2 drawdown of such systems. In coastal systems, on the other hand, while there is a 100% efficiency in the uptake of upwelled NO_3^-. This is, however, offset by a benthic remineralization flux component which, depending on its magnitude, can determine the CO_2 source - sink nature of an upwelling centre. The key to this CO_2 source - sink character are the mechanisms which govern the C:N stoichiometry because, as the data show, the $C_{Org} : C_{Ing}$ stoichiometry in the Benguela System plays an insignificant role. The ensuing discussion addresses these mechanisms in the surface layer during the ageing of newly upwelled waters. It focuses on their role in determining the CO_2 air - sea gradient by offsetting the C:N disequilibrium induced by the benthic remineralization flux (Chapter 5). This discussion is therefore complementary to the one presented in Chapter 5 for sub-surface remineralization.

The results presented above and summarized on Table (6.7), point to two characteristics of the CO_2 variability in the Benguela System which have a bearing on the modelling of CO_2 source sink dynamics:

- There are a number of upwelling centres (Cape Frio, Luderitz, Cape Columbine and Cape Peninsula) where measured or modelled post-bloom PCO_2 values were lowered to levels below atmospheric equilibrium ($PCO_2 < 360matm$) inducing a potential CO_2 drawdown from the atmosphere. This is in contrast to those upwelling centres (Walvis Bay

and Namaqua) where the final post bloom PCO_2 is well above atmospheric equilibrium (PCO_2 > 600 μatm).

Upwelling Centre	PCO2 UPW	PCO2 AUW	ΔCO2	ΔNO3	C:N
CF	626	335	140	21.57	6.42
WB	1243	612	125	19.47	6.42
LZ	458	324	126	13.67	13.3
NQ	2971	707	203	15.27	13.3
CC	656	171	307	18.51	16.61
CP	656	174	311	18.73	16.61

Table 6.7: Summary of the changes in PCO_2 and NO_3^- at each of the 6 upwelling centres in the Benguela System. The PCO_2 values apply to newly upwelled water (UPW) and post-bloom or aged upwelled water (AUW). ΔCO_2 is the magnitude of the CO_2 loss in μM units and similarly for ΔNO_3^-. C:N is the stoichiometry of the ΔCO_2: ΔNO_3^- change. From a mechanistic perspective, the interesting aspect of this summary is that it establishes that the upwelling centres have different hierarchies depending on whether one chooses UPW or AUW characteristics. (see text for discussion).

- However, the amount by which CO_2 or NTAcy is lowered in the surface domain at each upwelling centre is variable and not necessarily a good predictor of PCO_2 and hence of whether a particular upwelling centre is a source or a sink of CO_2.

These results indicate that the prediction of CO_2 source - sink behaviour in the Benguela System requires an understanding of more than one biogeochemical mechanism and, in all likelihood, they interact with each other in the surface layer domain with varying scales of space and time. Present insight indicates that there are *three* such processes in the Benguela System which have a potentially important impact on CO_2 fluxes between the atmosphere and the surface layer:

- *The biogeochemical characteristics* (CO_2 and NO_3^-) of waters which outcrop at upwelling centres which were earlier shown to be determined by the characteristics of the sub-surface remineralization fluxes.

- *The C:N uptake stoichiometry* in the surface layer where any value larger than that which is predicted by the Redfield ratio (Rr) could potentially result in a CO_2 sink larger than that which predicted by offsetting a sub-surface C:N disequilibrium.
- *The C_{Org}:C_{Ing} uptake stoichiometry* and the role of coccolithophore activity.

The mechanistic details which drive the first process have been addressed in detail in the context of sub-surface remineralization (see Chapter 5). Two points need to be re-emphasised:

- It is not the magnitude of the C and N remineralization fluxes which is of importance but their stoichiometry. NO_3^- is the limiting nutrient for new production in the surface domain and any disequilibium in the stoichiometry of the remineralization flux (where C:N > 6.6) will reduce the scope for surface photosynthesis to induce a CO_2 drawdown from the atmosphere. Such a limitation can only be overcome by a similar or larger opposing disequilibrium in the surface layer uptake of CO_2 and NO_3^-.
- The magnitude of the impact of this process is governed by the distance / time that ISW is advected from the "gate" site, over organic rich sediments to an upwelling centre.

If the PCO_2 in the surface layer after the post upwelling bloom were only governed by the impact of the sub-surface remineralization flux, that is, phytoplankton uptake was constrained by the Redfield ratio, the predicted order of decreasing CO_2 drawdown potential would be (see pre-bloom PCO_2 values in Table 6.7):

LZ > CF > CC ~ CP > WB > NQ

On the left are the upwelling centres located at gate sites where benthic remineralization flux (BRF) effects are least and on the right are the upwelling centres in mid sector where the BRF impact is greatest.

The actual order given by the results post bloom PCO_2 in Aged Upwelled Waters (AUW) summarized on Table (6.7) is:

CC ~ CP > LZ ~ CF > WB > NQ

This indicates that an additional process is playing an important mediating role: the process governs the C:N uptake stoichiometry of primary productivity in the surface domain. The results summarized on Table (6.7) show that there are significant differences in the overall ΔCO_2: ΔNO_3^- uptake stoichiometry from ISW to AUW mainly between the northern sector on the one hand (C:N = 6.42) and the central and southern sectors on the other (C:N = 13.30 and 16.61 respectively). The re-arrangement of the upwelling centre hierarchy in terms of the final PCO_2 values is driven by the C:N stoichiometry which characterized the uptake of bulk CO_2 and NO_3^- at the time of sampling. The southern sector has the greatest CO_2 drawdown potential because of the combination of lowest sub-surface remineralization flux (PCO_2 in UPW; Table 6.7) and highest C:N uptake stoichiometry. The Luderitz and Cape Frio cells are intermediate due to a combination of lower NO_3^- (13.67 μM) and high C:N 13.31 at LZ or less favourable C:N 6.42 stoichiometry and higher NO_3^- (20μM) at CF). The cells where CO_2 ingassing is predicted to never occur, WB and NQ, are characterized by a sub-surface re-mineralization flux of a magnitude and stoichiometry which cannot be compensated by surface uptake stoichiometry. The goal of the ensuing discussion is to address the mechanistic basis of these observations as a way to justify their use in the box model (Chapter 7).

6.4.1 C: N uptake stoichiometry in the surface layer: contradictions with existing paradigms.

The relationship between carbon and nitrogen cycling in the surface ocean is governed by two widely used and interrelated paradigms:

- C:N stoichiometry is predicted by the Redfield ratio (Rr) of 6.6 which characterizes the C and N uptake by phytoplankton (Redfield *et al.*, 1963).
- Carbon uptake by phytoplankton is partitioned into ***new*** and ***regenerated*** production pathways which are conveniently defined both conceptually and empirically by their respective uptake of oxidized (NO_3^-) and reduced (NH_4^+, urea) nitrogen species (Dugdale and Goering, 1967; Probyn, 1985). The numerical relationship between new and regenerated nitrogen uptake rates is defined by the f-ratio (Eppley and Peterson, 1979; King, 1987; Platt *et al.*, 1989). The f-ratio (eq. 6.1) is the proportion that NO_3^- uptake represents of the total nitrogen uptake including *inter alia* NO_3^-, NH_4^+ and urea (Eppley and Peterson, 1979; King, 1987). It is a useful parameter to calculate the partitioning of carbon into new production / export flux and regenerated production fractions:

$$f = \frac{\mu NO3}{\mu NO3 + \mu NH4 + \mu urea}$$

These widely used paradigms form the basis for a range of operational approaches to constrain new production and by association, carbon export production from the surface ocean (Eppley and Peterson, 1979; Chavez and Smith, 1995; Ducklow, 1995). These methods fall into two main categories covering a range of scales of variability; *in vitro* measurements (^{14}C, ^{15}N, O_2) sample short time scales (hours) and *bulk type* measurements integrate short term variability into time scales of days - seasons depending on the event turn over rate or the deployment time (Platt *et al.*, 1989). There are three main numerical definitions of export production which incorporate the parameters returned by the sampling methods:

Export Prdcn (C) = New Prdcn (C) = Total Net Prdcn * f-ratio eq. 6.2a

Export Prdcn (C) = New Prdcn (C) = [NO_3^-] * Rr eq. 6.2b

Export Prdcn (C) = New Prdcn (C) = F_Z (Vertical Flux Rate) eq. 6.2c

Total Net production (P_T) is usually determined by either ^{14}C or O_2 *in vitro* methods corrected for the endogenous respiration component. The [NO_3^-] term is the nitrate supply rate to the euphotic zone and Rr is the classical Redfield ratio (6.6) which theoretically defines the stoichiometry of C:N uptake by phytoplankton. F_Z is the vertical flux rate of organic carbon out of the surface layer as measured by sediment traps which is, in terms of the working paradigms, the only direct assessment of new production integrated over longer time scales determined by the sampling and deployment frequency (Eppley and Peterson, 1979; Packard *et al.*,1988, Platt *et al.*, 1989).

One of the sources of greatest concern at present is the degree of disagreement in the estimates of new and total production in the global oceans whose relationship is theoretically constrained by the f-ratio (Platt *et al.*, 1989; Ducklow, 1995). This problem was the subject of a detailed review by Platt *et al.*, , 1989 where it was suggested that new production was being underestimated. At the heart of the problem is the issue of matching the scale limitations of the sampling methods with the needs of regional and basin scale modelling of carbon fluxes or food web dynamics (Platt *et al.*, 1989). The basic assumption underlying the scaling up process is that of spatial and temporal constancy in the integrated dynamics of the surface ocean. This assumption appears to be increasingly questioned given the most recent evidence on the role played by mesoscale eddies in surface layer turbulence and NO_3^- supply rates in the open ocean (Platt *et al.*, 1989). It has been well established that the f-ratio increases with increasing NO_3^- supply rate (Probyn, 1992) hence the decoupling of production sampling scales and physical turbulence scales will underestimate the f-ratio. This problem is particularly pertinent to upwelling systems which are characterised by physically driven by synoptic scale pulsing of equatorward winds (Brink *et al.*, 1995; Hutchings *et al.*, 1995). The f-ratio reflects the physiological adaptation of the seeding community to changing turbulence conditions which drive the

nitrogen supply rates (Brink *et al.*, 1995; Hutchings *et al.*, 1995). In upwelling systems such as the Benguela the relationship between the f-ratio and NO_3^- supply is well characterised showing an initial intermediate f-ratio (say ~ 0.4-0.5) (NO_3^- 20 - 10μM), increasing to f-ratio ~ 0.8-0.9 during the shift up phase (NO_3^- 10 - 2 μM) declining to f-ratio < 0.2 with NO_3^- limitation < 2μM (Probyn, 1985; Probyn, 1987; Probyn, 1988; Probyn. 1992). This variability provides scope for data aliasing which can only be resolved by a temporally integrated f-ratio defined as <f> (Platt *et al.*, 1989) :

$$< f >= \frac{\int_0^t f dt}{t} \qquad \text{eq. 6.3}$$

Similar to the f-ratio, which governs the classical definition of new production, the second case (eq. 6.2b) which defines new production relative to NO_3^- supply rate depends very sensitively on the assumption that the C:N stoichiometry of uptake is correctly predicted by the Rr. However, as was discussed above, there is increasing evidence derived from changes to bulk concentration of TCO_2 and NO_3^- that question the robustness of the Rr (Sambrotto *et al.*, ., 1993; Banse, 1994). This evidence has serious implications not only for the NO_3^- based estimates of carbon export flux but poses questions about the relationship between the f-ratio and the partitioning of carbon between new and regenerated production.

The data from both the central and southern sectors of the Benguela System yielded C:N stoichiometries of 13.31 and 16.61 which are more than double the Redfield ratio. If such stoichiometries are part of the biogeochemical character of a system or part of it, any modelling based on the standard notions could seriously underestimate the carbon export flux.

The implication of a high C:N ratio in the uptake of bulk CO_2 and NO_3^- is that part of the NO_3^- pool is being re-cycled as NH_4^+ / urea in the euphotic zone and potentially being used by the same bloom to fix more carbon. Thus, while the actual uptake ratio by the phytoplankton may remain consistent with the Redfield ratio, a C:N disequilibrium develops in the regeneration pathway. The nitrogen rich fractions of the cell metabolites (amino acids and proteins) are remineralized at a higher rate providing a regeneration stoichiometry smaller than Rr and simultaneously turning the export flux into a magnitude larger than the Rr. The implication is that re-mineralized NH_4^+ is enhancing the export of carbon. In such a situation measurement of the f-ratio by ^{15}N uptake and equation 1 or 2 would produce a lower than expected value even though the carbon export component is higher. The question which arises is, could a temporally integrated low f-ratio still reflect an enhanced carbon export flux ? A mechanistically based answer is proposed below.

6.4.2 The decoupling of C and N uptake: a simple model

A mechanistic insight of the factors driving remineralization is best provided by a spreadsheet model reflecting the elemental (C and N) pathways and resulting stoichiometries (Fig. 6.5) under a range of scenarios. The conceptual version of the model shows two phytoplankton boxes (G_0- G_1), linking on to further steps each of which has three fluxes associated with them; the uptake flux (U_i), the export flux (F_i) and the regeneration flux (R_i), where for each flux there is also an elemental pathway for carbon and nitrogen (Fig. 6.5). While G_0 is provided with its nitrogen requirements by the initial flux of NO_3^-, the remaining boxes (G_1 ...G_i) are supplied by remineralized flux of NH_4^+ through flux R_i. The magnitude of Ri is given by (1 - f) (King, 1987). This model is used to demonstrate, through a series of numerical scenarios, how the interaction of the C:N stoichiometries of the uptake and regeneration pathways hold the key to the observed non-Redfield values in the Benguela System and other surface ocean systems. The

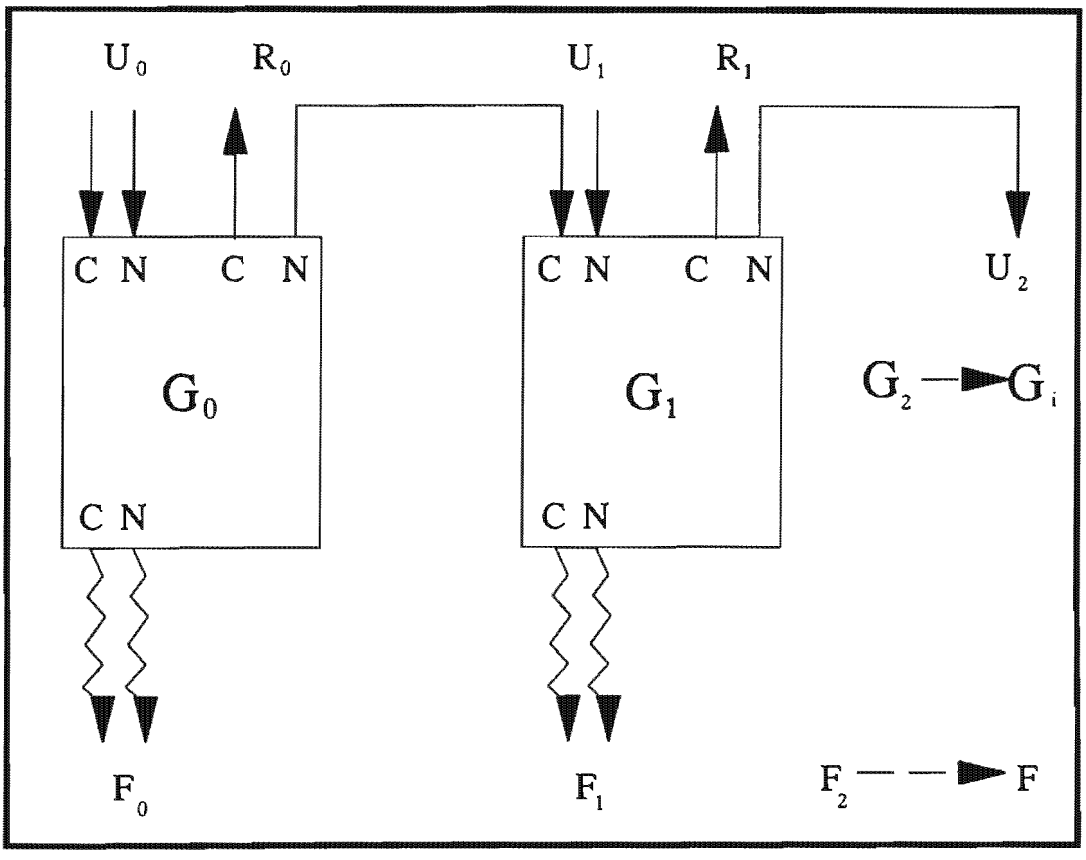

Fig. 6.5: A conceptual model illustrating the three main metabolic pathways for carbon and nitrogen associated with their sequential uptake and regeneration by a phytoplankton bloom. Each stage (Gi) has an uptake flux (Ui), an export flux (Fi) and a regeneration flux (Ri). The number of stages depends on the recycling efficiency = (1-f ratio)(see text for detailed discussion)

spreadsheet based model scenarios are depicted below with a structure which is as similar as possible to the conceptual version above (Fig. 6.5). The input parameters are at the top, the fluxes U_i, R_i and F_i are in the middle block and the export fluxes and their stoichiometry are located at the bottom (Table 6.8 - 6.10).

Scenario 1: Assumptions: f-ratio = 1.00 (Table 6.8).

This is the simplest and most artificial form of the model where the bloom G_0 grows and senesces with no remineralization occuring (Table 6.8). All the carbon (CO_2) and nitrogen (NO_3^-) fixed through U_0 is exported through flux F_0 where in both cases the C:N stoichiometry is strictly Redfield with the result that the recycle number R_0=0 and no secondary biomass compartments Gi arise. The recycling efficiency E_R and the recycling number are both 0. The output of this scenario simulates the widely used rule that the carbon export flux equals new production which in turn can be predicted by the product of the NO_3^- flux and the Rr (eq. 6.2b). A more realistic scenario has to incorporate a re-cycling component.

Scenario 2: assumptions: f-ratio = 0.3 and C:N of $U_i = R_i = 6.6$ (Table 6.9)

In this scenario a NO_3^- re-cycling component is introduced and simulated through the f-ratio of 0.3 which is close to the typical value found in the Benguela System (Probyn. 1992). There is no C:N disequilibrium between U_i and R_i and both remain constrained by the Rr. In this case E_R is 0.7 = 1 - f which in effect means that the magnitude of R_i is always 70% of Ui with the balance being lost through the export flux F_i. A spreadsheet based scenario pertaining to this example is depicted on Table (6.9). As before, the magnitude of the initial NO_3^- flux is 25.00 units and the C:N stoichiometry $Ui=R_i=6.6$. This scenario generates a series of compartments G_i (only 9 are shown) until the re-cycled flux F_i --> 0. Conceptually, these compartments

Table 6.8: Spreadsheet Model Depicting the relationship between the f ratio, C:N stoichiometry and the carbon flux out of the surface mixed layer

Scenario 1: f Ratio: 1; Ui ratio (6.6) = Ri ratio (6.6)
Result: Carbon Export (165) = Redfield New Production (25 * 6.6 = 165)

INPUT PARAMETERS

f Ratio	f	1	NR	0.00
Recycle Efficiency	ER	0	Ui ratio	6.6
Recycle Number	Nc	0.00	Ri ratio	6.6

MODEL OUTPUT

FLUXES			G0	G1	G2	G3	G4	G5	G6	G7	G8
Regeneration	Ri flux	C	0.00	0.00	0.00	0.00	0.00	0.00	0.00	0.00	0.00
		N	0.00	0.00	0.00	0.00	0.00	0.00	0.00	0.00	0.00
Uptake	Ui flux	C	165.00	0.00	0.00	0.00	0.00	0.00	0.00	0.00	0.00
		N	25.00	0.00	0.00	0.00	0.00	0.00	0.00	0.00	0.00
Export	Fi flux	C	165.00	0.00	0.00	0.00	0.00	0.00	0.00	0.00	0.00
		N	25.00	0.00	0.00	0.00	0.00	0.00	0.00	0.00	0.00
Fi flux Stoichiometry		C:N	6.60	#DIV/0!	#DIV/0!	#DIV/0!	#DIV/0!	#DIV/0!	#DIV/0!	#DIV/0!	#DIV/0!

SUMMARY OF TOTAL EXPORT FLUXES

Total Carbon Export	Sum Fi (C)	165.00
Total Nitrogen Export	Sum Fi (N)	25.00

Table 6.9: Spreadsheet Model Depicting the relationship between the f ratio, C:N stoichiometry and the carbon flux out of the surface mixed layer

Scenario 2: f Ratio: 0.3; Ui ratio (6.6) = Ri ratio (6.6)
Result: Carbon Export (165) = Redfield New Production (25 * 6.6 = 165)

INPUT PARAMETERS

f Ratio	f	0.3	NR	2.33
Recycle Efficiency	ER	0.7	Ui ratio	6.6
Recycle Number	Nc	2.33	Ri ratio	6.6

MODEL OUTPUT

FLUXES			G0	G1	G2	G3	G4	G5	G6	G7	G8
Regeneration	Ri flux	C	115.50	80.85	56.60	39.62	27.73	19.41	13.59	9.51	6.66
		N	17.50	12.25	8.58	6.00	4.20	2.94	2.06	1.44	1.01
Uptake	Ui flux	C	165.00	115.50	80.85	56.60	39.62	27.73	19.41	13.59	9.51
		N	25.00	17.50	12.25	8.58	6.00	4.20	2.94	2.06	1.44
Export	Fi flux	C	49.50	34.65	24.26	16.98	11.88	8.32	5.82	4.08	2.85
		N	7.50	5.25	3.68	2.57	1.80	1.26	0.88	0.62	0.43
Fi flux Stoichiometry		C:N	6.60	6.60	6.60	6.60	6.60	6.60	6.60	6.60	6.60

SUMMARY OF TOTAL EXPORT FLUXES

Total Carbon Export	Sum Fi (C)	164.94
Total Nitrogen Export	Sum Fi (N)	24.99

Table 6.10: **Spreadsheet Model Depicting the relationship between the f ratio, C:N stoichiometry and the carbon flux out of the surface mixed layer**

Scenario 3: f Ratio: 0.3; Ui ratio (6.6) > Ri ratio (3.5)
Result: Carbon Export (345.7) > Redfield New Production (25 * 6.6 = 165)

INPUT PARAMETERS

f Ratio	f	0.3	N_R	2.33
Recycle Efficiency	ER	0.7	Ui ratio	6.6
Recycle Number	Nc	2.33	Ri ratio	3.5

MODEL OUTPUT

FLUXES			G0	G1	G2	G3	G4	G5	G6	G7	G8
Regeneration	Ri flux	C	61.25	42.88	30.01	21.01	14.71	10.29	7.21	5.04	3.53
		N	17.50	12.25	8.58	6.00	4.20	2.94	2.06	1.44	1.01
Uptake	Ui flux	C	165.00	115.50	80.85	56.60	39.62	27.73	19.41	13.59	9.51
		N	25.00	17.50	12.25	8.58	6.00	4.20	2.94	2.06	1.44
Export	Fi flux	C	103.75	72.63	50.84	35.59	24.91	17.44	12.21	8.54	5.98
		N	7.50	5.25	3.68	2.57	1.80	1.26	0.88	0.62	0.43
Fi flux Stoichiometry		C:N	13.83	13.83	13.83	13.83	13.83	13.83	13.83	13.83	13.83

SUMMARY OF TOTAL EXPORT FLUXES

Total Carbon Export	Sum Fi (C)	345.70
Total Nitrogen Export	Sum Fi (N)	24.99

should not be equated to a series of blooms but as temporal "snapshots" of the same main bloom started by the initial NO_3^- input at G_0. Each compartment partitions 70% of its C and N into R_i as CO_2 and NH_4^+ and 30% through export flux F_i. As can be seen, despite the significant remineralization mechanism (f = 0.3) this simulation provides a final result of total carbon and nitrogen export flux which still follows the basic paradigm: carbon export flux is the product of the NO_3^- flux and the Rr. The problem with this result is that the stoichiometry of the export flux and hence that of bulk $\Delta CO_2 : \Delta NO_3^-$ is still constrained by the Redfield ratio. The biogeochemical characteristics of the export flux also drive the stoichiometry of the changes in the concentrations of the bulk water parameters such as TCO_2 and NO_3^-. The Redfield stoichiometry from this model scenario still does not reflect results from this and other studies (Sambrotto *et al.*, 1993) where the stoichiometry of the changes in TCO_2 and NO_3^- in the surface layer are of the order of double the R_r (13.3 - 16.6). This inconsistency indicates that mechanistically the scenario 2 simulation is still inadequate. The problem lies with the assumption that the C:N stoichiometries of U_i and R_i equal R_r. A C:N disequilibrium between U_i and R_i is necessary to generate and F_i with the C:N stoichiometry which is consistent with observations.

Scenario 3: assumptions: f-ratio = 0.3 and U_i = 6.6 ; R_i = 3.5

This scenario is identical to the previous one except on one detail: there is a stoichiometric disequilibrium between the uptake U_i and regeneration R_i fluxes (Table 6.10). The uptake is still constrained by the rule that it is governed by the physiological needs of the cell which are well simulated by the Redfield ratio (Redfield *et al.*, 1963). The remineralization stoichiometry is set to that which characterizes protein and amino acids (~ 3.5) which are suggested to be the most heterotrophically labile fraction of phytoplankton cellular matter. Such a stoichiometric disequilibrium between U_i and R_i resulted in a final simulation of the export flux stoichiometry which is now

close to that which has been observed in both the Benguela System and elsewhere (C:N = 13.83). From the carbon export flux perspective the most important result is that the magnitude of the flux is much larger (346 units cf 165 units for scenario 2) than that which was modelled by the straight application of the Rr driven export flux paradigm (scenarios 1 and 2). The carbon export flux is defined by the product of the NO_3^- input flux and the C:N stoichiometry of the export flux or alternatively, the C:N stoichiometry of the concentration changes to the bulk water components ΔTCO_2 and ΔNO_3^-.

In this case: C export = 25 * 13.83 = 345.75

These last two scenarios (2 and 3) are suggested to provide the upper and lower boundaries of carbon export from a marine system such as the Benguela. Besides providing a framework from which to study the mechanics of carbon fluxes, this type of modelling shows how important relatively poorly understood foodweb eco-physiological dynamics of are in governing the predictability of both conceptual and numerical models. This applies not only to the stoichiometric relationships but also to the nature of the export flux: that is whether the nitrogen depleted carbon is exported into the POC or DOC pools (Sambrotto *et al.*, 1993; Toggweiler, 1993).

This is the area of greatest uncertainty in the field of CO_2 biogeochemistry where both the magnitude of the DOC reservoir and its kinetics are still the subject of much speculation (Hedges, 1992). While the model scenario 3 predicts that there should be a nitrogen depleted export flux it cannot specify any criteria to quantitatively partition this flux into the POC and DOC pools. The relative importance of this partitioning is the subject of an ongoing debate which is tending to a consensus as DOC methodological uncertainties are removed (Ducklow, 1995; Williams, 1995).

6.4.3 Partitioning of carbon export flux into POC and DOC fluxes.

In the earliest published discussion on the topic, (Sambrotto *et al.*, 1993) proposed that the way to reconcile the observed non-Redfield character of TCO_2 - NO_3^- (ΔCO_2: ΔNO_3^- ~ 8-10) net removal from the surface layer was by invoking a particle export flux similarly depleted in nitrogen. This was justified by the elevated C:N = 8.8 ratios of particulates collected at 100m in one of the sampled areas (Bransfield Str). Although Sambrotto *et al.* 1993 did suggest that DOC could play a role in their observations they concluded that this was not sufficient to account for the changes. This view was criticised by Toggweiler, 1993 on the basis that there is globally little evidence that the C:N ratios of particles collected in sediment traps are significantly higher than the Redfield ratio. This was supported by most particle flux studies (Copin-Montegut and Copin-Montegut, 1983; Anderson and Sarmiento, 1994). However, Toggweiler 1993 does not dispute the view that the carbon is indeed being channelled to a nitrogen depleted pool of organic matter as was predicted by the box model above and the Sambrotto *et al.*, . (1993) data. His suggestion is that in view of the lack of convincing evidence from sediment traps, that such a reservoir of N depleted organic matter cannot be sinking and must therefore be channelled into the domain of DOC/DON. The study and understanding of DOC/DON dynamics in the ocean is the "Achilles heel" of marine biogeochemistry largely due to the combined effects of the amorphous structure of DOM and methodological uncertainties in recent times (Duursma and Dawson, 1981; Hedges, 1992). These issues make it difficult to unambiguously constrain the role of DOC as a carbon sink. The recent consensus that earlier methods were providing reliable data has however, lead to a re-assessment of their use in the context of carbon budgeting. A recent investigation of four historical data sets comprising measurements in the 4 main pools of carbon in the ocean (Williams, 1995) has lent very strong support to the Toggweiler, 1993 view that the nitrogen depleted pool is indeed in the dissolved and not the particulate fraction. This re-working of the historical data showed two essential points:

- That despite short term variability, the magnitudes of the changes to the POC and DOC pools were comparable
- The C:N stoichiometry of DOM is highly variable but mostly > 2 * Rr.

It appears that there is a strong seasonality to the variation in the magnitude of the DOC/DON pools (Williams, 1995). Typically, from the spring to the end of summer there is a build up of the DOC pool because, it is suggested, phytoplankton outcompete bacteria in sequestering recycled nitrogen (Blight *et al.*, 1995; Williams, 1995). With the drop in irradiance and weakening of stratification in the winter, bacteria gain the advantage and are able to metabolize the accumulated DOC in the surface layer. In a later follow up study which looked at food web dynamics linked to changes in DOC / POC pools (Blight *et al.*, 1995), it was shown that low molecular weight DOC compounds derived mainly from phytoplankton exudates were metabolised in a time scale of hours - days. In contrast, higher molecular weight compounds derived from micro and meso zooplankton grazing were metabolized in a time scale of weeks (Blight *et al.*, 1995). No mention was made of a third, and from a perspective of CO_2 export, perhaps the most important mechanism: the formation of heterotrophically resistant macromolecules of humic and fulvic acids (Duursma and Dawson, 1981). The long term carbon export potential of the DOC pool rests with the rates of formation of heterotrophically resistant DOC associated with the third option.

The interaction of these mechanisms has major implications for the CO_2 source - sink behaviour of a system such as the Benguela where DOC may be the single most important but at present, unquantified carbon reservoir. It becomes critical to know what proportion of the seasonal accumulation of DOC is not metabolised but gets exported out of the system as refractory material unavailable to heterotrophic activity. This also represents the fraction of new production which is not available to the foodweb. The natural formation of refractory DOM such as humic and fulvic acids has been the

subject of intense interest over the past 30 years but the basics of the mechanisms and their rates remain elusive (Duursma and Dawson, 1981). In view of the magnitude of the DOM reservoir which is 10 times larger than the POM and our lack of insight into its mechanics and temporal dynamics there is an urgent need to make this the focus of future work in upwelling systems.

The spreadsheet model scenario simulations above and the field data from studies (Williams, 1995) emphasise that some care has to be exercised in the use of the f-ratio to predict the carbon export flux. The box model simulations show that there are two realistic possibilities where the same f-ratio has quite different implications for the carbon export flux.

In the first instance (model scenario 2), the low f-ratio (0.3) occurs with a net export flux stoichiometry unchanged relative to the Redfield ratio. This scenario is interpreted to correspond with a situation where the f-ratio truly reflects the fraction of total production which is exported. That is the f-ratio is low because of the relatively high turnover rates of regenerated production associated with small cells which do not contribute to the export flux. Both the export and regenerated uptake dynamics stay close to the Redfield ratio. This is in effect the type of ideal scenario which is assumed to pervade the global ocean and allow predictions of carbon export based on either the NO_3^- flux or the f-ratio and total net production (eqs. 6.2a and 6.2b).

In the second, instance (model scenario 3), the simulation is close to that which is observed in the central and southern sectors of the Benguela System as well as other surface ocean system: that is the f-ratio is low (0.3) but the C:N stoichiometry of the net export flux is larger than the Redfield ratio. Here the f-ratio is low because a proportion of the new NO_3^- is being remineralized but instead of it being consumed by the pico/nanno plankton which drive regenerated production, it is re-utilized by the same bloom to generate more biomass and most importantly a larger carbon export flux. The carbon flux reflects its combined export as POC and DOC.

Several points arise from the foregoing discussion which have implications for the modelling of carbon fluxes.

- Inspite of the apparent importance of the DOC export pathway, there appears to be no evidence to dismiss the paradigm that the particulate carbon (POC) export flux can be predicted from the product of NO_3^- supply rate and the Rr (eq. 6.2b). In fact, sediment trap data support this view (Anderson and Sarmiento, 1994). If this is correct then, it allows the total magnitude of the DOC component to be calculated by difference as follows:

Total export (POC + DOC)		$E_T = NO_3^- * C:N$	eq. 6.4a
Export	POC	$E_P = NO_3^- * R_r$	eq. 6.4b
Export	DOC	$E_D = E_T - E_P$	eq. 6.4c

(where C:N > Rr). If C:N = Rr then DOC = 0

- If the particulate flux stoichiometry remains constrained by the Rr, overall C:N stoichiometry can only be measured from changes to the bulk CO_2 and NO_3^- concentrations. These bulk measurements should become part of the standardized parameters provided in the course of biological production measurements in the surface layer. In so doing a fuller description of the production and export fluxes is obtained which also integrates temporal variability.

- In scenario 3 the f-ratio is low not because it reflects the predicted partitioning of carbon into new and regenerated production, but because the new NO_3^- is being remineralized as NH_4^+ and re-utilized by the same cells that were taking up the upwelled NO_3^-: ie: NH_4^+ is sustaining new production. Such an f-ratio cannot be used to calculate new production from a concomitant value of total net production (P_T) because it would underestimate the new production term. It is suggested that in similar

scenarios where a *low f-ratio is accompanied by a high C:N stoichiometry* for the *bulk CO_2 and NO_3^- concentration change,* that the f-ratio is defined as follows:

$$f_{CN} = f * [C:N]_{obs} / R_r \qquad \text{eq. 6.5}$$

In terms of these definitions (eq.1 and eq. 5) the f and f_{CN} ratios have ecologically explicit significance.

The interesting outcome of these expressions is that the carbon export flux (E_F) cannot be defined as one number given by either eqs. 6.6a or eq. 6.6b:

$$E_F = f * P_T \qquad \text{eq. 6.6a}$$
$$E_F = f_{CN} * P_T \qquad \text{eq. 6.6b}$$

Rather, it is constrained to somewhere between that which is predicted by the standard assumptions of scenario 2 (C:N = Rr) (eq. 6.6a) which provides the lower boundary and those predicated by scenario 3 (C:N > Rr) (eq. 6.6b) which provides the upper boundary. How close the CO_2 export is to one or the other ultimately depends on the extent and kinetics of oxidation of the DOC pool. This is the subject of a detailed treatment in the modelling Chapter 7.

6.4.4 The C_{Org}: C_{Ing} stoichiometry of carbon fluxes:

Following on the above discussion which emphasised the important role played by C:N stoichiometry in driving CO_2 uptake and export the role of the C_{Org}: C_{Ing} stoichiometry on PCO_2 change in the Benguela System is disappointingly small. All vector plots showed that the stoichiometry of NTAcy : NTAlk were larger than 10 implying that changes in NTAlk driven by the

biologically controlled deposition of $CaCO_3$ was insignificant in the time scales of sampling.

There was direct observational evidence for the presence of coccolithophorids in water samples collected at the inshore sectors of both the Henties Bay and the Hondeklip Bay transects (Giraudeau, 1992; Giraudeau and Bailey, 1995). However, given present estimates of the carbon fixed by coccolithophores it can be shown that the observed standing stocks ($100\text{-}400*10^3$ cells/l) would not have impacted on the NTAlk. The most recent published values for the carbon content associated with coccolithophores indicate that the average values are 0.5pg carbon / coccolith and that coccolithophore cells have a range of 20-50 coccoliths / cell (Fernandez *et al.*, 1993). Given that the standing stocks ranged from $100*10^3$ - $400*10^3$ cells / l the estimated change to NTAlk is 0.25 - 1 μM based on 30 coccoliths /cell) which is below the detection limit of existing methodology on total alkalinity.

This result has to be reconciled with the observation that $CaCO_3$ is not only the largest carbon component but the single largest of any biogeochemical sediment component in the Benguela System (Rogers and Bremner, 1991). Only in a very restricted area close to shore does $CaCO_3$ contribution to the sediment composition drop to 5% but in contrast over at least 75% of the shelf and slope the $CaCO_3$ contribution is above 50% (Rogers and Bremner, 1991). In much of the inshore areas it is diluted by both terrigenous inputs from the Orange and Olifants rivers as well as siliceous diatom frustules (Rogers and Bremner, 1991). One of the major shortcoming in our present understanding of $CaCO_3$ biogeochemistry in the Benguela System is the lack of a quantitative assessment of whether $CaCO_3$ in the sediments originates from surface coccolithophore production or sub-surface / benthic foraminiferal activity. Resolving this issue would certainly go some way to assessing whether coccolithophores play an underrated role in the transport of carbon to the sediments. The only qualitative study on the distribution of

coccolithophores shows them to be widely distributed but with an increasing proportion of the total $CaCO_3$ towards the outer shelf (Giraudeau, pers.com.).

Coccolithophores could play an important long term role as a carbon export pathway despite very low contribution to surface production because of the system being almost completely supersaturated with respect to calcite. This could occur despite the fact that $CaCO_3$ deposition results potentially in an increase of PCO_2 (Robertson *et al.*, 1994). However, field observations show that, for coccolithophores, the concomitant photosynthesis takes up the resulting CO_2 with a stoichiometry of 1:1 (Robertson *et al.*, 1994; Sikes and Fabry, 1994). In such a scenario coccolithophore blooms would not change the PCO_2 but would still export carbon as $CaCO_3$. Literature based evidence for the frequency of coccolithophore bloom observations indicate that the frequency increases during periods of reduced upwelling wind stress (Mitchell-Innes and Winter, 1987). As was shown earlier the variability in upwelling wind stress has both seasonal and inter annual components (see Chapter 4). Coccolithophores are likely to be best adapted to the stratified quiescent conditions which develop in extended breaks between upwelling events which are typical of the late summer in both the northern and southern Benguela sectors. Being small with very low sinking rates (Honjo, 1976), coccolithophores are likely to be best adapted to seeding through the fugitive strategy which characterizes dinoflagellates (Hutchings *et al.*, 1995). This adaptive strategy predicts that their abundance or bloom frequency would be highest in the northern and southern extremes of the Benguela System where seasonal variations of equatorward wind stress are most pronounced as well as during El Nino periods (Shannon and Nelson, 1996). The largest bloom in the southern Benguela was observed in a period when both seasonal and El Nino conditions coincided (Mitchell-Innes and Winter, 1987).

On the basis of these observations it is suggested that the role of coccolithophores in carbon fluxes in the Benguela System is almost insignificant in the short term. However, because the system is

supersaturated with respect to calcite there is an ongoing accumulation of coccolithophore derived $CaCO_3$ in the sediments which is likely to be of importance in long term. This aspect of the phytoplankton ecology in the Benguela System needs to be addressed in a more coherent way combining:

- remote sensing for spatial and temporal coverage (Groom and Holligan, 1987; Balch and Byrne, 1994) which could be included into a SeaWifs programme.
- ground truth measurements with cell counts and water column carbonate measurements particularly during the most likely bloom period : late summer.
- greater focus on the $CaCO_3$ composition of sediments where the relative contribution by coccoliths needs to be quantified.

Chapter 7

7. Carbon Fluxes in the Benguela System: A Box Model Approach

7.1 Background

The physical and biogeochemical mechanisms which drive carbon fluxes in the various stages of the upwelling cycle of the Benguela System have been addressed in some detail in the foregoing chapters. The results and discussion in Chapters 4, 5 and 6 had two goals; firstly, to assess the extent to which the field data from this study are consistent with existing physical and biogeochemical models of the Benguela System and secondly, where appropriate, to create new ideas or hypotheses. The combined body of existing and new conceptual models were used to define the set of assumptions which underpin the carbon flux box model for the Benguela System. The box model is therefore a synthesis of this study in that its assumptions synthesise our understanding of key processes which drive carbon fluxes through the system. The box model is also a numerical platform from which quantitative predictions of carbon fluxes emerge. These can be expressed as hypotheses and tested through well-focused field process or monitoring studies whose results provide an indication of how well the nature and dynamics of carbon fluxes in the Benguela System are understood. The numerical output not only addresses the core hypothesis of this study,

- The Benguela upwelling system is an important CO_2 sink by virtue of its high primary production and sediment organic carbon accumulation rates,

but also serves to identify gaps in our understanding and to provide an objective framework against which future sampling strategies can be designed to test its rules and predictions.

One of the key issues arising from the results in Chapter 6 was the non-Redfield character of CO_2 and NO_3^- uptake in the surface layer in both the central and southern sectors. The importance of this result to the modelling of air - sea CO_2 fluxes is that DOC production is an intrinsic result of such observed C:N disequilibria (Toggweiler, 1993; Ducklow, 1995). The resulting air -sea CO_2 flux will necessarily depend on what proportion of the DOC production is remineralized back to CO_2 and what proportion is exported out of the surface layer. As no specific measurements exist for DOC dynamics in the Benguela System the quantitative basis through for the role of DOC in the model had to be obtained from the literature.

The fate of DOC in the surface layer is largely driven by a combination of physical and biogeochemical processes such as lateral advection, downward flux driven by turbulent diffusion across the thermocline, aggregation of macro molecules - colloids into sinking particles and heterotrophically driven respiration. Thus, while the physical processes enhance the role of DOC as a CO_2 sink by shifting it away from the air - sea interface, its oxidative breakdown opposes this effect. The net role of DOC as a CO_2 sink therefore depends on the relative rates of the physical and biogeochemical processes. Recent studies have shown that the vertical downward turbulent diffusion flux of DOC can be comparable to the POC flux (Guo *et al* 1995). In the Gulf of Mexico, a calculated DOC flux ($3.6*10^{-4}$ mol C m^{-2} d^{-1}) driven by turbulent diffusion had a magnitude 44% of the measured POC flux ($8.1*10^{-4}$ mol C m^{-2} d^{-1}) (Guo *et al* 1995). There are no DOC profiles for the Benguela System but, as will be shown below, the modelled magnitudes of DOC and POC production fluxes are comparable in both the central and southern sectors. This suggests that in parts of the system physically driven export of DOC from the surface layer may as important as POC export fluxes. There are no data

to verify this suggestion so it has to be left as an hypothesis which can be tested in future work on the Benguela System.

A number of approaches have been adopted recently to understand and quantitatively model biogeochemically driven DOC dynamics in the surface ocean. A detailed 3 year time series study from the Menai Straits (Blight *et al* 1995) suggested that the phasing of primary production and bacterioplankton respiration was governed by the nature of the substrate (DOM) made available by phytoplankton to bacteria. Specifically, while low molecular weight (LMW) substrates (bloom exudates) could lead to a phasing time scale of hours - days, high molecular weight (HMW) substrates (senescence and grazing waste) delayed the phasing to a time scale of weeks - months (Blight *et al* 1995). The phasing period is important because the longer it is the greater the relative impact of physical export pathways. The study showed that in general, diatom blooms couple more effectively to grazer foodwebs resulting in smaller and delayed community respiration than phaeocystis blooms (Blight *et al* 1995). In the Benguela System regeneration pathways are important particularly in the southern sector where activity of the microbial loop is elevated (Probyn, 1987; Brink *et al* 1995; Hutchings *et al* 1995). It is therefore expected that LMW DOC production will also be correspondingly high. This leads to an intriguing potential relationship between f-ratio, LMW - HMW DOC production and foodweb dynamics. This is expressed as an hypothesis which will need to be tested by a directed field programme:

- Phytoplankton blooms with a high f-ratio (dominated by new production) produce a larger proportion of HMW DOC which maximizes magnitude of the physically driven (turbulent mixing) export of DOC. This enhances the role of DOC as a carbon export flux contributing to the potential of the Benguela System as a CO_2 sink.

Curiously, although the focus of the Menai study was to establish a mechanistic link between phytoplankton and bacterial activity through the

nature of DOM, there were no concurrent DOC data to support the hypothetical pathways and their time scales. However, the conceptual model appears to be internally consistent and forms a useful basis for an approach to DOC work linked to plankton dynamics in the Benguela System. Another recent study on the dynamics of DOC in coastal environments (Gulf of Mexico and Mid - Atlantic Bight) (Guo *et al.*,1995), where changes in concentrations of three molecular weight ranges (1, 3 and 10 kDa) were measured, appeared to contradict the predictions of the Menai Straits study by indicating that the larger molecular weight fraction showed a greater reactivity than the bulk DOC pool. This was concluded from the lower concentrations of HMW DOC in the water column (Guo *et al.*,1995). It is however possible that their observations could reflect a lower relative production of HMW compounds in their systems.

Studies of DOC dynamics emphasise in a mechanistic way that the proportion of labile to non-labile DOC is a useful guide to predicting its role as a part of a carbon export flux from the surface ocean. In the absence of such a bulk type relationship for the Benguela System a global one was chosen which included both coastal and open ocean samples (Sondergaard and Middelboe, 1995). The average labile DOC fraction of total DOC for marine samples was given as 19 ± 12%. *The figure used to further constrain the impact of DOC remineralization on CO_2 fluxes in the Benguela System box model was the upper limit of 30%.*

The objectives of this Chapter are:

- to use field and historical data to constrain the estimated annual CO_2 source -sink character of the Benguela System. This is done for each upwelling centre as well as for the system as whole.
- to identify key factors or potential natural perturbations which have a first order impact on the magnitude and direction of the CO_2 air - sea flux in the Benguela System.

- to validate the model outputs by critically discussing the modelled organic carbon fluxes against historical data sets.
- to assess the impact that realistic variability in each of these key factors has on the magnitude and direction of the air - sea CO_2 flux in the Benguela System.

The approach used in the development and application of the box model is:

- to define the conceptual basis for the box model: the **assumptions**
- to define the numerical basis for the box model: physical and biogeochemical **inputs** and relationships between variables.
- to execute the spreadsheet model in **two modes**:

1. **standard mode** runs in which the input is constrained by field data. Two aspects of the output from this mode are discussed in detail:

- the net annual sea - air CO_2 fluxes in the Benguela System. This output is used to address the first hypothesis of this study (see Chapter 1).
- the organic carbon fluxes in the Benguela System. This output is used to assess the extent to which model predicted new production driven carbon export fluxes converge with field results from the Benguela System.

2. **perturbation mode** where key input variables such as stoichiometry (C:N and C_{Org}: C_{Ing}) and temperature are allowed to vary. Three aspects are investigated with the output of this mode:

- the impact of a realistic variation of the remineralization and uptake C:N stoichiometry on the predicted annual air - sea CO_2 fluxes in the Benguela System
- the impact of realistic variations of the C_{Org} : C_{Ing} stoichiometry on the predicted annual air - sea CO_2 fluxes in the Benguela System
- the impact of realistic variations ($18 \pm 2^{\circ}C$) of the atmospheric equilibrium temperature on the predicted annual air - sea CO_2 fluxes in the Benguela System

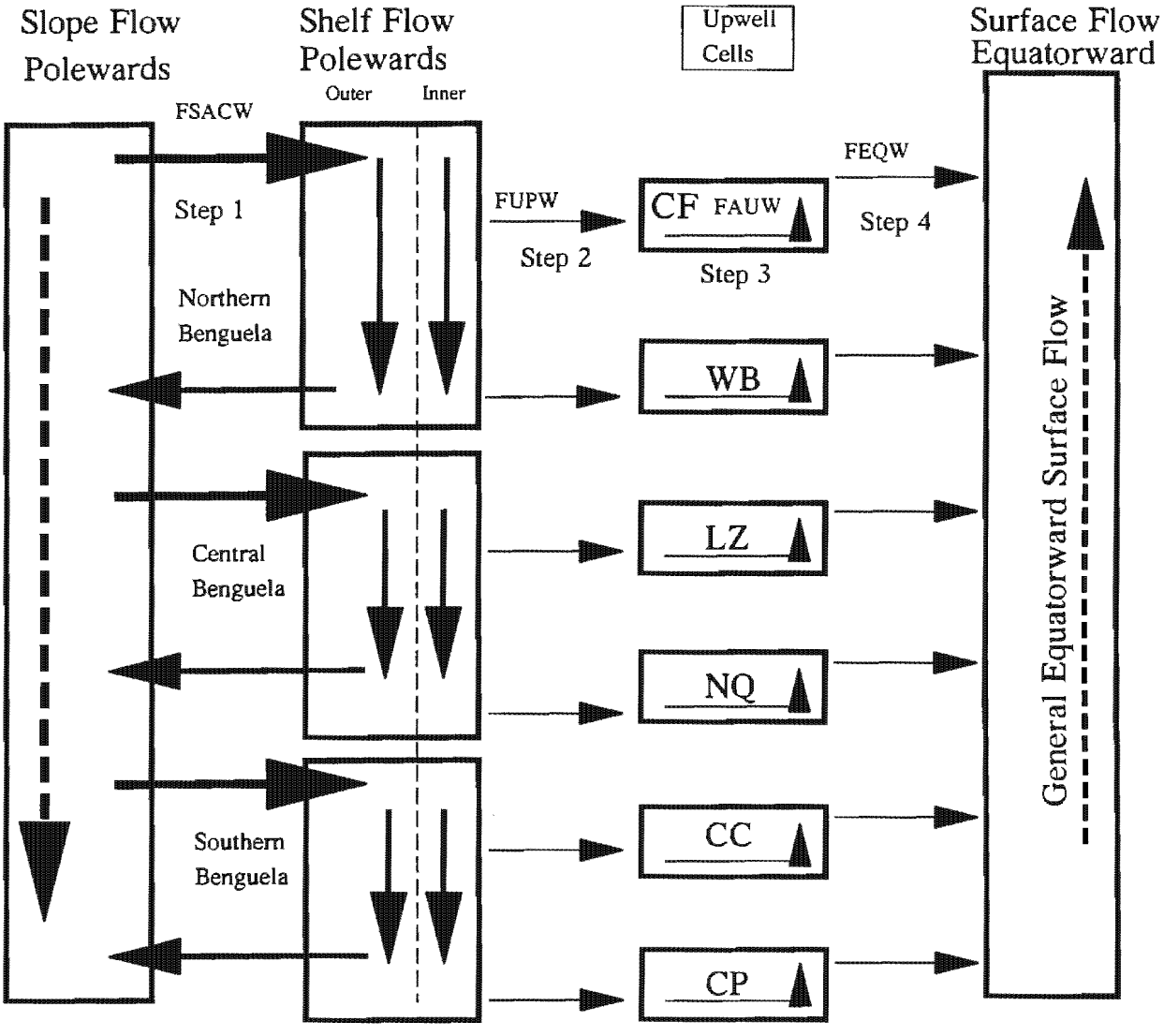

Fig. 7.1: The conceptual model of the Benguela System as formulated in terms of the "Gate Hypothesis" (see Chapter 4) which forms the basis for the advective fluxes of carbon to be quantified with the box model. It shows that South Atlantic Central Water (SACW) is advected to the surface in two steps. In step 1 it is advected onto the shelf from the slope as a flux FSACW at one of 3 "gates" which mark the northern boundary of each sector (northern, central and southern Benguela). On the shelf SACW is entrained onto the poleward flow of Inner Shelf Water (ISW) from where, in the vicinity of one of the 6 upwelling centres, it is advected to the surface in step 2 as a flux of newly upwelled water (FUPW). The surface part of the upwelling cycle is also composed of 2 steps. Step 3 is the physical and biogeochemical ageing of upwelled water as a flux FAUW associated with each upwelling centre. Aged upwelled water is finally entrained into the surface equatorward flux (FEQW) as step 4. To the north of each "gate" there is a compensatory offshore flux.

7.2 Model Assumptions

The quantitative model is constructed around the physical advective characteristics and biogeochemical stoichiometric characteristics which were formulated and discussed in earlier (see Chapters 4, 5 and 6). The key aspects of the underlying assumptions are set out below.

7.2.1 **Physical assumptions**: Advective Flux Pathways

The physical structure of the model is based on the "Gate" hypothesis which was presented in Chapter 4 and is conceptually depicted in Fig. 7.1. The key assumptions are:

1. the Benguela System is divided into 3 sectors (northern , central and southern) whose boundaries are defined by inflows of new SACW onto the shelf which define the "gates".
2. upwelling in each sector of the Benguela System is a 4 step process with 2 subsurface (1 and 2) and 2 surface steps (3 and 4): in step 1: SACW is advected from the slope and onto the shelf where in the inner shelf it becomes poleward flowing inner shelf water (ISW). In step 2: at each upwelling centre a flux (F_{UPW}), driven by equatorward wind stress, is upwelled from F_{ISW}. The box model only deals with fluxes associated with step 2 and subsequent surface fluxes, it does not quantify carbon or water fluxes associated to step 1.
3. The surface part of the upwelling cycle also has two steps: step 3: newly upwelled water which outcrops at the surface is physically aged by sun warming resulting is a flux of aged upwelled water (F_{AUW}) within the upwelling front. In this flux the temperature will typically increase from 10-12 °C to 18°C. The main post-upwelling bloom occurs in this step. In step 4 aged upwelled water feeds into the general equatorward surface flow to which it contributes a water flux F_{EQW}. For continuity in the model it is assumed that: $F_{UPW} = F_{AUW} = F_{EQW}$

4. Upwelling water fluxes ($F_{UPW} = F_{AUW} = F_{EQW}$) in this model are themselves modelled from Ekman transport model (Neumann and Pierson, 1966; see Appendix 7.1). It is assumed that the equatorward wind stress from each of the upwelling centres has a strong functional relationship with upwelling rates. This is strongly supported by a detailed study carried out at various upwelling centres by Lenz, 1992 and summarized by Smith, 1995.
5. Hourly wind records were obtained for the appropriate years (1992 and 1994) at all upwelling centres except Cape Frio. There are no continuous wind records for Cape Frio. This was overcome by making the assumption that the wind record from Luderitz was a suitable proxy for Cape Frio. The basis for this choice was that the spatial and temporal synthesis of seasonal wind characteristics in the Benguela System from Boyd, 1987 showed both Luderitz and Cape Frio to be characterized by similarly persistently strong equatorward winds (see Chapter 4). These characteristics differed from those which prevail in the vicinity of the intermediate Walvis Bay area where winds are more moderate Boyd, 1987. It is likely that the seasonality of wind strength differs between the two sites by virtue of their different latitudes but the model uses only the total annual Ekman transport which is likely to differ less significantly between the two upwelling centres.
6. it is assumed that the annual Ekman flux calculated for the 6 upwelling centres defined above (CF, WB, LZ, NQ, CC, CP; see Fig. 7.1) account for 100% of the upwelled waters which outcrop in the Benguela System.

7.2.2 **Biogeochemical assumptions:** Parameter concentrations and stoichiometry

The key assumptions which underlie the biogeochemical framework of the model are:

- the transport of dissolved components (CO_2 and NO_3^-) through the upwelling cycle is governed by physical fluxes. In this way, annual fluxes of biogeochemical components through the upwelling cycle at each

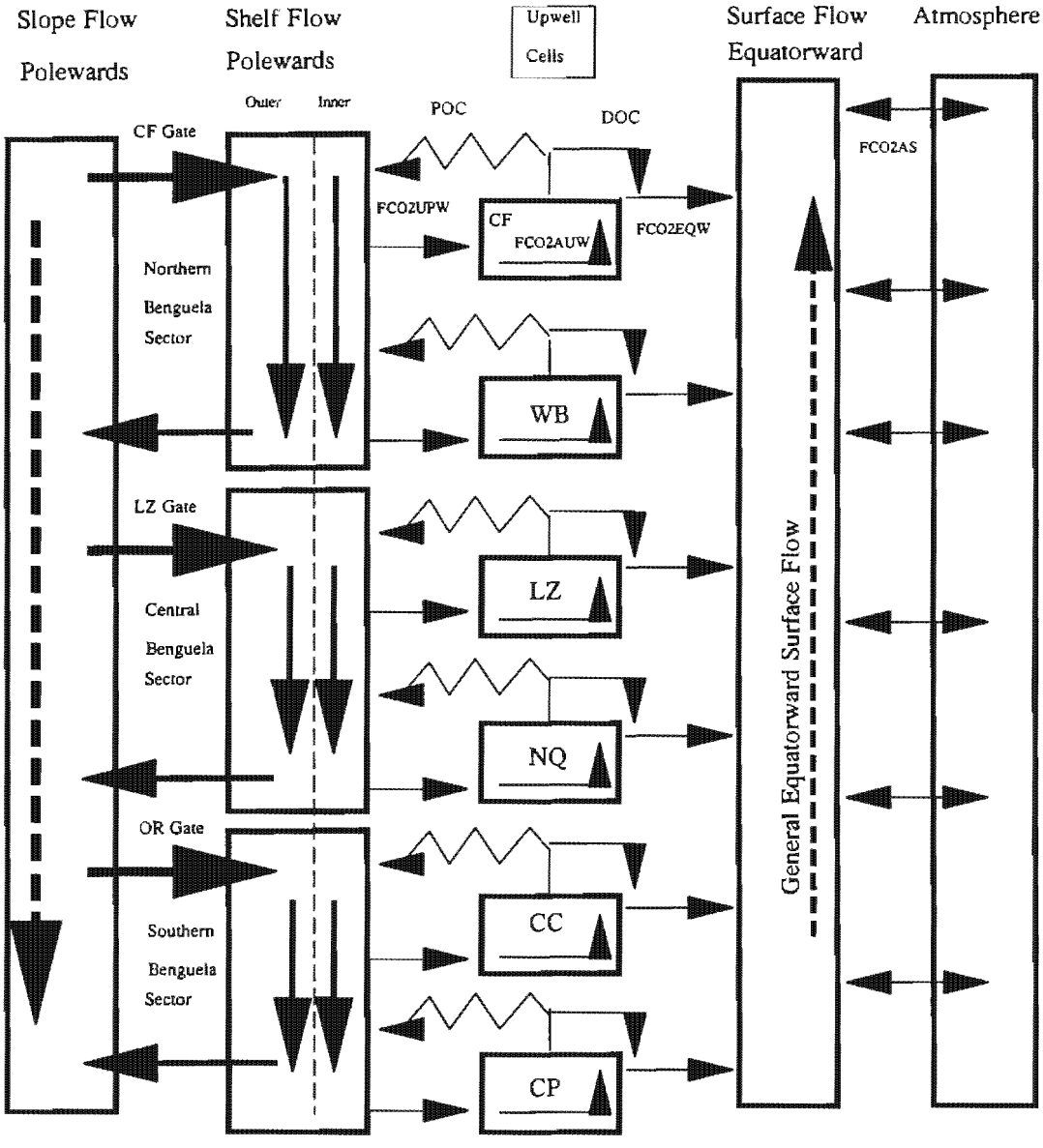

Fig. 7.2: The conceptual model of the Benguela System including the biogeochemical fluxes pathways. It shows that each physical flux has associated with it a corresponding carbon flux. For purposes of clarity only the fluxes of one upwelling cell (Cape Frio: CF) are labelled. It shows that the carbon fluxes arising from biological activity (NO_3^- driven new production)(FCO2BIO) split into two fractions: a particulate flux (POC) and a dissolved (DOC) flux. The long-term CO_2 equilibration with the atmosphere (FCO2AS) occurs as part of step 4 of the upwelling cycle.

upwelling centre are calculated from the product of the physical flux and the concentration of the chemical component (TCO_2 or NO_3^-). The extent to which the physical conceptual model for the Benguela System underpins the biogeochemical fluxes is depicted in Fig. 7.2 which shows all the carbon fluxes which will be modelled including the air - sea flux component. The fluxes are addressed in detail below under model outputs.

- the C:N stoichiometry of CO_2 and NO_3^- uptake in the surface layer can be used to quantify the partitioning of total new production into particulate (POC) and dissolved (DOC) export fluxes (see Chapter 6).
- the role of the inorganic carbon pump (C_{Ing}) in the Benguela System is insignificant but the C_{Org} : C_{Ing} stoichiometry is functionally included into the model calculations for the sake of completeness and to allow perturbation "experiments" to be conducted.
- the concentrations of CO_2 and NO_3^- from the transects are appropriate to simulate the biogeochemical characteristics of waters which upwell at the Walvis Bay (WB)(Henties Bay transect), Namaqua (NQ)(Hondeklip bay transect) and Cape Columbine (CC)(Olifants River transect) upwelling centres. For the centres for which there was no field data their biogeochemical characteristics were taken from the SACW in the respective sector's gate site (Cape Frio (CF) and Luderitz (LZ)). In the case of Cape Peninsula (CP) its characteristics were set to be identical to Cape Columbine. The biogeochemical boundary conditions are therefore set by the characteristics of the appropriate SACW and ISW.
- Atmospheric pCO_2 was set to the constant value of 360µatm.

7.3 Model Inputs and Outputs

The calculation of carbon fluxes F_{CO2} (mostly defined as 10^6 tons C y^{-1}) is done with the generic expression (eq. 7.1) of the water flux, Ekman transport F_W (m^3y^{-1}), and the total dissolved carbon concentration TCO_2 (g C m^{-3}).

$$F_{CO2} = F_W * TCO_2 \qquad \text{eq. 7.1}$$

This expression defines the two of the three critical inputs for the box model: the water flux, modelled using Ekman transport driven by equatorward wind stress (Neumann and Pierson, 1966), and carbon and nitrogen concentrations. The third input type are the stoichiometric relationships (C:N and C_{Org} : C_{Ing}) which are important not only to predict the partitioning of the new production into POC and DOC fluxes but also allow the model to be run on the basis of NO_3^- concentration changes and carbon (TAcy and TAlk) inputs only at boundary conditions. These physical and biogeochemical inputs are now examined in more detail.

7.3.1 **Physical Inputs:** Equatorward Wind Driven Ekman Transport

The magnitude of carbon fluxes in a coastal upwelling system such as the Benguela is strongly dependent on rates at which the NO_3^- rich sub-surface shelf waters (~ 20mmolm^{-3} in the Benguela System) are advected into the euphotic zone (Chapman and Shannon, 1985). This vertical water flux is in turn driven by synoptic scale equatorward wind forcing (Shannon and Nelson, 1996). The integrated annual upwelling at any one particular upwelling centre is a function of not only the strength but also the frequency and persistence of equatorward wind events (Nelson, pers.com.). Equatorward wind stress in the Benguela System has three main scales of variability (Shannon and Nelson, 1996):

- the synoptic scale is driven by the frequency of low pressure systems in the South Atlantic Ocean which modulate the upwelling intensity. This variability is particularly pronounced in the southern half of the system.
- the seasonal variability is governed by the meridional shifts of the South Atlantic High.

- the interannual variability is largely driven by the impact of El Nino Southern Oscillation (ENSO) events on the spatial and temporal characteristics of pressure gradients in the South East Atlantic.

For the purposes of this study only the total annual upwelling rates are of concern. The temporal resolution of the box model is low by virtue of the nature of the biogeochemical data which does not provide any temporal component. However, the synoptic scale dynamics are integrated into the calculated annual upwelling flux through the Ekman transport model (Neumann and Pierson, 1966; G. Nelson, Pers.Com.). At each of the 6 main upwelling cells the annual upwelling rates were derived by integrating the Ekman transport over four calendar quarters from hourly wind records. Although this approach provides some insight into the seasonal (quarterly) dynamics of upwelling, only the total annual figure is used to calculate carbon fluxes. The annual figure is realistic in that it incorporates not only the short-term synoptic variability but the also the seasonal signal. The longer term interannual variability is addressed by comparing two annual data sets which reflect ENSO and non-ENSO conditions. The potential impact of interannual variability was addressed by calculating Ekman transport at all 6 main upwelling centres in two years when winds in the Benguela System was modulated by ENSO (1992) or non ENSO (1994) conditions (Anon., 1993, 1994).

The Ekman transport associated with each wind record was calculated using the relationships between Ekman transport, wind stress and Coriolis force whose theoretical basis is described in detail by Neumann and Pierson, 1966 (see Appendix 7.1).

The results of this calculation series and further numerical treatment to derive total Ekman transport at the 6 chosen upwelling centres are summarized in Tables 7.1 and 7.2 for 1992 and 1994 respectively. Each upwelling centre has 4 entries referring to each quarter of the year. Each upwelling centre also

Ekman Fluxes at the main upwelling centres of the Benguela						1992														
Centre		Lat	Length (m)	F Coriolis	Factor	Quarter	Model Output (Quarter)	Upwell Time	Quarter Time	Upwell Time %	Ekman Flux Specific/Q	Ekman Flux Specific/Q	Ekman Flux Specific/Y	Ekman Flux (Total/Q)	Ekman Flux (Total/Y)	Quarter upwell rates	Annual upwell rates /cell	Annual upwell rates /sector	Sector %	Annual upwell rates Total
			m	s-1	kgm-3s		m2s-1	(hours)	(hours)		Kg/m/Q	m3/m/Q	m3/m/y	m3/Q	m3/y	Sv	Sv	Sv		Sv
Cape Frio	CF	18	5.00E+04	4.494E-05	35.29	1	137607.4	1977	2184	91	1.748E+10	1.70E+07	4.68E+07	8.52E+11	2.34E+12	1.08E-01	2.96E-01			
		18	5.00E+04	4.494E-05	35.29	2	64086.5	1956	2184	90	8.141E+09	7.93E+06		3.97E+11		5.05E-02				
		18	5.00E+04	4.494E-05	35.29	3	59544.3	1935	2208	88	7.564E+09	7.37E+06		3.69E+11		4.64E-02				
		18	5.00E+04	4.494E-05	35.29	4	116584.9	1992	2208	90	1.481E+10	1.44E+07		7.22E+11		9.08E-02				
Walvis	WB	22.5	1.00E+05	5.566E-05	28.49	1	22061.2	1915	2184	88	2.263E+09	2.21E+06	1.93E+07	2.21E+11	1.93E+12	2.81E-02	2.44E-01	5.40E-01	39	
		22.5	1.00E+05	5.566E-05	28.49	2	41223.9	1934	2184	89	4.229E+09	4.12E+06		4.12E+11		5.24E-02				
		22.5	1.00E+05	5.566E-05	28.49	3	66236.2	1992	2208	90	6.795E+09	6.62E+06		6.62E+11		8.33E-02				
		22.5	1.00E+05	5.566E-05	28.49	4	63436.8	1917	2208	87	6.507E+09	6.34E+06		6.34E+11		7.98E-02				
Luderitz	LZ	27	1.80E+05	6.603E-05	24.02	1	137607.4	1977	2184	91	1.19E+10	1.16E+07	3.18E+07	2.09E+12	5.73E+12	2.66E-01	7.25E-01			
		27	1.80E+05	6.603E-05	24.02	2	64086.5	1956	2184	90	5.542E+09	5.40E+06		9.72E+11		1.24E-01				
		27	1.80E+05	6.603E-05	24.02	3	59544.3	1935	2208	88	5.149E+09	5.02E+06		9.03E+11		1.14E-01				
		27	1.80E+05	6.603E-05	24.02	4	116584.9	1992	2208	90	1.008E+10	9.83E+06		1.77E+12		2.22E-01				
Namaqua	NQ	30	6.00E+04	7.272E-05	21.81	1	12318	1727	2184	79	967118648	9.43E+05	3.13E+06	5.66E+10	1.88E+11	7.19E-03	2.37E-02	7.49E-01	54	
		30	6.00E+04	7.272E-05	21.81	2	7278	1574	2184	72	571414964	5.57E+05		3.34E+10		4.25E-03				
		30	6.00E+04	7.272E-05	21.81	3	9144	1670	2208	76	717919542	7.00E+05		4.20E+10		5.28E-03				
		30	6.00E+04	7.272E-05	21.81	4	12110	1790	2208	81	950788020	9.27E+05		5.56E+10		6.99E-03				
Columbine	CC	33	3.50E+04	7.921E-05	20.02	1	83038.2	1864	2184	85	5.985E+09	5.83E+06	1.30E+07	2.04E+11	4.55E+11	2.60E-02	5.76E-02			
		33	3.50E+04	7.921E-05	20.02	2	16936.8	1390	2184	64	1.221E+09	1.19E+06		4.16E+10		5.30E-03				
		33	3.50E+04	7.921E-05	20.02	3	25768.5	1495	2208	68	1.857E+09	1.81E+06		6.34E+10		7.97E-03				
		33	3.50E+04	7.921E-05	20.02	4	59323.8	1812	2208	82	4.276E+09	4.17E+06		1.46E+11		1.84E-02				
Cape Point	CP	34.5	2.50E+04	8.238E-05	19.25	1	86482.9	1826	2184	84	5.994E+09	5.84E+06	1.35E+07	1.46E+11	3.38E+11	1.86E-02	4.28E-02	1.00E-01	7	1.39E+00
		34.5	2.50E+04	8.238E-05	19.25	2	8158.3	861	2184	39	565433072	5.51E+05		1.38E+10		1.75E-03				
		34.5	2.50E+04	8.238E-05	19.25	3	25092.9	1071	2208	49	1.739E+09	1.70E+06		4.24E+10		5.33E-03				
		34.5	2.50E+04	8.238E-05	19.25	4	80518	1496	2208	68	5.581E+09	5.44E+06		1.36E+11		1.71E-02				

Table 7.1: The Ekman fluxes calculated for each of the 6 upwelling centres of the Benguela System with the 1992 hourly wind data from the respective upwelling centres. The only exception was Cape Frio which got the wind record from Luderitz as a proxy for its own. Quarterly values were computed for each upwelling centre and added up to determine the annual fluxes. The Length column refers to the length of coastline (m) at the base of each upwelling centre. These values were used to calculate Total Ekman Fluxes from the Specific Ekman Fluxes which which are expressed as per metre of coastline. The upwelling rates are expressed as Svedrups (Sv).

Ekman Fluxes at the main upwelling centres of the Benguela						1994														
Centre		Lat	Length (m)	F Coriolis	Factor	Quarter	Model Output (Quarter)	Upwell Time	Quarter Time	Upwell Time %	Ekman Flux Specific/Q	Ekman Flux Specific/Q	Ekman Flux Specific/y	Ekman Flux (Total/Q)	Ekman Flux (Total/Y)	Quarter upwell rates	Annual upwell rates /cell	Annual upwell rates /sector	Sector %	Annual upwell rates Total
			m	s-1	kgm-3s		m2s-1	(hours)	(hours)		Kg/m/Q	m3/m/Q	m3/m/y	m3/Q	m3/y	Sv	Sv	Sv		Sv
Cape Frio	CF	18	5.00E+04	4.494E-05	35.29	1	77794	2040	2184	93	9.883E+09	9.63E+06	3.02E+07	4.82E+11	1.51E+12	6.13E-02	1.91E-01			
		18	5.00E+04	4.494E-05	35.29	2	46185.2	2009	2184	92	6.121E+09	5.97E+06		2.98E+11		3.79E-02				
		18	5.00E+04	4.494E-05	35.29	3	40249	1801	2208	82	5.113E+09	4.98E+06		2.49E+11		3.13E-02				
		18	5.00E+04	4.494E-05	35.29	4	77794	2040	2208	92	9.883E+09	9.63E+06		4.82E+11		6.06E-02				
Walvis	WB	22.5	1.00E+05	5.566E-05	28.49	1	35055.2	1536	2184	70	3.596E+09	3.50E+06	1.98E+07	3.50E+11	1.98E+12	4.46E-02	2.50E-01	4.41E-01	40	
		22.5	1.00E+05	5.566E-05	28.49	2	60234.6	2112	2184	97	6.179E+09	6.02E+06		6.02E+11		7.66E-02				
		22.5	1.00E+05	5.566E-05	28.49	3	51147.9	1941	2208	88	5.247E+09	5.11E+06		5.11E+11		6.43E-02				
		22.5	1.00E+05	5.566E-05	28.49	4	51147.9	1941	2208	88	5.247E+09	5.11E+06		5.11E+11		6.43E-02				
Luderitz	LZ	27	1.80E+05	6.603E-05	24.02	1	77794	2040	2184	93	6.727E+09	6.56E+06	2.06E+07	1.18E+12	3.70E+12	1.50E-01	4.68E-01			
		27	1.80E+05	6.603E-05	24.02	2	46185.2	2009	2184	92	4.167E+09	4.06E+06		7.31E+11		9.30E-02				
		27	1.80E+05	6.603E-05	24.02	3	40249	1801	2208	82	3.48E+09	3.39E+06		6.11E+11		7.68E-02				
		27	1.80E+05	6.603E-05	24.02	4	77794	2040	2208	92	6.727E+09	6.56E+06		1.18E+12		1.48E-01				
Namaqua	NQ	30	6.00E+04	7.272E-05	21.81	1	43129.2	1727	2184	79	3.386E+09	3.30E+06	6.40E+06	1.98E+11	3.84E+11	2.52E-02	4.86E-02	5.17E-01	47	
		30	6.00E+04	7.272E-05	21.81	2	8000	1574	2184	72	628101087	6.12E+05		3.67E+10		4.67E-03				
		30	6.00E+04	7.272E-05	21.81	3	10595.3	1670	2208	76	831864931	8.11E+05		4.86E+10		6.12E-03				
		30	6.00E+04	7.272E-05	21.81	4	21863.7	1790	2208	81	1.717E+09	1.67E+06		1.00E+11		1.26E-02				
Columbine	CC	33	3.50E+04	7.921E-05	20.02	1	118053	1798	2184	82	8.509E+09	8.29E+06	2.12E+07	2.90E+11	7.40E+11	3.69E-02	9.36E-02			
		33	3.50E+04	7.921E-05	20.02	2	29417.8	1344	2184	62	2.12E+09	2.07E+06		7.23E+10		9.20E-03				
		33	3.50E+04	7.921E-05	20.02	3	41351.7	1449	2208	66	2.981E+09	2.91E+06		1.02E+11		1.28E-02				
		33	3.50E+04	7.921E-05	20.02	4	112243.4	1812	2208	82	8.09E+09	7.89E+06		2.76E+11		3.47E-02				
Cape Point	CP	34.5	2.50E+04	8.238E-05	19.25	1	125195	1939	2184	89	8.677E+09	8.46E+06	1.73E+07	2.11E+11	4.31E+11	2.69E-02	5.46E-02	1.48E-01	13	1.11E+00
		34.5	2.50E+04	8.238E-05	19.25	2	23611	1185	2184	54	1.636E+09	1.59E+06		3.99E+10		5.07E-03				
		34.5	2.50E+04	8.238E-05	19.25	3	32772	1312	2208	59	2.271E+09	2.21E+06		5.53E+10		6.96E-03				
		34.5	2.50E+04	8.238E-05	19.25	4	73822	1765	2208	80	5.116E+09	4.99E+06		1.25E+11		1.57E-02				

Table 7.2: The Ekman fluxes calculated for each of the 6 upwelling centres of the Benguela System with the 1994 hourly wind data from the respective upwelling centres. The only exception was Cape Frio which got the wind record from Luderitz as a proxy for its own. Quarterly values were computed for each upwelling centre and added up to determine the annual fluxes. The Length column refers to the length of coastline (m) at the base of each upwelling centre. These values were used to calculate Total Ekman Fluxes from the Specific Ekman Fluxes which which are expressed as per metre of coastline. The upwelling rates are expressed as Svedrups (Sv).

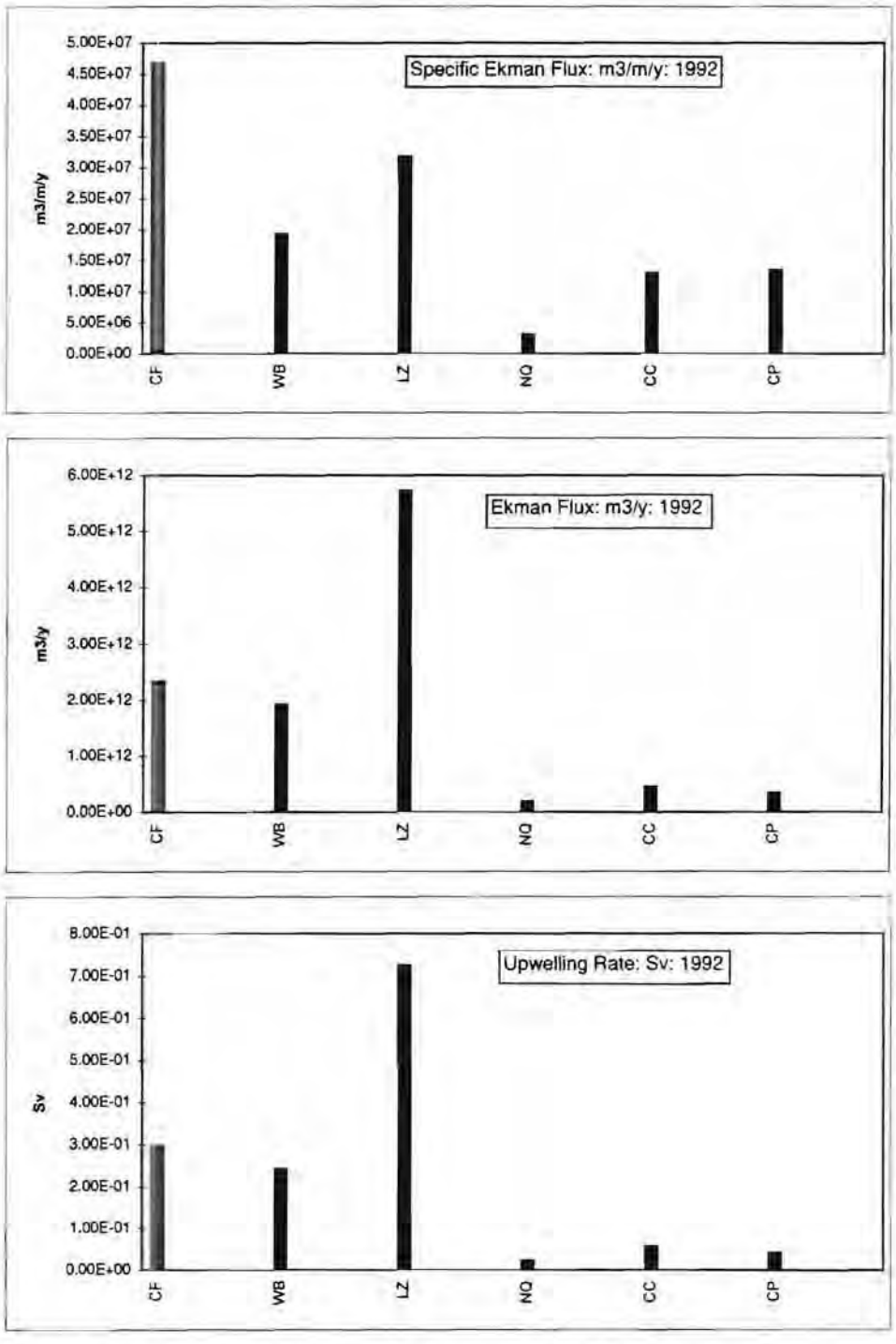

Fig. 7.3: Plots of the computed Ekman fluxes at each of the 6 upwelling centres. The Specific Ekman Flux (Fig. 7.3a) is a measure of relative wind transport and shows that, in 1992, there was a visible difference in wind transport between the three northerly centres (CF, WB and LZ) and the southerly group (NQ, CC and CP). This difference is accentuated when the actual Ekman flux (including the upwelling base length scale) is computed Figs. 7.3b and 7.3c. The upwelling flux at the Luderitz centre is the largest. This indicates that during ENSO conditions sharp differences in upwelling flux result between the northern and southern halves of the Benguela System.

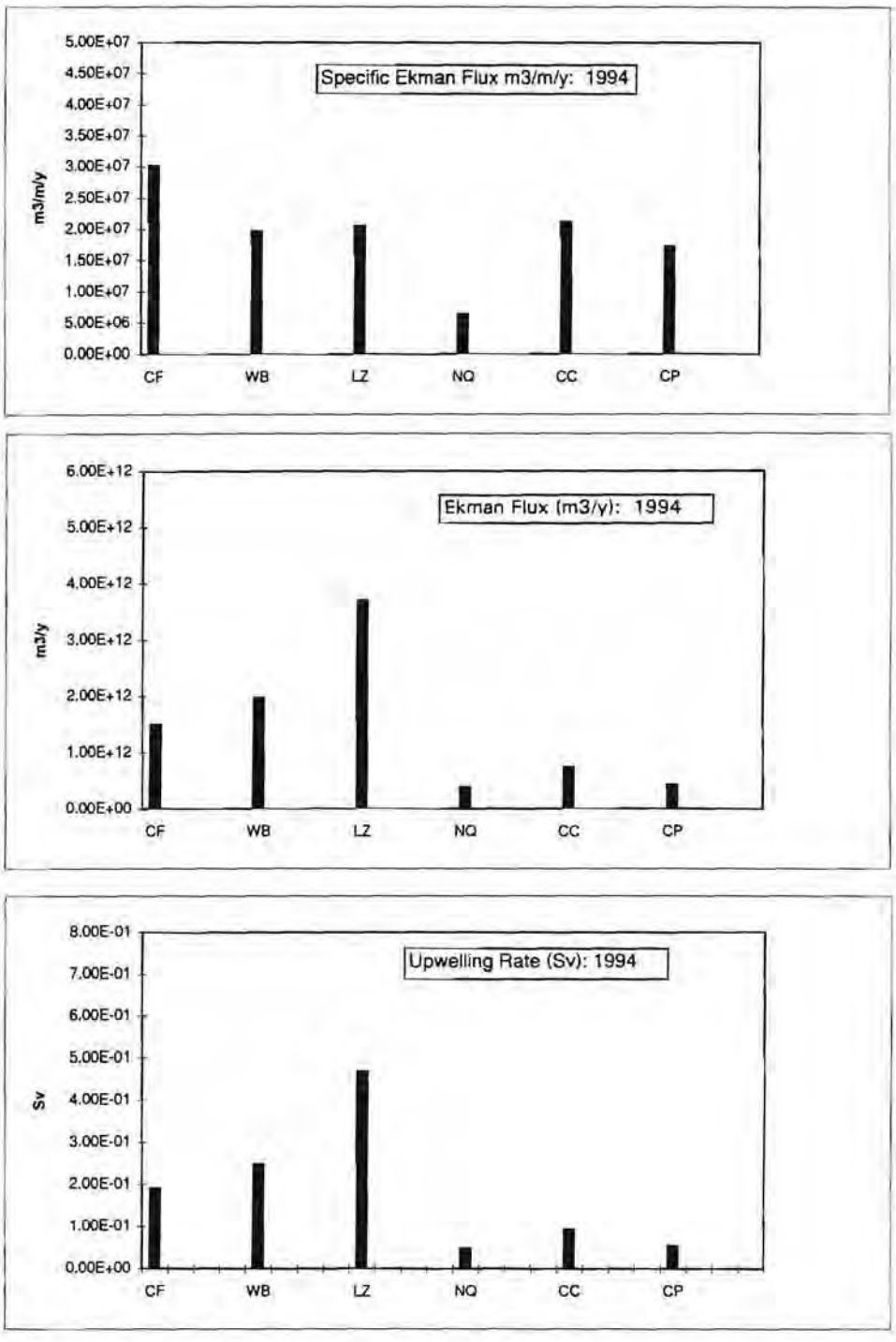

Fig. 7.4: Plots of the computed Ekman fluxes at each of the 6 upwelling centres. The Specific Ekman Flux (Fig. 7.4a) is a measure of relative wind transport and shows that, in 1994, with the exception of the Namaqua centre (NQ), there were small differences in the total annual wind. Once the coastline length factor is included, major differences in upwelling fluxes (Figs.7.4b, 7.4c) become apparent with Luderitz being the dominant source of upwelled water. These plots show that meridional differences are lessened in non-ENSO conditions. cf. Figs. 7.3a, 7.3b and 7.3c.

has an appropriate latitude (Lat), an upwelling coast length (Length m), Coriolis term (F) and a Factor which refers to the $C_D\rho_{air}/f$ term of eq.(A.3 in the appendix). The air drag coefficient of 0.0013 for the Benguela System was obtained from (Kamstra, 1985), ρ_{air} value was 1.22 kgm^{-3} and the Coriolis parameter value was defined for each centre according to its latitude. The integrated quarterly output from the Ekman model (Model Output) is shown with the total time (hours) of active upwelling, the total time (hours) of the particular quarter and an informative percentage upwelling time (Tables 7.1 and 7.2). The calculated Ekman flux is then shown in a variety of numerical formats of which the Annual Specific Ekman flux ($m^3m^{-1}y^{-1}$), Total Ekman flux (m^3y^{-1}) and Upwelling Rates (Sv) are the most important. Included are also percentage contribution by each of the three sectors to the total upwelling rate in the Benguela System.

The three Ekman transport formats defined above were calculated for the 6 upwelling centres and are depicted for both 1992 and 1994 in Figs. 7.3a-c, 7.4a-c. The specific Ekman transport per metre of coastline plots depict relative wind activity in so far as the magnitudes are proportional to V^2. The lower two plots depict total Ekman transport volume at each centre as a total annual value (m^3y^{-1}) and as a rate ($m^3s^{-1}*10^{-6}$ or Sv). These incorporate the coastline length term. The following features should be noted:

Firstly, in the case of the specific Ekman transport ($m^3m^{-1}y^{-1}$) (Figs. 7.3a and 7.4a) there is a noticeable contrast between the total upwelling wind activity in the northern (CF, WB and LZ) and the southern (NQ, CC and CP) halves of the Benguela System. This contrast is particularly marked in 1992 when the Benguela was reflecting the effects of a general ENSO event (Shannon and Nelson, 1996).

Under these conditions the summer southward excursion of the South Atlantic high pressure system is limited which has the dual effect of decreasing total equatorward wind stress in the southern Benguela System while at the same

time increasing it in the northern sectors. The net effect is enhancement of the meridional differences in the system. In contrast, during 1994 when normal non-ENSO conditions had returned the total activity in the northern half decreased while in both the NQ and CP centres it increased. The lower than expected activity at CC is attributed to a localized but as yet unexplained shutoff of equatoward wind stress earlier than expected in February 1994 (J. Taunton-Clark, pers.com.). The impact of this potential bias on the non-ENSO upwelling rates was investigated by using the 1980 (a peak non-ENSO year in the Benguela System) CC wind data to calculate Ekman transport rates. The total Ekman transport at CC was recalculated to be 60% higher than the 1992 when ENSO conditions predominated. The impact of this difference is small because of the small contribution by the southern sector to the total upwelling (see sector % in Tables 7.1 and 7.2). However, its effect on carbon fluxes is quantified in the discussion on the model outputs.

Secondly, the real differences in upwelling between the northern and southern halves of the Benguela System become apparent when the respective lengths of coastline are included to calculate total upwelling fluxes (Figs. 7.3b,c and 7.4b,c). The respective coastline lengths were defined as the distance over which the inner shelf and coastline were relatively straight to allow the development of stable upwelling (G. Nelson, pers.com.). Here, not only does the well- described dominance of the Luderitz cell becomes evident but the meridional contrast increases. The contrast between the sectors is emphasised by the percentage breakdown of the upwelling fluxes between the 3 sectors of the Benguela System (Tables 7.1 and 7.2). The southern Benguela, whether defined as part of a 3- or 2-sector system, is a minor contributor to the total upwelling flux. This sensitivity to the chosen length of coastline raises the question whether the criterion used to determine the length of coastline is acceptable. The best test of the robustness of this approach is a comparison of the calculated upwelling flux at Luderitz (0.73 Sv in 1992 and 0.49 Sv in 1994) and the equatorward flow of upwelled derived water to the north of the same centre determined from ADCP measurements

(0.7 Sv) (Gordon et al., 1995 in Shannon and Nelson, 1996). The two approaches are in reasonable agreement indicating that the length of the base of the Luderitz upwelling cell of 180km, and hence its length criterion decided on prior to the availability of the comparative flux value, was approximately correct.

Thirdly, the total upwelling flux of 1.4 Sv in 1992 and 1.0 Sv in 1994 is significantly lower than the 3.3 Sv calculated for the Peruvian system (Wyrtki, 1963) but for a total coastline length of 1800km it provides an average of 0.5 - 0.8 Sv / 1000km which is within the global average of 0.5 - 2 Sv / 1000 km for coastal upwelling systems (Brink *et al* 1995). The total estimate upwelling rate from all coastal upwelling systems is 15 Sv (Brink *et al* 1995) and the Benguela System is estimated to contribute 7 - 10%. However, if the Benguela System were divided into the two halves (northern and southern sub-systems with the boundary between the LZ and NQ cells) which have historically been widely used, the northern half contributes 88-90% of the total. Given that upwelling rates are likely to be central to the carbon flux dynamics it is expected that measured biogeochemical parameters should reflect this meridional asymmetry. Three reported characteristics of the Benguela System reflect this asymmetry: the extent and magnitude of organic carbon accumulation in the sediments off Namibia (), the phytoplankton biomass (Brown *et al* 1991) and fish production (Hutchings. 1992).

7.3.2 **Biogeochemical Inputs:** parameter concentrations and stoichiometry

The matrix of physical and biogeochemical inputs (Model Inputs: Volumes, Concentrations and Stoichiometry) are shown on Tables 7.3a-c. Each table refers to the model inputs and outputs for a particular sector based on 1992 wind data. This 1992 matrix is only shown for descriptive purposes as the model outputs which are pertinent to the discussion below are separately summarized for each run. Each table shows the water fluxes defined earlier

grouped into 3 categories (Sub-surface Shelf Fluxes [F_{SACW}, F_{ISW}]; X Upwelling Centre and Y Upwelling Centre where X ,Y refer to the name of the upwelling centre and where each has F_{UPW}, F_{AUW}, F_{EQW} water fluxes. Each flux is fully described in terms of volume (Ekman transport), temperature, salinity and a number of carbon and nitrogen parameter concentrations and stoichiometries (Tables 7.3a-c). There are two levels of carbon and nitrogen input parameter in the spreadsheet form of the box model:

- The primary biogeochemical inputs (shaded in Table 7.3a only) are the boundary conditions (*carbon [NTAlk, NTAcy] and nitrogen [NO_3^-] parameters concentrations in SACW associated with the particular sector*). The NO_3^- concentration changes *[ΔNO_3]* between the "gate" site and upwelling cell(s) as well as the C:N and C_{Org}:C_{Ing} (Org:Ing) regeneration and uptake stoichiometries of $\Delta CO2$: ΔNO_3^- and ΔCO_2:ΔCO_3^{2-} respectively both in sub-surface and surface domains. These inputs are all values obtained from field data. From these inputs the remainder of the biogeochemical input variables, the secondary input variables, can be calculated from basic principles.
- The secondary type of biogeochemical inputs comprise those carbon and nitrogen parameter concentrations (not shaded on Tables 7.3a-c) which are necessary for the CO_2 flux calculations but are computed from the primary input values. For example, the NTACY and NTALK characteristics of F_{ISW} are calculated from the [NO_3^-], the NTACY and the NTALK of F_{SACW} as well as the ΔNO_3^-, C:N and COrg:CIng which govern the biogeochemical change between the two. Similarly, while the upwelling centre near the "gate" gets its initial biogeochemical characteristics from unmodified SACW, the mid sector upwelling centre gets the same from ISW. The fact that the secondary input values used for the 1992 and 1994 standard runs are the same as the field data is because all the primary inputs are also taken from the field data. That is, for the purposes of the standard runs the model is driven by the same field data. However, allowing the secondary variables to be computed from primary variables provides greater flexibility for the model when it

Box Model of Carbon Fluxes in the Benguela System

Sector: Northern
Run: 1992 winds; Standard Inputs

Model Inputs: Volumes, Concentrations and Stoichiometry

SUB-SURFACE SHELF FLUXES

	Upwelling Step	Flux m3/y	Temp	Sal	NO3	ΔNO3	C:N	Rr	N-Rr	Org:Ing	ΔCO2	NTAcy	ΔCO3	NTAlk	NTCO2	ATMEQ ΔNTACY	ATMEQ ΔCO2
New SACW	FSACW	5.00E+13	12.50	35	21.57	-0.12	-825			66		2519		2383	2239		
Inner Shelf Mod	FISW	4.77E+13	12.50	35	21.45						99	2717	2	2386	2339		

CAPE FRIO UPWELLING CENTRE FLUXES

	FUPW	2.34E+12	12.50	35	21.57	-21.57	6.6	6.6	6.6	66		2519		2383	2239		
	FAUW	2.34E+12	18.00	35	0						-142	2234	-2	2379	2094	-10	-5
	FEQW	2.34E+12	18.00	35	0							2244		2379	2099		

WALVIS BAY UPWELLING CENTRE FLUXES

	FUPW	1.93E+12	12.50	35	21.45	-21.45	6.6	6.6	6.6	66		2717		2386	2339		
	FAUW	1.93E+12	18.00	35	0						-142	2434	-2	2382	2196	188	94
	FEQW	1.93E+12	18.00	35	0							2246		2382	2102		

MODEL OUTPUTS: CARBON FLUXES

CARBON FLUXES	TYPE	CAPE FRIO	WALVIS BAY	TOTAL
Upwelling Flux	FCO2UPW	62.9E+6	54.2E+6	117.0E+6
Equator. Water	FCO2EQW	59.0E+6	48.7E+6	107.6E+6
Aged Water	FCO2AUW	58.8E+6	50.9E+6	109.7E+6
Biological Flux	FCO2BIO TOC	-4.0E+6	-3.3E+6	-7.3E+6
	POC	-4.0E+6	-3.3E+6	-7.3E+6
	DOC	000.0E+0	000.0E+0	000.0E+0
Air-Sea Flux	FCO2AS	-136.5E+3	2.2E+6	2.0E+6

Notes:
Inputs: Concentrations
All concentration units: mmolm-3

Outputs: Carbon Fluxes
Units: tons C / y
(-)ve sign => CO2 ingassing flux: Air ---> Sea

Table 7.3a A spreadsheet display of the box model showing the inputs (water fluxes, parameter concentrations and stoichiometry) and the outputs (carbon fluxes) for the northern sector (Cape Frio: CF and Walvis Bay: WB). The upwelled water fluxes were generated from the 1992 wind data (see Table 7.1). All other runs are displayed as a table of outputs only. The definitions for each of the input and output variables can be found in Tables 7.4 and 7.5.

FSACW	Flux of South Atlantic Central Water (Step 1)
FISW	Flux of Inner Shelf Water
FUPW	Flux of Newly Upwelled Water (Step 2)
FAUW	Flux of Aged Upwelled Water (Step 3)
FEQW	Flux of Equatorward Water (Step 4)
FCO2UPW	CO2 flux in Newly Upwelled Water
FCO2AUW	CO2 flux in Aged upwelled Water
FCO2EQW	CO2 flux in Equatorward water
FCO2BIO	CO2 fixed by the new production as POC and DOC
FCO2AS	Net Air - sea flux of CO2

Box Model of Carbon Fluxes in the Benguela System

Sector: Central
Run: 1982 winds; Standard Inputs

Model Inputs: Volumes, Concentrations and Stoichiometry

SUB-SURFACE SHELF FLUXES

	Upwellin Step	Flux m3/y	Temp	Sal	NO3	ΔNO3	C:N	Rr	N-Rr	Org:Ing	ΔCO2	NTAcy	ΔCO3	NTAlk	NTCO2	ATMEQ ΔNTACY	ATMEQ ΔCO2
New SACW	FSACW	5.00E+13	10.00	35	13.67	6.41	41.19			-56		2480		2413	2234		
Inner Shelf Mod	FISMW	4.43E+13	10.00	35	20.08						264	3008	-5	2404	2494		

LUDERITZ UPWELLING CENTRE FLUXES

	FUPW	5.73E+12	10.00	35	13.67	-13.67	13.3	6.6	20	41		2480		2413	2234		
	FAUW	5.73E+12	18.00	35	0						-182	2116	-6	2404	2048	-143	-71
	FEQW	5.73E+12	18.00	35	0							2259		2404	2119		

NAMAQUA UPWELLING CENTRE FLUXES

	FUPW	1.88E+11	10.00	35	20.08	-20.08	13.3	6.6	20	41		3008		2404	2494		
	FAUW	1.88E+11	18.00	35	0						-267	2474	-7	2391	2220	226	113
	FEQW	1.88E+11	18.00	35	0							2248		2391	2107		

MODEL OUTPUTS: CARBON FLUXES

CARBON FLUXES		LUDERITZ	NAMAQUA	TOTAL
Upwelling Flux	FCO2UPW	153.6E+6	5.6E+6	159.3E+6
Equator. Water	FCO2EQW	145.7E+6	4.8E+6	150.5E+6
Aged Water	FCO2AUW	140.8E+6	5.0E+6	145.8E+6
Biological Flux	FCO2BIO TOC	-12.5E+6	-602.5E+3	-13.1E+6
	POC	-6.2E+6	-299.0E+3	-6.5E+6
	DOC	-6.3E+6	-303.5E+3	-6.6E+6
Air-Sea Flux	FCO2AS	-4.9E+6	254.8E+3	-4.6E+6

Notes: Inputs: Concentrations
All concentration units: mmolm-3

Outputs: Carbon Fluxes
Units: tons C / y
(-)ve sign => CO2 ingassing flux: Air —> Sea

Table 7.3b A spreadsheet display of the box model showing the inputs (water fluxes, parameter concentrations and stoichiometry) and the outputs (carbon fluxes) for the central sector (Luderitz: LZ and Namaqua NQ upwelling centres).

Box Model of Carbon Fluxes in the Benguela System

Sector: Southern
Run: 1992 winds; Standard Inputs

Model Inputs: Volumes, Concentrations and Stoichiometry

SUB-SURFACE SHELF FLUXES

	Upwellin Step	Flux m3/y	Temp	Sal	NO3	ΔNO3	C:N	Rr	N-Rr	Org:Ing	ΔCO2	NTAcy	ΔCO3	NTAlk	NTCO2	ATMEQ ΔNTACY	ATMEQ ΔCO2
New SACW	FSACW	5.00E+13	10.00	35	16.16	2.57	26.07			-12		2435		2389	2200		
Inner Shelf Mod	FISMW	4.95E+13	10.00	35	18.73						67	2569	-6	2378	2261		

CAPE COLUMBINE UPWELLING CENTRE FLUXES

	FUPW	4.55E+11	10.00	35	18.73	-18.73	16.61	6.6	26.62	60		2569		2378	2261		
	FAUW	4.55E+11	18.00	35	0						-311	1947	-5	2367	1945	-290	-145
	FEQW	4.55E+11	18.00	35	0							2237		2367	2090		

CAPE PENINSULA UPWELLING CENTRE FLUXES

	FUPW	3.38E+11	10.00	35	18.73	-18.73	16.61	6.6	26.62	60		2569		2378	2261		
	FAUW	3.38E+11	18.00	35	0						-311	1947	-5	2367	1945	-290	-145
	FEQW	3.38E+11	18.00	35	0							2237		2367	2090		

MODEL OUTPUTS: CARBON FLUXES

CARBON FLUXES	TYPE		. COLUMBIN	. PENINSUL	TOTAL
Upwelling Flux	FCO2UPW		12.3E+6	9.2E+6	21.5E+6
Aged Water	FCO2AUW		10.6E+6	7.9E+6	18.5E+6
Equator. Water	FCO2EQW		11.4E+6	8.5E+6	19.9E+6
Biological Flux	FCO2BIO	TOC	-1.7E+6	-1.3E+6	-3.0E+6
		POC	-675.0E+3	-501.4E+3	-1.2E+6
		DOC	-1.0E+6	-760.4E+3	-1.8E+6
Air-Sea Flux	FCO2AS		-792.3E+3	-588.5E+3	-1.4E+6

Notes: **Inputs: Concentrations**
All concentration units: mmolm-3

Outputs: Carbon Fluxes
Units: tons C / y
(-)ve sign => CO2 ingassing flux: Air —> Sea

Table 7.3c A spreadsheet display of the box model showing the inputs (water fluxes, parameter concentrations and stoichiometry) and the outputs (carbon fluxes) for the southern sector (Cape Columbine: CC and Cape Peninsula: CP upwelling centres).

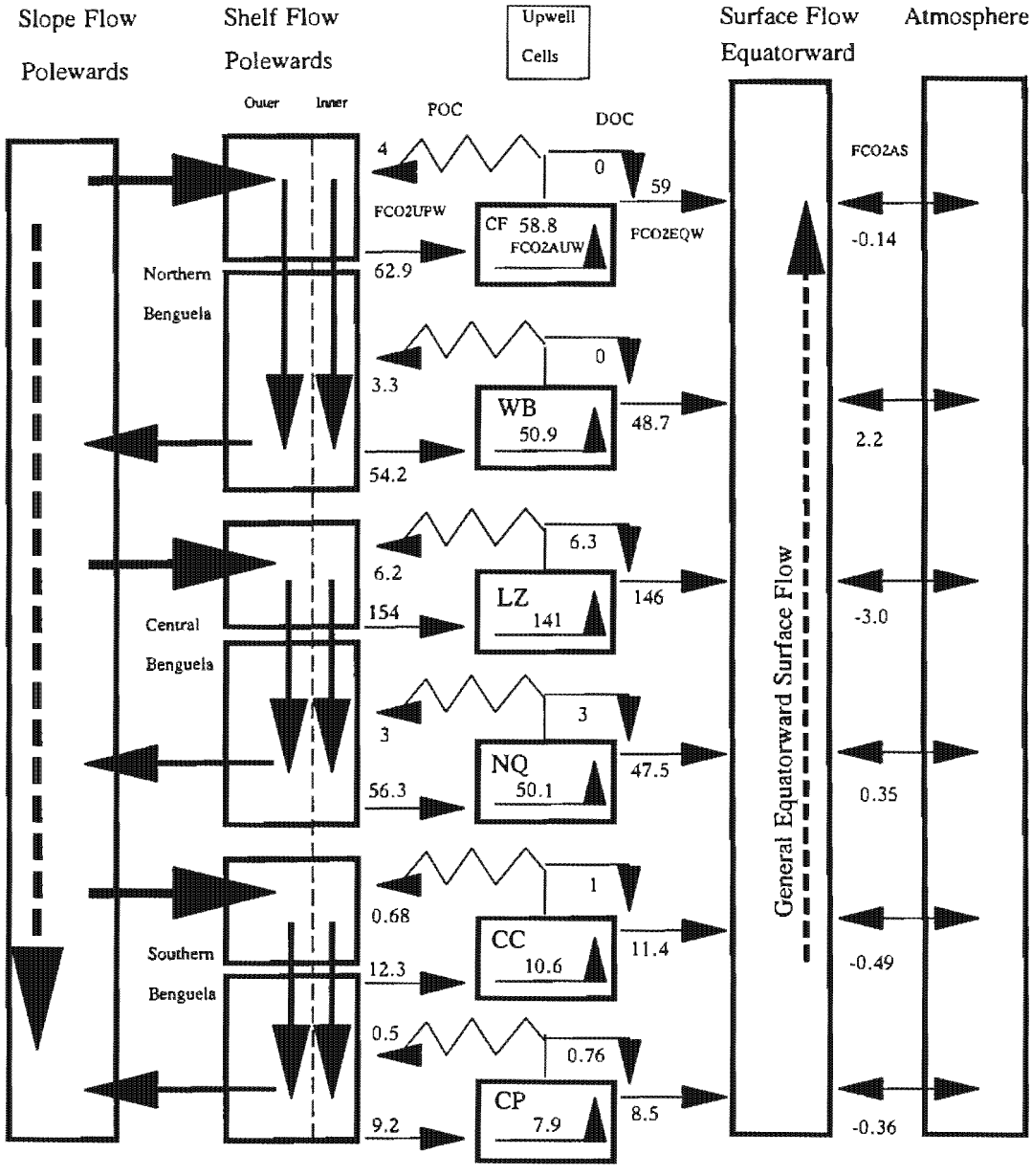

Fig. 7.5: The biogeochemical version of the conceptual Benguela system model with each of the fluxes quantified using the output from the 1992 model run whose output is summarised in Table 7.6. All the flux values are expressed in million tons of carbon / year. It shows that the carbon fluxes in the southern sector are one order of magnitude lower than those in the central and northern sectors. The fluxes associated with the Luderitz cell are in turn one order of magnitude larger than the remainder.

becomes necessary to test the sensitivity of the outputs to specific perturbations.

Table 7.4: Biogeochemical Input Variables: definitions and units

NO_3^- :	Nitrate concentration ($mmolm^{-3}$)
ΔNO_3^-	Nitrate concentration change between model compartments ($mmolm^{-3}$).
C:N	$\Delta CO2$: ΔNO_3^- stoichiometry between model compartments. Any C:N value greater than the Redfield Ratio (6.6) is divided into a Redfield (Rr) and non Redfield (N-Rr) components which have been suggested in this study to determine the partitioning of the carbon flux into POC and DOC.
Rr	Standard Redfield Ratio (= 6.6) component of the C:N value. This value determines the magnitude of the POC flux (see Table 7.5 and Chapter 6).
N-Rr	Non - Redfield Ratio component of the C:N value. This value determines the DOC flux. (N-Rr = 2 x C:N - Rr)
Org:Ing	Stoichiometry of the organic:inorganic carbon pumps and a primary variable. In the Benguela where the inorganic pump is mostly not significant the value tends to be large. It is included for completeness and to cater for the possible testing of coccolithophore driven scenarios
$\Delta CO2$	CO_2 change which is associated with a given combination of C:N and ΔNO_3^-. ($\Delta CO_2 = \Delta NO_3 * C:N$). (units $mmolm^{-3}$)
NTACY	Total Acidity for a given compartment or flux normalized to a salinity of 35psu. This value can either be a primary input variable (F_{SACW}) or a derived secondary input variable. In the latter case it can be derived as $NTACY_j = NTACY_i + 2^* \Delta[CO_2]$ as is the case for F_{ISW} and F_{AUW} or from CO_2 equilibrium model as is the case for F_{EQW}. The latter is the NTACY value which characterizes the equatorward flux in equilibrium with the atmosphere (pCO2 = 360 µatm) at the defined temperature and salinity. (Units: $mmolm^{-3}$)
ΔCO_3^{2-}	the change in CO_3^{2-} concentration between compartments in the model. It is calculated from the NTACY and Org:Ing values: $\Delta CO_3^{2-} = \Delta CO2 / Org:Ing$. Given the very low activity of the inorganic pump in the Benguela this is usually a very small number and it magnitude on the model output may be prone to apparent rounding errors even though its use in other calculations uses the real value.
NTALK	Total Alkalinity value for a given compartment normalized to a salinity of 35psu. It is a primary input variable (value for F_{SACW}), a secondary input variable where for both F_{ISW} and F_{AUW} $NTALK_j = NTALK_i + 2 * \Delta[CO_3^{2-}]$. In the case of F_{EQW} NTALK = NTALK (F_{AUW}); that it there is no change between aged upwelled water and equatorward water.
NTCO2	Total dissolved CO_2 normalized to a salinity of 35psu. In all cases the value is derived from the expression for the interrelationship between capacity parameters (see chapter 5) NTCO2 = (NTACY + NTALK - BT) / 2.
ATMEQ	The net change in NTACY when PCO_2 partial pressure in F_{AUW} (ΔNTACY) equilibrates with the atmosphere (pCO2 = 360 µatm) during the equatorward surface flow. It magnitude is given by the difference $\Delta NTACY = NTACY(F_{AUW}) - NTACY(F_{EQW})$. A negative sign implies a net ingassing from the atmosphere and vice versa for a positive value. (see NTACY definition above).
ATMEQ (ΔCO_2)	The concomitant CO_2 change which accompanies the ΔNTACY defined (ΔCO_2) above. From its original definition: $\Delta CO_2 = \Delta NTACY / 2$

7.3.3 Model Outputs: Carbon Fluxes

The model outputs are shown as a separate block in the same (Tables 7.3a-c) as the inputs and also graphically depicted in Fig. 7.5.

Table 7.5: Biogeochemical Output Variables: Carbon Flux definitions and units (all units are tons C y^{-1})

FCO2UPW:	**CO_2 upwelling flux** is the total CO_2 transported from F_{SACW} or $\{F_{ISW}\}$ to the surface by the annual Ekman flux at each upwelling centre. Its magnitude is the product of the Ekman transport volume (F_{UPW}) and the corresponding NTCO2 concentration for the appropriate upwelling centre.
FCO2BIO:	**CO_2 biological flux** is the portion of the upwelled carbon flux which is taken up by the NO_3^- driven new primary production at a particular upwelling centre. The total organic carbon (TOC) component can be partitioned into two fractions of particulate organic carbon (POC) and dissolved organic carbon (DOC). The TOC component is calculated from the product of TOC = NO_3^- * C:N. That is the NO_3^- concentration taken up from newly upwelled waters (usually the final NO_3^- is 0) and the C:N ratio which for a particular upwelling centre characterises the relative uptake of CO_2 and NO_3^- after newly upwelled waters outcrop. The POC fraction is defined according to the rules suggested in Chapter 6; POC = NO_3^- * Rr ; The product of the total NO_3^- uptake and the Redfield Ratio (6.6) which follows the standard definition of new production. The DOC fraction which has a nitrogen depleted character given by the stoichiometry N-Rr is calculated as the difference between TOC and POC.
FCO2AUW	**CO_2 flux in aged upwelled water** is the total dissolved CO_2 remaining in the surface waters after the main post upwelling blooms by which time the temperature has also equilibrated to approximately 18°C typical of the Benguela System. The magnitude of this flux is given by the product: $F_{CO2AUW} = F_{AUW}$ * $NTCO_2$: which is the Ekman volume flux and the total dissolved CO_2 remaining in AUW after the TOC fraction has been removed.
FCO2EQW	**CO_2 flux in the equatorward surface flow** of old upwelled waters is given by the product: FCO2EQW = F_{EQW} * NTCO2 : that is the equatorward flux from a particular upwelling centre and its total dissolved CO_2 after it has equilibrated with atmospheric pCO_2 which in this modelling study is taken to be 360µatm where the water temperature was 18°C and the salinity 35psu.
FCO2AS	The **CO_2 flux across the Air - Sea boundary** is given by the difference FCO2AS = FCO2AUW - FCO2EQW. That is, if the final post bloom value of CO_2 in aged upwelled waters (FCO2AUW) is lower than that for the same waters equilibrated with atmospheric CO_2 (FCO2EQW) then the net CO_2 flux will be ingassing to a magnitude given by the difference. The reverse is also true. In this model the negative sign for FCO2AS implies an ingassing flux and a positive sign implies an outgassing flux.

These comprise the modelled magnitudes of the carbon fluxes at each step of the upwelling cycle: F_{CO2UPW} (step 2), F_{CO2AUW} (step 3) and F_{CO2EQW} (step 4) Fig. 7.5. It also includes the biologically driven (F_{CO2BIO}) organic carbon flux which generates the TOC flux which is in turn partitioned (by the C:N stoichiometry) into POC and DOC fluxes. Most importantly, the air - sea CO_2 flux (F_{CO2AS}) arises as the net result of all physical and biogeochemical processes which drive the changes to PCO_2 in upwelled waters until they reach thermal equilibrium with the atmosphere. The carbon flux outputs computed from the 1992 model run (Tables 7.3a-c) are shown in Fig. 7.5 to emphasise the link between the fluxes and the conceptual view of the pathways. The definitions and computations which give rise to these outputs are presented in more detail in Table 7.5.

In the section below the model results are discussed in detail with a view to addressing the three initial hypotheses and providing new insights into carbon biogeochemistry in the Benguela System. This is done in two parts: the first part the runs are constrained by real data with a view to testing the first and main hypothesis of this study (see Chapter 1) as well as validating the model predictions with comparative published field data. the second part, the perturbation runs, is where the sensistivity of air - sea CO_2 fluxes to changes in key biogeochemical (stoichiometric ratios) and physical (surface layer temperature) forcing factors is quantified.

7.4 Model Results I: Standard Runs: 1992 and 1994 winds

These first two model runs aim to address the primary hypothesis of this study: that the Benguela System should be a CO_2 sink by virtue of its very high productivity rates and high levels of organic carbon in the sediments, especially on the Namibian shelf. The two model runs share the same biogeochemical inputs. These comprise primary input carbon and nitrogen parameter values obtained from the field data as represented by the 1992 run in Tables 7.3a-c. The physical inputs are calculated separately for 1992 and

1994 winds which, contrast ENSO (1992) and non-ENSO (1994) conditions in the Benguela System.

The outputs of the two runs are summarized separately in Table 7.6 for 1992 and Table 7.7 for 1994. In each output set the matrix shows the carbon fluxes (tons C y^{-1}) for each of the 3 upwelling cycle steps (upwelling flux, aged water flux and equatorward water flux), the organic carbon fluxes (TOC, POC and DOC) and the air - sea CO_2 flux. The latter is defined in three forms: the first, (CO2) represents the magnitude of the air - sea CO_2 flux if none of the DOC is re-oxidized. That is, it is the upper boundary of the flux at each upwelling centre. The second (+ DOC), is the CO_2 flux if 100% of the DOC fraction is oxidized in the surface layer making it a lower boundary for the flux magnitude. The third (+ 30% DOC) is the flux if only 30% of the DOC is oxidised. The basis and significance of this value is addressed below. Flux values are shown for each upwelling centre, for each sector and a total for the whole Benguela System. The aim of this comparison is to assess not only whether the Benguela System is a source or a sink of CO_2 but to what extent this outcome is dependent on the complete preservation or oxidation of DOC. That is, to what extent does DOC contribute to the CO_2 sink- source character of the Benguela System ?

Two aspects of the outputs are addressed in particular detail: firstly, *the air - sea CO_2 flux* which provides the basis for analysing the CO_2 source - sink character of the Benguela System and secondly, *the organic carbon fluxes* which are used to validate the output as they are the only component for which comparable historical field data exists.

7.4.1 Net air - sea CO_2 fluxes in the Benguela System

The magnitudes of the CO_2 fluxes (FCO2AS) (Tables 7.6 and 7.7) between the atmosphere and the surface layers in the Benguela System are graphically depicted in Figs. 7.6a, 7.6b for 1992 and 1994. At this stage, the plots contrast only the extreme scenarios of 0 or 100% DOC oxidation. The

Summary Output for Model Runs: **All Upwelling Cells**
Run Type: **1992 winds; Standard Inputs**

Flux	Type		CF	WB	LZ	NQ	CC	CP	Northern CF+WB	Central LZ+NQ	Southern CC+CP	TOTAL
Upwelling Flux	FCO2UPW		62.9E+6	54.2E+6	153.6E+6	5.6E+6	12.3E+6	9.2E+6	117.0E+6	159.3E+6	21.5E+6	297.8E+6
Aged Water	FCO2AUW		58.8E+6	50.9E+6	140.8E+6	5.0E+6	10.6E+6	7.9E+6	109.7E+6	145.8E+6	18.5E+6	274.0E+6
Equator. Water	FCO2EQW		59.0E+6	48.7E+6	145.7E+6	4.8E+6	11.4E+6	8.5E+6	107.6E+6	150.5E+6	19.9E+6	278.0E+6
Biological Flux	FCO2BIO	TOC	-4.0E+6	-3.3E+6	-12.5E+6	-602.5E+3	-1.7E+6	-1.3E+6	-7.3E+6	-13.1E+6	-3.0E+6	-23.3E+6
		POC	-4.0E+6	-3.3E+6	-6.2E+6	-299.0E+3	-675.0E+3	-501.4E+3	-7.3E+6	-6.5E+6	-1.2E+6	-15.0E+6
		DOC	000.0E+0	000.0E+0	-6.3E+6	-303.5E+3	-1.0E+6	-760.4E+3	000.0E+0	-6.6E+6	-1.8E+6	-8.4E+6
Air-Sea Flux	FCO2AS	No DOC	-136.5E+3	2.2E+6	-4.9E+6	254.8E+3	-792.3E+3	-588.5E+3	2.0E+6	-4.6E+6	-1.4E+6	-4.0E+6
		+DOC	-136.5E+3	2.2E+6	1.4E+6	558.4E+3	231.4E+3	171.9E+3	2.0E+6	2.0E+6	403.3E+3	4.4E+6
		+ 30% DO	-136.5E+3	2.2E+6	-3.0E+6	345.9E+3	-485.2E+3	-360.4E+3	2.0E+6	-2.7E+6	-845.6E+3	-1.5E+6

Table 7.6: Numerical summary of the model output fluxes for the 1992 model run. The carbon fluxes (tons C y-1) are shown for each upwelling cell, for each sector (northern, central and southern) as well as an overall total value (TOTAL). The three FCO2AS fluxes are: No DOC: 0% DOC remineralization, + DOC: 100% DOC remineralization and +30% DOC: 30% remineralization of DOC. Negative values imply a downward flux.

Summary Output for Model Runs: All Upwelling Cells
Run Type: 1994 winds; Standard Inputs

Flux	Type		CF	WB	LZ	NQ	CC	CP	Northern CF+WB	Central LZ+NQ	Southern CC+CP	TOTAL
Upwelling Flux	FCO2UPW		40.6E+6	55.6E+6	99.2E+6	11.5E+6	20.1E+6	11.7E+6	96.2E+6	110.7E+6	31.8E+6	238.6E+6
Aged Water	FCO2AUW		38.0E+6	52.2E+6	90.9E+6	10.2E+6	17.3E+6	10.1E+6	90.1E+6	101.2E+6	27.3E+6	218.6E+6
Equator. Water	FCO2EQW		38.0E+6	49.9E+6	94.1E+6	9.7E+6	18.6E+6	10.8E+6	88.0E+6	103.8E+6	29.4E+6	221.2E+6
Biological Flux	FCO2BIO	TOC	-2.6E+6	-3.4E+6	-8.1E+6	-1.2E+6	-2.8E+6	-1.6E+6	-5.9E+6	-9.3E+6	-4.4E+6	-19.6E+6
		POC	-2.6E+6	-3.4E+6	-4.0E+6	-610.7E+3	-1.1E+6	-639.4E+3	-5.9E+6	-4.6E+6	-1.7E+6	-12.3E+6
		DOC	000.0E+0	000.0E+0	-4.1E+6	-619.9E+3	-1.7E+6	-969.7E+3	000.0E+0	-4.7E+6	-2.6E+6	-7.3E+6
Air-Sea Flux	FCO2AS	No DOC	-88.1E+3	2.2E+6	-3.2E+6	520.5E+3	-1.3E+6	-750.5E+3	2.1E+6	-2.6E+6	-2.0E+6	-2.5E+6
		+DOC	-88.1E+3	2.2E+6	900.3E+3	1.1E+6	376.4E+3	219.2E+3	2.1E+6	2.0E+6	595.6E+3	4.8E+6
		+ 30% DO	-88.1E+3	2.2E+6	-1.9E+6	706.5E+3	-789.1E+3	-459.6E+3	2.1E+6	-1.2E+6	-1.2E+6	-344.7E+3

Table 7.7 Numerical summary of the model output fluxes for the 1994 model run. The carbon fluxes (tons C y-1) are shown for each upwelling cell, for each sector (northern, central and southern) as well as an overall total value (TOTAL). The three FCO2AS fluxes are: No DOC: 0% DOC remineralization, + DOC: 100% DOC remineralization and +30% DOC: 30% remineralization of DOC. Negative values imply a downward flux.

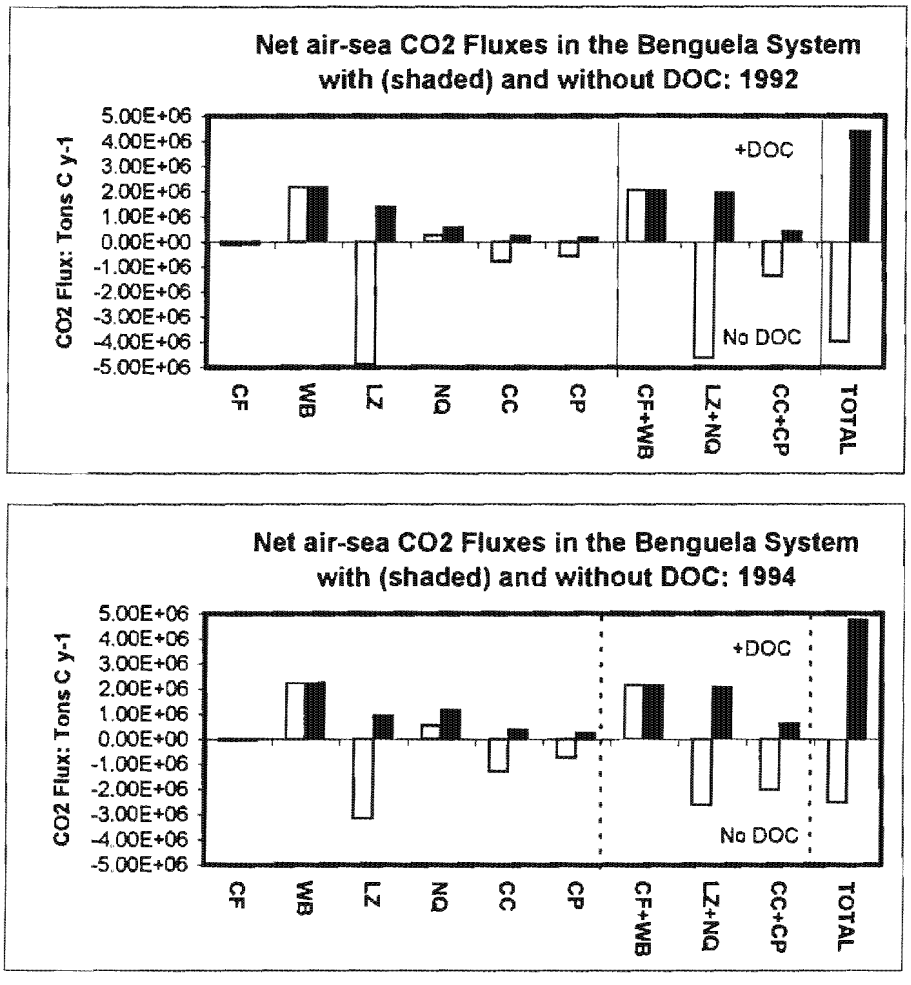

Fig. 7.6a, b: Two plots showing the net air - sea flux of CO2 in the Benguela System for the 1992 and 1994 winds. Fluxes are shown at each individual upwelling centre, combined for each of the 3 sectors and as a system total (TOTAL) Two extreme scenarios are shown for each year: No DOC assumes that n of the DOC is re-oxidized to CO2 and +DOC (shaded) assumes that 100% of DOC is oxidised. It shows the extent to which DOC synthesis and oxuidation dynamics govern the CO2 source - sink behaviour of the system

following features should be noted (Figs. 7.6a, 7.6b and Tables 7.6 and 7.7):

Firstly, for both 1992 and 1994 the Benguela System as a whole (TOTAL) is a net sink of CO_2 if the potential complete oxidation of the DOC fraction is excluded (No DOC). This upper boundary magnitude of the CO_2 sink is -3.99*10^6 tons C y^{-1} and -2.54*10^6 tons C y^{-1} in 1992 and 1994 respectively. The decrease under non-ENSO conditions (1994) is unexpected because the Benguela System is seen to be windier and more productive. The decreased CO_2 ingassing flux is attributed to the decreased upwelling rates at Luderitz when, in non-ENSO conditions, the South Atlantic high pressure cell increases its southward shift during the summer. This was discussed in the context of the Ekman transport (see section on Model Inputs).

Secondly, if the opposite extreme is taken that the whole DOC fraction of production is completely oxidised to CO_2 (+ DOC) (Figs. 7.6a and 7.6b) then the system as a whole (TOTAL) becomes a net source of CO_2 with a degassing flux of 4.39*10^6 and 4.78*10^6 tons C y^{-1} in 1992 and 1994 respectively (Tables 7.6 and 7.7). This outcome is reflected by all the upwelling cells except those in the northern sector (CF and WB) where the C:N ratio of CO_2 uptake in the surface layer was 6.4 ~ 6.6 which in terms of the model would result in no DOC production. For these two cells the air - sea CO_2 fluxes with or without DOC oxidation are the same.

Thirdly, the largest single CO_2 sink in the Benguela System is the Luderitz upwelling cell (LZ) which, when DOC oxidation is excluded, accounts for 76% of the total CO_2 ingassing in 1992 (-4.9*10^6 tons C y^{-1}) and 60% (-3.2*10^6 tons C y^{-1}) in 1994. In contrast, the other CO_2 sinks located in the Southern sector (CC and CP) are an order of magnitude smaller (< 1.3*10^6 tons C y^{-1}) (Tables 7.6 and 7.7). The relative magnitude of the Luderitz sink means that the system as whole responds very sensitively to changes in the upwelling flux and biogeochemical characteristics of the Luderitz cell. This result suggests the intriguing hypothesis that, depending on the early diagenesis

kinetics of DOC, the Benguela System may be a larger CO_2 sink during ENSO years when the South Atlantic high pressure cell persists in its northerly position. This results in increased persistence of equatorward winds in the Luderitz area which through the larger Ekman flux would cause a larger CO_2 drawdown.

Fourthly, the largest and most persistent CO_2 source is the Walvis Bay (WB) upwelling cell in the northern sector. The net outgassing at this upwelling centre appears, in contrast to Luderitz, to be largely insensitive to ENSO conditions in the Benguela System. The magnitude of the 1992 CO_2 flux ($2.18*10^6$ tons C y^{-1}) is not significantly different to the 1994 value ($2.23*10^6$ tons C y^{-1}). This persistent CO_2 source reflects the impact of the benthic remineralization rates in the Namibian shelf sediments coupled with its large C:N disequilibrium (see Chapter 5). This generates a large CO_2 input into the inner shelf water without the concomitant NO_3^- required to sequestrate it at the surface. The net effect, enhanced by surface warming, is the outgassing of CO_2. The Namaqua upwelling centre is also a persistent net CO_2 source with a flux which is typically an order of magnitude smaller than the WB centre. This again reflects the meridional changes in Ekman transport (see Figs. 7.3 and 7.4). The contrast in the CO_2 source - sink character between the adjacent WB and LZ cells is a consequence of the "gate" hypothesis which predicts that they are located in different sectors because their source waters come from different input pathways.

The single most important issue arising from these model predictions is the sensitivity of the net CO_2 source - sink characteristics of the Benguela System to the diagenesis characteristics of DOC. Thus, although changes in the Ekman transport bring about interannual variability in the magnitude of the fluxes, it is the impact of the DOC which ultimately determines whether the system and its individual components are net sinks or sources. It should be noted that the role of POC in remineralization was incorporated through the benthic remineralization fluxes (Chapter 5). For this reason, it is thought that

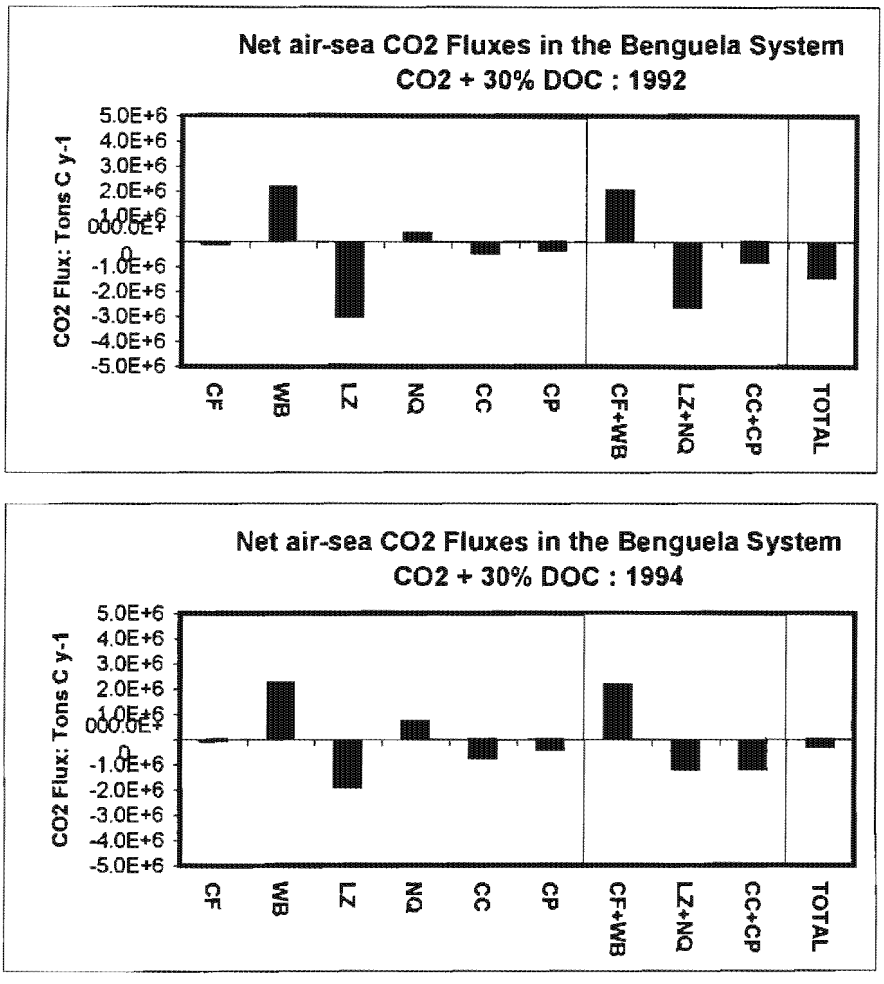

Figs. 7.7a,b: The net air - sea CO2 fluxes in the Benguela system corrected for a 30% oxidation of the DOC fraction of the organic carbon flux. It shows that the system remains a net CO2 sink in both 1992 and 1994. It emphasises the importance of the Luderitz upwelling cell in offsetting the CO2 source character of the Walvis Bay centre.

these extreme scenarios on the potential role of DOC need to be constrained further to provide a more realistic estimate of their impact on CO_2 fluxes. The estimated range of the CO_2 source - sink variability in the Benguela System ($\pm$ $4*10^6$ tons C y^{-1}) provided by the model has to be narrowed by making use of existing insights into the diagenesis of DOC in the ocean. This was done by applying the ocean average of 30% remineralization of DOC as being a first order estimate of the proportion of DOC which is oxidised to CO_2 (Sondergaard and Middelboe, 1995).

The box model output was recalculated using this value and the graphic output is depicted in Figs. 7.7a and 7.7b for the 1992 and 1994 runs. The numerical magnitudes are shown in Tables 7.6 and 7.7. The net effect on the Benguela System as a whole (TOTAL) was to maintain a net CO_2 sink of $1.47*10^6$ tons C y^{-1} in 1992 and $0.35*10^6$ tons C y^{-1} in 1994. In both years there is a coherence in the net CO_2 fluxes within each sector where the northern sector is a net CO_2 source whereas both the central and southern sectors are net sinks (Figs. 7.7a and 7.7b). As before, the main single CO_2 sink is the Luderitz cell whose magnitude is still one order of magnitude larger than the southern Benguela System sinks (CC and CP). This confirms that its variability largely determines the CO_2 sink behaviour of the Benguela System.

Overall, the Benguela System can be considered to be a marginal CO_2 sink with the magnitude of the air - sea flux being largely determined by the meridional distribution of wind stress. Because of the dominance of the Luderitz cell, the more the wind stress favours the northern half of the Benguela System the greater the CO_2 ingassing and sink potential. This character is different to the sustained CO_2 outgassing which characterises open ocean upwelling in both the Pacific and Atlantic equatorial oceans (Watson, 1995). Relative to global CO_2 air - sea fluxes the magnitudes of the net CO_2 fluxes in the Benguela System (- 0.35 to $-1.47 * 10^6$ tons C y^{-1}) are very small. In the context of the estimated magnitude of the "missing carbon"

$\pm 1000 * 10^6$ tons C y^{-1} the Benguela System CO_2 sink can account for about 0.1%.

The two most important factors minimizing the sink potential of the Benguela System are:

- the benthic remineralization coupled to a strong C:N disequilibrium in the northern sector and
- a relatively weak upwelling wind stress in the southern sector.

It is clear therefore that the bathymetric (wide shelf) and physical dynamics on the northern sector which allow the build up of organic rich sediments along the inner shelf are a key factor for the reduced CO_2 sink potential of the system. It could be expected that any comparable system in which the sedimentation flux is readily exported onto the slope sediments as a result of either a narrow shelf and or strong benthic boundary layer turbulence will enhance its CO_2 sink potential. Such a systems might be the NW African upwelling system where the sediments are characterised by low organic content and coarse particles (Summerhayes *et al* 1995) or the Peruvian system characterised by a narrow shelf (Smith, 1995). Given that both these systems also have upwelling rates (Peru; 3.3 Sv and NW Africa; 2-3) it is predicted that both will be larger CO_2 sinks than the Benguela System although the long term burial may occur off the shelf.

One of the key concerns in respect of these results and predictions is that there are no independent CO_2 data with which to validate the CO_2 fluxes. This means that alternative proxy variables, in this case organic carbon fluxes, have to be used to allow comparisons with the relatively large production data sets from the Benguela System.

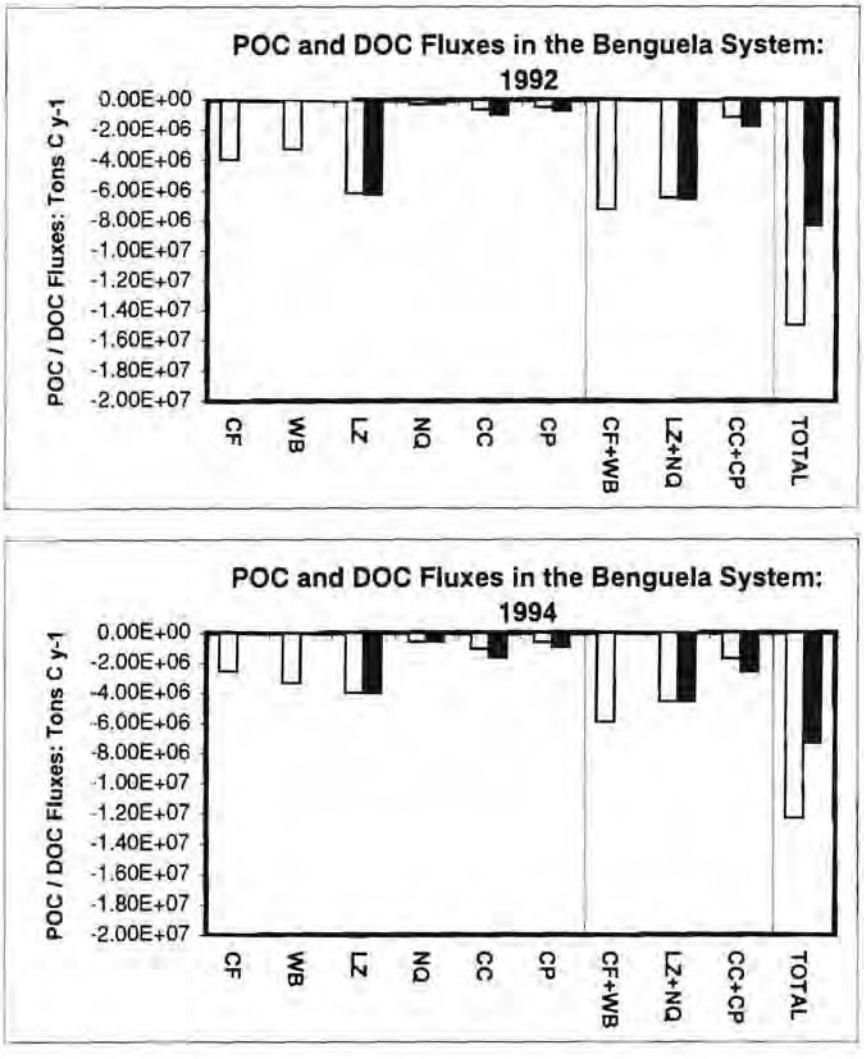

Figs. 7.8a,b The magnitude of the POC and DOC (shaded) fluxes from each upwelling centre, each sector and total of the Benguela System in 1992 and 1994. It shows that in both the central and southern sectors that the POC and DOC fluxes are comparable. Luderitz is again the source of the larges fluxes and the southern sector the smallest contributor to the total.

7.4.2 Organic Carbon Fluxes Predicted by the Model for the Benguela System

The box model gives numerical predictions about the CO_2 flux between the Benguela System and the atmosphere which in the absence of direct PCO_2 data are difficult to validate. The only model output for which comparable field data exist are the POC fluxes which can be related to published total and new production measurements in the system (Brown *et al* 1991; Probyn. 1992). The foregoing discussion emphasised that organic carbon dynamics (production - sinking - oxidation) play a key role in both the short term and long term magnitude and direction of the air - sea CO_2 flux.

The magnitudes of the POC and DOC fluxes modelled in the Benguela System using the same 1992 and 1994 wind data sets are graphically depicted in Figs. 7.8a and 7.8b and numerically summarized in Tables (7.6 and 7.7). The TOC (POC + DOC) flux is dependent on two forcing factors (see definitions in Table 7.5):

- The equatorward wind stress which provides the NO_3^- flux and,
- The C:N ratio of measured bulk CO_2 : NO_3^- uptake stoichiometry which governs the partitioning of TOC into POC and DOC.

The effect of both factors can be seen from the meridional variability of POC (Figs. 7.8a and 7.8b) which resembles that which was predicted from the Ekman transport (Figs. 7.3 and 7.4) as well as the changes in the relative size of the DOC fraction which reflects a variable C:N ratio (Chapter 6; Table 6.7). The POC flux which was defined in the model as [NO_3^- * R_r * F_{UPW}] (Table 7.5) is dependent only on the NO_3^- concentration and the upwelled water flux (F_{UPW}) which is driven by the equatorward wind stress. Thus, if NO_3^- concentrations and the C:N stoichiometry (Rr = 6.6) were constant for all upwelling centres then the POC flux would only be driven by changes in the equatorward wind stress and would mimic the Ekman transport exactly. The

fact that NO_3^- in upwelled waters does change (particularly with Luderitz where in this study NO_3^- concentration (13.67μM) was lower than other centres (18-20μM) accounts for the limited differences in the meridional variability of Ekman transport and POC flux. Despite this factor, the same sharp break is observed in the POC fluxes between Luderitz (LZ) and Namaqua (NQ) upwelling centres (Figs. 7.8a and 7.8b) which was the most significant feature of the Ekman transport (Figs. 7.3 and 7.4). The meridional asymmetry of the POC fluxes is emphasised by the percentage contribution of each sector to the total POC flux in the 1992 and (1994) model runs: northern sector (NB): 49% (49%); Central sector (CB): 43% (38%); southern sector (SB): 8% (13%). Though the SB contribution increased sharply from 8 to 13% its overall contribution is still not large especially considering that the 13% is likely to be an upper limit. A significant part of this increase was due to a decrease in the wind stress at Luderitz and hence a reduced POC flux contribution from this centre. Thus the overall Benguela System total POC flux modelled for ENSO conditions in 1992 was $15*10^6$ tons y^{-1} and the 1994 non-ENSO total was a lower $12.6*10^6$ tons C y^{-1} which clearly shows that the drop from LZ had a dominant effect over the concomitant increase in both Cape Columbine (CC) and Cape Peninsula (CP) upwelling centres.

In both the central and southern sectors upwelling centres where the C:N ratio is > Rr (Redfield ratio), DOC plays an important role (see Chapter 6). The modelled magnitude of the DOC flux increases from insignificant in the northern sector (C:N ~ Rr) to 50% of TOC in the central sector and 60% of TOC in the southern sector (Tables 7.6 and 7.7). The extent to which this DOC flux contributes to the CO_2 sink - source character of the Benguela System is difficult to calculate at present because of the lack of field observations. The best possible attempt at this deficiency is to use the approach from the previous section where a global relationship of 30% labile DOC is used to reduce the uncertainty of its impact on the air -sea CO_2 flux (Sondergaard and Middelboe, 1995). However its role as a CO_2 sink in the Benguela System will remain uncertain and one of the most critical gaps in

our understanding of the system until a concerted effort is made to include DOC into the routine production measurements.

The modelled and measured organic carbon fluxes through Benguela System are now critically discussed in order to define their magnitudes and to assess the reliability of the model predictions.

Comparison of model and field based organic carbon fluxes:

The Benguela System has historically been viewed as a 2 sector system (Northern and Southern Benguela) divided by the intense Luderitz upwelling cell which forms an environmental boundary between the Northern and Southern Benguela System (Shannon and Nelson, 1996). The difficulty which arises in a comparative exercise using spatially and temporally averaged historical production and biomass data (Table 7.8a) is that those were done on the basis of a 2 sector Benguela System (Shannon and Nelson, 1996). The boundary of the two sector system is taken to be at the Orange river which locates the important Luderitz cell in the northern sector. This does not allow the 3 sector approach adopted in this study to be easily compared with existing published data (Table 7.8a). For the purposes of such a comparison the modelled data is redefined for a 2 sector Benguela System where the organic carbon fluxes from CF, WB and LZ are grouped into the northern sub-system and the NQ, CC and CP are grouped into the southern sub-system. (Table 7.8b). **All references to northern and southern Benguela sub-systems below imply the use of a 2 sector approach and not the 3 sector system proposed in this study.** The spatially and temporally averaged historical data from the northern and southern sub-systems of the Benguela show that while there is little difference in total production between the two sectors ($77*10^6$ vs $76*10^6$ tons Cy^{-1} respectively) (Table 7.8a) the northern sector ($2.6*10^6$ tons C) accounts 80% of the total phytoplankton biomass. The elevated phytoplankton biomass in the northern

Table 7.8a: A Table showing a range of typical published biological parameters from both the Benguela and Peruvian systems. These values emphasise the higher rates of new production in the Peruvian system relative to the Benguela. It also shows that although the total production (tons C y-1) in the northern and southern Benguela sub-systems are comparable, the former accounts for 80% of the total biomass (2.6E+06 tons C). This is supported by the higher f-ratio in the northern sub-system

Physical and production parameters for the Benguela and Peruvian systems

Sub-System	Upwelling Flux (Sv)	Prodcn Total	Prodcn New	f-Ratio	Biomass /area	Area	Total Biomass	Prodcn Total (TP)	PB
		gCm-2d-1	gCm-2d-1		gCm-2	m2	(tons C)	tons C y-1	
Northern		1.1	0.16	0.35	14.3	179.0E+9	2.6E+6	77.4E+6	0.07
Southern		3.5	0.3 - 1.9	0.2	6.45	104.0E+9	670.0E+3	76.4E+6	0.54
Peru	3.3	2.3 - 5.7	0.8 - 2.4	0.5	20 - 40				0.49

Table 7.8b: Model results which are comparable to the values in Table 7.8a. They show that the total modelled carbon (POC) export flux is 13.6 million tons C y-1 but that the DOC production makes a significant contribution to the total value of new production (TOC). The f-ratios are lower than the measured values. (see text for discussion)

Model Based Organic Carbon Fluxes in the Benguela System

(Average of 1992 and 1994 model runs)

Sub-System	Ekman Flux Sv	POC tons C y-1	DOC tons C y-1	TOC tons C y-1	f-Ratio POC/TP
Northern Benguela	1.10	11.7E+6	5.2E+6	16.9E+6	0.15
Southern Benguela	0.16	1.9E+6	2.7E+6	4.6E+6	0.02
Total		13.6E+6	7.9E+6	21.5E+6	

sub-system indicates that its annual new production, which generates biomass, is substantially higher than in the southern sub-system. The fact that the same contrast is not reflected by the total production values is an indication that a larger proportion of total production in the southern sub-system is dominated by regenerated production. For completeness, the data set also includes total, new production rates and f - ratios from both the Benguela and Peruvian systems. The comparative model data are shown in Table (7.8b) where the Ekman, POC and DOC fluxes are averages of the 1992 and 1994 model outputs. Averaging of contrasting ENSO and non-ENSO years makes the historical and model data more comparable and averages are only used for comparative purposes.

The modelled POC fluxes, which represent new production in the Dugdale and Goering, 1967 and Eppley and Peterson, 1979 sense, show that there is a strong contrast between the northern and southern sector values. The POC flux in the northern sector accounts for 86% of the total new production which is in close agreement with the equivalent contrast (80%) of biomass estimates from the historical data sets (Table 7.8a). Given that both parameters are independently closely related to total annual new production in each sector, their convergence provides some confidence in the quantitative prediction of the model.

This result is consistent with the observed difference in the modelled Ekman transport (Northern Sector 1.10 Sv and Southern Sector 0.16 Sv)(Table 7.8b) which governs NO_3^- supply rate, new production and both the POC and biomass. The lack of sensitivity of total production values to the large differences in the Ekman transport suggest that total production in the Benguela System as a whole is largely driven by regenerated (NH_4^+, Urea) rather than new (NO_3^-) nitrogen. This is confirmed by the f-Ratio calculated using POC and total production fluxes (TP) where the f -ratio is defined as:

$$f = \frac{\text{New Prodcn}}{\text{Total Prodcn}} = \frac{POC}{TP}$$

and calculated as 0.15 for the northern and 0.02 for the southern sectors respectively (Table 7.8b). These values are significantly lower than those determined from *in situ* ^{15}N isotope dilution methods (Probyn. 1992). These showed ranges of 0.15 - 0.55 (mean 0.35) in the northern sector and 0.02 - 0.7 [mean 0.3 autumn; 0.2 summer (Probyn, 1992) for the southern sector (Table 7.8a). There are two possible explanations for this discrepancy:

- The first is that the comparison draws on two data sets whose temporal and spatial scales are completely different. This is a well recognized problem in global data sets) which is the cause of uncertainty in estimates of primary production and other oceanographic variables (Platt *et al.* 1989. Isotope dilution measurements are *in situ* instantaneous measurements of the nitrogen uptake rate whereas the net uptake data in this study are derived from bulk characteristics which integrate over longer space and time scales. There is little doubt that the measured f-Ratio is a highly variable parameter which depends on the particular stage of synoptic scale bloom dynamics and seasonal scale successional dynamics. The way in which isotope dilution and bulk property measurements could be reconciled with each other would be through time series of which there are none for the Benguela System. This problem also applies to the ^{14}C uptake measurements on which the total production values are based. However, the these ^{14}C based averages for total net production were calculated from a large data base of 122 values covering wide spatial and temporal scales (Brown *et al* 1991).

- The second explanation is that most field measurements in the Benguela System focus on productive areas during the active upwelling cycles. That is, most phytoplankton directed work looks for active bloom development during upwelling periods which, it is suggested, introduces

an uncertain bias towards higher f-Ratios. This problem would apply particularly to the southern Benguela sub-system which not only has temporal gaps between upwelling events but also a significant low or non upwelling season from April to August (; Shannon and Nelson, 1996). The use of hourly wind record from each appropriate upwelling centre would incorporate such variability and, it is suggested, produce results which reflect a temporally integrated reality more accurately. That is, lower f-ratios.

The spatial and temporal scales of the data set used in this study also impose their own significant limitations. Spatially they only cover a section rather than an area (1 line rather than a grid) and temporally, while bulk data reflects a synoptically integrated signal, it does not reflect the seasonal variability. These factors will in all likelihood introduce other aliasing impacts which opens the possibility that the f-Ratios calculated from this study may be too low. The real annually averaged f-Ratio is hypothesised to lie between the two estimates (^{15}N dilution method and bulk estimates) but this will only be confirmed when sampling strategies are adopted which converge the spatial and temporal scales of *in situ* and bulk measurements. This hypothesis does not change the observation that carbon turnover in the Benguela System is largely dominated by regenerated pathways whose role in net removal of CO_2 is small. Short term and long term CO_2 changes are driven by the much smaller new production pathways where the Northern Benguela System is the only significant part of the system.

In physical terms the northern Benguela sub-system comprises 5% of the total area of coastal upwelling systems and contributes 7% (1.1 Sv) of the estimated Ekman transport based on the total of 15 Sv for coastal upwelling systems (Chavez and Smith, 1995). In biological terms the northern sub-system makes a contribution of 1.5% ($11.7*10^6$ tons C y^{-1}) to present estimates of new production from coastal upwelling systems ($800*10^6$ tons C $m^{-2}y^{-1}$) (see Table 1.2) which in turn contributes approximately 11% to global

new production (see Table 1.2). There is a discrepancy between the Ekman flux (7%) and new production (1.5%) contributions from the northern sub-system to coastal upwelling but this is not thought to be significant. It is likely that with greater certainty in the physical and new production controlling variables that these relative estimates could converge significantly. On this scale of magnitude the contribution by the southern sub-system to global coastal new production is insignificant (< 0.1%).

While new production driven POC flux is important in short term CO_2 changes in the surface layer, the longer term role of the Benguela System as a CO_2 sink is determined by the burial flux which impacts on time scales of > 10^5 years (Watson, 1995). The magnitude and implications of the burial flux in the Benguela System are addressed in detail below using a diagrammatic depiction of the calculated carbon pathways and fluxes through both the northern and southern Benguela System.

Comparative Carbon Fluxes through the northern and southern sub-systems of the Benguela

The carbon fluxes obtained from the box model and from published production data in both the northern (CF, WB, LZ) and southern (NQ, CC, CP) sectors of the Benguela System are summarised in Figs. 7.9 and 7.10. **All the carbon flux magnitudes are expressed as million tons y^{-1}** and similarly, **reservoir sizes as million tons** and where necessary additional figures such as percentage partitioning of a flux, uncertain fluxes [?] or reservoir sizes [TCO_2] are provided. The upwelled and equatorward fluxes are depicted as [IN] and [OUT] respectively, the magnitude of the CO_2 reservoir in the surface layer (assuming an average depth of 25m) is expressed as [SL-TCO_2], zooplankton production as [ZOO] and fish production as [FISH]. The air - sea flux of CO_2 is depicted as [FCO2AS], the burial flux as [BURIAL] and the benthic regeneration flux as [BREG]. All the model generated values were taken from the averaged outputs of the 1992

Carbon Fluxes Through the Northern Benguela System

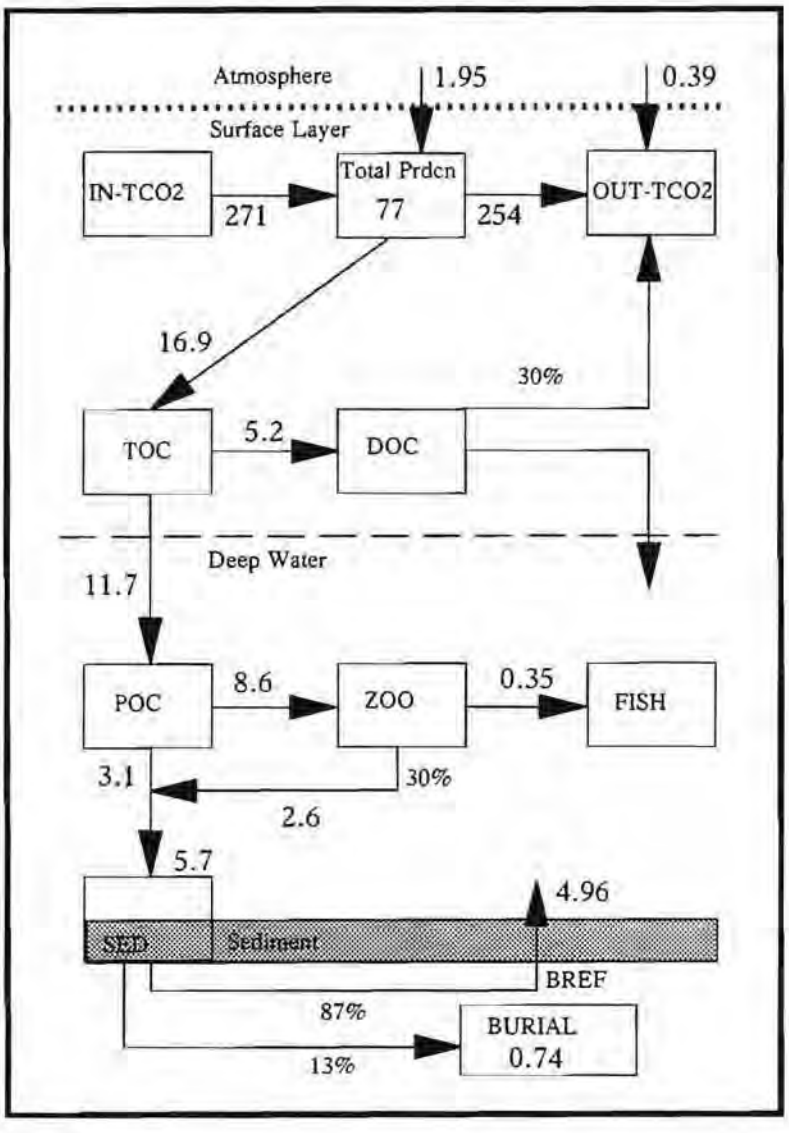

Fig. 7.9: The biological carbon fluxes through the northern Benguela sub-system which using the convensional boundaries of the system includes the Cape Frio, Walvis Bay and Luderitz upwelling cells. The values are averages of the fluxes calculated from both the 1992 and 1994 model runs. It shows that when the post bloom surface water TCO_2 is corrected for a 30% remineralization of DOC the net ingassing flux of CO_2 from the atmosphere reduces from 1.95 to 0.39 milion tons carbon / year. (see text for discussion)

Carbon Fluxes Through the Southern Benguela System

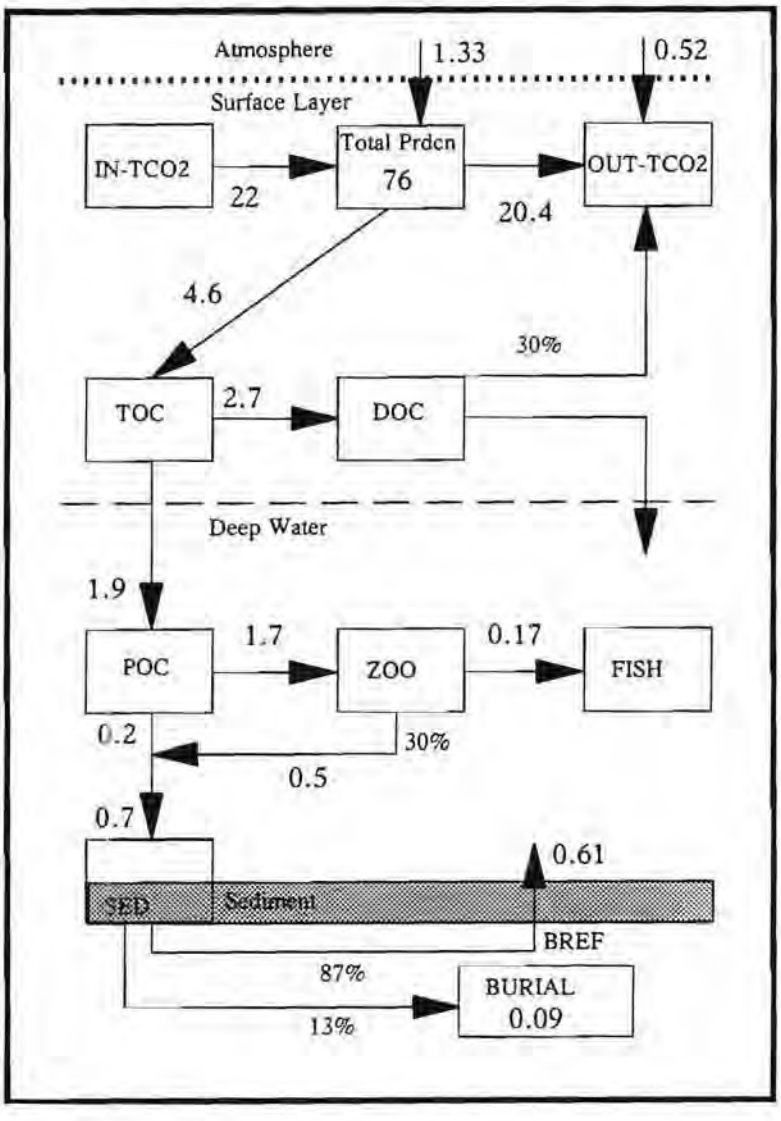

Fig. 7.10: The biological carbon fluxes through the southern Benguela sub-system which using the conventional boundaries of the system includes the Namaqua, Cape Columbine and Cape Peninsula upwelling cells. The values are averages of the fluxes calculated from both the 1992 and 1994 model runs. It shows that when the post bloom surface water TCO_2 is corrected for a 30% remineralization of DOC the net ingassing flux of CO_2 from the atmosphere reduces from 1.33 to 0.52 milion tons carbon / year. This makes the net CO_2 ingassing fluxes of the southern and northern sub-systems comparable despite much larger biological fluxes being associated with the northern sub-system. The reason is the much higher sub-surface remineralization flux in the northern sub-system. In the southern sub-system zooplankton fecal pellet flux (0.5) is suggested to make a larger contribution to the sedimentation flux than the phytoplankton detrital (POC) flux (0.2). (see text for discussion)

and 1994 runs (Table 7.8b). The carbon fluxes through the northern and southern sub-systems in a 2 sector Benguela are now discussed in more detail.

The Northern Benguela Sub-System (CF, WB, LZ)

The carbon fluxes show that in this sector the annual physically driven carbon (TCO_2) through flow (IN: 271 and OUT 254) turns over the surface layer reservoir [TCO_2: 118] approximately twice and that total production [TOTAL PRDCN] of 77 turns the same reservoir over about 1.5 times. These magnitudes provide an indication of the degree of physical and biogeochemical activity or turnover. The total production rates comprise both the regenerated and new production fluxes but only the latter is of consequence to the CO_2 fluxes across the air-sea boundary. In terms of the model the upwelled NO_3^- flux generates a "new production" flux of both POC and DOC which when combined become TOC. The new production driven TOC (POC + DOC) flux generates a short term net CO_2 drawdown flux of 1.95 but on the longer term the latter depends on the subsequent kinetics of diagenesis of the DOC fraction. The fate of the DOC fraction is the greatest source of uncertainty in that the magnitude of both lateral and vertical fluxes which govern part of its role as a pathway for the removal of CO_2 cannot be quantified. The box model assumed an oxidative remineralization flux of 30% of the DOC production rate which results in a re-adjustment of the net sea - air CO_2 flux to a reduced ingassing of 0.39. The net POC flux, which represents new production in the classical sense (Dugdale and Goering, 1967), is 11.7 and it gets partitioned into a foodweb pathway [ZOO] and [FISH] and a direct sedimentation flux [POCSED]. The production rates of the food web components were obtained from Verheye *et al.* 1992 for the zooplankton and Hutchings, 1992 for the fish. The zooplankton production includes both meso and macro zooplankton components. Zooplankton [ZOO] production [8.6] partitions approximately 3/4 of the POC flux and is itself partitioned into a faecal pellet sedimentation flux [FPSED] of 2.6 and fish

production [0.35]. Fish production in the northern Benguela System is 2 orders of magnitude lower than the new production POC flux and 1 order of magnitude lower than the sedimentation flux. The magnitude of the faecal pellet sedimentation flux was given by a 30% waste factor which was derived as an average of a range of empirical estimates (Verheye et al., 1992). The net POC sedimentation flux [POCSED] of 3.1 combined with the faecal pellet flux [FPSED] to form the total sedimentation flux [FSED] of 5.7 which amounted to about 50% of the original POC flux. This is in good agreement with the prediction of the fraction of POC which sediments out on relatively shallow (~200m) productive shelf areas (Middelburg et al., 1993). Equally importantly, these fluxes suggest that the sedimentation flux in the northern Benguela System has approximately equal contributions from phytoplankton detritus of 3.1 and faecal pellets of 2.6. Historical measurements from this region support an important role from faecal pellects (Bishop et al., 1978) but these predictions need to be checked with sediment trap deployments.

The partitioning of this sedimentation flux into a burial [BURIAL] and benthic regeneration (BREG) fluxes was estimated adopting the widely-used figure of 87% for the fraction which is regenerated (Middelburg et al., 1993). This resulted in a burial flux of 0.74 and a concomitant benthic regenerated flux (BREG) of 4.96. The burial flux governs the long term role of the northern Benguela sub-system as a CO_2 sink and gives rise to the spatially widely distributed accumulations of organic rich sediments (Fig. 4.27). The question is: can the estimated burial flux be validated through an independent approach ? This was done using the sediment accumulation rate of $1 mm y^{-1}$ (Bremner, pers.com.), an average 5% POC content in the sediment, 80% porosity from direct observation and a spatial distribution over 25% of the 179,000 km^2 of shelf area. These input data yield an organic carbon burial rate of about $1*10^6$ tons y^{-1} which is in very good agreement with the result from the model $0.74*10^6$ tons y^{-1}.

Globally, the total POC annual burial rates have been estimated to be $157*10^6$ tons C y^{-1} (Berner, 1982) of which approximately 3.4% ($5.4*10^6$ tons C y^{-1}) occurs in equatorward wind-driven coastal upwelling systems (Berner, 1982) (excludes Arabian sea system). The calculated burial rate for the northern Benguela System ($0.74 *10^6$ tons C y^{-1}) accounts for 14% of the burial in coastal upwelling systems. This is approximately 3 times larger than the contribution from comparative physical characteristics such as Ekman transport and area discussed above (~ 5%). It suggests that the northern Benguela System is more efficient than the average coastal upwelling systems in sequestrating organic carbon into the long term burial reservoir. One can only speculate about this but the following three explanations seem plausible and worth further investigation:

Firstly, the potential role of efficient particle aggregation which has been widely observed in coastal ocean (Ittekkot, 1993). This could include organic aggregates "ballasted" with lithogenic particles delivered into the surface layer via aeolian pathways (Ittekkot, 1993). There is strong evidence to support the latter in the northern Benguela sub-system both from remote sensing imagery showing plumes of dust being blown offshore by catabatic wind events (Shannon, 1985) and from the sediment record which defines the boundaries of aeolian dust on the Benguela System shelf (Dingle *et al* 1987). The question which is critical for predictive numerical modelling is whether these "ballasted" fluxes occur throughout the upwelling season as part of synoptic scale events or as one or two major inputs. Addressing this question is important not only because of the need to constrain the sedimentation flux but also to allow reasonable predictions of how climate change may impact carbon flux dynamics in the Benguela System. Climate change linked to global warming is likely to alter the spatial and temporal characteristics of the equatorward wind in the Benguela System. If aeolian particle fluxes are an important part of the mechanism for mass accumulation rates in this system then the future carbon fluxes will be closely coupled to wind strength, direction and persistence characteristics throughout the Benguela System.

Secondly, the physical dynamics of the BBL which are poorly understood in all upwelling systems (Lenz and Trowbridge, 1991) are likely in the future be shown to be a key factor in governing the rate and location of organic carbon burial in sediments. The BBL dynamics are suggested to control the efficiency of burial through their impact on resuspension of sediments, the transport of a nepheloid layer which will spread the organic particles over the shelf or carry them off the shelf onto the slope area and through the ventilation rates of the sediments which impact on their redox character and oxidation rates. *Thirdly*, the proposed idea of massively pulsed production which overcomes the short term capacity of the system to re-mineralize it (Summerhayes, 1983). The fact that the northern sub-system appears to be characterised by a relatively efficient burial mechanism does not mean that other systems such as the Peruvian or NW African ones are less effective. It may simply be a question of whether the burial occurs on or off the shelf. Off NW Africa for example the sediments are largely characterised by coarser sand particles compared to the muds on the Namibian shelf (Rogers and Bremner, 1991). It is possible that in the former the sedimentation flux is carried off the shelf by stronger BBL turbulent flow and deposited on the slope. This aspect of the Benguela System is completely unknown but it is predicted that the sites where inner shelf water is advected off the shelf ("gate sites") are prime areas to locate such slope deposits. This makes it necessary to study the problem of burial in a holistic way and extend the spatial scale of sampling to include the shelf and slope areas particularly in areas where the poleward flow is directed off the shelf.

The Southern Benguela Sub-System (NQ, CC, CP)

The carbon flux pathways for the southern Benguela sub-system were structured in an identical manner to that of the northern sub-system (Fig.7.10). This carbon flow diagram emphasises the contrasts between the two sub-systems. In the southern sub-system, the magnitude of total production is almost identical to the northern sub-system value of 76. This indicates that primary production turns the entire surface layer [SL-TCO2]

reservoir of 70 over annually. Furthermore, the upwelled CO_2 flux [IN-TCO2] is now approximately 1/3 of the magnitude of both the total production and the surface layer TCO_2 reservoir. These carbon flux characteristics in the surface layer domain lend further support to the view discussed earlier that the southern sub-system relies on regenerated pathways to a greater extent than the northern sector. This in turn is consistent with the suggestion that the southern sub-system has a more active microbial loop than the northern counterpart (Brink *et al* 1995).

The TOC flux of 4.6 generates a net CO_2 ingassing flux of 1.33 which when corrected for the 30% remineralization of the DOC fraction remains a net ingassing flux with a reduced magnitude of 0.52. As was the case previously, the fate and magnitude of the DOC reservoir is completely unknown which in the case of the southern Benguela System is more significant because of its relatively larger contribution (60% cf. 30% in the northern sub-system) to the TOC flux. In further contrast to the northern sub-system, the magnitude of the POC flux 1.9 is only slightly larger the zooplankton production flux of 1.7 (Verheye *et al.*, 1992). This suggests the possible notion that zooplankton production in the southern sector close to being limited by the magnitude of new production. It also indicates that the resulting direct POC sediment flux [POCSED] of 0.2 is smaller than the faecal pellet flux from zooplankton [ZOO] production of 0.5. This large contribution from faecal pellet flux to the sedimentation flux (~70%) is expected to be reflected in the sediment record for this region. This will need to be checked through sediment trap measurements.

The resulting burial flux using the same 13% burial factor is 0.09 which is an order of magnitude smaller than the equivalent of 0.74 for the northern sub-system. This is suggested to be a strong factor in the contrasting spatial distribution and concentration of POC in the sediments of both sectors. This burial rate is small enough to be less than the annual fish production of 0.17

suggesting the interesting notion that fishing in the southern Benguela sub-system is potentially a larger carbon export mechanism factor than sediment burial.

The Benguela system as a whole contributes a burial flux of ~ $0.85 * 10^6$ tons C y^{-1} which is ~ 0.5% of the total carbon burial in the oceans and 16% of the organic carbon burial in eastern boundary coastal upwelling areas. This is a strong indication of the importance of the biological pump in this system. It emphasises the need to focus on the northern sub-system as the key to measuring and modelling carbon fluxes in the Benguela System. It should however be re-stated that the model also shows the extent to which the Luderitz upwelling cell is the biogeochemical centre of gravity of the system and any future work must place its emphasis accordingly.

7.5 Model Results Part II: Perturbation Runs

The results and discussion presented above focus mainly on a " status quo" scenario which did not provide an insight into how sensitive the CO_2 flux predictions were to realistic changes in the key controlling parameters. The ensuing discussion addresses the need for a sensitivity analysis of predicted air - sea CO_2 fluxes to variability in C:N and C_{Org} : C_{Ing} stoichiometries and surface layer temperatures.

7.5.1 C:N Stoichiometry of Remineralization and Uptake

The stoichiometry or coupling of the C and N remineralization and uptake pathways has been shown to be one of the key factors underlying the observed PCO_2 values in the Benguela System and the modelled air -sea CO_2 fluxes. In the standard model runs the stoichiometric relationships were those which were measured in the field and considered to be system properties or in the model, primary input variables. The question which arises is, what if the C:N ratios of remineralization and uptake were allowed to vary ?

Run Character	Year	Perturbation	DOC factor	FCO2AS
Standard	1992	ENSO	+30% DOC	-1.50E+06
	1994	non-ENSO	+30% DOC	-3.50E+05
C:N	1992	Max. D.Down	+30% DOC	-7.00E+06
	1992	Std	+30% DOC	-1.50E+06
	1992	Min. D.Down	+30% DOC	4.40E+06
Org:Ing	1992	1:10	+30% DOC	-3.77E+05
Sol. Pump	1992	16	+30% DOC	-3.70E+06
	1992	18	+30% DOC	-1.50E+06
	1992	20	+30% DOC	7.00E+05

Table 7.9: A summary of the perturbation model runs. It shows that the biogeochemical mechanisms with the greatest scope to change the magnitude of the source - sink behaviour of the Benguela System is the C:N stoichiometry of benthic remineralization and surface uptake. Depending on their extremes they can turn the system as a whole into a significant sink (7 million tons C / year) or source (4.4 million tons C / year) of CO_2. Increasing the contribution of inorganic carbon pump to a $C_{Org} : C_{Ing}$ stoichiometry of 10:1 decreases the magnitude of the sink by an order of magnitude. Increasing the temperature of the surface layer to 20°C from the 18°C used in the standard model runs also turn the system into a net source of CO_2 but by a small margin (0.7 million tons C / year).

What would be the impact on CO_2 fluxes and how sensitive are these to such a variability ? This problem was investigated by running two scenarios which represented the potential extreme impacts relative to the standard observations. Outputs from the three comparative scenarios are shown in Table 7.9 and are all compared to the 1992 model run (standard scenario).

In the first scenario the C:N ratio of benthic remineralization was set to the Redfield ratio (6.6) but the surface uptake ratio remained unchanged from the observed values. It was shown in Chapter 6 that one of the main reasons why upwelled water in the Benguela System has a weak CO_2 ingassing potential is because of the strong de-coupling of the benthic carbon and nitrogen remineralization fluxes. In this problem, which is most strongly observed in the northern sector, the CO_2 remineralization flux is much larger than the NO_3^- flux which at the surface governs and limits the carbon new production export flux. The first perturbation aims to assess what impact re-setting the benthic remineralization flux C:N ratio to Redfield (6.6) would have on air - sea CO_2 fluxes. Such a scenario might be expected from a well ventilated poleward sub-surface flow where nitrification rates are high. The results show that after the 30% DOC correction is applied the impact of this perturbation ($-7*10^6$ tons C y^{-1}) is to increase the magnitude of the CO_2 sink by a factor of 5 relative to the standard 1992 run reference figure of ($-1.5*10^6$ tons C y^{-1}). This scenario reflects the maximum C:N driven CO_2 sink potential for the Benguela System with the observed surface uptake C:N ratios.

In an alternative extreme the benthic remineralization flux C:N ratio was fixed at the observed values and the surface uptake C:N stoichiometry was reduced to a common Redfield ratio (6.6) value. This is the "classical" scenario in the sense that many carbon flux calculations, especially those based on new production measurements (Waldron, 1996) make the assumption that the NO_3^- flux * Rr is the carbon export flux which will then provide a quantitative estimate of the CO_2 sink potential. The results show that in this scenario the system becomes a strong net CO_2 source ($4.4*10^6$

tons C y^{-1}). This emphasises the importance of the measurement and modelling of non-Redfield behaviour by C:N stoichiometry of phytoplankton uptake as a key to correctly predicting the CO_2 source - sink nature of an upwelling system such as the Benguela. Assuming Redfield behaviour will underestimate the CO_2 sink potential.

7.5.2 Carbon pump stoichiometry: Org:Ing

The water column field data obtained in the course of this study showed little evidence of inorganic carbon pump (C_{Ing}) activity (see Chapter 6). However, there is alternative evidence to question whether the spatial and temporal sampling scales of this study were adequate to address C_{Org}: C_{Ing} stoichiometry adequately. The alternative evidence fits into two temporal scales:

- short term bloom events: coccolithophore blooms have been periodically observed in the Benguela System (Giraudeau and Bailey, 1995). Given that coccolithophore activity has been largely overlooked by the ecological studies in the Benguela System, it is possible that their incidence may be more frequent than expected.
- long term sediment accumulation: it was shown in Chapter 6 that $CaCO_3$ is the single most important geochemical constituent of sediments on the Benguela System shelf. Even taking into account the $CaCO_3$ vs. POC preservation factor this is the most compelling evidence that over the long -term, coccolithophore activity in the surface layer in the Benguela System is the most important carbon export pathway.

The question which arises on the basis of the above two points is: is the long term accumulation of $CaCO_3$ the result of a few large events or a continuous low level flux ?

The spreadsheet model was used to assess the impact of a shift in the carbon pump stoichiometry from a negligible contribution by the C_{Ing} pump

(adopted in all standard runs) to 10:1 C_{Org} : C_{Ing} stoichiometry. That is, giving the C_{Ing} pump a small (10%) but realistic and significant role. This stoichiometry is a compromise between what is expected from large bloom events where C_{Org} : C_{Ing} is ~ 1:1 (Robertson *et al* 1994) and its low level pico-plankton activity. The summarized output fluxes of the run are shown in Table 7.9. Like all perturbation runs its inputs are based on the 1992 wind data set. It shows that the effect of a 10:1 stoichiometry corrected for a 30% DOC remineralization is to reduce the CO_2 ingassing flux by an order of magnitude from the standard 1992 magnitude of $-1.5*10^6$ tons C y^{-1} to $-3.77*10^5$ tons C y^{-1}. The reduction of the ingassing flux is consistent with the fact that $CaCO_3$ deposition leads to an increase in the PCO_2 (see Chapter 3) which reduces the air - sea gradient and consequently the ingassing flux.

The lack of knowledge about the ecological dynamics of coccolithophores particularly *Emiliania huxlei* is being addressed in the context its recognized importance in of global carbon flux (Westbroek *et al* 1993). Similarly, not enough is known to predict how coccolithophores in the Benguela System will respond to climate change and alter the C_{Org}: C_{Ing} stoichiometry. However, it is speculated that given that coccolithophores are part of the nanno/pico plankton ecology they are subject to similar turbulence driven seeding and blooming constraints (see Chapter 1). This is supported by the increased incidence of coccolithophore blooms during El Nino periods when there is a decreased wind activity especially in the southern Benguela System. Given this, it is suggested that if global warming increases coastal equatorward wind activity as predicted by Bakun, 1990 that this will further depress coccolithophore activity in the Benguela System.

The significance of this relationship with turbulence is that the factor which enhances coccolithophore activity, reduced wind induced turbulence, decreases new production rates and vice versa. Thus, the impact of a 10:1 stoichiometry on CO_2 fluxes predicted by the model will be an underestimate because under such a scenario there would have been a similar decrease in

the new production driven POC flux. This coupled relationship has the effect of amplifying the effect of one or other dominant mechanisms on PCO_2 and air - sea CO_2 fluxes.

Two hypotheses are proposed as a result of these results:

- the long term build up of $CaCO_3$ in the Benguela System sediments is mainly the result of a continuous but low level coccolithophore activity strongly modulated by nanno- and pico-plankton dynamics.
- the contribution of the inorganic carbon pump C_{Ing} driven by coccolithophore activity is inversely correlated to new production.

7.5.3 Temperature: the solubility pump

The aim of investigating the role of temperature is to constrain the impact of the solubility pump on the net air - sea CO_2 flux. This model run entails simulating two scenarios which might be expected to arise in the context of global climate change: the first is a warming scenario where the equilibrium temperature of the surface layer is 20°C cf. 18°C used for the standard runs and the second, is a cooling scenario where the surface layer temperature is 16°C. All the biogeochemical characteristics remain unchanged so that the only factor contributing to change is the impact of the temperature of the equatorward surface flow on the solubility of CO_2. The results are summarized in Table 7.9 (which include the standard 18°C values).

The outputs show two significant features:

- While in the cooler 16°C scenario the Benguela System remains a sink (-$3.7*10^6$ tons C y^{-1}) regardless of whether the DOC component is included, in the warmer 20°C scenario it become a significant CO_2 source ($0.69*10^6$ tons C y^{-1}) when the DOC remineralization is included.

- The overall effect of the 2°C change in temperature is to change the magnitude of the flux for the whole Benguela System by $2.2*10^6$ tons C y^{-1} relative to the standard 18°C scenario or approximately $1*10^6$ tons C y^{-1} /°C.

These are only approximate values because both scenarios were calculated relative to a fixed atmospheric pCO_2 of 360μatm whereas in reality the atmospheric pCO2 would also be changing. Such a concomitant change would influence the magnitude of the gradient across the air sea interface. The impact of the concomitant changes to the atmospheric pCO_2 on the flux would be asymmetrical. Under the warmer scenario atmospheric pCO_2 increases and the effect would be to reduce the magnitude of the outgassing flux whereas under the cooling 16°C scenario with lower pCO_2 the inverse would hold and the ingassing flux would be larger than that which is predicted above. Such an asymmetrical response by CO_2 fluxes to changes in the solubility pump predict that the rates of atmospheric pCO_2 decrease associated to planetary cooling would be far higher than for an equivalent Greenhouse driven warming.

7.6 Appendix 1:

Generically, the Ekman mass transport per metre of coastline ($Kgm^{-1}s^{-1}$) is given by eq. A.1. In this study, this variable is called the *specific* Ekman transport to differentiate it from *total* Ekman transport which includes the coastal length scale and is defined by Kgs^{-1} or m^3s^{-1} units.

$$S_x = \int_0^D u\,dz \qquad \text{eq. A.1}$$

This expression is the integral of the water velocities between the surface and the Ekman depth (D). This can be expanded and simplified to the expression in eq. A.2

$$S_x = \frac{\varrho V_0 D}{\pi\sqrt{2}} = \frac{\tau_y}{f} \qquad \text{eq. A.2}$$

where the Ekman transport S_x is more simply shown to be function of wind stress (τ_y) and Coriolis parameter (f). The wind stress in turn, is defined by the product of the equatorward wind speed (V^2), air density (ϱ_{air}) and the drag coefficient (C_D)(eq. A.3):

$$S_x = \frac{C_D \varrho_{air} V^2}{f} \quad \text{(Dimensions: } ML^{-1}T^{-2}\text{)} \qquad \text{eq. A.3}$$

The basic units for Ekman transport in eq. A.3 are [$Kgm^{-1}s^{-2}$] which with density (ϱ) convert to volume as [$m^3m^{-1}s^{-2}$] and finally when integrated over a quarter (3 months) becomes [$m^3m^{-1}s^{-1}Q^{-1}$]. This implies an upwelling rate (volume/second) per Quarter per metre of active upwelling coastline. The quarterly Ekman transport was calculated at each upwelling site by solving eq. 3 through the following steps (G. Nelson, Pers.Com):

- The year long hourly wind record was divided into the 4 quarters.
- The hourly wind vectors were resolved into meridional (N-S) (v) and zonal (E-W)(u) components.
- The meridional (v) component was filtered using a 72 hour moving average filter to remove the high frequency noise (< 2.5 days) to in order to isolate wind events while not inducing problems of data aliasing (G. Nelson, Pers.Com). Spectral analysis of pressure changes in the Benguela System has in the past shown that periods of 3-6 days are an intrinsic part of the variability (G. Nelson, Pers.Com). The numerical output from this filter was compared to an alternative 3 day Thompson filter. This had a sharp cut-off at 3 days and its response does not show

the same ringing characteristics of a moving average filter which can contaminate the output. The comparison showed that differences were no larger than 5%.

- The filtered hourly meridional component was rectified to resolve the northward upwelling inducing component which was then squared to obtain the V^2 term of eq. A.3. An example of the output at this stage is graphically depicted in Fig. A.1 for the first quarter of 1992 wind record from Cape Columbine. It shows the rectified output of V^2 (m^2s^{-2}) which is then integrated to provide the quarterly value for V^2.

The integrated V^2 term was then multiplied out with the variables from eq. A.3 to produce an Ekman transport value ($Kgm^{-1}s^{-1}$) for the particular quarter.

Chapter 8

8. Closure

8.1 Conclusions

This study is a process orientated work which set out to test three hypotheses that embody contemporary understanding of carbon fluxes in the Benguela System and the underlying physical and biogeochemical driving mechanisms. The hypotheses are:

- The Benguela upwelling system is an important CO_2 sink by virtue of its high primary production and sediment organic carbon accumulation rates,
- The carbon export flux and the magnitude of the CO_2 sink in the Benguela System can be predicted from the C:N stoichiometry provided by the Redfield Ratio.
- The inorganic carbon pump through coccolithophore production plays a minimal role in driving changes to the magnitude of both the carbon export flux and the air - sea CO_2 flux in the Benguela System

This synthesis of the study aims to assess the extent to which the work was able to address the three hypotheses and in doing so also present the highlights of the work and its findings.

- Hypothesis 1: The Benguela upwelling system is an important CO_2 sink by virtue of its high primary production and sediment organic carbon accumulation rates.

The carbon fluxes which define the CO_2 source - sink character of the Benguela System were quantified using a spreadsheet box model. The two main model runs contrasted the annual carbon fluxes under ENSO (1992)

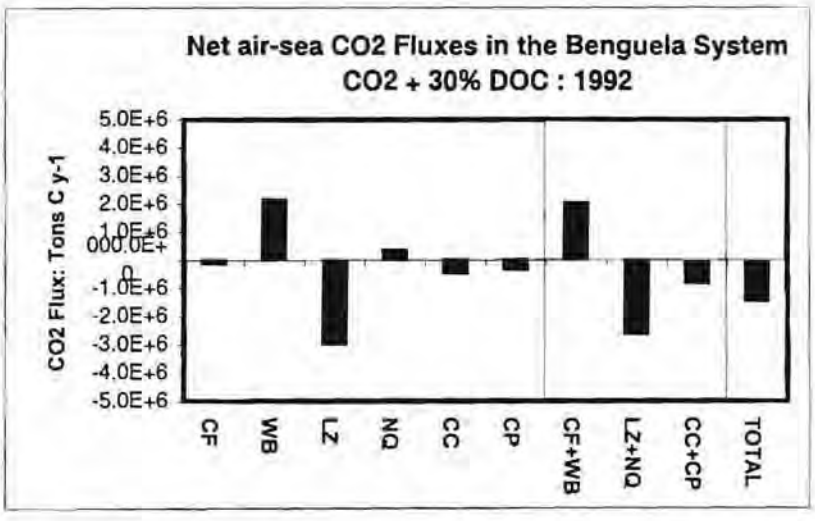

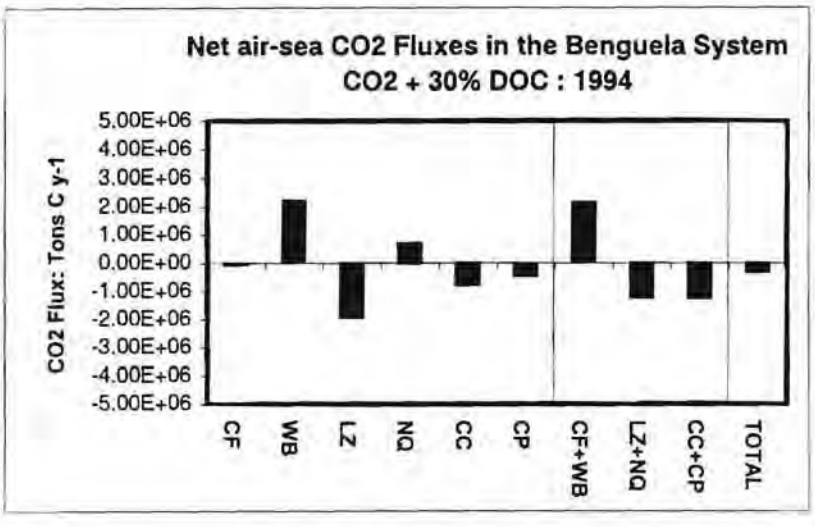

Figs. 8.1a,b: The net air - sea CO2 fluxes in the Benguela system corrected for a 30% oxidation of the DOC fraction of the organic carbon flux. It shows that the system remains a net CO2 sink in both 1992 and 1994. It emphasises the importance of the Luderitz upwelling cell in offsetting the CO2 source character of the Walvis Bay centre.

and non-ENSO (1994) conditions which provide the system with its most extreme interannual character (Shannon and Nelson, 1996). The modelled air - sea flux of CO_2 (tons C y-1) is shown in Fig. 8.1a,b which depicts the fluxes for each of the six main upwelling cells: Cape Frio (CF), Walvis Bay (WB), Luderitz (LZ), Namaqua (NQ), Cape Columbine (CC) and Cape Peninsula (CP) (Lutjeharms and Meewvis, 1987), for each of the 3 sectors: northern (CF & WB), central (LZ & NQ) and southern (CC & CP) and an overall system total (TOTAL). These CO_2 fluxes were modelled assuming that 30% of the DOC flux associated with new production was re-oxidized to CO_2 (Sondergaard, 1995; Blight *et al.*, 1995). The plots show that:

- Under both ENSO (1992) and non-ENSO (1994) conditions, the Benguela System as a whole (TOTAL) is a net sink of atmospheric CO_2. The magnitude of the CO_2 sink flux is 1.5 and 0.34 million tons C y^{-1} in 1992 and 1994 respectively.
- Counter-intuitively, the magnitude of the total CO_2 sink flux increases under ENSO conditions. The explanation lies in the source - sink behaviour of the individual upwelling cells, particularly Luderitz under both ENSO and non-ENSO conditions.
- The Luderitz upwelling cell is the largest single CO_2 sink in the system by one order of magnitude. Small shifts in its upwelling flux , which drives the CO_2 sink character, govern the overall character of the system. Under ENSO conditions, when the South Atlantic High pressure cell is located north of its average summer position (Shannon and Nelson, 1996), upwelling is depressed in the southern half of the system (NQ, CC and CP) but enhanced at Luderitz. By contrast, under non-ENSO conditions when upwelling increases in the southern half, the increase is not enough to offset the simultaneous decrease at Luderitz. This shows that ENSO conditions increase the contrast in fluxes between the northern and southern halves of the system relative to the non-ENSO years.
- The two most extreme upwelling centres are the adjacent Walvis Bay and Luderitz cells.

- The net air - sea CO_2 fluxes in each of the three sectors of the system show that in both years the northern sector was a CO_2 source whereas the central and southern sectors were consistent sinks. This suggests that south of 25°S the Benguela System is, on an annual average, a CO_2 sink.

These model results support the first hypothesis.

- Hypothesis 2: The carbon export flux and the magnitude of the CO_2 sink in the Benguela System can be predicted from the C:N stoichiometry provided by the Redfield Ratio.

The most important mechanistic insight gained from this study is that the Redfield C:N stoichiometry is the exception rather than the rule in the Benguela System. This applies to both remineralization and uptake processes. The measured C:N dis-equilibria are concluded to be the single most important biogeochemical factor governing the direction and magnitude of the air - sea flux in the Benguela System. The two most important aspects of this control are:

- The dis-equilibria which develop in the remineralization of CO_2 and NO_3^- in shelf sediments which are typically > 50 result in a reduction of the CO_2 drawdown potential of upwelled waters as NO_3^- is the limiting nutrient for primary production.
- Dis-equilibria in CO_2 and NO_3^- uptake at the surface (typical range 6.4 - 17) can to some extent offset the impact of remineralization but the impact is limited because: a) the C:N stoichiometry of uptake is always smaller than that of remineralization and b) according to most recent ideas (Toggweiler, 1993; Williams, 1994) most of the carbon production which induces the shift away from Redfield stoichiometry is partitioned into nitrogen poor DOM. The role of DOC as a CO_2 sink depends on the

magnitudes of the labile and heterotrophically resistant fractions which are undefined in the Benguela System. The model results show that the production and fate of DOC which is linked to the C:N disequilibrium hold the key to whether the Benguela System is a CO_2 sink or source. The use of a literature-based 30% fraction of labile DOC (Sondergaard, 1995) for the Benguela System provides a first step in addressing one of the most important gaps in our understanding.

Two mechanisms are proposed to account for the remineralization and uptake dis-equilibria. Adsorption of NH_4^+ to sediment and sedimenting biogenic and lithogenic particulates and a C:N dis-equilibrium in the C:N stoichiometries of regeneration and uptake. The conclusion is that the use of Redfield stoichiometries to calculate carbon export from either nitrogen uptake measurements or nitrogen flux estimates will underestimate the resulting carbon export flux as both POC and DOC. Measurement of bulk CO_2 and NO_3^- stoichiometric change should be a central component to production studies.

- Hypothesis 3: The inorganic carbon pump through coccolithophore production plays a minimal role in driving changes to the magnitude of both the carbon export flux and the air - sea CO_2 flux in the Benguela System.

In view of the recent view that the role of coccolithophores in the global carbon budget has been largely underestimated (Westbroek et al., 1993), its role in the Benguela System was investigated using a novel Total Acidity (TAcy) - Total Alkalinity (TAlk) vector plot method which is a modification of the widely used Deffeys diagrams. These plots were used to independently quantify the impact of the organic (C_{Org}) and inorganic (C_{Ing}) carbon pumps on the observed changes to TCO_2 in water samples. The results strongly support the hypothesis that carbonate deposition and remineralization make a very small contribution to changes in the carbonate chemistry of the water

column in the Benguela System. However, it should also be noted that this conclusion is not consistent with the observation based on historical sediment geochemistry that $CaCO_3$ is the single most important carbon reservoir in the sediments. It was concluded that $CaCO_3$ deposition through coccolithophore activity is not significant in experimental time scales but that because the system is super-saturated with respect to calcite, that it will accumulate in the sediments despite low $CaCO_3$ production rates.

8.2 Other Highlights

8.2.1 The "Gate" Hypothesis

The data suggest that the Benguela System can be divided into three distinct sectors on the basis of there being three input points of South Atlantic Central water (SACW) from the slope onto the shelf as opposed to generalised inflow across the length of the shelf. This 3-sector system is conceptually described in Fig. 8.2. It shows that each sector has an inflow of fresh SACW and an outflow of shelf modified SACW. Each inflow acts as a "gate" limiting the further poleward advection of SACW from the northerly sector. Water does not outcrop at each upwelling centre directly from the slope but as a 2-step process. Once through the "gate" SACW is entrained into poleward flow and the part which outcrops is the inner shelf water. The implications of this for carbon flux modelling are:

- the biogechemical characteristics of upwelled waters are governed by the distance of the upwelling cell from the "gate" rather than by SACW.
- Biogenic detrital material (POC) may be exported out of the shelf onto the slope at very specific sites.

The average carbon fluxes (million tons C y^{-1}) for both 1992 and 1994 are modelled for each stage of the upwelling cycle and shown next to their

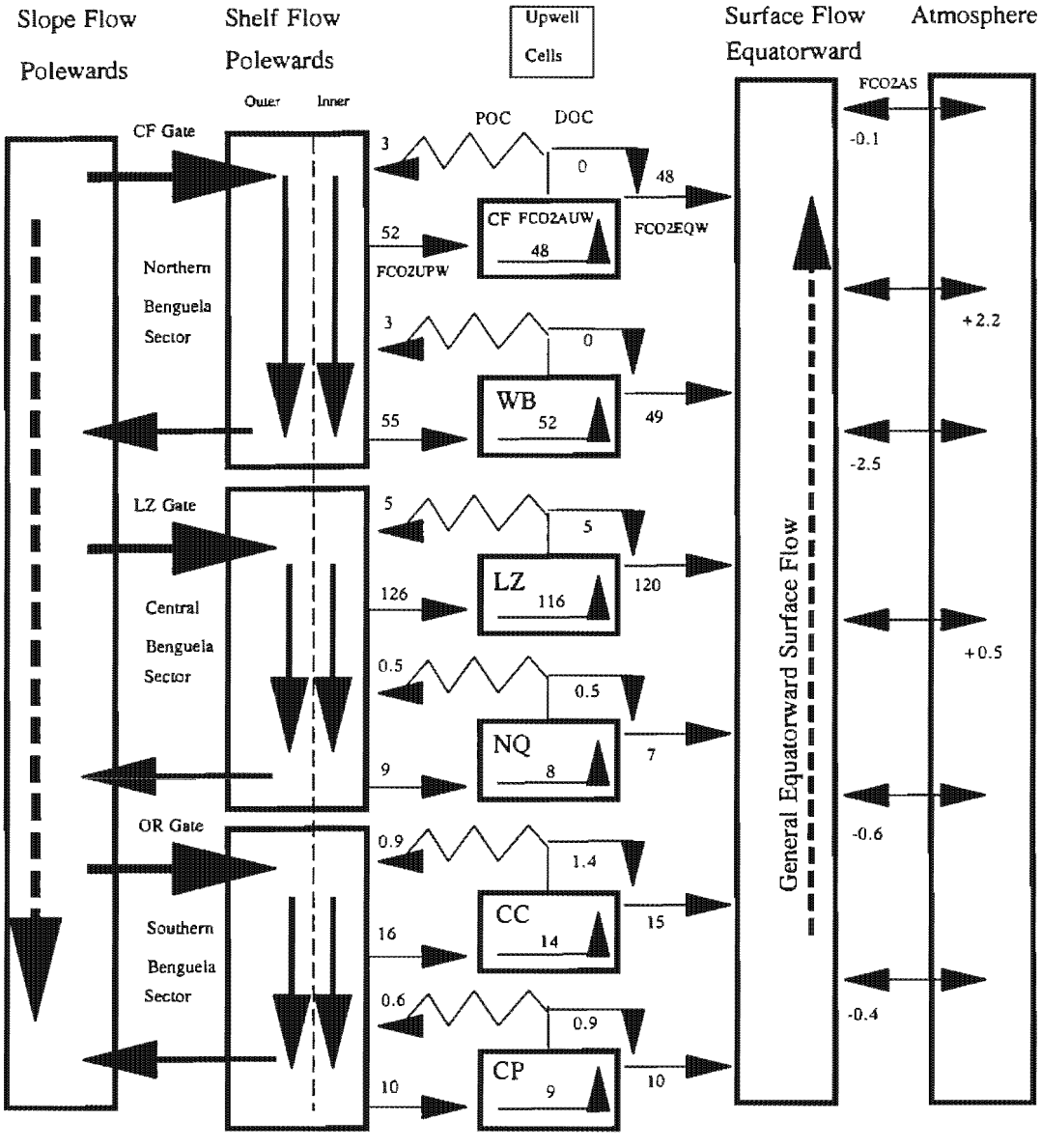

Fig. 8.2: The biogeochemical version of the "Gate" hypothesis Benguela system model with each of the fluxes quantified using the averaged outputs from the 1992 and 1994 model runs. All the flux values are expressed in million tons of carbon / year. It shows that the carbon fluxes in the southern sector are one order of magnitude lower than those in the central and northern sectors. The fluxes associated with the Luderitz cell are in turn one order of magnitude larger than the remainder. It also shows the positions of the 3 "gates" (Cape Frio CF Gate; Luderitz LZ Gate and Olifants River OR Gate). The fluxes are as follows: FCO2UPW is the flux of CO_2 advected to the surface in newly upwelled water; FCO2AUW is the flux of CO_2 advected on the surface during the ageing of upwelled water and FCO2EQW is the flux of CO_2 advected equatorward as part of the general surface flow. The biological fluxes POC and DOC are shown coming off each upwelling centre. There are 6 upwelling centres Cape Frio (CF), Walvis Bay (WB), Luderitz (LZ), Namaqua (NQ), Cape Columbine (CC) and Cape Peninsula (CP). The air - sea CO_2 flux at each upwelling centre is shown (FCO2AS) where the negative value implies a drawdown flux.

respective flux arrows. The caption provides information on the flux labels. On the basis of this work it is suggested that the following areas of future research would assist in understanding and quantifying the carbon budget of the Benguela and comparable systems:

- DOC production and remineralization rates.
- Greater emphasis in processes in the northern areas of the Benguela System in particular, the Luderitz and Walvis Bay upwelling cells which offer the greatest contrast in the system.
- More emphasis on time series experiments which would not only address event scale variability but also assist in converging the carbon flux estimates based on in situ measurements and bulk concentration changes (Platt et al., 1989).
- Benthic boundary layer processes. Remineralization is the process which most significantly reduces the scope for upwelling systems, such as the Benguela to be CO_2 sinks. The extent to which this happens depends completely on the poorly understood benthic boundary layer physical and biogeochemical dynamics.

8.2.2 The Total Acidity - Total Alkalinity Vector Plots

Total Alkalinity and Total Acidity vector plots are an extremely useful set of co-ordinates with which to model the stoichiometry of perturbations to the carbonate system in the marine environment. Such a model quantitatively separates out in a direct way the effects of the two biogeochemical pumps (C_{Org} and C_{Ing}) and in doing so overcome a major shortcoming of the Deffeys approach. Furthermore, by superimposing PCO_2 isopleths in such a vector model (using equilibrium chemistry) the relative effects of the two biological pumps on PCO_2 change can be quantified. The vector model emphasised how PCO_2 changes are primarily governed by the stoichiometry (C_{Org}:C_{Ing}) rather than the total magnitude (C_{Org} + C_{Ing}) of the biological pumps. Finally,

the effects of temperature on PCO_2 and its impact on air -sea CO_2 flux are addressed. In this regard the vector model indicates how the heating up of upwelled waters has a profound negative impact on the CO_2 sink potential of such systems with consequences in respect of the feedbacks of global warming.

9. Literature Cited

AGENBAG, J.J. AND L.V. SHANNON 1988 - A suggested physical explanation for the existence of a physical boundary at 24°30'S in the Benguela system. *South African Journal of Marine Science* **6**: 119-132.

AIKEN, J., G.F. MOORE AND P.M. HOLLIGAN 1992 - Remote sensing of oceanic biology in relation to global climate change. *Phycology* **28**: 579-590.

ALMGREN, T., D. DYRSSEN AND S. FONSELIUS 1983 - Determination of Alkalinity and Total Carbonate. In *Methods of Sea Water Analysis*, 2nd Ed. Grasshoff, K., M. Ehrhardt and K. Kremling. (Eds). Verlag-Chemie, Weinheim: p. 99-124.

ALTABET, M.A. AND R. FRANCOIS 1994 - Sedimentary nitrogen isotopic ratio as a recorder for surface ocean nitrate utilization. *Global Biogeochemical Cycles* **8**: 103-116.

ANDERSON, L.A. AND J.L. SARMIENTO 1994 - Redfield ratios of remineralization determined by nutrient data analysis. *Global Biogeochemical Cycles* **8**: 65-80.

ANDREWS, W.R.H. AND L. HUTCHINGS 1980 - Upwelling in the Southern Benguela Current. *Progress in Oceanography* **9**: 1-81.

ANGEL, M.V., M.A. BAARS, R.T. BARBER, F.P. CHAVEZ, M. KASTNER, M. LEINEN, J.R.E. LUTJEHARMS, G. REVERDIN AND G.B. SHIMMIELD 1995 - Group report: How do open ocan upwelling systems operate as integrated physical, chemical and biological systems and influence the geological record. In *Upwelling in the ocean: modern processes and ancient records*, Summerhayes, C.P., K.-C. Emeis, M.V. Angel, R.L. Smith and B. Zeitzschel. (Eds). John Wiley & Sons, Chichester: p. 193-220.

ANTOINE, D. AND A. MOREL 1995 - Modelling the seasonal course of upper ocean PCO_2: validation of the model and sensitivity studies. *Tellus* 47B: 122-144.

ARCHER, D. AND E. MAIER - REIMER 1994 - Effect of deep-sea sedimentary calcite preservation on atmospheric CO_2 concentration. *Nature* 367: 260 - 263.

BAILEY G.W. 1987 - The role of regeneration from the sediments in the supply of nutrients to the euphotic zone in the southern Benguela system. In *The Benguela and comparable ecosystems.* Payne AIL, Brink KH, Mann KH, and Hilborn R (Eds). *South African Journal of Marine Science.* **5**: 273-286.

BAILEY, G.W. 1990 - Organic carbon flux and development of oxygen deficiency on the modern Benguela continental shelf south of 22oS: spatial and temporal variability. In *Modern and Ancient Continental Shelf Anoxia*, Tyson, R.V. and T.H. Pearson. (Eds). Geological Society: p. 171-183.

BAILEY, G.W. AND P. CHAPMAN 1985 - The nutrient status of the St Helena Bay region in February 1979. In *South African Ocean Colour and Upwelling Experiment*, Shannon, L.V. (Ed.). Sea Fisheries Research Institute, Cape Town: p. 125-145.

BALCH, W.M. AND C.F. BYRNE 1994 - Factors affecting the estimate of primary production from space. *Journal of Geophysical Research* **99**: 7555-7570.

BANG, N.D. 1973 - Characteristics of an intense ocean frontal system in the upwell regime west of Cape Town. *Tellus* **25**: 256-265.

BANG, N.D. AND W.R.H. ANDREWS 1974 - Direct current measurements of a shelf-edge frontal jet in the southern Benguela system. *Journal of Marine Research* **32**: 405-417.

BANSE, K. 1994 - Uptake of inorganic carbon and nitrate by marine plankton and the Redfield ratio. *Global Biogeochemical Cycles* **8**: 81-84.

BARANGE M., PILLAR S.C., AND HUTCHINGS L. 1992 - Major pelagic borders of the Benguela ecosystem according to euphausiid species distribution. In *Benguela trophic functioning.* Payne AIL, Brink KH, Mann KH, and Hilborn R (Eds). *South African Journal of Marine Science.* **12**: 3-18.

BARANGE, M. AND S.C. PILLAR 1992 - Cross-shelf circulation, zonation and maintenance mechanisms of the euphausiids *Nyctophanes capensis* and *Euphausia hanseni* (Euphausiacea) in the northern Benguela upwelling system. *Continental Shelf Research* **12**: 1027-1042.

BARBER, R.T. AND R.L. SMITH 1981 - Coastal upwelling ecosystems. In *Analysis of marine ecosystems*, Longhurst, A.R. (Ed.). Academic Press, London: p. 31-68.

BARNOLA, J.M., D. RAYNAUD, C. LORIUS AND Y.S. KOROTKEVICH 1994 - Historical CO2 record from the Vostok ice core. In *Trends '93: A compendium of data on global change*, Boden, T.A., D.P. Kaiser, R.J. Sepanski and F.W. Stoss. (Eds). Oak Ridge, USA; Carbon Dioxide Information Analysis Centre: p. 7-10.

BARNOLA, J.M., D. RAYNAUD, Y.S. KOROTKEVICH AND C. LORIUS 1987 - Vostok ice core provides 160,000 year record of atmospheric CO2. *Nature* **329**: 408-414.

BARNOLA, J.M., M. ANKLIN, J. PORCHERON, D. RAYNAUD, J. SCHWANDER AND B. STAUFFER 1995 - CO2 Evolution During the Last Millenium as Recorded by Antarctic and Greenland Ice. *Tellus* **47B**: 264-272.

BATES, R.G. 1973 - *Determination of pH, Theory and Practice*. Wiley, New York: 479pp.

BERGER, W.H., V.S. SMETACEK AND G. WEFER 1989 - Ocean productivity and paleo-productivity -an overview. In *Productivity of the oceans: present and past*, Berger, W.H., V. Smetacek and G. Wefer. (Eds). Wiley, Chichester: p. 1-34.

BERNER, R.A. 1976 - Inclusion of adsorption in the modelling of early diagenesis. *Earth and Planetary Science Letters* **29**: 333-340.

BERNER, R.A. 1982 - Burial of Organic Carbon and Pyrite Sulphur in the Modern Ocean: Its Geochemical and Environmental Significance. *American Journal of Science* **282**: 451-473.

BIRCH, G.F. 1975 - Sediments on the continental margin off the west coast of South Africa. Joint Geological Survey - University of Cape Town Marine Geoscience Bulletin **6**: 1-142.

BISHOP, J.K.B., D.R. KETTEN and J.M. EDMOND - The chemistry, biology and vertical flux of particulate matter from the upper 400m of the Cape basin in the southeast Atlantic Ocean. *Deep Sea Research* **25**: 1121-1161.

BLIGHT, S.P., T.L. BENTLEY, D. LEFEVRE, C. ROBINSON, R. RODRIGUES, J. ROWLANDS AND P.J.L. WILLIAMS 1995 - Phasing of autotrophic and heterotrophic plankton metabloism in a temperate coastal ecosystem. *Marine Ecology Progress Series* **128**: 61-175.

BOATMAN, C.D. AND J.W. MURRAY 1982 - Modelling exchangeable NH4+ adsorption in marine sediments: process and controls of adsorption. *Limnology and Oceanography* **27**: 99-110.

BOLIN, B. 1986 - How much CO_2 will remain in the atmosphere: *The carbon cycle and projections for the future*, SCOPE, 29, edited by B. Bolin, B. Dos, J. Jager, J. Warwick and R.A. Warwick, Wiley and Sons, Chichester.

BOYD, A.J. 1987 - The Oceanography of the Namibian Shelf. Ph.D. Thesis, University of Cape Town, South Africa, 1-190.

BREMNER, J.M. 1981 - Sediments on the continental margin off South West Africa between latitudes 17° and 25°S. Joint Geological Survey - University of Cape Town Marine Geoscience Bulletin **10**: 1-233.

BREMNER, J.M. 1983 - Biogenic sediments on the South West African (Namibian) continetal margin. In *Coastal upwelling: Its sedimentary record Part B: Sedimentary records of ancient coastal upwelling*, Thiede, J. and E. Suess. (Eds). Plenum Press, New York: p. 73-103.

BREWER, P.G. 1979. Carbon dioxide and climate, *Oceanus*, 13-17.

BRINK, K.H., F.F.G. ABRANTES, P.A. BERNAL, R.C. DUGDALE, M. ESTRADA, L. HUTCHINGS, R.A. JAHNKE, P.J. MULLER AND R.L. SMITH 1995 - Group Report: How do Coastal Upwelling Systems Operate as Integrated Physical, Chemical and Biological Systems and Influence the Geological Record ? The Role of Physical Processes in Defining the Spatial Structures of Biological and Chemical Variables. In *Upwelling in the Ocean: Modern Processes and Ancient Records*, Summerhayes, C.P., K.-C. Emeis, M.V. Angel, R.L. Smith and B. Zeitzschel. (Eds). John Wiley & Sons, Chichester: p. 103-124.

BROECKER, W.S. AND T.-H. PENG 1982 - *Tracers in the sea.* Lamont-Doherty Geological Observatory, New York: pp 690.

BROECKER, W.S. AND T.-H., PENG 1984 - The climate - chemistry connection, In: J.E Hansen, and T. Takahashi (Eds). Climate processes and climate sensitivity, *Geophysical Monograph Series*. 29: 327-336, AGU, Washington DC.

BROECKER, W.S. AND T.-H., PENG - 1987. The role of $CaCO_3$ compensation in the glacial to interglacial atmospheric CO_2 change, *Global Biogeochemical Cycles*, 1: 15-39.

BROECKER, W.S. AND T.-H. PENG, 1989 - The cause of the glacial to interglacial atmospheric CO_2 change: a polar alkalinity hypothesis, *Global Biogeochemical Cycles*, **3**: 215-239.

Broecker, W.S. and Takahashi T., 1982 - Is there a tie between atmospheric CO_2 content and ocean circulation ? In: J.E Hansen, and T. Takahashi (Eds), Climate processes and climate sensitivity, *Geophysical Monograph Sereis* **29**: 314-326, AGU, Washington DC.

BROWN P.C. AND HUTCHINGS L. 1987 - The development and decline of phytoplankton blooms in the southern Benguela system: 1. Drogue movements, hydrography and bloom development. In *The Benguela and comparable ecosystems.* Payne AIL, Gulland JA, and Brink KH (Eds). *South African Journal of Marine Science.* **5**: 357-392.

BROWN P.C. AND HUTCHINGS L. 1987a - The development and decline of phytoplankton blooms in the southern Benguela upwelling system: 2. Nutrient relationships. In *The Benguela and comparable ecosystems.* Payne AIL, Gulland JA, and Brink KH (Eds). *South African Journal of Marine Science.* **5**: 393-410.

BROWN, P.C., S.J. PAINTING AND K.L. COCHRANE 1991 - Estimates of phytoplankton and bacterial biomass and production in the northern and southern Benguela ecosystems. *South African Journal of Marine Science* **11**: 537-564.

CALLENDAR, G.S. 1938 - The artificial production of carbon dioxide and its influence on temperature. *Quarterly Journal of the Royal Meteorological Society* **64**: 223-240.

CALLENDAR, G.S. 1958 - On the amount of carbon dioxide in the atmosphere. *Tellus* **10**: 243-248

CHAPMAN P AND SHANNON LV. 1985 - The Benguela ecosystem Part II. chemistry and related processes. In *Oceanography and Marine Biology. An Annual Review.* **23**. Barnes M. (Ed.). Aberdeen University, Press Aberdeen. 183-251.

CHAPMAN P. AND SHANNON L.V. 1987 - Seasonalinity in the oxygen minimum layers at the extremeties of the Benguela system. In *The Benguela and comparable ecosystems.* Payne AIL, Gulland JA, and Brink KH (Eds). *South African Journal of Marine Science.* 5: 85-94.

CHAVEZ, F.P. AND S.L. SMITH 1995 - Biological and Chemical Consequences of Open Ocean Upwelling. In *Upwelling in the Ocean: Modern Processes and Ancient Records*, Summerhayes, C.P., K.-C. Emeis, M.V. Angel, R.L. Smith and B. Zeitzschel. (Eds). Wiley & Sons, Chichester: p. 149-170.

CHAVEZ, F.P. AND J.R. TOGGEWEILER 1995 - Physical Estimates of Global New production: The Upwelling Contribution. In *Upwelling in the Ocean: Modern Processes and Ancient Records*, Summerhayes, C.P., K.-C. Emeis, M.V. Angel, R.L. Smith and B. Zeitzschel. (Eds). Wiley & Sons, Chichester: p. 313-336.

CHEN-T.A. 1978 - Decomposition of calcium carbonate and organic carbon in the deep ocean, *Science*, **201**: 735 - 736.

CODISPOTI, L.A., G.E. FRIEDRIECH AND D.W.HOOD 1986 - Variability in the inorganic carbon system over the southeastern Bering Sea during spring 1980 and spring - summer 1981, *Continental Shelf Research* **5**, 133-160.

COPIN-MONTEGUT, C. AND G. COPIN-MONTEGUT 1983 - Stoichiometry of carbon, nitrogen and phosphorus in marine particulate matter. *Deep-Sea Research* **30**: 31-46.

CRAWFORD R.J.M. 1987 - Food and population variability in five regions supporting large stocks of anchovy, sardine and horse mackerel. In *The Benguela and comparable ecosystems*. Payne AIL, Gulland JA, and Brink KH (Eds). *South African Journal of Marine Science*. **5**: 735-757.

CULBERSON, C.H. 1981 - Direct Potentiometry. In *Marine Electrochemistry: A Practical Introduction*, Whitfield, M. and D. Jagner. (Eds). John Wiley & Sons, Chichester: p. 187-262.

CULLEN, J.J. 1991 - Hypotheses to explain high nutrient conditions in the open sea. *Limnology and Oceanography* **36**: 1578-1599.

CURRIE, R. 1953 - Upwelling in the Benguela Current. *Nature* **171**: 497-500.

CUSHING, D.H. 1969 - Upwelling and fish production. *FAO Fisheries Technical Papers* **84**: 1-40.

DE BAAR, H.J.W AND E. SUESS 1993 - Ocean carbon cycle and climate change - An introduction to the interdisciplinary Union Symposium, *Global and Planetary Change*, **8**, VII - XI.

DEACON, E.L. 1977 - Gas transfer to and across an air - water interface. *Tellus* **29**: 363-374.

DEDECKER, A.H.B. 1970 - Notes on an oxygen-depleted sub-surface current off the west coast of South Africa. *Investigational Reports of the Division of Sea Fisheries, South Africa* **84**: 1-19.

DEFANT, A. 1936 - Das Kaltwasserauftriebsgebiet vor der Kuste Sudwestafrikas. *Landerkdl. Forschung. , Festchr. N. Krebs* 52-66.

DEFFEYS, K.S., 1965 - Carbonate equilibria: a graphic and algebraic approach, Limnology and Oceanography **10**: 412-426.

DENMAN, K.L. AND A.E. GARGETT 1995 - Biological-physical interactions in the upper ocean: the role of vertical and small scale transport processes. *Annual Reviews of Fluid Mechanics* **27**: 383-413.

DENMAN, K.L., E. HOFFMANN AND H. MARCHANT 1996 - Marine biotic response to environmental change and feedbacks to climate. In *IPCC scientific assessment of climate change*, Houghton, J.T. and L.G. Meira. (Eds). Cambridge University Press, Cambridge: p. 10.1-10.40.

DICKSON, A.G. 1984 - pH scales and proton transfer reactions in saline media such as sea water. *Geochimica and Cosmochimica Acta* **48**: 2299-2308.

DICKSON, A.G. 1990 - The Oceanic Carbon Dioxide System: Planning for Quality Data. *JGOFS News (US)* **2**: 2-10.

DICKSON, A.G. 1993 - pH Buffers for Sea Water Media Based on the Total Hydrogen Ion Concentration Scale. *Deep-Sea Research* **40**: 107-118.

DICKSON, A.G. 1994 - The Measurement of Sea Water pH. *Marine Chemistry* **44**: 131-142.

DICKSON, A.G. 1995 - Quality Control of Oceanic Carbon Dioxide Measurements. *First JGOFS International Scientific Symposium, Villefranche-sur-Mer, France* 8(Abstract)

DICKSON, A.G. AND F.J. MILLERO 1987 - A Comparison of the Equilibrium Constants for the Dissociation of Carbonic Acid in Sea Water Media. *Deep-Sea Research* **34**: 1733-1743.

DINGLE, R.V. AND G. NELSON 1993 - Sea Bottom Temperature, Salinity and Oxygen on the Continental margin off South Western Africa. *South African Journal of Marine Science* **13**: 33-49.

DINGLE, R.V., G.F. BIRCH, J.M. BREMNER, R.H. DE DECKER, A. DU PLESSIS, J.C. ENGLEBRECHT, M.J. FINCHAM, T. FITTON, B.W. FLEMMING, R.I. GENTLE, S.H. GOODLAD, A.K. MARTIN, E.G. MILLS, G.J. MOIR, R.J. PARKER, S.H. ROBSON, J. ROGERS, D.A. SALMON, W.G. SIESSER, E.S.W. SIMPSON, C.P. SUMMERHAYES, F. WESTALL, A. WINTER AND M.W. WOODBOURNE 1987 - Deep Sea Sedimentary Environments around Southern Africa (South East Atlantic and South Western Indian Oceans). *Annals of the South African Museum* **98**: 1-27.

DOE, 1994. Handbook of methods for the analysis of the various parameters of the carbon dioxide system in sea water. A.G. Dickson and C. Goyet Editors), Version 2.0, U.S. Department of Energy.

DUCKLOW, H.W. 1995 - Ocean Biogeochemical Fluxes: New production and Export of Organic Matter from the Upper Ocean. *Reviews of Geophysics* **33**:

DUGDALE, R.C. AND J.J. GOERING 1967 - Uptake of new and regenerated forms of nitrogen in primary productivity. *Limnology and Oceanography* **12**: 196-206.

DUURSMA, E.K. AND R. DAWSON 1981 - *Marine Organic Chemistry: Evolution, Composition, Interactions and Chemistry of Organic Matter in Seawater*. Elsevier, Amsterdam: pp.521.

DYRSSEN, D. AND L.G. SILLEN 1967 - Alkalinity and total carbonate in sea water. A plea for p - T independent data. *Tellus* **19**: 113-121.

ENTING, I.G., C.M. TRUDINGER AND R.J. FRANCEY 1995 - A synthesis inversion of the concentration of $d^{13}C$ of Atmospheric CO2. *Tellus* **47B**: 35-52.

EPPLEY, R.W. AND B.J. FETERSON 1979 - Particulate organic matter flux and planktonic new production in the deep ocean. *Nature* **282**: 677-680.

EPPLEY, R.W., E.H. RENGER AND W.G. HARRISON 1979 - Nitrate and phytoplankton production in southern California coastal waters. *Limnology and Oceanography* **24**: 483-494.

ETCHETO, J., J. BOUTIN AND L. MERLIVAT 1991 - Seasonal variation of the CO2 exchange coefficient over the global ocean using satellite wind speed measurements. *Tellus* **43B**: 247-255.

ETHERIDGE, D.M., I.P. STEELE, J.M. BARNOLA, C.W. WOOKEY AND G.I. PEARMAN 1993 - A high resolution atmospheric CO2 record from Law dome ice cores and air in the firn. *4th International CO2 Conference*, Carqueiranne, France: 184-185.(Abstract)

FARMER, D.M., C.L. MCNEIL AND B.D. JOHNSON 1993 - Evidenece for the importance of bubbles in increasing air-sea gas flux. *Nature* **361**: 620-623.

FARRINGTON J.W. 1992 - Macromolecular organic matter working group report. In *Marine Organic Geochemistry: Review and Challeges for the Future.* Farrington JW (Ed.). *Marine Chemistry.* **39**: 39-50.

FENCHEL, T. AND T.H. BLACKBURN 1979 - *Bacteria and Mineral Cycling.* Academic Press, London: pp225.

FERNANDEZ, E., P. BOYD, P.M. HOLLIGAN AND D.S. HARBOUR 1993 - Production of organic and inorganic carbon within a large-scale coccolithophore bloom in the northeast Atlantic Ocean. *Marine Ecology Progress Series* **97**: 271-285.

FIELD, J.G., C.L. GRIFFITHS, E.A.S. LINLEY, P. ZOUTENDYK AND R.A. CARTER 1981 - Wind Induced Water Movements in a Benguela Kelp Bed. In *Coastal Upwelling*, Richards, F.A. (Ed.). American Geophysical Union, Washington: p. 507-513.

GARGETT, A.E. 1984 - Vertical eddy diffusivity in the ocean interior. *Journal of Marine Research* **42**: 359-393.

GARRISON, D.L. 1981 - Monterey Bay phytoplankton. II. Resting spore cycles in coastal diatom populations. *Journal of Plankton Research* **3**: 137-156.

GIRAUDEAU, J. 1992 - Distribution of Recent nannofossils beneath the Benguela system: southwest African continental margin. *Marine Geology* **108**: 219-237.

GIRAUDEAU, J. AND G.W. BAILEY 1995 - Spatial dynamics of coccolithophore communities during an upwelling event in the southern Benguela system. *Continental Shelf Research* **15**: 1825-1852.

GIRAUDEAU, J., P.M.S. MONTEIRO AND K. NIKODEMUS 1993 - Distribution and malformation of living coccolithophores in the northern Benguela upwelling system off Namibia. *Marine Micropaleontology* **22**: 93-110.

GLIBERT, P.M., F. LIPSCHULTZ, J.J. MCCARTHY AND M.A. ALTABET 1982 - Isotope dilution models of uptake and remineralization of ammonium by marine plankton. *Limnology and Oceanography* **27**: 639-650.

GORDON HR AND MOREL A. 1983 - Remote Assessment of Ocean Colour for Interpretation of Satellite Visible Imagery: A Review. In *Lecture notes on coastal and estuarine studies.* 4. Springer-Verlag, Berlin. 1-114.

GOWER, J.F.R. 1981 - *Oceanography from Space.* New York; Plenum Press: pp.978

GRAN, G. 1952 - Determination of the equivalence point in potentiometric titrations Part II. *Analyst* **77**: 661-671.

GRASSHOFF, K. 1983 - Determination of Oxygen. In *Methods of Sea Water Analysis*, 2nd Ed. Grasshoff, K. and M. Ehrhardt. (Eds). Verlag-Chemie, Weinheim: p. 61-72.

GROOM, S.B. AND P.M. HOLLIGAN 1987 - Remote sensing of Coccolithophore blooms. *Advances in Space Research.* **7**: 73-78.

GUASTELLA L.A. 1992 - Sea surface heat exchange at St Helena bay and implications for the southern Benguela upwelling system. In *Benguela Trophic Functioning.* Payne AIL, Brink KH, Mann KH, and Hilborn R (Eds). *South African Journal of Marine Science.* **12**: 61-70.

GUO, L., H. SANTSCHI AND K.W. WARNKEN 1995 - Dynamics of dissolved organic carbon (DOC) in oceanic environments. *Limnology and Oceanography*. **40**: 1392-1403.

HANSEN, J. AND S. LEBEDEFF 1988 - Global surface air temperatures update through 1987. *Geophysical Research Letters* **15**: 323-326.

HANSSON, I. 1973 - A new set of pH scales and standard buffers for sea water. *Deep-Sea Research* **20**: 479-491.

HANSSON, I. AND D. JAGNER 1973 - Evaluation of the accuracy of Gran plots by means of computer calculations. Application of the potentiometric titration of the total alkalinity and carbonate content of sea water. *Analytica Chimica Acta* **65**: 363-372.

HARRISON, W.G. 1978 - Experimental measurements of nitrogen remineralization in coastal waters. *Limnology and Oceanography* **23**: 684-694.

HART, T.J. AND R. CURRIE 1960 - The Benguela Current. *Discovery Reports* **31**: 123-297.

HEDGES, J.I. 1992 - Global biogeochemical cycles: progress and problems. *Marine Chemistry* **39**: 67-93.

HSIEH, W.W. AND G.J. BOER 1992 - Global climate change and ocean upwelling. *Fisheries and Oceanography* **1**: 333-338.

HONJO, S. 1976 - Coccoliths: Production, transportation and sedimentation. *Marine Micropaleontology* **1**: 65-79.

HUNTSMAN, S.A., K.H. BRINK, R.T. BARBER AND T. BLASCO 1981 - The Role of Circulation and Stability in Controling the Relative Abundance of Dinoflagellates and Diatoms Over the Peru Shelf. In *Coastal Upwelling*, Richards, F.A. (Ed.). Washington; American Geophysical Union: p. 357-365.

HUTCHINGS, L. 1981 - The Formation of Plankton Patches in the Southern Benguela Current. In *Coastal Upwelling*, Richards, F.A. (Ed.). Washington; American Geophysical Union: p. 496-506.

HUTCHINGS L. 1992 - Fish harvesting in a variable environment - searching for rules or searching for exceptions. In *Benguela Trophic Dynamics.* Payne AIL, Brink KH, Mann KH, and Hilborn R (Eds). *South African Journal of Marine Science.* **12**: 297-318.

HUTCHINGS, L., G.C. PITCHER, T.A. PROBYN AND G.W. BAILEY 1995 - The Chemical and Biological Consequences of Coastal Upwelling. In *Upwelling in the Ocean: Modern Processes and Ancient Records*, Summerhayes, C.P., K.-C. Emeis, M.V. Angel, R.L. Smith and B. Zeitzschel. (Eds). Chichester; John Wiley & Sons: p. 65-82.

IPCC 1990 - *Climate Change: The IPCC Scientific Assessment.* Cambridge University Press, Cambridge, UK: pp.365

IPCC 1996 - *Climate Change 1995 - The science of climate change: summary for policymakers.* Cambridge University Press, Cambridge: pp

ITTEKKOT, V. 1993 - The abiotically driven biological pump in the ocean and short term fluctuations in atmospheric CO2 contents. *Global and Planetary Change* **8**: 17-26.

JAGNER, D. 1981 - Potentiometric titrations. In *Marine Electrochemistry: A practical Introduction*, Whitfield, M. and D. Jagner. (Eds). Chichester; John Wiley & Sons: p. 263-300.

JAMES A.G. 1987 - Feeding ecology, diet and field based studies on feeding selectivity of the Cape anchovy *Eugraulis capensis* Gilchrist. In *The Benguela and comparable ecosystems.* Payne AIL, Gulland JA, and Brink KH (Eds). *South African Journal of Marine Science.* 5: 673-692.

JGOFS. 1990 - The Joint Global Ocean Flux Study - Science Plan. **5**: pp61.

JGOFS. 1992 - Joint Global Ocean Flux Study - Implementation Plan. **9**: pp80.

JOHNSON, K.M., P.J.L. WILLIAMS, L. BRANDSTROM AND J.M. SIEBURTH 1987 - Coulometric TCO2 Analysis for Marine Studies: Automation and Calibration. *Marine Chemistry* **21**: 117-133.

KAMSTRA, F. 1985 - Environmental features of the southern Benguela with special reference to the wind stress. In *South African Ocean Colour and Upwelling Experiment*, Shannon, L.V. (Ed.). Cape Town; Sea Fisheries Research Institute: p. 13-28.

KEELING, C.D. 1960 - The concentration and isotopic abundance of carbon dioxide in the atmosphere. *Tellus* **12**: 200-203.

KEELING, C.D. 1968 - Carbon dioxide in surface ocean waters. Global distribution. *Journal of Geophysical Research* **73**: 4543-4553.

KEELING, C.D. AND T.P. WHORF 1993 - Trends in atmospheric CO2 since the eruption of Pinatubo in 1991. *4th International CO2 Conference*, Carqueiranne, France(Abstract).

KEELING, C.D. AND T.P. WHORF 1994 - Atmospheric CO2 records from sites in the SIO air sampling network. In *Trends '93: A compendium of data on global change*, Boden, T.A., D.P. Kaiser, R.J. Sepanski and F.W. Stoss. (Eds). Oak Ridge, USA; Carbon Dioxide Information Analysis Centre: p. 16-26.

KEIR, R.A. 1993 - Cold surface ocean ventilation and its effect on atmospheric CO_2, Journal of Geophysical Research 98: 849 - 856.

KING, F.D. 1987 - Nitrogen recycling efficency in steady state oceanic environments. *Deep-Sea Research* **34**: 843-856.

KING, F.D. AND A.H. DEVOL 1979 - Estimates of vertical eddy diffusion through the thermocline from phytoplankton nitrate uptake rates in the mixed layer of the eastern tropical Pacific. *Limnology and Oceanography* **24**: 645-651.

KOROLEFF, F. 1983 - Determination of Nutrients. In *Methods of Sea Water Analysis*, 2nd Ed. Grasshoff, K. and M. Ehrhardt. (Eds). Weinheim; Verlag-Chemie: p. 125-188.

LENZ, S.J. 1992 - The surface boundary layer in coastal upwelling regions. *Journal of Physical Oceanography* **24**: 1517-1539.

LENZ, S.J. AND J.H. TROWBRIDGE 1991 - The bottom boundary layer over the northern California shelf. *Journal of Physical Oceanography* **21**: 1186-1201.

LEWIS, M.R., E.P.W. HORNE, J.J. CULLEN, N.S. OAKEY AND T. PLATT 1984 - Turbulent motions may control phytoplankton photosynthesis in the upper ocean. *Nature* **311**: 149-150.

LISS, P.S. 1983 - Gas transfer: experimental and geochemical implications. In *Air - sea exchange of gases and particles*, Liss, P.S. and W.G.N. Slinn. (Eds). Berlin; Reidel: p. 241-298.

LISS, P.S. AND L. MERLIVAT 1986 - Air -sea gas exchange rates: introduction and synthesis. In *The role of air-sea exchange in geochemical cycling*, Buat-Menard, P. (Ed.). D. Reidel Publishing Co. p. 113-127.

LOEWENTHAL, R.E. AND C.V.R. MARAIS 1984 - *Carbonate Chemistry of Aquatic Systems: high salinity waters*. Ann Arbor Science, Boston..

LONGHURST, A.R. AND W.G. HARRISON 1989 - The biological pump: profiles of plankton production and consumption in the upper ocean. *Progress in Oceanography* **22**: 47-123.

LUTJEHARMS J.R.E. AND MEEUVIS J.M. 1987 - The extent and variability of south-east Atlantic upwelling. In *The Benguela and comparable ecosystems.* Payne AIL, Gulland JA, and Brink KH (Eds). *South African Journal of Marine Science.* **5**: 51-62.

LUTJEHARMS J.R.E. AND STOCKTON P.L. 1987 - Kinematics of the upwelling front off southern Africa. In *The Benguela and comparable ecosystems.* Payne AIL, Gulland JA, and Brink KH (Eds). *South African Journal of Marine Science.* **5**: 35-50.

LUTJEHARMS J.R.E. AND VALENTINE H.R. 1987 - Water types and volumetric considerations of the South-East Atlantic upwelling regime. In *The Benguela and comparable ecosystems.* Payne AIL, Gulland JA, and Brink KH (Eds). *South African Journal of Marine Science.* **5**: 63-72.

MACISAAC, J.J., R.C. DUGDALE, R.T. BARBER, D. BLASCO AND T.T. PACKARD 1985 - Primary production cycle in an upwelling centre. *Deep-Sea Research* **32**: 503-529.

MACKIN, J.E. AND R.C. ALLER 1984 - Ammonium adsorption in marine sediments. *Limnology and Oceanography* **29**: 250-257.

MAIER-REIMER, E., 1993. The biological pump in the greenhouse, *Global and Planetary Change*, **8**: 13-16.

MARGALEF, R. 1978 - Life-forms of phytoplankton as survival alternatives in an unstable environment. *Oceanologica Acta* **1**: 493-509.

MELILLO, J., C. PRENTICE, E. SHULTZE, G. FARQUHAR AND O. SALA 1996 - Terrestrial ecosystems: responses to global environmental change and feedbacks to climate. In *IPCC second scientific assessment of climate change*, Houghton, J.T. and L.G. Meira. (Eds). Cambridge University Press, Cambridge: p. 9.1-9.36.

MERBACH, C., C.H. CULBERSON, J.E. HAWLEY AND R.M. PYTKOWICZ 1973 - Measurement of the apparent dissociation constants of carbonic acid in sea water at atmospheric pressure. *Limnology and Oceanography* **18**: 897-907.

MIDDELBURG, J.J., T. VLUG AND F.J.W.A. VAN DER NAT 1993 - Organic matter mineralization in marine systems. *Global and Planetary Change* **8**: 47-58.

MILLERO, F.J. 1979 - The Thermodynamics of the Carbonate System in Sea Water. *Geochimica and Cosmochimica. Acta* **43**: 1651-1661.

MILLIMAN, J.D. 1993 - Production and accumulation of calcium carbonate in the ocean: budget of a nonsteady state. *Global Biochemical Cycles* **7**: 927-957.

MITCHELL, J.F.B. 1989 - The "Greenhouse " effect and climate change. *Reviews of Geophysics* **27**: 115-139.

MITCHELL-INNES, B.A. AND A. WINTER 1987 - Coccolithophores: a major phytoplankton component in mature upwelled waters off the Cape Peninsula, South Africa in March, 1983. *Marine Biology* **95**: 25-30.

MOLONEY C.L. 1992 - Simulation studies of trophic flows and nutrient cycles in Benguela upwelling foodwebs. In *Benguela trophic functioning.* Payne AIL, Brink KH, Mann KH, and Hilborn R (Eds). *South African Journal of Marine Science.* **12**: 457-476.

MONTEIRO, P.M.S., A.G. JAMES, A.D. SHOLTO-DOUGLAS AND J.G. FIELD 1990 - The $d^{13}C$ trophic position isotope spectrum as a tool to define and quantify carbon pathways in marine food webs. *Marine Ecology Progress Series* **78**: 33-40.

MURRAY, J.W., R.T. BARBER, M.R. ROMAN, M.P. BACON AND R.A. FEELY 1994 - Physical and biological controls on carbon cycling in the equatorial Pacific. *Science* **266**: 58-65.

NATHAN, Y., J.M. BREMNER, R.E. LOEWENTHAL AND P.M.S. MONTEIRO 1993 - Role of bacteria in phosphorite genesis. *Geomicrobiology Journal* **11**: 69-76.

NEFTEL, A., E. MOOR, H. OESCHGER AND B. STAUFFER 1985 - Evidence from polar ice cores for the increase in atmospheric CO2 in the past two centuries. *Nature* **315**: 45-47.

NEFTEL, A., H. FRIEDLI, E. MOOR, H. LOTSCHER, H. OESCHGER, U. SIEGENTHALER AND B. STAUFFER 1994 - Historical CO2 record from the Sipple Station ice core. In *Trends '93: A compendium of data on global change*, Boden, T.A., D.P. Kaiser, R.J. Sepanski and F.W. Stoss. (Eds). Oak Ridge, USA; Carbon Dioxide Information Analysis Centre: p. 11-14.

NELSON, G. 1985 - Notes on the physical oceanography of the Cape Peninsula upwelling system. In *South African Ocean Colour and Upwelling Experiment*, Shannon, L.V. (Ed.). Cape Town; Sea Fisheries Research Institute: p. 63-96.

NELSON, G. 1989 - Poleward motion in the Benguela area. In *Poleward flows along eastern ocean boundaries*, Neshyba, S.J., C.N.K. Mooers, R.L. Smith and R.T. Barber. (Eds). New York; Springer: p. 110-130.

NELSON, G. AND L. HUTCHINGS 1983 - The Benguela upwelling area. *Progress in Oceanography* **12**: 333-356.

NEUMANN, G. AND W.J. PIERSON 1966 - *Principles of Physical Oceanography.*; Prentice-Hall, London: pp. 545.

NEWMAN, G.G. AND D.E. POLLOCK 1974 - A mass stranding of rock-lobsters *Jasus lalandii* (H Milne-Edwards 1837) at Elands Bay, South Africa (Decapoda, Palinuridae). *Crustaceana* **26**: 1-4.

PACKARD, T.T., M. DENIS AND P. GARFIELD 1988 - Deep-ocean metabolic CO2 production: calculations from ETS activity. *Deep-Sea Research* **35**: 371-392.

PAYNE, A.I.L., J.A. GULLAND AND K.H. BRINK 1987 - *The Benguela and comparable ecosystems. South African Journal of Marine Science* **5**: pp.957

PAYNE, A.I.L., K.H. BRINK, K.H. MANN AND R. HILBORN 1992 - *Benguela trophic functioning. South African Journal of Marine Science* **12**: pp. 1108

PITCHER G.C., BROWN P.C., AND MITCHELL-INNES B.A. 1992 - Spatio-temporal variability of phytoplankton in the southern Benguela upwelling system. In *Benguela trophic functioning*. Payne AIL, Brink KH, Mann KH, and Hilborn R (Eds). *South African Journal of Marine Science*. **12**: 439-456.

PITCHER, G.C. 1990 - Phytoplankton seed populations of the Cape Peninsula upwelling plume, with particular reference to resting spores of *Chetoceros* (Bacillariophyceae) and their role in seeding upwelling waters. *Estuarine, Coastal and Shelf Science* **31**: 283-301.

PITCHER, G.C., A.J. RICHARDSON AND J.L. KORRUBEL 1996 - The use of sea temperatures in characterizing mesoscale heterogeneity of phytoplankton in an embayment of the southern Benguela upwelling system. *Journal of Plankton Research* **18**:

PITCHER, G.C., D.R. WALKER AND B.A. MITCHELL-INNES 1989 - Phytoplankton sinking rate dynamics in the southern Benguela upwelling system. *Marine Ecology Progress Series* **55**: 261-269.

PITCHER, G.C., D.R. WALKER, B.A. MITCHELL-INNES AND C.L. MOLONEY 1991 - Short-term variability during an anchor station study in the southern Benguela upwelling system: Phytoplankton dynamics. *Progress in Oceanography* **28**: 39-64.

PLATT, T. AND S. SATHYENDRANATH 1988 - Oceanic primary production: estimation by remote sensing at regional and larger scales. *Science* **241**: 1613-1620.

PLATT, T., W.G. HARRISON, M.R. LEWIS, W.K.W. LI, S. SATHYENDRANATH, R.E. SMITH AND A.F. VEZINA 1989 - Biological production of the oceans: the case for consensus. *Marine Ecology Progress Series* **52**: 77-88.

PROBYN, T.A. 1985 - Nitrogen uptake by size fractionated phytoplankton populations in the southern Benguela upwelling system. *Marine Ecology Progress Series* **22**: 249-259.

PROBYN, T.A. 1987 - Ammonium regeneration by microplankton in an upwelling environment. *Marine Ecology Progress Series* **37**: 53-64.

PROBYN, T.A. 1988 - Nitrogen utilization by phytoplankton in the Namibian upwelling region during the austral spring. *Deep-Sea Research* **35**: 1387-1404.

PROBYN, T.A. 1990 - Size-fractionated measurements of nitrogen uptake in aged upwelled waters: Implications for pelagic food webs. *Limnology and Oceanography* **35**: 202-210.

PROBYN T.A. 1992 - The inorganic nitrogen nutrition of phytoplankton in the southern Benguela: new production, phytoplankton size and implications for pelagic foodwebs. In *Benguela trophic functioning.* Payne AIL, Brink KH, Mann KH, and Hilborn R (Eds). *South African Journal of Marine Science.* 12: 411-420.

PYTKOWICZ, R.M. 1983 - *Equilibria, non-equilibria and natural waters.* John Wiley & Sons; New York: pp 353.

QUAY, P.D., B. TILBROOK AND C.S. WONG 1992 - Oceanic uptake of fossil fuel CO_2: Carbon-13 evidence. *Science* **256**: 74-79.

REDFIELD, A.C., B.H. KETCHUM AND F.A. RICHARDS 1963 - The influence of organisms on the composition of sea water. In *The Sea*, Hill, M.N. (Ed.). Interscience, New York: p. 26-77.

REID, J.L. 1989 - On the total geostrophic circulation of the South Atlantic Ocean: Flow patterns, tracers and transports. *Progress in Oceanography* **23**: 149-244.

REVELLE, R. AND E. SUESS 1957 - Carbon dioxide exchange between the atmosphere and the ocean. *Tellus* **9**: 18-27.

REVERDIN, G. 1995 - The Physical Processes of Open Ocean Upwelling Systems. In *Upwelling in the Ocean: Modern Processes and Ancient Records*, Summerhayes, C.P., K.-C. Emeis, M.V. Angel, R.L. Smith and B. Zeitzschel. (Eds). Chichester; Wiley & Sons: p. 125-148.

RHAMSTORF, S. 1994 - Rapid climate transitions in a coupled ocean - atmosphere model. *Nature* **372**: 82-85.

RICHARDS, F.A. 1981 - *Coastal Upwelling.* Washington; American Geophysical Union: pp 529.

RICKER, W.E. 1984 - Computation and use of central trend lines. *Canadian Journal of Zoology* **62**: 1897-1905.

ROBERTSON, J.E., C. ROBINSON, D.R. TURNER, P.M. HOLLIGAN, A.J. WATSON, P. BOYD, E. FERNANDEZ AND M. FINCH 1994 - The impact of a coccolithophore bloom on oceanic carbon uptake in the northeast Atlantic during summer 1991. *Deep-Sea Research* **41**: 297-250.

ROGERS J AND BREMNER JM. 1991 - The Benguela Ecosystem. Part IV. Marine-Geological aspects. In *Oceanography and Marine Biology. An Annual Review.* 29. Barnes M. (Ed.). Aberdeen University Press, Aberdeen. 1-85.

RYTHER, J.H. 1969 - Photosynthesis and Fish Production in the Sea. *Science* **166**: 72-76.

SAMBROTTO, R.N., G. SAVIDGE, C. ROBINSON, P. BOYD, T. TAKAHASHI, D.M. KARL, C. LANGDON, D. CHIPMAN, J. MARRA AND L. CODISPOTI 1993 - Elevated consumption of carbon relative to nitrogen in the surface ocean. *Nature* **363**: 248-250.

SARMIENTO, J.L., J.C. ORR AND U. SIEGENTHALER 1992 - *Journal of Geophysical Research* **97**: 3621-3645.

SHACKLETON NJ AND PISIAS NG. 1985 - Atmospheric Carbon Dioxide, Orbital Forcing and Climate. In *The Carbon Cycle and Atmospheric CO2: Natural Variations from the Archean to the Present.* 32. American Geophysical Union. 303-317.

SHANNON LV. 1985 - The Benguela Ecosystem Part I: Evolution of the Benguela, Physical Features and Processes. In *Oceanography and Marine Biology. An Annual Review.* 23. Barnes M. (Ed.). Aberdeen; Aberdeen University Press. 105-182.

SHANNON LV AND PILLAR SC. 1986 - The Benguela Ecosystem Part III. Plankton. In *Oceanography and Marine Biology. An Annual Review.* 24. Barnes M. (Ed.). Aberdeen; Aberdeen University Press. 65-170.

SHANNON, L.V. AND G. NELSON 1996 - The Benguela: Large scale features and processes and system variability. In *The South Atlantic: present and past circulation*, Wefer, G., W.H. Berger, G. Siedler and D. Webb. (Eds). Berlin; Springer-Verlag:

SHANNON L.V., CRAWFORD R.M., POLLOCK D.E. ET AL. 1992 - The 1980's - a decade of change in the Benguela Ecosystem. In *Benguela Trophic Dynamics*. Payne AIL, Brink KH, Mann KH, and Hilborn R (Eds). *South African Journal of Marine Science*. 12: 271-297.

SHOLTO-DOUGLAS, A.D., J.G. FIELD, A.G. JAMES AND N.J. VAN DER MERWE 1990 - $^{13}C/^{12}C$ and $^{15}N/^{14}N$ isotope ratios in the southern Benguela ecosystem: indicators of foodweb relationships among different size classes of plankton and pelagic fish; differences between fish muscle and bone collagen tissues. *Marine Ecology Progress Series* **78**: 23-31.

SIEGENTHALER, U. 1990 - El Nino and atmospheric CO_2. *Nature* **345**: 295-296.

SIEGENTHALER, U. AND F. JOOS 1992 - *Tellus* **44B**: 186-207.

SIEGENTHALER, U. AND H. OESCHGER 1987 - Biospheric CO_2 emissions during the past 200 years reconstructed by deconvolution of ice core data. *Tellus* **39B**: 140-154.

SIEGENTHALER, U. AND J.L. SARMIENTO 1993 - Atmospheric carbon dioxide and the ocean. *Nature* **365**: 119-125.

SIEGENTHALER, U., 1986. Carbon Dioxide: its natural cycle and anthropogenic perturbation. In: P. Buat-Menard, (Ed), The role of air-sea exchange in geochemical cycling, 209-247, D. Riedel Publishing Co.

SIEGFRIED, W.R. AND J.G. FIELD 1981 - A description of the Benguela Ecology Programme 1982 -1986. *South African National Scientific Programmes Report* **54**: 1-39.

SIKES, C.S. AND V.J. FABRY 1994 - Photosynthesis, CaCO3 deposition, coccolithophorids and the global carbon cycle. In *Regulation of atmospheric CO2 and O2 by photosynthetic carbon metabolism*, Tolbert, N.E. and J. Preiss. (Eds). Oxford University Press, Oxford: p. 217-233.

SKIRROW, G. 1975 - The Dissolved Gases: Carbon Dioxide. In *Chemical Oceanography*, 2nd Ed. Riley, J.P. and G. Skirrow. (Eds). Academic Press, London: p. 1-181.

SMITH, R.L. 1995 - The Physical Processes of Coastal Upwelling Systems. In *Upwelling in the Ocean: Modern Processes and Ancient Records*, Summerhayes, C.P., K.-C. Emeis, M.V. Angel, R.L. Smith and B. Zeitzschel. (Eds). Chichester; John Wiley & Sons: p. 39-64.

SONDERGAARD, M. AND M. MIDDELBOE 1995 - A cross-system analysis of labile dissolved organic carbon. *Marine Ecology Progress Series* **118**: 283-294.

STUMM, W. AND J.J. MORGAN 1970 - *Aquatic Chemistry: An Introduction Emphasising Chemical Equilibria in Natural Waters*. Wiley - Interscience, New York: pp. 583

SUMMERHAYES, C.P., K.-C. EMEIS, M.V. ANGEL, R.L. SMITH AND B. ZEITZSCHEL 1995 - Upwelling in the Ocean: Modern Processes and Ancient Records. In *Upwelling in the Ocean: Modern Processes and Ancient Records*, Summerhayes, C.P., K.-C. Emeis, M.V. Angel, R.L. Smith and B. Zeitzschel. (Eds). John Wiley & Sons, Chichester: p. 1-38.

TAKAHASHI, T. 1989 - The carbon dioxide puzzle. *Oceanus* **32**: 22-29.

TANS, P.P., I.Y. FUNG AND T. TAKAHASHI 1990 - Observational Constraints on the Global carbon Budget. *Science* **247**: 1431-1438.

TAUNTON-CLARK, J. 1985 - The formation, growth and decay of upwelling tongues in response to the mesoscale wind field during summer. In *South African Ocean Colour and Upwelling Experiment*, Shannon, L.V. (Ed.). Sea Fisheries Research Institute Cape Town: p. 47-62.

TAYLOR, N.K. 1995 - Seasonal Uptake of Anthropogenic CO2 in an Ocean General Circulation Model. *Tellus* **47B**: 145-169.

THACKERAY, J.F., N.J. VAN DER MERWE, J.A. LEE-THORP, A. SILLEN, J.L. LANHAM, R. SMITH, A. KEYSER AND P.M.S. MONTEIRO 1990 - Changes in Carbon Isotope Ratios in the late Permian Recorded in Therapsid Tooth Apatite. *Nature* **347**: 751-753.

TOGGWEILER, J.R. 1993 - Carbon overconsumption. *Nature* **363**: 210-211.

TOGGWEILER, J.R. and CARSON S., 1995. What are upwelling systems contributing to the global carbon budget ?, In: C.P. Summerhayes, K.-C. Emeys, M.V. Angel, R.L. Smith, B. Zeitchel. (Editors) Upwelling in the ocean: Modern Processes and Ancient Records, Dahlem Workshop Report ES 18, John Wiley, Chichester. p 337-360.

TSUNOGAI, S. AND NORIKI S., 1991. Particulate fluxes of carbonate and organic carbon in the ocean. Is the marine biological activity working as a sink of atmospheric carbon ? *Tellus* **43B**: 256-266.

UNESCO 1994 - Protocols for the Joint Global Ocean Flux Study (JGOFS) core measurements. *Manuals and Guides* **29**: 1-170.

VOLK, T. AND M.I. HOEFFERT 1985 - Ocean carbon pumps: analysis of relative strengths and efficiencies in ocean driven atmospheric CO2 changes. *Geophysical Monograph Series* **32**: 99-110.

WALDRON H.N. AND PROBYN T.A. 1992 - Nitrate supply and potential new production in the Benguela upwelling system. In *Benguela Trophic Functioning*. Payne AIL, Brink KH, Mann KH, and Hilborn R (Eds). *South African Journal of Marine Science*. 12: 29-40.

WALDRON, H.N. 1996 - Regional estimates of potential new production in the southern Benguela upwelling system. Ph.D. Thesis, University of Cape Town, 1-101.

WALLACE, D.W.R. 1995 - Monitoring Global Ocean Carbon Inventories. OOSDP background Report **5**: 1-54.

WANNINKHOF, R. 1992 - Relationship between wind speed and gas exchange over the ocean. *Journal of Geophysical Research* **97**: 7373-7382.

WATSON, A.J. 1995 - Are Upwelling Zones Sources or Sinks of CO2 ? In *Dahlem Workshop Reports ES 18*, Summerhayes, C.P., K.-C. Emeis, M.V. Angel, R.L. Smith and B. Zeitzschel. (Eds). Chichester; Wiley & Sons: p. 321-336.

WESTBROEK, P., C.W. BROWN, J. VAN BLEIJSWIJK, C. BROWNLEE, G.J. BRUMMER, M. CONTE, J. EGGE, E. FERNANDEZ, R. JORDAN, M. KNAPPERTSBUSCH, J. STEFELS, M. VELDHUIS, P. VAN DER WAL AND J. YOUNG 1993 - A model system approach to global climate forcing. The example of *Emiliania huxlei*. *Global and Planetary Change* **8**: 27-46.

WHITFIELD, M. AND D.R. TURNER 1981 - Sea water as an electrochemical medium. In *Marine Electrochemistry: A Practical Introduction*, Whitfield, M. and D. Jagner. (Eds). John Wiley & Sons, Chichester: p. 3-66.

WILLIAMS, P.J.L. 1995 - Evidence for the seasonal accumulation of carbon rich dissolved organic material, its scale in comparison with changes in particulate material and the consequential effect on net C/N assimilation ratios. *Marine Chemistry* **51**: 17-29.

WYRTKI, K. 1963 - The horizontal and vertical field of motion in the Peru current. *Bulletin of the Scripps Institute for Oceanography* **8**: 313-346.